WAVE INDUCED NEARSHORE CURRENTS: A STUDY OF THE FORCING, MIXING AND STABILITY CHARACTERISTICS

by

Uday Putrevu and Ib A. Svendsen

RESEARCH REPORT NO. CACR-91-11

December, 1991

CENTER FOR APPLIED COASTAL RESEARCH

Department of Civil Engineering
University of Delaware
Newark, Delaware 19716

TABLE OF CONTENTS

LIST OF FIGURES

LIST OF TABLES

ACKNOWLEDGMENT

The work reported here was funded by NOAA Office of Sea Grant, Department of Commerce, under Grant No. AA-D-SG040 (Project No. R/OE 6).

Chapter 1

INTRODUCTION

Waves breaking on a beach set up mean currents in the nearshore region. These mean currents play a crucial role in the hydrodynamics of the coastal zone. Of particular concern in recent years has been beach erosion and water quality in the coastal ocean.

An understanding of the nearshore circulation patterns is fundamental to the modelling of the sediment transport in the surf-zone which is required to predict coastal erosion/accretion. Predictions of pollutant dispersal in coastal waters also require a knowledge of nearshore circulations. Clearly, therefore, there exists a need for comprehensive models that predict the effects of various factors on nearshore circulation patterns.

Because of their complexity, comprehensive models of coastal processes have long been restricted to physical models. Physical models are both time consuming and expensive and are plagued by scale effects. Also, the isolation of the effects of different terms in the governing equations on the circulation is not always possible by using physical models. Numerical models do not have these shortcomings but require that the fundamental processes be well understood. The present work is an effort to understand the various mechanisms controlling the mean circulation in the nearshore region.

The circulation in the nearshore region may be studied either using time dependent models that account for wave propagation or by using a wave averaged model that assumes that the motion may be split into a "wave" part and a "current" part. The advantage of the first type of models is that there is no need to differentiate between the wave and current parts of the motion. This is a significant advantage while dealing with the motion above the wave trough level. The disadvantage is that such models are extremely time consuming. The second type of models assume that the wave motion is already known. For this to be a good assumption the quasi-uniform wave approximation should hold and

the width of the surf-zone should be at least several times the wavelength at breaking (Battjes 1988).

The mean circulation in the nearshore region is usually studied using the wave averaged equations of mass, momentum and energy. It turns out that the concept of the radiation stress introduced by Longuet-Higgins & Stewart (1960) is fundamental when dealing with the wave averaged equations. This quantity represents the interaction of the waves and currents and plays a role similar to the role of the Reynolds' stresses in ensemble averaged equations.

Since the introduction of the concept of the radiation stress the wave averaged equations have been used successfully to make significant progress with regard to the understanding of the mechanisms responsible for various phenomena in the nearshore region. An extremely lucid account of the radiation stress and its early applications is given by Longuet-Higgins & Stewart (1964). Pioneering contributions that have used the concept of radiation stress to explain various phenomena in the nearshore region include the variations of the mean water surface in the nearshore region (Longuet-Higgins & Stewart 1963, Bowen *et al.* 1968), the phenomenon of "surf-beat" (Longuet-Higgins & Stewart 1962, Symmonds *et al.* 1982), predictions of longshore currents (Bowen 1969a, Thornton 1970, Longuet-Higgins 1970), mechanisms for rip-currents (Bowen 1969b, Dalrymple & Lozano 1978), undertow modelling (Dyhr-Nielsen & Sorensen 1970, Dally 1980, Borecki 1982, Svendsen 1984b), side band instability of wave groups to explain extremely low frequency motions in the nearshore (Shemer *et al.* 1991).

1.1 A brief overview of nearshore circulation on a long, straight beach

In this section we give a very brief overview of the presently accepted view of the mean circulation patterns in the nearshore region. Some of the phenomena mentioned below are investigated further in the present thesis. In such a situation, a brief review of the state of the art is presented at the beginning of the appropriate chapter. In the following the chapter referred to at the end of a paragraph contains the brief review of the phenomenon discussed in that particular paragraph. For the references to work

not developed in this thesis and a general review of the state of the art of nearshore hydrodynamics, we refer the reader to the review article by Battjes (1988).

As gravity waves advance from deep water, they begin to feel the bottom and shoal. As they shoal, in the absence of energy dissipation the cross-shore component of the radiation stress increases and this causes a set-down of the mean water surface. Subsequent to wave breaking the wave height decreases and this causes a decrease of the radiation stress which causes a set-up of the mean water surface. (Chapter 3.)

The different contributions to the radiation stresses are not evenly distributed over depth. This creates an imbalance at every depth location. This imbalance drives the undertow which is a return current that balances the volume flux due to the waves in the direction of propagation. (Chapter 5.)

If the incoming wave train approaches the shore obliquely, the decrease of the longshore component of the radiation stress in the cross-shore direction sets up a current parallel to the shore, the so-called longshore current. (Chapter 5.)

On long, straight coasts one often finds rip currents – narrow currents that flow seaward and are often regularly spaced along the beach. Several mechanisms have been proposed to explain these currents.

If the incoming wave train has some time variability (due to groupiness, for example) then the set-up and set-down become time dependent and a low frequency motion, the so called surf-beat, becomes associated with the time variation of the mean water surface.

The shallow water equations admit free wave solutions that are bound to the shore and are progressive or standing in the alongshore direction. The wave motions represented by these solutions are called edge waves and are interference patterns that are trapped near the shoreline by refraction. They have exponentially decaying amplitudes in the cross-shore direction. Edge waves have frequencies that are much lower than the incident gravity waves and combined with the surf-beat form the so-called infra-gravity band of motions in the nearshore region.

Recently extremely low frequency motions (with frequencies significantly lower than

that of edge waves) have been observed in the nearshore region. These motions were identified and mechanisms to explain these motions were proposed after the publication of the review article by Battjes and, therefore, do not figure in that article. (Chapter 7.)

1.2 Outline of the present work

The present work concentrates on the mean circulation on a long, straight beach. We do not account for rip-currents here. Traditional low frequency motions in the surf-zone, *viz.*, surf-beats and edge waves are not addressed in this thesis. We refer the reader to the recent work of Schaffer (1990) in addition to Battjes (1988) for a discussion of the state of the art of infra-gravity motions.

In chapter 2 we derive the equations that govern the mean circulation and water level variation in the nearshore region. The equations derived here allow for the possibility of the currents having a vertical structure. These equations are then simplified for the case of a long straight beach. We also give an extensive discussion of the simplifications afforded by the assumption of alongshore uniformity.

Chapter 3 analyzes available measurements of set-up and wave height variations in order to determine the proper variation of the radiation stresses and energy dissipation rates across the surf-zone. The procedure is then extended to the 2D horizontal situation to estimate variations of the longshore component of the radiation stress which acts as a forcing for the longshore currents.

In the alongshore direction the forcing is resisted by the bottom stress. A quadratic bottom friction formulation is presented in chapter 4. Some interesting implications of the quadratic law are discussed there.

Chapter 5 discusses the prediction of 2D horizontal currents and the extraction of the vertical structure from these currents. A perturbation scheme is developed for the longshore current prediction. The numerical scheme developed is used to study the effects of various factors on longshore currents.

Chapter 6 examines the effect of the interaction of the longshore current and the undertow. The mixing caused by this interaction is analyzed in order to determine whether

the interaction could account for the mixing level required to predict cross-shore variations of the longshore current.

Recent work by Bowen & Holman (1989) suggests that longshore currents may be unstable to perturbations of the velocity field and the resulting motions (termed "shear waves") may possibly explain the observed low-frequency motions in the surf-zone (Tang & Dalrymple 1988, Oltman-Shay *et al.* 1989). Chapter 7 uses a numerical technique to solve the stability equation and extends the stability analysis carried out by Bowen & Holman to more general situations. Also, the effect of a longshore bar on the stability characteristics is examined in some detail. Estimates of the viscous threshold and relevance to laboratory measurements are also given.

Chapter 8 summarizes the work and concludes the same with suggestions for future work.

This report has four appendices. Appendix A contains figures that show the variations of the experimental data analyzed in chapter 3. In appendix B we show, following James (1974a), that the longshore component of the radiation stress is conserved outside the surf-zone. Appendix C contains the details of a derivation of an equation in chapter 5. The numerical scheme used in chapter 7 is described in appendix D.

1.3 Important notations and terminology used in this report

In this report, we will find it convenient to use a co-ordinate system that measures the cross-shore distance from the mean shore line. Therefore, we will have $x = 0$ representing the mean shore line and positive x representing the region of interest. The measurements analyzed in chapter 3 were, for the most part, reported using the cross-shore co-ordinate increasing towards the shoreline. Visser (1982, 1984) reports his measurements using a co-ordinate system that originates at the mean shoreline and is increasing seawards. To avoid confusion, we have, in chapter 3, plotted Visser's measurements using a co-ordinate system that increases towards the mean shoreline. The origin of this co-ordinate system is fixed at the wave maker location. When plotting the original data points from the experiments analyzed in chapter 3 we use the upper case X to denote the cross-shore co-ordinate increasing towards the shoreline.

Other important variables that will be used here include, h_0 the undisturbed depth of the water column, $b = (\overline{\xi})$ the set-up, $h = h_0 + b$ the total depth of the water column, H the wave height, η the instantaneous free surface measured from the mean water level, $\xi = b + \eta$ the instantaneous free surface measured from the still water level, $\zeta = z + h_0$ the distance from the bottom, h_b the total water depth at the break point, $x = x_b$.

In a number of discussions we will be using the description *linear theory estimate* of the radiation stress, or mass flux, *etc.* What is meant by this is the estimate of the radiation stresses/mass fluxes derived using the results of linear wave theory. All these are second order quantities and are correct to that order.

Chapter 2

DERIVATION OF THE EQUATIONS GOVERNING THE WAVE AVERAGED MEAN CIRCULATION

In this chapter we will derive and discuss equations that govern the mean circulation in the nearshore region. The depth integrated equations as well as equations governing the depth variations are derived. The depth integration of the continuity and momentum equations for the case of currents that are constant over depth are well known, and, when these integrated equations are wave averaged they lead to the familiar equations governing the mean quantities (set-up and currents) in the nearshore region (see, *e.g.*, Phillips 1977 p. 62 or Mei 1983 p. 454). The equations derived in the present chapter are valid for the case where the currents have a vertical variation.

For the continuity equation the extension to currents varying with depth is straightforward. The depth integration of the momentum equations, on the other hand, turns out to add more than just algebraic complexity relative to the case where the currents are constant over depth.

It also turns out that the equation governing the depth variation of the currents cannot be integrated directly to give the integrated equations. The reason for this is also analyzed here.

In this thesis we concentrate on the case of a long, straight beach with straight and parallel depth contours. The general equations derived are simplified for that topography. An extensive discussion of the simplifications afforded by this topography is also given.

2.1 Depth integration of the governing equations

2.1.1 Definitions of the velocities and boundary conditions

Let $u_i(t)$ be the instantaneous fluid velocity in the x_i direction ($i = 1, 2$) and w be the vertical velocity (throughout this chapter we will use the indices i, j to represent the horizontal co-ordinates, velocities, *etc.*; the vertical co-ordinate and velocity will be covered separately by z and w). These velocities are split into current and oscillatory parts. Below trough level the splitting into the two parts is straightforward – we define the mean of the velocity to be the current. Above trough level, the splitting is not so straightforward. In this region there is water only part of the time and the usual definition of the currents as the time average of the instantaneous velocity does not work very well. This is because there is a net mass flux due to the waves in the direction of wave propagation and some of the non-zero time averaged velocity is due to the wave motion itself. Assuming that there is no current above trough level is not satisfactory either. For the time being, we will assume that there is a current above trough level.

As suggested by the discussion above, the specification/determination of this current requires additional discussion. One way to specify the current above trough level could be to assume that the mathematical expression that is valid below trough level is valid above that level too. This assumption is implicit in the derivations given in Phillips (1977) and Mei (1983). These derivations are for currents that do not vary with the vertical coordinate and anything other than the assumption that the current has the same value both below and above the trough level would be inconsistent. However, there seems to be reason to believe that this suggestion might not model the physical situation accurately (see chapter 6).

The oscillatory part of the velocity is further split into a wave part and a turbulent fluctuation. In the present work we use a definition of the wave velocity (and, therefore, the current) similar to that used by Phillips (1977). This definition is slightly different from that used by Mei (1983).

To clearly isolate the mechanisms responsible for the creation of the currents, the current is split, following Phillips, into a "return" current and an "external" current. The

"return" current is envisaged as being forced by reasons of continuity and the "external" current is defined as the part that is forced by momentum considerations. The depth integrated value of the external current should equal the externally imposed mass flux. The return current compensates for the wave induced mass flux if there is a constraint on the flow, *e.g.*, a wall that blocks off the flow. If there is no such constraint then the return current would be zero. The benefit of the splitting adopted here will become apparent while discussing the depth integration of the momentum equations. Mathematically, these definitions read

$$u_i(x_j,z,t) = u_{oi}(x_j,z,t) + U_{ri}(x_j,z) + U_{ci}(x_j,z) \tag{2.1}$$

where U_r stands for the return current and U_c the external current. u_o represents the oscillatory component which is further split as below

$$u_{oi}(x_j,z,t) = u_{wi}(x_j,z,t) + u_i'(x_j,z,t) \tag{2.2}$$

The subscript w is used to denote the wave induced velocity and a prime the turbulent fluctuation. Below trough level ($z < \xi_t$, see figure 2.1 which defines the various vertical co-ordinates and locations used in this thesis) we have

$$\overline{u_{wi}(x_j,z,t)} = 0 \tag{2.3}$$

The overbar represents a time average (over a wave period). Between trough and crest the wave induced velocity gives

$$\overline{\int_{\xi_t}^{\xi} u_{wi}(x_j,z,t)dz} = Q_{si} \tag{2.4}$$

where $\vec{Q_s}$ is the volume flux due to the wave motion. In addition,

$$\overline{u_i'(x_j,z,t)} = 0 \tag{2.5}$$

throughout the water column. Furthermore, for later convenience we assume that the return current is zero above trough level.

The kinematic free surface and bottom boundary conditions read (summation over the repeated index is implied)

Kinematic Free Surface Boundary Condition (KFSBC) (at $z = \xi(x_j,t)$)

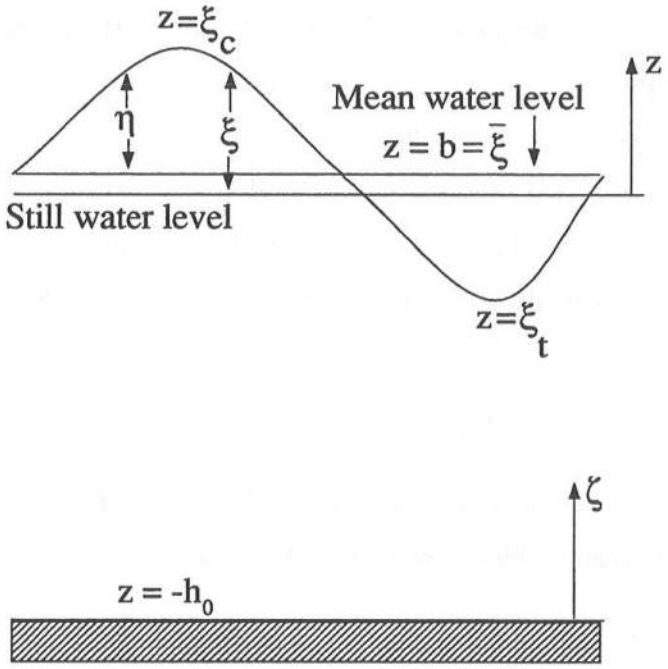

Figure 2.1: Definition sketch for the vertical co-ordinates

$$\frac{\partial \xi}{\partial t} + u_j \frac{\partial \xi}{\partial x_j} = w \tag{2.6}$$

The above condition is applied at the instantaneous free surface $z = \xi(x_j, t)$.

Bottom Boundary Condition (BBC) (at $z = -h_0(x_j)$, top of the bottom boundary layer)

$$-\left(u_{wj} + U_j\right) \frac{\partial h_0}{\partial x_j} = \left(w_w + W\right) \tag{2.7}$$

Because the BBC is applied at the top of the boundary layer only the wave and current parts will satisfy the BBC. The turbulent fluctuations will, in general, not satisfy the BBC at the top of the boundary layer. This is related to the layered approach where the boundary layer supplies a stress condition for the core/middle layer. This approach is described in the next section.

2.1.2 Depth integration of the continuity equation

The continuity equation reads

$$\frac{\partial u_j}{\partial x_j} + \frac{\partial w}{\partial z} = 0 \tag{2.8}$$

Integrating the above from $z = -h_0$ to $z = \xi$ using Leibniz' rule and using the KFSBC and BBC leads to

$$\frac{\partial \xi}{\partial t} + \frac{\partial}{\partial x_j}\int_{-h_0}^{\xi} u_j dz - \left(u_j' \frac{\partial h_0}{\partial x_j} + w'\right)_{-h_0} = 0 \tag{2.9}$$

Time averaging the above and introducing the splitting of the horizontal velocity vector leads to

$$\frac{\partial}{\partial x_j}\int_{-h_0}^{\bar{\xi}} (U_{cj} + U_{rj})\, dz + \frac{\partial}{\partial x_j}\overline{\int_{\xi_t}^{\xi} u_{wj} dz} = 0 \tag{2.10}$$

or introducing (2.4)

$$\frac{\partial}{\partial x_j}\left[\int_{-h_0}^{\bar{\xi}} U_{cj} dz + \int_{-h_0}^{\xi_t} U_{rj} dz + Q_{sj}\right] = 0 \tag{2.11}$$

2.1.3 Depth integration of the momentum equations

The horizontal momentum equations neglecting the viscous stresses (outside the bottom boundary layer) read

$$\frac{\partial u_i}{\partial t} + \frac{\partial u_i u_j}{\partial x_j} + \frac{\partial u_i w}{\partial z} = -\frac{1}{\rho}\frac{\partial P}{\partial x_i} \tag{2.12}$$

We will first integrate the above equation up to trough level. The reason for doing this is that, in order to overcome the difficulty of dealing with the fluid motion above trough level, some authors (Hansen & Svendsen 1984, Stive & Wind 1986) have suggested that a three layered description of the fluid column be used. In such a model the water column is divided into three layers – the bottom boundary layer, the middle layer and a surface layer. The momentum equation is solved in the middle layer with stress conditions applied at the bottom of the middle layer and at the top of the middle layer. These stresses represent the interaction of the middle layer with the other two layers. This approach is an extension of the more common two-layer approach wherein the water column is split into a boundary layer and a core layer. If the boundary stresses can be specified without reference to the fluid motion in the boundary and surface layers, the three layer approach is an attractive one for it reduces the complexity of the problem considerably.

Integrating (2.12) from $z = -h_0$ to the trough level $z = \xi_t$ leads to, after using (2.7),

$$\frac{\partial}{\partial t}\int_{-h_0}^{\xi_t} u_i dz + \frac{\partial}{\partial x_j}\left(\int_{-h_0}^{\xi_t} u_i u_j dz\right) - (u_i u_j)_{\xi_t}\frac{\partial \xi_t}{\partial x_j} + (u_i w)_{\xi_t} =$$
$$-\frac{1}{\rho}\left\{\frac{\partial}{\partial x_j}\int_{-h_0}^{\xi_t} P dz - P_{\xi_t}\frac{\partial \xi_t}{\partial x_i} - P_{-h_0}\frac{\partial h_0}{\partial x_i} + \tau_i(-h_0) + \tau_{ij}(-h_0)\frac{\partial h_0}{\partial x_j}\right\} \tag{2.13}$$

where

$$\tau_i(-h_0) = -\rho u_i' w')_{-h_0} \tag{2.14}$$

and

$$\tau_{ij}(-h_0) = -\rho u_i' u_j')_{-h_0} \tag{2.15}$$

The τ_i and τ_{ij} terms might require some explanation. These terms represent the turbulent stresses at the top of the bottom boundary layer. The level $z = -h_0$ represents the top of the bottom boundary layer. As pointed out before, at this location the bottom boundary condition as specified by (2.7) applies only to the wave and current parts and does not apply to the turbulent fluctuation. These terms represent this residue. These terms are equivalent to the τ_{i3} and τ_{ij} that Mei finds in his derivation (see Mei 1983, p. 456, equation 2.14).

Time averaging (2.13) leads to

$$\frac{\partial}{\partial x_j}\left(\int_{-h_0}^{\xi_t} \overline{u_i u_j} dz\right) - (\overline{u_i u_j})_{\xi_t}\frac{\partial \xi_t}{\partial x_j} + (\overline{u_i w})_{\xi_t} = -\frac{1}{\rho}\left\{\frac{\partial}{\partial x_j}\int_{-h_0}^{\xi_t} \overline{P} dz - \overline{P}_{\xi_t}\frac{\partial \xi_t}{\partial x_i} - \right.$$
$$\left. \overline{P}_{-h_0}\frac{\partial h_0}{\partial x_i} + \overline{\tau_i(-h_0) + \tau_{ij}(-h_0)\frac{\partial h_0}{\partial x_j}}\right\} \tag{2.16}$$

To use (2.16) to predict the time averaged currents we need to know the effective shear stress at trough level $\overline{P}_{\xi_t}\partial\xi_t/\partial x_i$. To evaluate this quantity we need either a description of the fluid motion above the trough level or a parametrization of this stress, perhaps, in terms of a convenient velocity similar to the one normally adopted for the bottom stress.

To evaluate the effective shear stress at trough level integrate (2.12) from $z = \xi_t$ to $z = \xi(t)$. After using the KFSBC we get

$$\frac{\partial}{\partial t}\int_{\xi_t}^{\xi} u_i dz + \frac{\partial}{\partial x_j}\int_{\xi_t}^{\xi} u_i u_j dz + (u_i u_j)_{\xi_t}\frac{\partial \xi_t}{\partial x_j} - (u_i w)_{\xi_t}$$
$$= -\frac{1}{\rho}\left\{\frac{\partial}{\partial x_j}\int_{\xi_t}^{\xi} P dz + P_\xi \frac{\partial \xi}{\partial x_i} - P_{\xi_t}\frac{\partial \xi_t}{\partial x_i}\right\} \tag{2.17}$$

which after time averaging and assuming that $P_\xi = 0$ leads to

$$\frac{\partial}{\partial x_j}\overline{\int_{\xi_t}^{\xi} u_i u_j dz} + (\overline{u_i u_j})_{\xi_t}\frac{\partial \xi_t}{\partial x_j} - (\overline{u_i w})_{\xi_t} = -\frac{1}{\rho}\left\{\frac{\partial}{\partial x_i}\overline{\int_{\xi_t}^{\xi} P dz} + \overline{P}_{\xi_t}\frac{\partial \xi_t}{\partial x_i}\right\} \tag{2.18}$$

Eliminating the quantity $\overline{P}_{\xi_t}\partial\xi_t/\partial x_i$ between (2.17) and (2.18) we get

$$\frac{\partial}{\partial x_j}\left[\int_{-h_0}^{\overline{\xi}} (U_{ci}U_{cj} + U_{ci}U_{rj} + U_{ri}U_{cj} + U_{ri}U_{rj})\, dz \right.$$
$$\left. + \overline{\int_{\xi_t}^{\xi} (u_{wi}U_{cj} + u_{wi}U_{rj} + u_{wj}U_{ci} + u_{wj}U_{ri})\, dz} + \overline{\int_{-h_0}^{\xi} u_i' u_j' dz} + \overline{\int_{-h_0}^{\xi} u_{wi}u_{wj} dz}\right]$$
$$= -\frac{1}{\rho}\left\{\frac{\partial}{\partial x_i}\overline{\int_{-h_0}^{\xi} P dz} - \overline{P}_{-h_0}\frac{\partial h_0}{\partial x_i} + \overline{\tau_i(-h_0)} + \overline{\tau_{ij}}(-h_0)\frac{\partial h_0}{\partial x_j}\right\} \tag{2.19}$$

The interpretation of (2.19) is relatively straightforward. The LHS represents the change in the mean momentum flux of the water column and the RHS the total force acting on the water column. The first term of the LHS represents the momentum flux due to the currents, the second due to the interaction of the currents with the wave induced velocities above trough level and the third and fourth terms represent respectively the mean momentum fluxes due to the turbulent fluctuations and the wave induced velocities respectively. The first term on the RHS represents the forcing from the mean pressure gradient, the second term contains the effect of the sloping bottom and the last two terms make up the bottom resistance.

Note that (2.19) could have been obtained more directly by integrating (2.12) from $z = -h_0$ to $z = \xi$ and time averaging after using the BBC and the KFSBC which is essentially what is done here, albeit, in a round about fashion. The reason for doing this is that if there were some means of specifying the effective shear stress at trough level externally then (2.16) may be used to calculate the currents below trough level. Also note

that (2.19) may be further simplified by the fact that we have, by definition, no return current above trough level.

In addition to information about the wave motion and the turbulent fluctuations, it is clear that to use (2.19) to predict mean currents the pressure variation needs to be determined. This is done by integrating the vertical momentum equation. The vertical momentum equation, neglecting viscous stresses, reads

$$\frac{\partial w}{\partial t} + \frac{\partial w u_j}{\partial x_j} + \frac{\partial w^2}{\partial z} = -\frac{1}{\rho}\frac{\partial}{\partial z}(P + \rho g z) \tag{2.20}$$

Integrating the above from $z = z_r(x_j, t)$ to $z = \xi$ leads to after using the KFSBC

$$\frac{P(z_r)}{\rho} = g(\xi - z_r) + \frac{\partial}{\partial t}\int_{z_r}^{\xi} w dz + \frac{\partial}{\partial x_j}\int_{z_r}^{\xi} u_j w dz - w^2(z_r) + (u_j w)_{z_r}\frac{dz_r}{dx_j} \tag{2.21}$$

The last term on the RHS is required to make the above applicable at any arbitrary location z_r which may, in general, be a function of the horizontal location. We will, in fact, need to apply this at the bottom which is a function of x_j. The mean pressure at the bottom is given by time averaging the above equation. This leads to

$$\overline{\frac{P(-h_0)}{\rho}} = g(\overline{\xi} + h_0) + \frac{\partial}{\partial x_j}\overline{\int_{-h_0}^{\xi} u_j w dz} - \overline{w'\left[w' + u_j'\frac{\partial h_0}{\partial x_j}\right]_{-h_0}} \tag{2.22}$$

after using the BBC.

The last term of (2.21) is only required to make it applicable at particular depth locations (like $z = -h_0$). This term term does not contribute to an integral over depth. With this understanding (2.21) may be integrated to result in

$$\int_{z_r}^{\xi}\frac{P(z)}{\rho}dz = g\left(\xi z_r - \frac{z_r^2}{2}\right) + \frac{\partial}{\partial t}\int_{z_r}^{\xi}\int_{z}^{\xi} w dz + \frac{\partial}{\partial x_j}\int_{z_r}^{\xi}\int_{z}^{\xi} u_j w dz + \frac{dz_r}{dx_j}\int_{z_r}^{\xi} u_j w dz - \int_{z_r}^{\xi} w^2 dz \tag{2.23}$$

A time average of the above evaluated at $z = -h_0$ leads to

$$\overline{\int_{-h_0}^{\xi}\frac{P(z)}{\rho}dz} = g\frac{\overline{(h_0+\xi)^2}}{2} + \frac{\partial}{\partial x_j}\overline{\int_{-h_0}^{\xi}\int_{-h_0}^{\xi} u_j w dz} - \overline{\int_{-h_0}^{\xi} w^2 dz} - \frac{\partial h_0}{\partial x_j}\overline{\int_{-h_0}^{\xi} u_j w dz} \tag{2.24}$$

Equation 2.19 requires that the quantity $\partial\left(\overline{\int_{-h_0}^{\xi} P dz}\right)/\partial x_i - \overline{P}_{-h_0}\partial h_0/\partial x_i$ be specified in order to calculate the currents. Using (2.24) and (2.22) to evaluate this quantity we find

$$\frac{1}{\rho}\left(\frac{\partial}{\partial x_i}\overline{\int_{-h_0}^{\xi} P dz} - \overline{P}_{-h_0}\frac{\partial h_0}{\partial x_i}\right) = \left[\frac{\partial}{\partial x_j}\overline{\int_{-h_0}^{\xi}\frac{P}{\rho}dz} - g\left(\frac{1}{2}\frac{\partial(h_0+\overline{\xi})^2}{\partial x_j} - (h_0+\overline{\xi})\frac{\partial\overline{\xi}}{\partial x_j}\right)\right]\delta_{ij} - \frac{\partial h_0}{\partial x_i}\frac{\partial}{\partial x_j}\overline{\int_{-h_0}^{\xi} u_j w dz} + \overline{w'\left[w' + u_j'\frac{\partial h_0}{\partial x_j}\right]_{-h_0}}\frac{\partial h_0}{\partial x_i} \quad (2.25)$$

We also define the radiation stress tensor S_{ij} by[1]

$$S_{ij} = \left[\overline{\int_{-h_0}^{\xi}\left(\overline{P}+P_w\right)dz} - \frac{1}{2}\rho g(h_0+\overline{\xi})^2\right]\delta_{ij} + \int_{-h_0}^{\xi_t}\rho U_{ri}U_{rj}dz + \overline{\int_{-h_0}^{\xi}\rho u_{wi}u_{wj}dz} \quad (2.26)$$

and excess momentum flux due to turbulent fluctuations (or the integrated Reynolds' stresses) by

$$S_{ij}' = \left[\overline{\int_{-h_0}^{\xi} P' dz} - \frac{1}{2}\rho g\overline{\xi'^2}\right]\delta_{ij} + \rho\overline{\int_{-h_0}^{\xi} u_i' u_j' dz} \quad (2.27)$$

Substituting (2.24) into (2.26) to get a more explicit formula for S_{ij} we get

$$S_{ij} = \rho\left[g\frac{\overline{\eta^2}}{2} + \frac{\partial}{\partial x_j}\overline{\int_{-h_0}^{\xi}\int_{-h_0}^{\xi} u_{wj}w_w dz} - \overline{\int_{-h_0}^{\xi} w_w^2 dz} - \frac{\partial h_0}{\partial x_j}\overline{\int_{-h_0}^{\xi} u_{wj}w_w dz} + \frac{\partial}{\partial x_j}\int_{-h_0}^{\xi_t}\int_{-h_0}^{\xi} U_{rj}W dz - \overline{\int_{-h_0}^{\xi} W^2 dz} - \frac{\partial h_0}{\partial x_j}\int_{-h_0}^{\xi_t} U_{rj}W dz\right]\delta_{ij} + \int_{-h_0}^{\xi_t}\rho U_{ri}U_{rj}dz + \overline{\int_{-h_0}^{\xi}\rho u_{wi}u_{wj}dz} \quad (2.28)$$

where $\eta = \left(\xi - \overline{\xi}\right)$ (see figure 2.1).

For later reference we note here that the radiation stress may be written in the following form

$$S_{ij} = S_{m,ij} + S_p\delta_{ij} \quad (2.29)$$

---

[1] This definition is similar to the one used by Phillips (1977) who includes terms similar to $\int_{\xi}^{\xi_t} U_{ri}U_{rj}dz$ in the radiation stress whereas Mei (1983) does not explicitly account for the same. These terms, however, are implicitly included in his definition since his definition of the wave induced velocity is slightly different from what we have used here (which follows from Phillips). Mei does not have $\overline{u_{wi}} = 0$ below trough level, instead he has $\overline{\int_{-h_0}^{\xi} u_{wi}dz} = 0$. Since there is a net shoreward mass flux above trough due to the wave motion, this implies that Mei includes the return current in his wave motion below trough level. The problem with using this approach is that the velocity one gets by time averaging velocity records is not the current that one calculates using the time averaged equations.

where

$$\begin{aligned} S_p &= \overline{\int_{-h_0}^{\xi} P dz} - \rho g(h_0+\overline{\xi})^2 \\ &= \rho\left[g\frac{\overline{\eta^2}}{2} + \frac{\partial}{\partial x_j}\overline{\int_{-h_0}^{\xi}\int_{-h_0}^{\xi} u_{wj}w_w dz} - \overline{\int_{-h_0}^{\xi} w_w^2 dz} - \frac{\partial h_0}{\partial x_j}\overline{\int_{-h_0}^{\xi} u_{wj}w_w dz} + \right. \\ &\quad \left. \frac{\partial}{\partial x_j}\int_{-h_0}^{\xi}\int_{-h_0}^{\xi_t} U_{rj}W dz - \overline{\int_{-h_0}^{\xi} W^2 dz} - \frac{\partial h_0}{\partial x_j}\int_{-h_0}^{\xi_t} U_{rj}W dz\right] \end{aligned} \tag{2.30}$$

$$S_{m,ij} = \rho\int_{-h_0}^{\xi_t} U_{ri}U_{rj}dz + \rho\overline{\int_{-h_0}^{\xi} u_{wi}u_{wj}dz} \tag{2.31}$$

In terms of the radiation stresses we find that (2.19) may be represented as follows

$$\begin{aligned} &\frac{1}{\rho}\left[\frac{d}{dx_j}\left(S_{ij}+S'_{ij}\right) + \left(\tau_i + \tau_{ij}\frac{\partial h_0}{\partial x_j}\right)\right] + \frac{\partial}{\partial x_j}\left[\int_{-h_0}^{\overline{\xi}}\left(U_{ci}U_{cj}+U_{ci}U_{rj}+U_{ri}U_{cj}\right)dz + \right. \\ &\left. \overline{\int_{\xi_t}^{\xi} u_{wi}U_{cj}+u_{wj}U_{ci}dz}\right] - \overline{w'\left[w'+u'_j\frac{\partial h_0}{\partial x_j}\right]_{-h_0}}\frac{\partial h_0}{\partial x_i} + \frac{\partial h_0}{\partial x_i}\frac{\partial}{\partial x_j}\overline{\int_{-h_0}^{\xi} u_j w dz} \\ &= -g(h_0+\overline{\xi})\frac{\partial\overline{\xi}}{\partial x_i} \end{aligned} \tag{2.32}$$

Mei (1983, p. 459) finds a term similar to the last term on the LHS of the above while integrating the momentum equations for currents independent of the depth. This term seems to represent the horizontal component (caused by the sloping bottom) of the contribution to the pressure from the vertical shear stresses. Mei shows that the contribution from this is negligible in comparison to the RHS and therefore may be neglected without any loss of accuracy. We will assume here that this term is negligible. The term just before this term is of order $(\partial h_0/\partial x)^2$ times the bottom friction term since

$$w'u'_j\frac{\partial h_0}{\partial x_j} = \tau_j\frac{\partial h_0}{\partial x_j} \tag{2.33}$$

and

$$(w')^2\frac{\partial h_0}{\partial x_i} \ll \tau_{ij}\frac{\partial h_0}{\partial x_j} \tag{2.34}$$

since we expect that $w' \ll u'$. Equations 2.33 and 2.34 imply that the third term on the LHS of (2.32) is significantly smaller than the bottom stress term included in the first term. This follows from the fact that the third term on the LHS represents the correction to the bottom stress from the sloping bottom. Therefore, this term may be neglected too. Making these assumptions and introducing the notation

$$\tau_{bi} = \tau_i(-h_0) + \tau_{ij}\frac{\partial h_0}{\partial x_j} \tag{2.35}$$

the depth integrated equations governing the mean currents in the nearshore region reduce to

$$\frac{1}{\rho}\left[\frac{d}{dx_j}\left(S_{ij}+S'_{ij}\right)+\tau_{bi}\right]+\frac{\partial}{\partial x_j}\left[\int_{-h_0}^{\overline{\xi}}\left(U_{ci}U_{cj}+U_{ci}U_{rj}+U_{ri}U_{cj}\right)dz+\right.$$
$$\left.\overline{\int_{\xi_t}^{\xi} u_{wi}U_{cj}+u_{wj}U_{ci}dz}\right] = -g(h_0+\overline{\xi})\frac{\partial\overline{\xi}}{\partial x_i} \tag{2.36}$$

In principle, given a description of the wave motion and a parameterization of the turbulent stresses (2.36) and (2.11) can be solved for the currents and water level variations if the depth variation of the currents is known. The next section deals with the derivation of the equations governing the depth variation.

Note that the time-averaged, depth integrated equations are strictly valid only in the region where there is water all the time. These equations are therefore not valid shoreward of the lowest run-down point and cannot predict quantities in the swash-zone.

2.2 Depth integration of the wave averaged equations

The time average of (2.12) may potentially be used to calculate the depth variation of the currents. Time averaging (2.12) leads to

$$\frac{\partial\overline{u_iu_j}}{\partial x_j}+\frac{\partial\overline{u_iw}}{\partial z}=\frac{-1}{\rho}\frac{\partial\overline{P}}{\partial x_i} \tag{2.37}$$

which with the splitting becomes

$$\frac{\partial}{\partial x_j}\left(\overline{u_{wi}u_{wj}+u'_iu'_j+U_iU_j}\right)+\frac{\partial}{\partial z}\left(\overline{u_{wi}w_w+u'_iw'+U_iW}\right)=\frac{-1}{\rho}\frac{\partial\overline{P}}{\partial x_i} \tag{2.38}$$

We now introduce the following turbulence closures

$$\overline{u'_iu'_j} = -\nu_{tx}\left(\frac{\partial U_i}{\partial x_j}+\frac{\partial U_j}{\partial x_i}\right) \tag{2.39}$$

$$\overline{u'_iw'} = -\nu_{tz}\left(\frac{\partial U_i}{\partial z}+\frac{\partial W}{\partial x_i}\right) \tag{2.40}$$

where, for later convenience, we have differentiated between the horizontal and vertical eddy viscosities. These closures reduce (2.38) to

$$\frac{\partial}{\partial z}\left(\nu_{tz}\frac{\partial U_i}{\partial z}\right)+\frac{\partial}{\partial z}\left(\nu_{tz}\frac{\partial W}{\partial x_i}\right)=\frac{\partial}{\partial x_j}\left(\overline{u_{wi}u_{wj}}+U_iU_j\right)+\frac{\partial}{\partial z}\left(\overline{u_{wi}w_w}+U_iW\right) \quad + \quad \frac{1}{\rho}\frac{\partial\overline{P}}{\partial x_i}-$$

$$\frac{\partial}{\partial x_j}\left[\nu_{tx}\left(\frac{\partial U_i}{\partial x_j}+\frac{\partial U_j}{\partial x_i}\right)\right] \qquad (2.41)$$

Note that the U_iW term is included in (2.41). This term is non-zero in the general situation. The mass flux due to the waves is expected to be a maximum at break point.[2] Therefore, the mass flux decreases shoreward of the break point. For that situation, continuity dictates that there has to be a net transfer of water downwards at trough level indicating that $W \neq 0$. Outside the surf-zone we expect, for similar reasons, that the vertical current has the opposite sign. Even in the case where there is no change in volume flux due to the waves, a non-horizontal bottom will cause a vertical current at the bed thereby inducing vertical currents elsewhere in the water column.

It is emphasized that the depth integration of (2.41) from $z = -h_0$ to the mean water level does not lead to the depth-integrated, time averaged momentum equation (2.36). This is because the upper limit of the integration is a function of time and, therefore, in the latter case we have the correlations between fluctuating quantities that are included by the procedure adopted whereas the first approach does not include the same. The depth integration from the bottom up to the trough level does yield the same result as (2.16). This is because the trough level is assumed to be independent of time and hence the integration and the time averaging are interchangeable. This is true only for regular, monochromatic waves.

The situation is somewhat similar to the calculation of the time average of a quantity like $\int_0^\xi u dz$ where both u and ξ are time dependent. If u is independent of z then the proper time average is given by $\overline{\int_0^\xi u dz} = \overline{u}\overline{\xi} + \overline{u'\xi'}$. Time averaging before integrating will only give the first term. Therefore, the depth integration and the time averaging are not interchangeable.

It is clear that the depth-integrated, time-averaged equations do not throw away any information that is required for the prediction of the currents and, when solved, should lead to the correct result. The discussion above indicates that the currents above trough

[2] According to linear long wave theory $Q_s = B_q H^2\sqrt{gh}/h$ where B_q is a constant. Outside the surf-zone $H^2\sqrt{gh}$ is a constant (according to Green's law) and therefore Q_s decreases with increasing h. Inside the surf-zone we expect $H^2\sqrt{gh}$ to decrease faster than h thus leading to Q_s being a maximum at the break point.

level cannot be predicted by a time averaged equation. To calculate the current above trough level, one would have to solve the time dependent equation (2.12) to calculate the velocity above trough level and time average this velocity to get the current after properly accounting for the mean velocity due to the wave motion (which is responsible for the mass flux due to the waves).

It has been suggested (Svendsen & Lorenz (1989) for the longshore component and deVriend & Kitou (1990) for the general situation) that (2.41) will lead to the depth-integrated, time averaged equation if the $\overline{u_{wi} w_w}$ term is properly accounted for. As we argued earlier, this requires adding to (2.41) the terms corresponding to $\overline{u'\xi'}$ in the example above.

2.3 Discussion of simplifications for a long, straight coast

From now on, in this thesis we deal exclusively with the situation on a long straight coast. Therefore, it is worthwhile to spend some time discussing the nature of the simplifications afforded by this topography.

2.3.1 The depth integrated equations on a long, straight coast

For the case of a long, straight coast with straight and parallel depth contours, we have $(\partial/\partial y = 0)$.[3] This simplifies the equations considerably.

An additional simplification is afforded by this simple topography. Because there is no barrier to stop the flow in the y direction, there is no return current in that direction and, therefore, $V_r = 0$. In addition, for the case where there is no net mass flux in the cross-shore direction (zero externally imposed mass flux) we will also have $U_c = 0$. This thesis deals only with this situation.

To simplify the notation, we shall from now on drop the subscripts on U and V with the understanding that these quantities will refer to the undertow (return current) and the longshore current (external current) respectively.

---

[3] We remove this restriction in a later chapter where we study the shear instability of longshore currents. In that case we allow periodicity in y for the motions induced by the instability.

Under the simplifications above, the wave averaged equations read

Continuity

$$\frac{d}{dx}\left(\int_{-h_0}^{\xi_t} U\,dz + Q_{sx}\right) = 0 \tag{2.42}$$

$x-$ momentum

$$\frac{1}{\rho}\left[\frac{d}{dx}\left(S_{xx} + S'_{xx}\right) + \tau_{bx}\right] = -g(h_0 + \bar{\xi})\frac{\partial \bar{\xi}}{\partial x} \tag{2.43}$$

$y-$ momentum

$$\frac{1}{\rho}\left[\frac{d}{dx}\left(S_{xy} + S'_{xy}\right) + \tau_{by}\right] + \frac{\partial}{\partial x}\left[\int_{-h_0}^{\xi_t} UV\,dz + \overline{\int_{\xi_t}^{\xi} u_w V\,dz}\right] = 0 \tag{2.44}$$

Equations 2.42 and 2.43 are similar to the corresponding equations found in Phillips and Mei. Their equations have currents constant over depth and hence in their equations the integrals involving the currents are readily evaluated. Equation 2.44 on the other hand contains a term that is not found in their equations. The additional term found here is the last term on the LHS of (2.44). This term is zero if the longshore current, V, is independent of the depth.

The interpretation of (2.44) is as follows: The first term represents the radiation stresses due to the waves and the turbulent fluctuations. The second term represents the bottom resistance and the last term represents the interaction of the undertow and the longshore current.

Note also that the only limiting assumptions made so far are 1) the currents are steady and 2) there is alongshore uniformity, *viz.*, $\partial/\partial y = 0$. This implies that (2.44) has all the terms necessary to predict steady longshore currents on long, straight beaches. In other words: If the assumptions leading to (2.44) are satisfied – and there are a lot of instances where they are – then incorrect predictions of the longshore currents must be due to incorrect modelling of one or more terms of (2.44).

Equation 2.44 is different from equations hitherto used to describe longshore currents in that it contains the UV term as well as the effects of the depth variation of V. Also note if the interaction between the undertow and longshore currents is neglected (or if the longshore current is independent of the vertical co-ordinate) then (2.44) reduces to

$$\frac{d}{dx}\left(S_{xy}+S'_{xy}\right)+\tau_{by}=0 \tag{2.45}$$

which is the equation usually solved for longshore currents (see, *e.g.*, Mei 1983, p. 471). In this equation the S'_{xy} term smoothens the longshore current by redistributing the current. That term has no net contribution when integrated across the entire extent of the longshore current. We will be returning to (2.45) a number of times in this thesis.

The τ_{by} term provides the resistance to the longshore currents. These are forced by gradients of the longshore component of the radiation stress and τ_{by} when integrated across the extent of the longshore current should equal the value of S_{xy} at breaking.

In the shore normal direction, $S'_{xx} \ll S_{xx}$ (because $u_w \gg u'$) and therefore may be neglected in (2.43). We make this simplification here and the $x-$ momentum equation reduces to

$$\frac{1}{\rho}\left[\frac{dS_{xx}}{dx}+\tau_{bx}\right]=-g(h_0+\overline{\xi})\frac{\partial\overline{\xi}}{\partial x} \tag{2.46}$$

The radiation stresses of relevance, *viz.*, S_{xx} and S_{xy} are given by

$$S_{xx} = \overline{\left[\int_{-h_0}^{\xi}\left(\overline{P}+P_w\right)dz-\rho g(h_0+\overline{\xi})^2\right]}+\rho\int_{-h_0}^{\xi_t}U^2dz+\rho\overline{\int_{-h_0}^{\xi}u_w^2dz} \tag{2.47}$$

$$S_{xy} = \rho\overline{\int_{-h_0}^{\xi}u_wv_wdz} \tag{2.48}$$

Introducing the expression for the pressure the cross-shore component of the radiation stress, S_{xx}, is given by

$$\begin{aligned}\frac{S_{xx}}{\rho} = {} & \overline{\frac{g(\xi-\overline{\xi})^2}{2}}+\int_{-h_0}^{\xi_t}U^2dz+\overline{\int_{-h_0}^{\xi}u_w^2dz}+\frac{d}{dx}\overline{\int_{-h_0}^{\xi}\int_{-h_0}^{\xi}u_ww_wdz}-\overline{\int_{-h_0}^{\xi}w_w^2dz} \\ & -\frac{dh_0}{dx}\overline{\int_{-h_0}^{\xi}u_ww_wdz}+\frac{d}{dx}\int_{-h_0}^{\xi_t}\int_{-h_0}^{\xi_t}UWdz-\overline{\int_{-h_0}^{\xi}W^2dz}-\frac{\partial h_0}{\partial x_j}\int_{-h_0}^{\xi_t}UWdz\end{aligned} \tag{2.49}$$

Typical sizes of the third, fourth, fifth and sixth terms on the RHS are u_w^2h, $h_xu_ww_wh$, w_w^2h and $h_xu_ww_wh$ respectively. Under normal surf-zone conditions we will have $h_x \ll 1$ and $w_w \ll u_w$. Therefore, these terms are generally much smaller than the third term and may be neglected. A similar consideration leads to the conclusion that the dominating term involving the currents is the U^2 term. We further know that $Q_s \ll |u_w|h$, therefore, it follows that

$$\int_{-h_0}^{\xi_t} U^2 dz \ll \overline{\int_{-h_0}^{\xi} u_w^2 dz} \tag{2.50}$$

and, therefore, to a reasonably good approximation we have

$$S_{xx} = \frac{\overline{g(\xi - \bar{\xi})^2}}{2} + \overline{\int_{-h_0}^{\xi} u_w^2 dz} = g\frac{\overline{\eta^2}}{2} + \overline{\int_{-h_0}^{b+\eta} u_w^2 dz} \tag{2.51}$$

where η is measured from the mean water level (see figure 2.1). The result (2.51) could have been arrived at, more simply, by assuming that the pressure is hydrostatic below the instantaneous water surface $P = \rho g(\xi - z)$ and neglecting the undertow contribution. Therefore, the assumption that the last three terms of the RHS of (2.49) may be neglected is equivalent to assuming that the pressure is hydrostatic. Under the approximations introduced above, we have, for a wave incident at an angle α to the $x-$ axis

$$S_{ij} = S_p \delta_{ij} + S_m e_{ij} \tag{2.52}$$

where

$$S_p = \rho g \frac{\overline{\eta^2}}{2} \tag{2.53}$$

$$S_m = \rho \overline{\int_{-h_0}^{b+\eta} |\mathbf{u_w}|^2 dz} \tag{2.54}$$

$$e_{ij} = \begin{Bmatrix} \cos^2\alpha & \frac{1}{2}\sin 2\alpha \\ \frac{1}{2}\sin 2\alpha & \sin^2\alpha \end{Bmatrix} \tag{2.55}$$

In the above $|\mathbf{u_w}|$ is the magnitude of the wave induced horizontal velocity. (2.52) implies that if the wave angle α and $\overline{\eta^2}$ are known then S_{xy} can be estimated from S_{xx}. We will exploit this in the next chapter where we analyze available measurements of set-up and wave height variations to get realistic variations of S_{xx}. We will then use (2.52) to estimate the longshore component of the radiation stress. The simplification achieved here is that we will be able to estimate the driving force for the longshore currents by using measurements of variations in the cross-shore direction that seemingly have very little to do with longshore currents.

2.3.2 Nature of simplifications

For the topography under discussion the nearshore circulation problem is typically solved as follows:

- The cross-shore momentum equation (2.46) is coupled with an energy equation to solve for the set-up and wave height variations.
- The continuity equation is used to determine the return current or the undertow (at least an average value).
- The longshore momentum equation (which is uncoupled from the cross-shore momentum and energy equations) is used to determine the longshore current.

So, fundamentally different approaches are used to solve for the currents. Also, there is a fundamental difference between the undertow and the longshore current. The undertow is a return current that is forced because there is no net mass flux in the cross-shore direction. The unknown quantity in the cross-shore direction is the set-up and the known quantity is the total mass flux which by continuity considerations dictates the undertow. In complete contrast, the known quantity in the longshore direction is the set-up ($\partial\overline{\xi}/\partial y = 0$) and the unknown quantity is the total mass flux in the longshore direction. This is determined by solving the momentum equation.

The decoupling of the longshore momentum equation from the other three equations is a great simplification which is, of course, possible only for the simple case of $\partial/\partial y = 0$. However, the price paid for this is that the nature of the longshore and cross-shore problems become fundamentally different and an approach that works for the solution of the cross-shore problem does not necessarily work in the longshore direction.

The clearest example of this comes while determining the boundary conditions for the depth variation of the currents. The depth variation of the currents is determined from (2.41) which is a second order PDE and hence two boundary conditions need to be specified. One condition is the relationship between the near bottom current and the bed shear stress. This condition is the same in both directions. The second condition is quite different in the two directions. For the undertow, as discussed earlier, the integrated continuity equation naturally provides the second condition. In the longshore direction the momentum equation provides the second condition.

Note that the depth variation of the undertow is determined by the momentum equation whereas the average value is determined from the continuity equation. We will return to this point below.

2.3.3 Depth variation of the currents

Under the simplifications provided by the long straight coast the undertow and longshore current depth variations are governed by (see equation 2.41)

Undertow

$$\frac{\partial}{\partial z}\left(\nu_{tz}\frac{\partial U}{\partial z}\right) = g\frac{\partial \bar{\xi}}{\partial x} + \frac{\partial}{\partial x}\left(\overline{u_w^2} + U^2\right) + \frac{\partial}{\partial z}\left(\overline{u_w w_w} + UW\right) - \frac{\partial}{\partial x}\left(2\nu_{tx}\frac{\partial U}{\partial x}\right) \tag{2.56}$$

Longshore current

$$\frac{\partial}{\partial z}\left(\nu_{tz}\frac{\partial V}{\partial z}\right) = \frac{\partial}{\partial x}\left(\overline{u_w v_w} + UV\right) + \frac{\partial}{\partial z}\left(\overline{v_w w_w} + VW\right) - \frac{\partial}{\partial x}\left(\nu_{tx}\frac{\partial V}{\partial x}\right) \tag{2.57}$$

In (2.56) the $\partial W/\partial x$ term has been neglected relative to equation 2.41. Assuming that the length scales of the currents in the x and z directions are given by l_x and l_z it is easy to show that $\partial W/\partial x \sim (l_x/l_z)^2 \partial U/\partial z$. Typically, for the wave induced currents, the appropriate scales are $l_z \sim h$ and $l_x \sim L$ (the wavelength). Therefore, $(l_z/l_x)^2 \ll 1$ and the neglect of the $\partial W/\partial x$ in (2.56) is justified. In the alongshore direction the corresponding term is $\partial W/\partial y$ which is zero for a long, straight coast.

As discussed previously, two conditions are required to solve equations 2.56 and 2.57 for the depth variation of the currents. In both longshore and cross-shore directions one condition is related to specifying the value of the velocity (depth-averaged value in the cross-shore direction and the near-bottom value for the longshore direction). The other condition applied is a stress condition. We could either specify a shear stress at tough level or one near the bottom. In principle, there is no difference between the two options.

Stive & Wind (1986) argue that the undertow is driven primarily by the shear stress at trough level and, hence, that is a better condition to adopt. The shear stress at the bed can then be calculated from the undertow profile. Svendsen & Hansen (1988) argued that the bottom stress calculated from this model is bound to be extremely unreliable since it is equivalent to determining the bottom stress as a difference between two large

quantities. They suggest using a condition that relates the bottom shear stress to the near-bottom velocity. We adopt the latter approach here since, typically, the bottom stress is the quantity of most practical interest and therefore, it is important to be able to estimate this quantity reasonably accurately.

Battjes (1988) suggests that the above conflict may be resolved by specifying both the shear stress at trough level as well as a bottom condition and treating the forcing for the undertow as an unknown. This suggestion has the shortcoming that it attempts to calculate the wave induced forcing below trough level using, among other things, the value of the shear stress at trough level. The estimation of the value of the shear stress at trough level requires making assumptions about the water motion above the trough level. These assumptions are necessarily cruder than the assumptions regarding the wave induced motions below trough level. Therefore, Battjes' suggestion would give an estimate of the wave induced forcing for the undertow that is less reliable than the one calculated directly from assumptions about the wave motion.

An additional problem arises with the undertow. Typically, (2.46) is solved to determine the variation of $\overline{\xi}$. This result is then substituted into (2.56) to calculate the forcing for the undertow. One constraint for the undertow comes from (2.42). The other, as discussed above, is a stress condition. It turns out that for the undertow there is a difference between the application of the shear stress at trough level and at the bottom.

The reason for this is that the momentum equation used to calculate the depth variation of the undertow is incompatible with the depth integrated momentum equation. This is because the turbulent stress terms that control the depth variation are neglected in the depth integrated equation. If these terms were retained in the depth integrated equation, as they are in the longshore direction, there is no principal difference between applying the boundary condition at trough level or at the bottom. In this case the momentum and continuity equations would have to be solved simultaneously to determine the set-up and the undertow.

The simplification offered by the decoupling of the continuity and momentum equations in the cross-shore direction leads to this inconsistency. If this decoupling is used,

clearly, one has to make a choice of the appropriate boundary condition that is to be applied.

2.4 Determination of the vertical current

It is evident from (2.56) and (2.57) that both the vertical current and its integral would be required to determine the depth variation of the currents. We proceed to determine these quantities in this section.

Consider the wave averaged continuity equation below trough level

$$\frac{\partial U}{\partial x} + \frac{\partial W}{\partial z} = 0 \tag{2.58}$$

This implies that

$$W(z) = -\int_{-h_0}^{z} \frac{\partial U}{\partial x} dz \; + \; W(-h_0) \tag{2.59}$$

The wave averaged BBC gives

$$W(-h_0) = -U_b \frac{\partial h_0}{\partial x} \tag{2.60}$$

Therefore, we get

$$W(z_r) = -\frac{\partial}{\partial x} \int_{-h_0}^{z_r} U dz \; + \; U_{z_r} \frac{\partial z_r}{\partial x} \tag{2.61}$$

where the last term is required to make the above applicable at $z = -h_0$. In order to evaluate the current profiles a depth integration of (2.61) is required. This is given by

$$\int_{-h_0}^{z} W dz = -\frac{\partial}{\partial x} \int_{-h_0}^{z} \int_{-h_0}^{z} U dz \; - \; \frac{\partial h_0}{\partial x} \int_{-h_0}^{z} U dz \tag{2.62}$$

because the last term of (2.61) does not contribute to the integral.

In addition to the vertical current and its integral found above, it is clear from (2.44), (2.46), (2.56) and (2.57) that to use the wave averaged equations to predict the mean quantities inside the surf-zone the variation of the radiation stress tensor across the surf-zone needs to be known. At the present time, there is no theory of wave motion inside the surf-zone that can give reliable estimates of the radiation stress. In the next chapter we analyze currently available measurements of the wave height and set-up in order to determine this variation.

Chapter 3

DETERMINATION OF THE FORCING FOR NEARSHORE WAVE-INDUCED CURRENTS

In this chapter we deal with the cross-shore variations of the set-up and the wave height. The emphasis is on the solution of (2.46) coupled with an energy equation. The major aim here is to determine the variation of S_{xx} accurately and use this variation to determine S_{xy} from (2.52). It is customary to use b to denote the set-up in models that predict set-up and wave height variations. We will do the same in this chapter.

3.1 Summary of previous work on set-up and wave height variations

Over the last two decades, numerous models have been proposed for the variations of the set-up and wave height across the surf-zone. These models invariably work with wave averaged equations and require that a description of the radiation stresses be available in terms of the wave height, wave period and the water depth.

Munk (1949) suggested that in the surf-zone the wave height is approximately proportional to the local water depth. This has become a very common assumption in surf-zone models. Le Mehaute (1962) first proposed that the wave averaged energy equation be used to determine the wave height decay across the surf-zone. He suggested that the energy dissipation rate in breaking waves be modelled by the dissipation rate in a bore of the same height. Horikawa & Kuo (1966) and Divoky *et al.* (1970) used this approach to calculate the wave height decay. The assumption that the energy dissipation in breaking waves is the same as that in a bore has become a frequently used assumption in models that solve the energy equation to determine the wave height variations.

Longuet-Higgins & Stewart (1962) applied the concept of the radiation stress and predicted a depression of the mean water surface (set-down) seaward of the break point

and an elevation of the same inside the surf-zone. In 1963 the same authors confirmed their predictions (quantitative for the set-down and qualitative for the set-up) by comparing the predictions with experimental data available at that time.

The first prediction of set-up variation across the surf-zone was due to Bowen *et al.* (1968). They also conducted experiments to examine the the accuracy of their predictions. They calculated the set-down outside the breaker zone using the lowest order estimate of the radiation stress and assuming energy conservation. Inside the surf-zone, they assumed that the wave height was a constant fraction of the depth and showed that the slope of the mean water surface is proportional to the bottom slope.

Their experimental results showed that the calculated set-down severely overpredicted the value near the break point. They also found that the mean water surface remained approximately horizontal for some distance shoreward of the break point and shoreward of this point the slope of the mean water surface agreed with their theoretical result surprisingly well. As they remark it is surprising that their experimental results agreed so closely with the predictions because there is no reason why the linear long wave approximation for the radiation stress should be valid.

Hwang & Divoky (1970) were the first to solve the energy and momentum equations simultaneously to determine the set-up and wave height. They used a bore dissipation model.

Dally *et al.* (1985) assumed that at any given depth there exists a "stable energy flux" and that the rate of energy dissipation was proportional to the energy flux in excess of this stable value. Using this model they calculated variations of set-up and wave height across the surf-zone. Their results indicated that the while prediction of the wave height variation was reasonable, the prediction of the mean water surface variation was poor.

Most of the above models that dealt with set-up variations used linear theory to calculate the wave averaged quantities like the radiation stresses and energy fluxes. The use of linear theory by early investigators simplified their analyses significantly and allowed them to demonstrate the mechanisms responsible for various phenomena in the surf-zone in an elegant manner. However, as mentioned above, already Bowen *et al.* (1968) expressed

concern that linear theory cannot be expected to give quantitatively correct results for the wave averaged quantities. A number of numerical models are currently available that use linear theory estimates of the various wave averaged quantities and contain empirical constants whose values are adjusted by comparison with measurements. Such models run the risk of compensating for the error in the wave qunatities by incorrectly modelling other terms. Unfortunately, at the present time, there is no wave theory that describes the wave motion inside the surf-zone to the extent that the integrated quantities can be calculated with confidence.

A step away from linear theory was made by James (1974a) who used a wave theory that is a combination of an approximation to cnoidal theory ("hyperbolic" wave theory) in the nearshore region and Stokes' wave theory further seawards to calculate the radiation stresses and predict set-up and set-down variations. His calculations showed better agreement with the measured values of the set-down outside the surf-zone in comparison with those of Bowen *et al.* indicating, not surprisingly, that the inaccuracies outside the breaker zone are directly related to the nonlinearity of the waves. Inside the surf-zone he found that the slope of the mean water level was somewhat smaller than that predicted by Bowen *et al.*

The first contribution to acknowledge the different nature of waves in the surf-zone was Svendsen (1984a) who included the "roller" contribution to the radiation stress and energy flux and found that this contribution greatly enhanced the wave averaged quantities. Svendsen assumed that the roller which is a mass of water that is carried shoreward by the wave moves with a speed that equals the celerity of the wave. Using this he estimated that

$$\int_{roller} \rho u^3 \approx \frac{\rho g H^2 c}{2} B_r \tag{3.1}$$

and

$$\int_{roller} \rho u^2 \approx \rho g H^2 B_r \tag{3.2}$$

where

$$B_r = \frac{Ah}{H^2 L} \tag{3.3}$$

in which A represents the area of the roller. He used the measurements of the roller area by Duncan (1981) to come up with estimates for the roller contribution to the radiation stress and the energy flux. Calculating both set-up and wave height variations he also utilized a simple version of the bore dissipation model for periodic waves developed by Svendsen *et al.* (1978) for modelling the energy dissipation in breaking waves.

The analysis of experimental data in the spirit of the present work was first carried out by Svendsen *et al.* (1978) who analyzed their measurements of wave height variations across the surf-zone and calculated the dissipation rate based on these measurements. They concluded that the dissipation rate in breaking waves is higher than in a bore of the same height. Using the general bore model of Svendsen *et al.* Svendsen & Madsen (1981) showed that the presence of turbulent fluctuations and the curvature of the streamlines increases the dissipation rate in a bore and suggested that this may be one reason why the dissipation in a breaking wave is higher than the traditional bore estimate. Stive (1984) analyzed the measurements of Stive & Wind (1982) to determine the variations of radiation stress and dissipation across the surf-zone. He found that near breaking linear long wave theory severely over predicted the radiation stress. His results for the dissipation rate also showed that the momentum flux due to the turbulence must be included in the general bore model to predict the actual dissipation in broken waves.

Stive & Wind (1982), Hansen & Svendsen (1984), Okayasu *et al.* (1986, 1988) and Okayasu (1989) measured, among other quantities, the variations of wave height and set up across the surf-zone. All these experiments were conducted using regular, monochromatic waves. Hansen (1990, 1991) analyzed these measurements and suggested empirical variations for a number of quantities of interest inside the surf-zone (like, *e.g.*, $B_0 = \overline{(\eta/H)^2}$).

3.2 Motivation for the present work

The analysis of existing measurements presented below was originally motivated by the necessity of determining the forcing for longshore currents. The longshore current is forced by spatial gradients of the longshore component of the radiation stress. It is evident from the discussions above that there is no satisfactory way of calculating this quantity for

surf-zone waves at the present time. To properly determine the forcing for the longshore current it is necessary to be able to predict the radiation stress in the direction of wave propagation. This is the topic addressed below.

3.2.1 Background

As shown in the previous chapter, S_{xx} and S_{xy} are closely related. On a long, straight beach the cross-shore component of the radiation stress balances the set-up. Therefore, if the set-up and the wave height are well predicted by a surf-zone model, we may have some confidence in the longshore component of the radiation stress being predicted by that model. Conversely, models that give poor predictions of the set-up and wave height almost certainly would give extremely unreliable estimates of the longshore current forcing.

All of the comprehensive surf-zone models (*e.g.,* Svendsen 1984a, Dally *et al.* 1985) solve the wave averaged equations momentum and energy equations to predict variations of set-up and wave height. The equations usually solved are

$$\frac{dS_{xx}}{dx} = -\rho g h \frac{db}{dx} \tag{3.4}$$

$$\frac{dE_f}{dx} = \mathtt{D} \tag{3.5}$$

Here E_f is the energy flux and $\mathtt{D}(< 0)$ is the energy dissipation rate. The bottom friction term has been neglected in (3.4) [see (2.46)]. Calculating the two terms of (3.4) on the basis of measurements of the velocity field, Stive & Wind (1982) found that these terms balanced one another to within experimental accuracy and hence concluded that the frictional contribution to the momentum balance was smaller than the uncertainty of their measurements. An analysis by Svendsen & Hansen (1988) shows that the friction term is of the order 5% of the terms retained. This suggests that (3.4) is a reasonable approximation, at least for the present purposes.

3.2.2 Predictions of currently available surf-zone models

Figure 3.1 presents the predictions of three different models for two experiments (Visser, experiment 1 and Stive & Wind experiment 1). Details of these experiments are

given later on. The predictions in this figure are based on

1. The model of Svendsen (1984a) (marked "Svendsen").

2. Two versions of the model suggested by Dally *et al.* (1985) (marked "Dally *et al.*" and "Dally *et al.* 1"). In the second version the wave set-up is artificially made to start at the point where the measurements begin to show a slope of the mean water surface.

3. A model that uses the B_0 variation suggested by Hansen (1990) and the roller area suggested by Okayasu (1989) to calculate the radiation stress and energy flux and uses a bore dissipation model (marked "Present").

It is clear from this figure that none of the above models accurately predict both the set-up and wave height variations. For example, the model of Dally *et al.* predicts the wave height fairly well but does not predict the set-up very well. This clearly indicates that the radiation stress used is quite inaccurate. A similar statement can be made when the set-up is well predicted but the wave height is not (for example, the predictions due to Svendsen's model).

The implication of the above is that none of these models would give accurate estimates of the longshore component of the radiation stress.

In this chapter we analyze currently available experimental measurements of the variations of set-up and wave height across the surf-zone to determine the variation of the cross-shore component of the radiation stress across the surf-zone. In addition, we also estimate the variations of the rate of energy dissipation and longshore component of the radiation stress based on these measurements. The analysis makes use of some of the empirical variations suggested by Hansen (1990).

The following dimensionless quantities are used in this chapter

$$P = \frac{S_{xx}}{\rho g H^2} \tag{3.6}$$

$$D = \mathtt{D}\frac{4hL}{\rho g H^3 c} \tag{3.7}$$

$$B = \frac{E_f}{\rho g H^2 c} \tag{3.8}$$

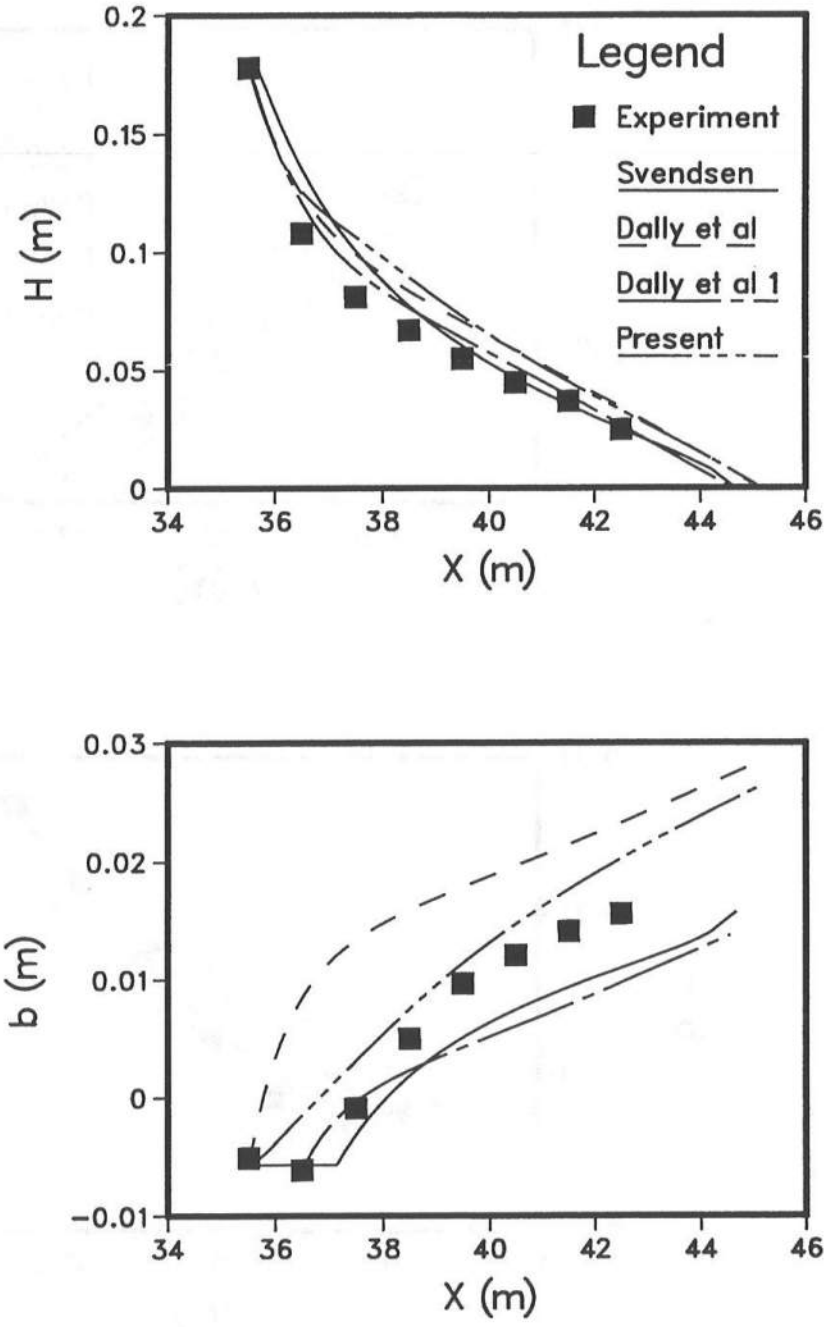

Figure 3.1: Predictions of wave height and set-up using existing models

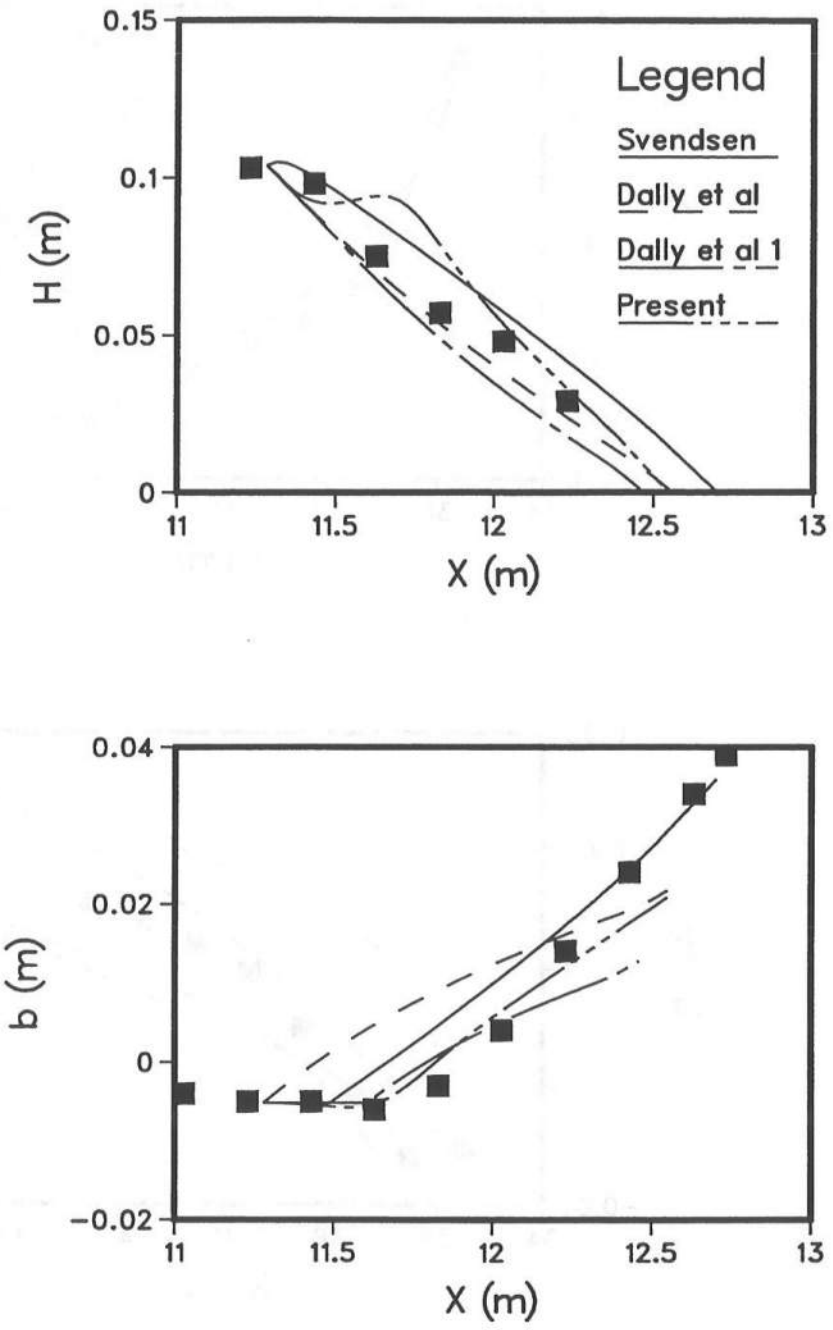

Figure 3.1: Continued

$$B_0 = \left(\frac{\overline{\eta^2}}{H^2}\right) \tag{3.9}$$

where c is the wave celerity, η is the instantaneous free surface elevation above the mean water surface, L is the local wavelength defined by $L = cT$ and P, B and D represent respectively the dimensionless radiation stress, energy flux and dissipation rate.

The results to be presented in this chapter follow directly from the measurements and do not presuppose the validity of any particular wave theory. The results for P, in particular, are quite general and have the effect of the roller as well as the effects of nonuniform pressure and velocity distributions. The roller effect though will formally be eliminated in equation 3.18 (which will be used to calculate B) is still reflected in B (and therefore in D) though the additional assumptions required to calculate B introduce some uncertainty into these results. The effect of these assumptions is also assessed in this chapter.

We emphasize here that this chapter is only aimed at analyzing the available experimental data to determine the variations of the dimensionless quantities and show that these quantities deviate significantly from the values usually used. We make no effort to provide empirical variations of the quantities for general use because we believe that the available data are too limited to provide accurate empirical variations. The analysis and results presented should help in planning future experiments aimed at providing accurate variations for the dimensionless quantities.

3.3 Determination of the radiation stress and the rate of energy dissipation

3.3.1 Determination of P

To determine the variation of the radiation stress across the surf zone we integrate (3.4) from a reference location x_r to a point x. This leads to

$$S_{xx}(x) = \int_x^{x_r} \rho g h \frac{db}{dx} dx \; + \; S_{xx}(x_r) \tag{3.10}$$

which after substituting (3.6) leads to

$$P = \frac{1}{H^2} \int_x^{x_r} h \frac{db}{dx} dx \; + \; P(x_r) \frac{H^2(x_r)}{H^2(x)} \tag{3.11}$$

It is clear from the above that to determine S_{xx} a boundary value is needed. In principle, any reference value could be chosen. This could, for example, be a place far seaward of breaking where a highly nonlinear wave theory (like that of Cokelet 1977) could be expected to give a fairly accurate estimate of S_{xx}. However, this choice has the drawback that if we wish to calculate P then (3.11) shows that any inaccuracy in the boundary value at a point where H is large will lead to extremely large inaccuracies near the shoreline where $H \to 0$. For the experiments we will be analyzing here this problem is avoided by using the shoreline (of the mean water level) as the reference point. For this case the boundary condition becomes $S_{xx}(x_r) = 0$ and hence the boundary term in (3.11) drops out. The value of P at the shoreline is then determined as a limit of the values near the boundary. This is discussed further in the following.

We see from (3.10) and (3.11) that the dimensionless radiation stress may be determined by using just experimentally measured values of b and H with no further approximations.

In principle, the radiation stress could also be calculated directly from the definition (2.26) if measurements of the vertical structure of the wave induced velocities and pressures are available. However, measurement of velocities under breaking waves, particularly above trough level, is extremely difficult (Stive & Wind 1982). This is significant because the higher velocities occur in this region and the region is a significant fraction of the total depth. This leads to a large uncertainty in the calculated result. Therefore, the present method of estimating the radiation stress, if carefully pursued, is considered the most accurate method of estimating the radiation stress that is possible at the present time.

3.3.2 Determination of B

The determination of the dimensionless energy flux, B, is required for the determination of D. Whereas P can essentially be determined using just measured quantities the determination of B from P requires some assumptions. These are discussed below.

If the vertical velocity is neglected the energy flux is given by

$$E_f \approx \int_{-h_0}^{b+\eta-roller} pu dz + \int_{roller} \rho u^3 dz \tag{3.12}$$

In the above "roller" refers to the region of recirculating water along the turbulent front.

As a generalization of the linear theory for arbitrary wave profiles and nonuniform velocities we assume that

$$u = c\frac{\eta}{h} f_u(z) \tag{3.13}$$

$$p = c\frac{\eta}{h} f_p(z) \tag{3.14}$$

We assume further that $f_u(z) = f_p(z)$.[4] Under this approximation the dimensionless energy flux is given by

$$B = B_0 \alpha_u + \frac{Ah}{2H^2 L} \tag{3.15}$$

where A is the area of the roller, and

$$\alpha_u = \frac{\overline{\int_{-h_0}^{b+\eta} u_w^2 dz}}{c^2 \overline{\frac{\eta^2}{h^2}} h} \tag{3.16}$$

In (3.15) we have used the approximation derived by Svendsen (1984a) for the roller contribution (see equations 3.1 and 3.2). A similar estimation of the dimensionless radiation stress yields

$$P = \left(\alpha_u + \frac{1}{2}\right) B_0 + \frac{Ah}{H^2 L} \tag{3.17}$$

(3.15) and (3.17) yield

$$B = \frac{P}{2} + B_0 \left(\frac{\alpha_u}{2} - \frac{1}{4}\right) \tag{3.18}$$

For the experiments analyzed here (with the exception of Visser's) the variation of the parameter B_0 has been determined on the basis of measurements of the free surface fluctuations by Hansen (1990). In our analysis we use the empirical variation suggested by Hansen. The reason for doing this that these variations show extremely good agreement with the actual variations and the differentiations become straightforward. In addition to this we need the value of α_u in order to evaluate B from P. Since B_0 is essentially a

[4] Linear wave theory has $f_p = \cosh k(h_0 + z)/\cosh kh$ and $f_u = f_p kh/\tanh kh$. For relatively long waves these variations show that $f_p \approx f_u$. Hence, although the waves are not linear, it indicates that this approximation may be reasonable.

measured quantity and since P follows directly from the measurements it is clear that the major source of inaccuracy for B is in the determination of α_u. From (3.18) it is clear that an error in the estimation of of α_u produces a smaller relative error in the value of B. Therefore, while the value of B calculated using (3.18) will be influenced by errors in α_u the errors introduced in B this way are smaller than the errors in α_u.

3.3.3 Calculation of the rate of energy dissipation

A rearrangement of the energy equation (3.5) after the substitution of (3.8) yields

$$D' = \frac{dH^2}{dx} + \left(\frac{c_x}{c} + \frac{B_x}{B}\right) H^2 \tag{3.19}$$

In the above

$$D' = \frac{\mathtt{D}}{\rho g c B} \tag{3.20}$$

If we assume that $c = \sqrt{gh}$ (3.19) becomes

$$D' = \frac{dH^2}{dx} + \left(\frac{h_x}{2h} + \frac{B_x}{B}\right) H^2 \tag{3.21}$$

In the above equation the LHS is a measure of the dissipation, the first term on the RHS is the total wave height variation and the terms in the parenthesis above contain the shoaling terms. Our results show that the first term is the dominant term of the RHS. Of the other two terms on the RHS, the first dominates near the shoreline, and the second, near breaking.

Equation 3.21 is used to determine the rate of energy dissipation. It is evident that in order to use (3.21) we need to estimate B and B_x. Furthermore, based on the magnitude of the terms above we expect that inaccuracies in B will have a relatively minor influence on the value of D' but D and $\mathtt{D}$ are directly influenced by the the value of B.

In a later section we will be comparing the results for the rate of energy dissipation to that in a bore to examine the validity of the bore model for this quantity. The nondimensional dissipation rate in a bore is given by

$$D_{bore} = \frac{h^2}{d_t d_c} \tag{3.22}$$

where d_t and d_c are the depths below the crest and trough respectively.

3.4 Analysis of experimental data

The data used to determine the variations of P and D come from the following experiments on plane slopes. Among other quantities, these experiments measured set-up and wave height variations across the surf-zone.[5]

1. Stive & Wind (1982) 1/40, two cases.
2. Hansen & Svendsen (1984) 1/35 one case.
3. Okayasu *et al.* (1986, 1988) 1/30 five cases and four 1/20 cases.
4. Visser (1982) 1/20 two cases and three 1/10 cases.

Visser actually reports seven cases. Of these, experiment 7 is a repetition of experiment 4 with a different bottom roughness. For the higher roughness (experiment 7) Visser did not measure the mean water level variations. He assumed that they were the same as those in experiment 4. To ensure a steady wave climate, his experiment 6 had to be conducted using much smaller wave heights than the other experiments thus resulting in much smaller set-up. Since Visser reports only the mean depth [accurate only to 0.1 cm (see also table 5.1)] from which the set-up has to be calculated this experiment has the highest uncertainty as far as the set-up variation is concerned. In fact, the set-up calculated from the reported depth for experiment 6 shows no consistent variation. Hence, experiments 6 and 7 are discarded here.

The relevant parameters for these experiments are shown in table 3.1. The parameters shown in the table are the deep water steepness, H_0/L_0, deep water surf-similarity parameter $\xi_0 = h_x/\sqrt{H_0/L_0}$ (Battjes 1974), ratio of wave height to water depth at breaking $\gamma_b = H_b/h_b$ and the parameter $S_b = h_x L_b/h$ (Svendsen & Hansen 1976).[6]

The determination of the dimensionless radiation stress and dissipation rates require the differentiation of b and H. In all these experiments measurements were taken

---

[5] The authors gratefully acknowledge the receipt of detailed original data from A. Okayasu and M. J. F. Stive. Additionally, we had access to the original data of the Hansen & Svendsen. Unfortunately, such detailed data was not available for Visser's experiments.

[6] Cnoidal theory was used to calculate L_b.

Table 3.1: Relevant parameters for the experiments analyzed

Source	Symbol	Slope	T (s)	H_0/L_0	γ_b	S_b	ξ_0	Breaker Type
Stive & Wind	S & W 1	1/40	1.79	0.032	0.86	0.36	0.140	Spilling
Stive & Wind	S & W 2	1/40	3.00	0.010	0.81	0.57	0.250	Plunging
Hansen & Svendsen	ISVA	1/35	2.00	0.020	0.85	0.47	0.204	Spilling
Okayasu *et al.*	OKS3C1	1/30	1.61	0.023	0.88	0.54	0.249	Plunging
Okayasu *et al.*	OKS3C2	1/30	1.97	0.010	0.96	0.82	0.327	Spilling
Okayasu *et al.*	OKS3C3	1/30	1.96	0.014	0.90	0.68	0.282	Spilling
Okayasu *et al.*	OKS3C4	1/30	1.12	0.046	0.86	0.39	0.156	Spilling
Okayasu *et al.*	OKS3C5	1/30	1.23	0.028	0.78	0.49	0.200	Spilling
Okayasu *et al.*	OKS2C1	1/20	2.00	0.014	1.07	1.04	0.424	Plunging
Okayasu *et al.*	OKS2C2	1/20	2.00	0.009	1.00	1.23	0.521	Plunging
Okayasu *et al.*	OKS2C3	1/20	1.17	0.050	0.87	0.55	0.223	Spilling
Okayasu *et al.*	OKS2C4	1/20	0.91	0.054	0.77	0.49	0.215	Spilling
Visser	Exp. 4	1/20	1.02	0.052	0.83	0.93	0.220	Plunging
Visser	Exp. 5	1/20	1.85	0.014	0.93	1.04	0.420	Plunging
Visser	Exp. 1	1/10	2.01	0.016	1.00	2.43	0.810	Plunging
Visser	Exp. 2	1/10	1.00	0.065	0.91	1.04	0.390	Plunging
Visser	Exp. 3	1/10	1.00	0.062	0.85	1.01	0.410	Plunging

at limited number of locations. Based on these data points a smooth curve was drawn by hand which was then represented by a spline approximation. The differentiations and integrations of the spline approximation are straightforward.

Figure 3.2 shows the original measurements along with the variations adopted for experiment S2C3 of Okayasu *et al.* Corresponding figures for the other experiments analyzed here are presented in Appendix A. The distance between the data points and the curves show the approximations introduced.

In all the cases there are very few measured points near the shoreline and hence the variations used near the shoreline are based on extrapolations of the variations away from the shoreline. The rationale used in these extrapolations is the following: For the set-up we assume that the slope of the mean water surface near the shoreline is constant.

On extremely steep slopes the mean water level steepens considerably near the shoreline. This is related to water level fluctuations in the swash zone. On mild slopes the swash oscillations are smaller leading to no significant steepening of the mean water surface. For example, Kobayashi *et al.* (1989) calculated the set-up for Stive & Wind's (1982) Experiment 1 by time averaging the results of a time dependent nonlinear shallow water model. Their results for the mean water surface show no steepening near the shoreline. The experiments analyzed here were, for the most part, conducted on relatively mild slopes (1/20 or milder), therefore, we expect no significant steepening of the mean water surface near the shoreline. Also, as pointed out before, there is very little data near the shoreline and using an extrapolation different from the one used here does not seem to be justified especially considering the limited amount of data available.

For extrapolation of the wave height near the shoreline we used a slightly different approach. Originally, the extrapolations were based on a natural continuation of the wave height variation away from the shoreline. The resulting wave height to water depth ratio was compared with the value of the same ratio determined from the measurements. In cases where the measured wave height to water depth ratio showed a smooth variation the wave heights near the shoreline were replaced by values derived from an extrapolation of the H/h values. The reason for doing this is that we expect this ratio to vary in a relatively

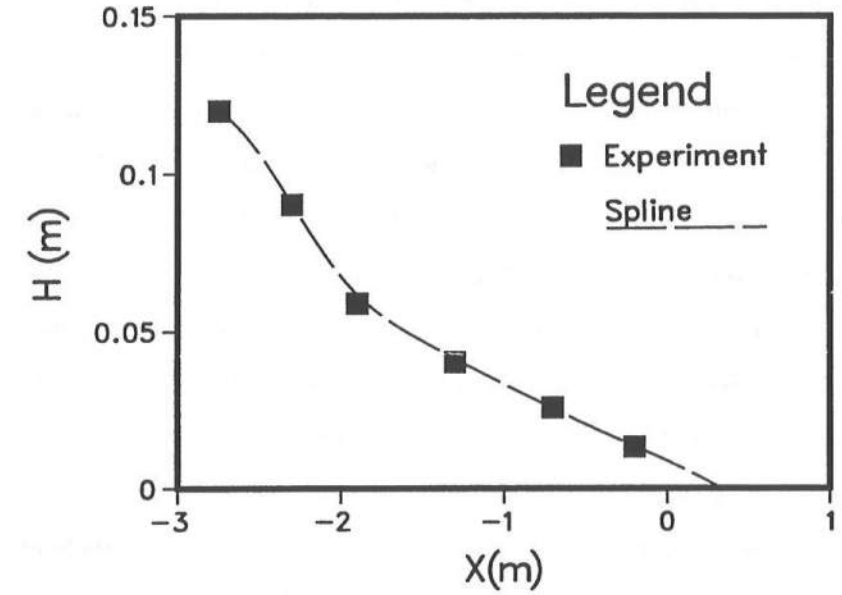

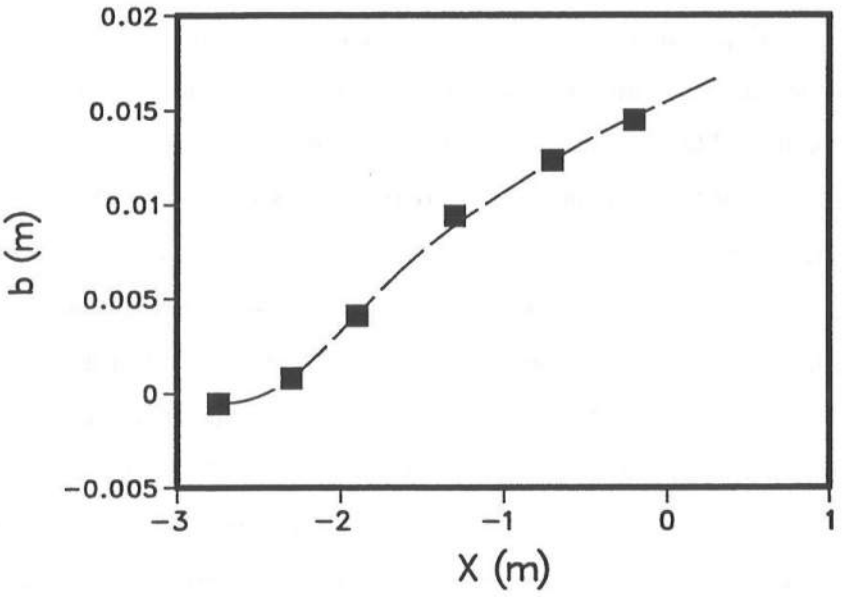

Figure 3.2: Experimental data and variations used

smooth manner. (In fact, many surf-zone models assume a constant value for this ratio.) A comparison of the "measured" H/h value and the variation used for experiment S2C3 of Okayasu *et al.* is shown in figure 3.3. As before, the corresponding figures for the other experiments are shown in appendix A. We see that in almost all the experiments the variation of this ratio is smooth (some of Visser's experiments are the only ones for which this is not true). Furthermore, in a number of the experiments this ratio is increasing towards the shoreline. This trend for the wave height to water depth ratio was first found by Horikawa & Kuo (1966) and a similar result is implied by the experimental results of Bowen *et al.* (1968).

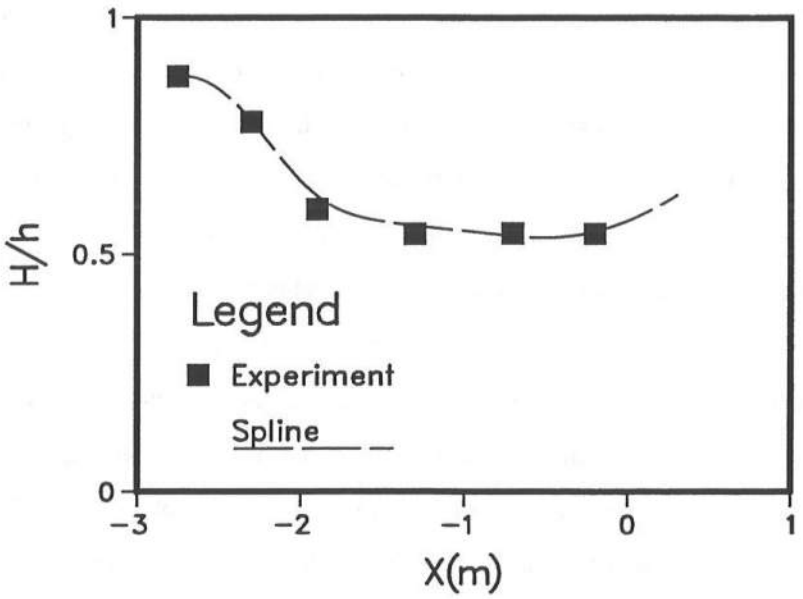

Figure 3.3: "Measured" variations of H/h and extrapolated values of Okayasu S2C3

We note that since H/h is a quantity that is calculated from independent measurements of set-up and wave height there is the possibility that errors in the two measurements add up while calculating this quantity. However, smooth variations of this quantity suggest that this is not the case.

3.4.1 Results for P

Figures 3.4 show the results for the variation of the nondimensional radiation stress for different values of the bottom slope parameter S_b. These figures show that P varies systematically across the surf-zone with S_b. In all cases the value of P at breaking is significantly smaller than that predicted by linear long wave theory ($P = 3/16$). The small value of P at breaking is consistent with results found by Cokelet (1977) for very steep symmetric waves propagating on a horizontal bottom. This result was also discussed by Svendsen (1984a). It represents the fact that the very steep waves are very peaky and have very little "substance" when compared with a linear wave of the same height.

Shoreward of the break point P increases sharply from the small value at breaking indicating a rather strong change in shape of the wave. This increase indicates a "filling" up of the wave or making it less "peaky" from the condition at breaking. In this region the set-up is nearly constant while the wave height is decreasing and thus P has to increase to keep the radiation stress constant. The variation of P in the inner surf-zone is much milder than the variations just shoreward of breaking thereby indicating that the changes in the wave shape are relatively small in this region.

The results from the experimental data by Visser differ somewhat from the rest of the data analyzed. Visser's experiments have rather large values of S_b (almost all of them have $S_b > 1$) and the values of P for Visser's experiments are significantly higher than those encountered in other experiments. A comparison of the variations of P for Visser's experiments 2 and 3 indicate that these two are not very similar though the experimental conditions are very similar (same period and slope, comparable deep water steepnesses, S_b's and γ_b's). The major difference in the two experimental conditions is the angle of incidence of the waves (24 and 12 degrees at breaking respectively). If the waves were equal, however, this difference should only lead to approximately 10% difference in the results for these two experiments near the break point and the difference would be expected to decrease significantly shoreward of this location. The actual results indicate an opposite trend (see figure 3.4e). The reason for this difference is not clear.

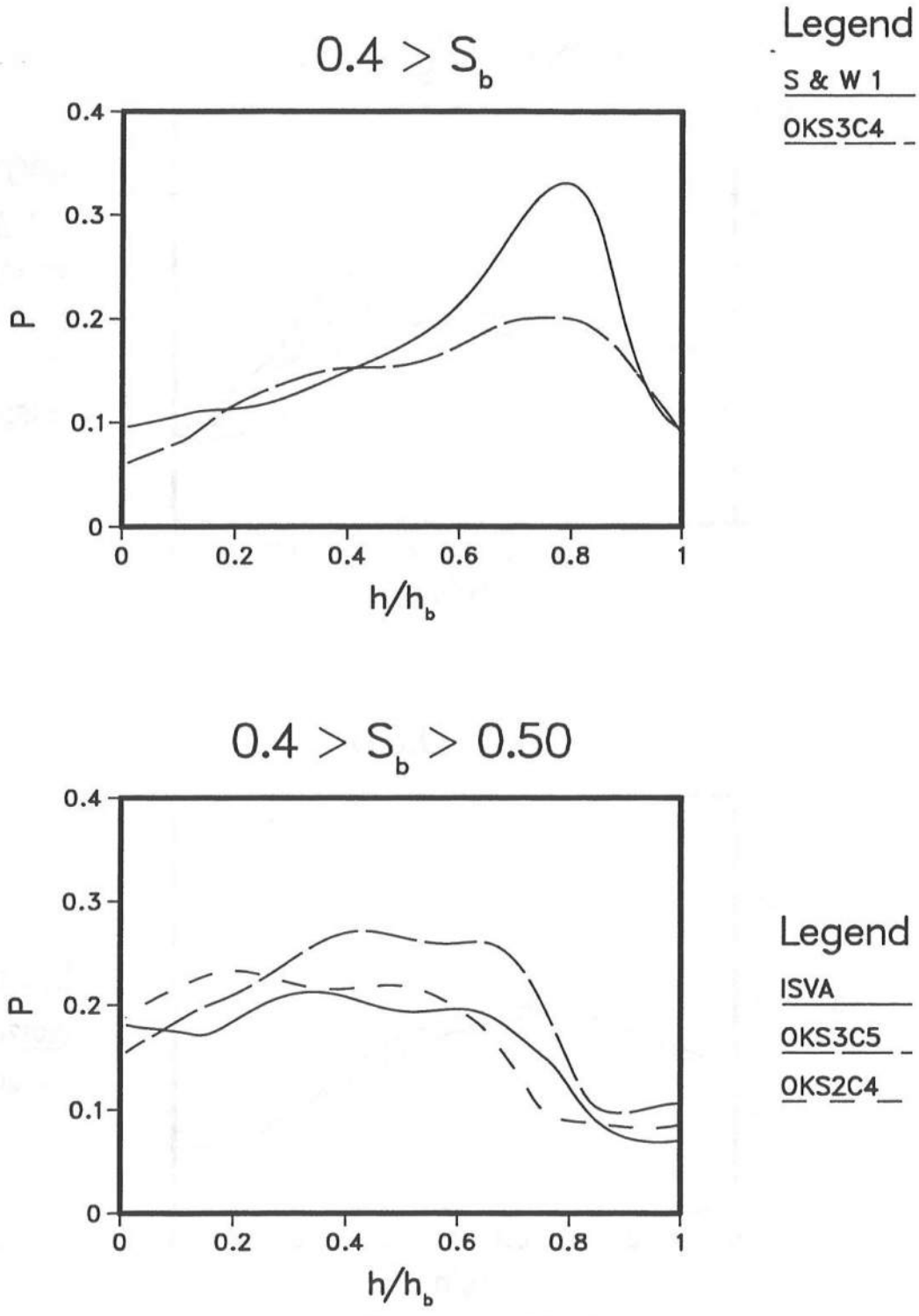

Figure 3.4: Variations of P for the experiments

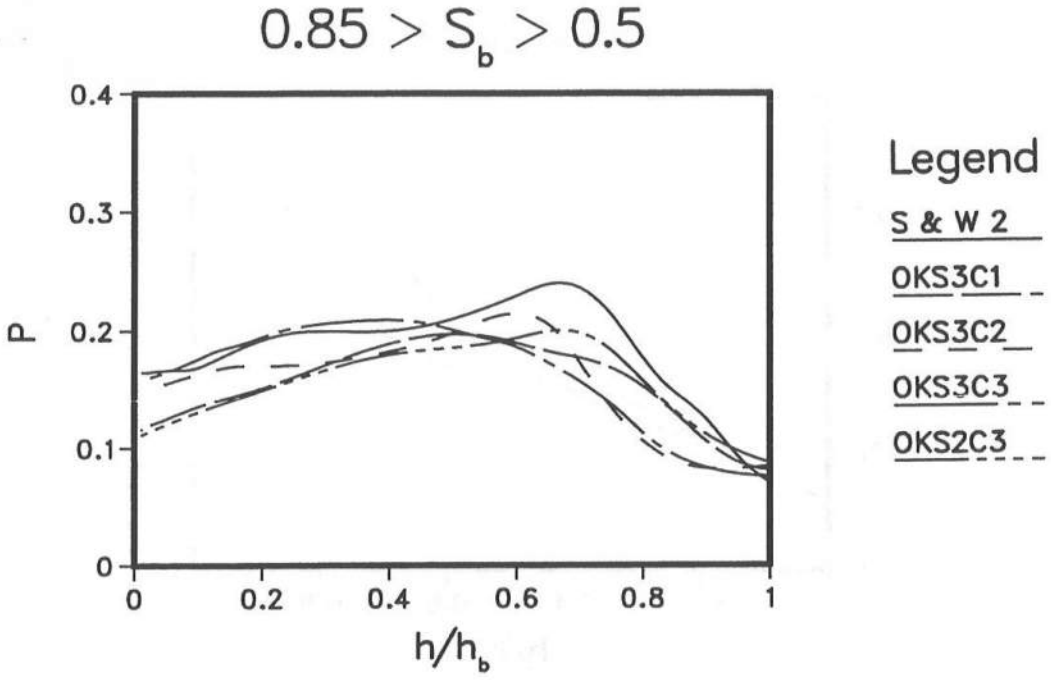

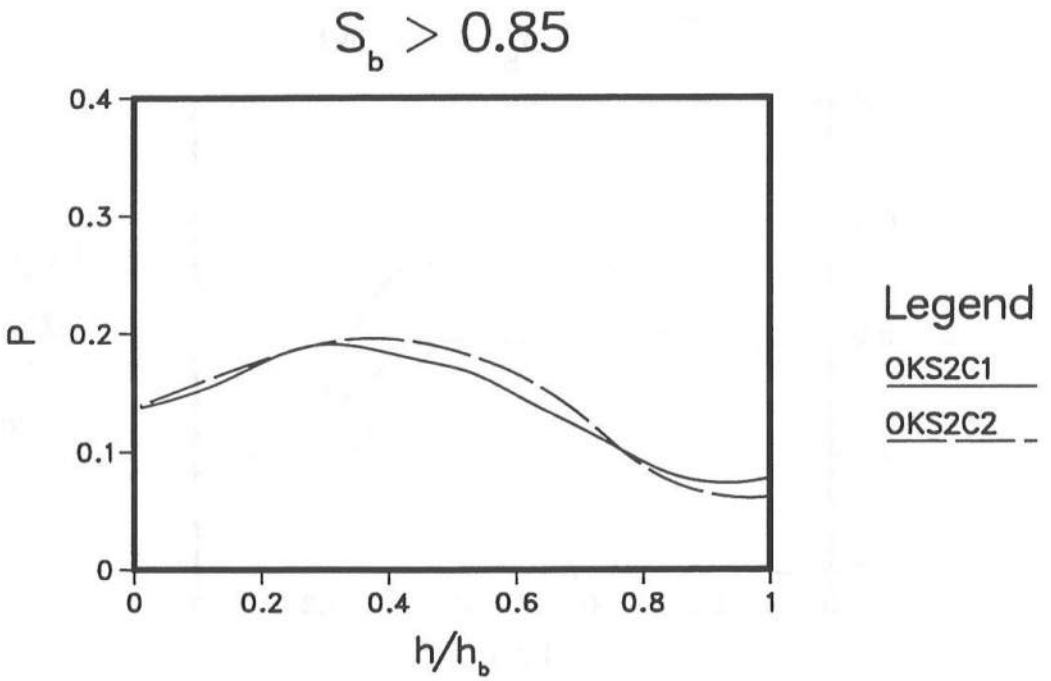

Figure 3.4: Continued

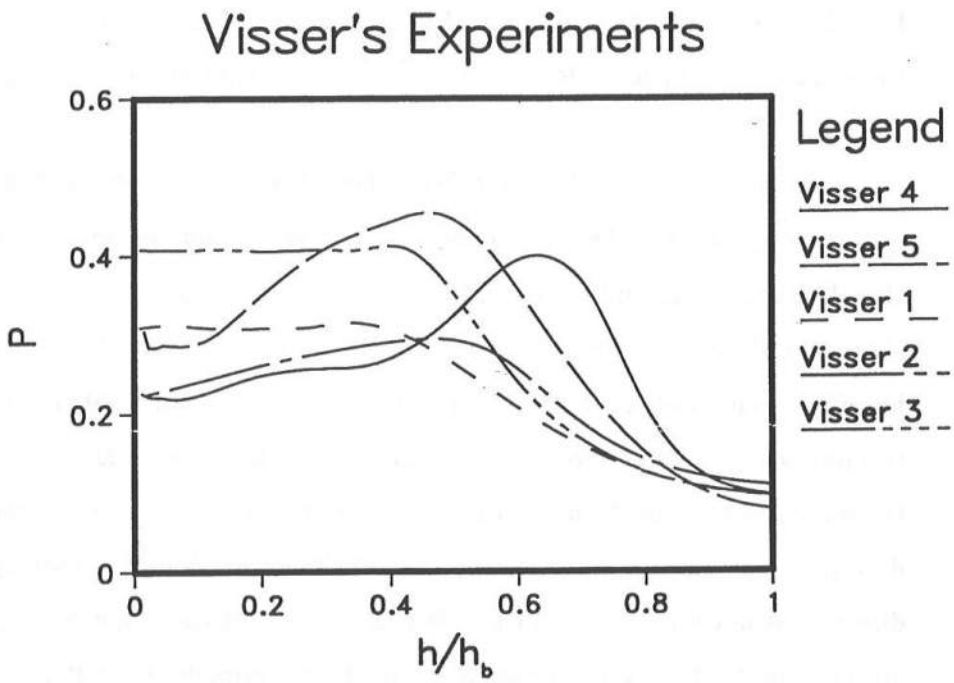

Figure 3.4: Continued

It is not completely clear if the wave averaged approach which presupposes quasi-uniform waves is applicable for the large S_b values found in Visser's experiments. Battjes (1988) suggests that the the quasi-uniform wave approximation requires that the width of the surf-zone be greater than the wavelength at breaking. However, the high P values cannot be attributed to this because except for Experiment 1 all other Visser experiments have S_b values that are comparable to the experiments with the higher S_b from other sources.

It is possible from (2.49) that a very strong undertow could significantly increase the radiation stress. The extremely steep slope of the mean water surface would certainly set up a reasonably strong undertow. It is tempting to forward this as a possible explanation for the large values of the radiation stresses encountered in Visser's experiments. However, before this explanation can be accepted, the following question needs to be answered: Why do Visser's experiments have such high slopes on the mean water surface (which, in turn, presumably, induce rather strong undertows) when other experiments with comparable

breaking conditions (for example, Visser exp. 5 and Okayasu S2C1 have similar conditions) induce a much milder slopes on the mean water surface (and, presumably, weaker undertows)?

Visser's experiments differ from the other experiments analyzed here in one important respect. All the other experiments were conducted in narrow wave flumes and therefore the set-up and wave height do not have any significant dependence on the alongshore co-ordinate. Visser's principal aim was to measure longshore currents and therefore his experiments were conducted in a wide wave tank (width $\sim$ 20 m). Though he took care to minimize alongshore nonuniformity, he found that there was about $\pm 10\%$ variation in the wave height from the mean value in the alongshore direction (see section 5.8 for a brief description of Visser's experimental layout). The variation of the set-up in the alongshore direction is not reported by Visser. It is possible that the alongshore nonuniformity plays an important role in the interpretation of the experimental results.

Note that the relative length of the transition zone seems to be well correlated with the parameter S_b. This is a consequence of the fact that S represents a change in depth encountered by the wave while it traverses one wavelength. This quantity therefore represents the way in which the wave "feels" the bottom. Small values of this quantity indicate that the wave is propagating on an essentially flat bottom and, therefore, the wave can adjust to the local conditions as it propagates. Recently, a number of different empirical formulas have been suggested for the width of the transition zone. While comparing the different expressions it is important to realize that there is no accepted quantitative definition of the transition point. Svendsen *et al.* (1978) and Okayasu (1989) define this point based on visual observations of the broken waves. Svendsen (1984a) and Nairn *et al.* (1990) define the transition point as the point where the set-up begins. Visser (1984) assumes that the transition takes place at the plunge point. Since, in general, these definitions do not coincide the width of the transition zone as predicted by the various empirical formulas will be quite different.

3.4.2 Results for B

As mentioned earlier, the deduction of B from P requires that additional assumptions be made. Specifically, we need to estimate either the momentum correction factor α_u or the area of the roller A. We have chosen here to estimate the momentum correction factor α_u. To estimate this coefficient we need to know the distribution of the wave induced velocity. Hansen (1990) determined this quantity below trough level. Above trough we assume that the wave induced velocity increases linearly to equal a fraction of the wave celerity at crest level. (The assumed variation of the wave induced velocity is shown in figure 3.5.) The assumed velocity profile is described by

$$u_w = \begin{cases} \beta c \frac{\eta}{h} & z + b \leq \eta_t \\ \beta c \frac{\eta}{h} + \frac{c}{H}\left[K - \beta c \frac{\eta}{h}\right](z - \eta_t) & z + b > \eta_t \end{cases} \tag{3.23}$$

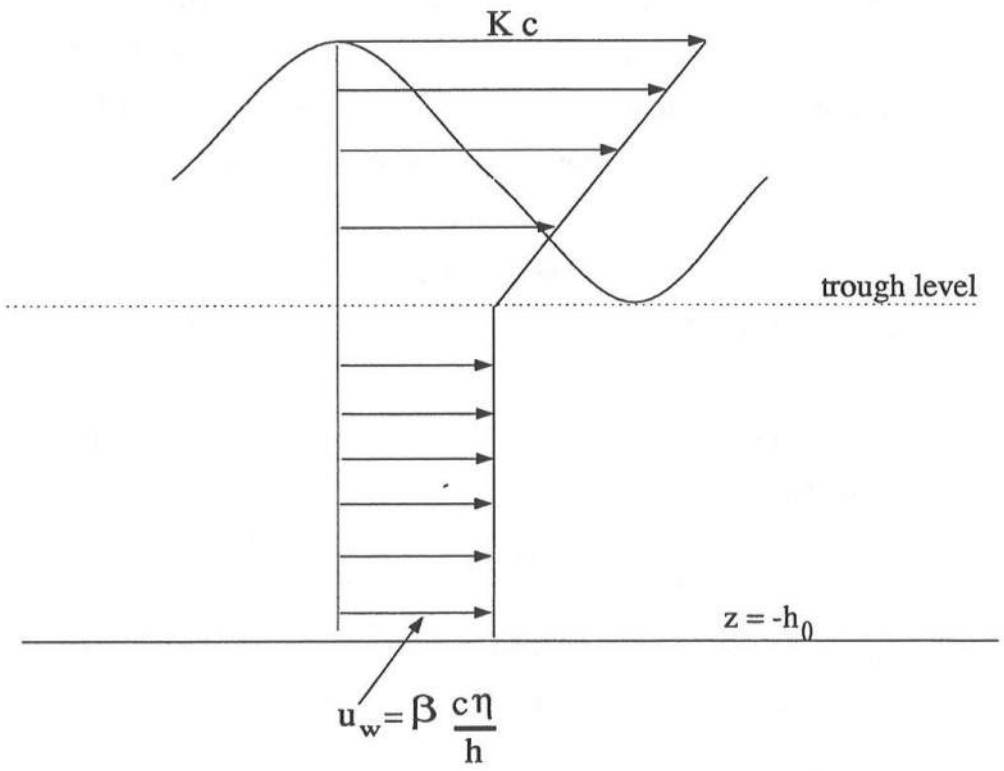

Figure 3.5: Assumed variation of the wave induced horizontal velocity

Extrapolations similar to the above were made by Stive & Wind (1982). Equation 3.23 indicates, after some fairly straightforward algebra, that

$$\overline{\int_{-h_0}^{\eta+b} u_w^2 dz} = Hc^2 B_0 \left\{ \left(\frac{\beta H}{h}\right)^2 h_t - \frac{\eta_t}{H}\left[\left(K - \beta\frac{\eta_c}{h}\right) + \beta\frac{H}{h}\right]^2 - \left(\frac{\eta_t}{H}\right)^3 \frac{\left(K - \beta\frac{\eta_c}{h}\right)^2}{3B_0} \right\} \tag{3.24}$$

where $h_t = h + \eta_t$ is the depth below trough. The correction coefficient may be calculated by substituting (3.24) into (3.16). Figure 3.6 shows the variation of α_u with K for a number of H/h values. These curves suggest that α_u is typically in the range $0.85 < \alpha_u < 1.3$. The variations plotted in this figure use $\beta = 0.7$, $B_0 = 0.1$ and $\eta_t/H = -0.4$. These values were chosen based on the variations suggested by Hansen (1990). Physically, we expect the velocity at the crest to be close to the wave celerity and the H/h plots presented earlier indicate that H/h is typically between 0.6 and 0.8 in the inner surf-zone and somewhat higher in the transition zone. For these values we see from figure 3.6 that α_u is slightly greater than 1. Note that since the roller contribution has already been accounted for the momentum correction factor will be somewhat smaller than the values estimated from figure 3.6.

Based on figure 3.6 we find that $\alpha_u = 1$ is a reasonable value to use. Later on in this chapter we will discuss the sensitivity of the results to this choice by comparing the results for $\alpha_u = 1, 1.3$.

For future reference (chapter 5) we note here that the extrapolated wave induced velocity profile gives

$$Q_{sw} = \overline{\int_{\eta_t}^{\eta} u_w dz} = \frac{cH^2 B_0}{h}\left[\left(1 + \frac{\eta_t}{H}\right)\beta + \frac{h}{H}\frac{K}{2}\left(1 + \frac{\eta_t^2}{H^2}\right)\right] \tag{3.25}$$

where Q_{sw} is the volume flux induced by the wave motion. Substituting the typical values for the various parameters we find that

$$\overline{\int_{\eta_t}^{\eta} u_w dz} \approx 1.3\frac{cH^2 B_0}{h} \tag{3.26}$$

The above forms one part of the volume flux due to the waves. A contribution due to the roller needs to be added to calculate the total mass flux.

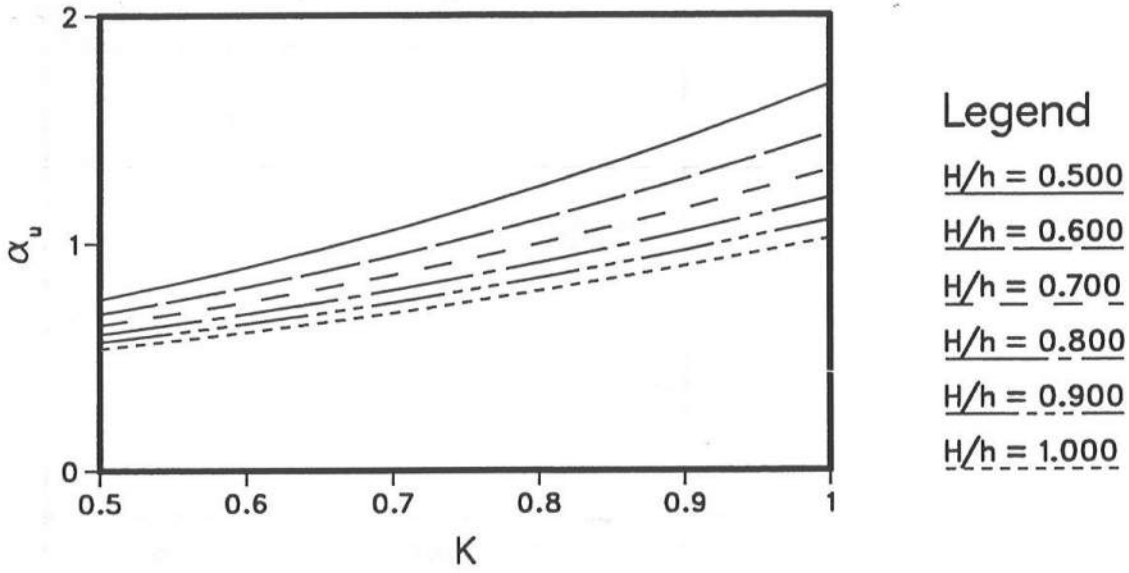

Figure 3.6: Variation of α_u with K

Figures 3.7 show the variations of B determined using the procedure described above. These plots show features essentially similar to those of P and all the comments made regarding the nondimensional radiation stress apply to this quantity too.

3.4.3 Results for D

Figures 3.8 show the variations of D/D_{bore} for the experiments analyzed (recall that $D < 0$). We see once again that the results are rather strongly grouped by the parameter S_b. For all the experiments the dissipation is close to zero at breaking indicating that even though there is a significant decrease of wave height near breaking there is very little change in the energy flux and therefore there must be a substantial change in the shape of the wave. This is consistent with the results we found earlier for P.

For smaller values of the parameter S_b the dissipation increases from zero to a value that is about one and a half times the dissipation in a bore. The dissipation rate then stays relatively constant at this value for a long stretch and then increases quite rapidly near the shoreline. As one progresses to higher and higher S_b values we see that

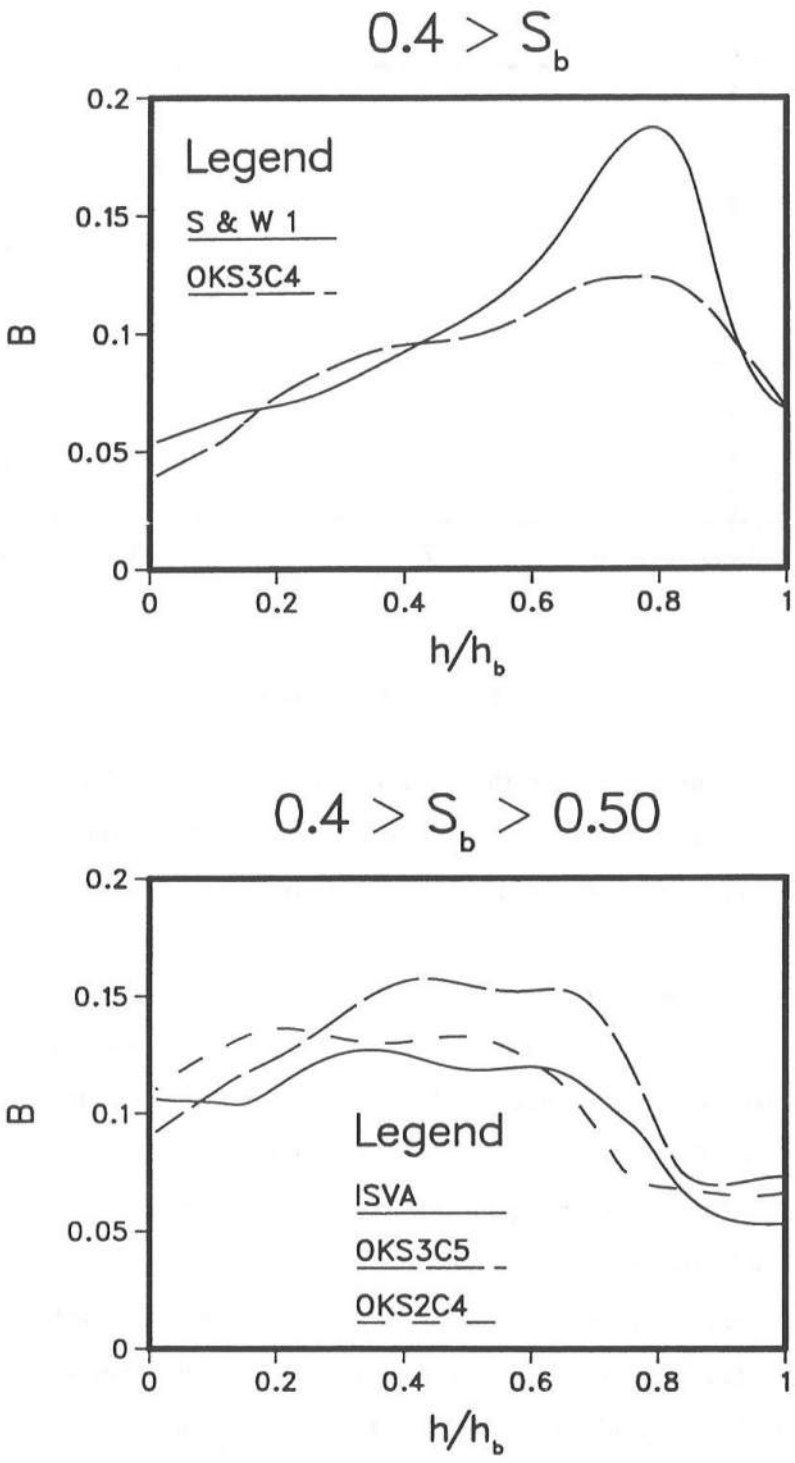

Figure 3.7: Variations of B for the experiments

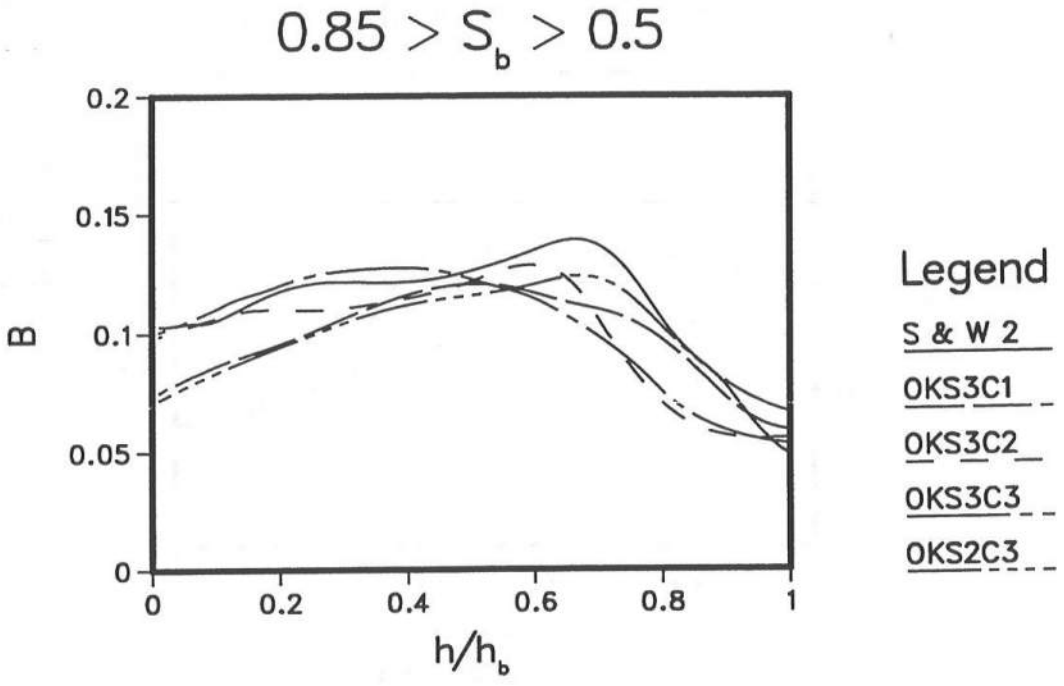

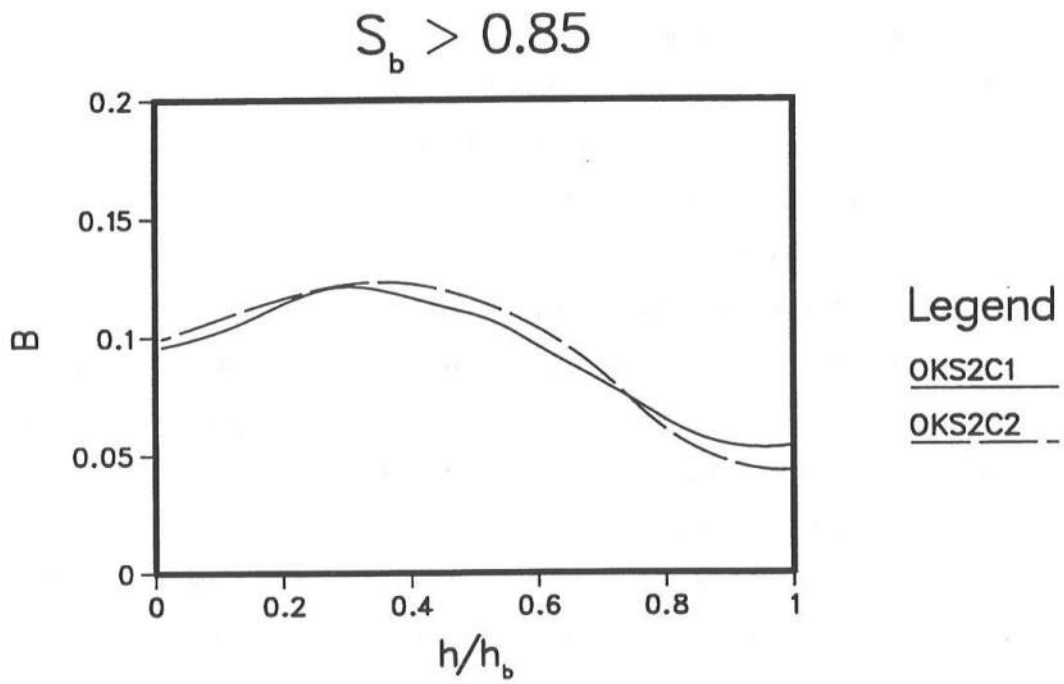

Figure 3.7: Continued

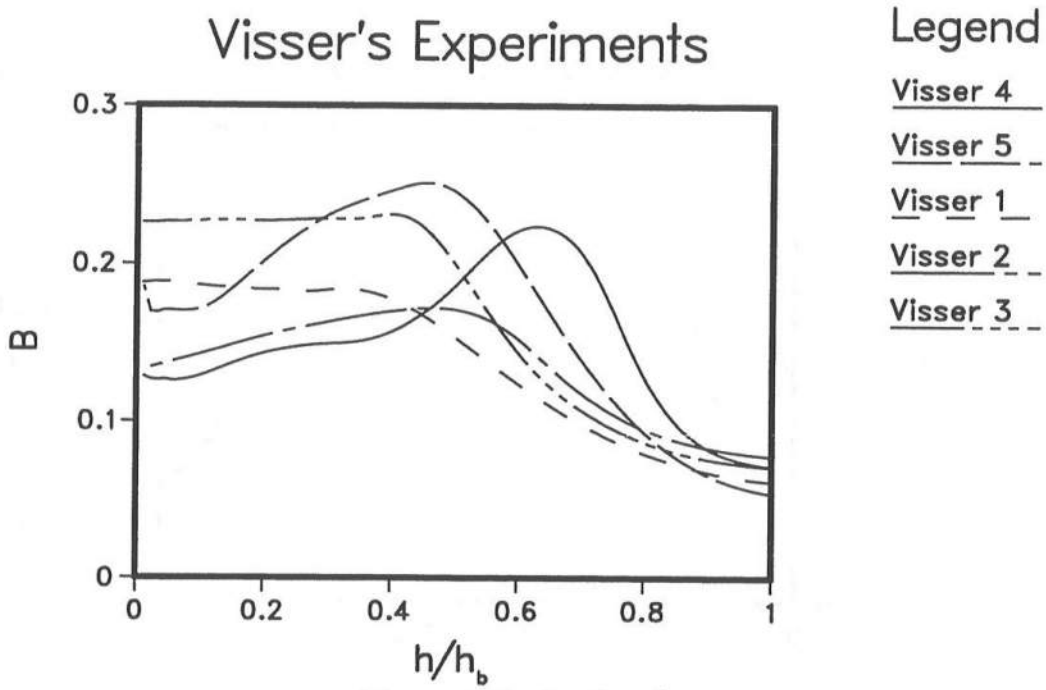

Figure 3.7: Continued

the stable value of D/D_{bore} is higher and that the wave propagates to smaller values of h/h_b equilibrium conditions are achieved. For the very high values of S_b we find that D/D_{bore} increases constantly from break point and there is no region in which it remains approximately constant indicating that the changes are so rapid that the wave does adjust to local conditions and reach an equilibrium situation. These results are also consistent with the results we found for P.

Similar to what we found with the variations of P the results from Visser's experiments are significantly different from the results derived from other experiments (figure 3.8d). Again, we see significant difference between the experimental results for experiments 2 and 3, where, based on the experimental parameters, we would not expect to see much difference. As before, the cause for this remains inexplicable.

All the dissipation curves show two strikingly common features. The first is that all of them show very little dissipation near the break point. This result was also discussed by Svendsen (1984a). The second is that all the curves in figures 3.8 show that near the shoreline the ratio D/D_{bore} tends to extremely large values. The reason for this is that

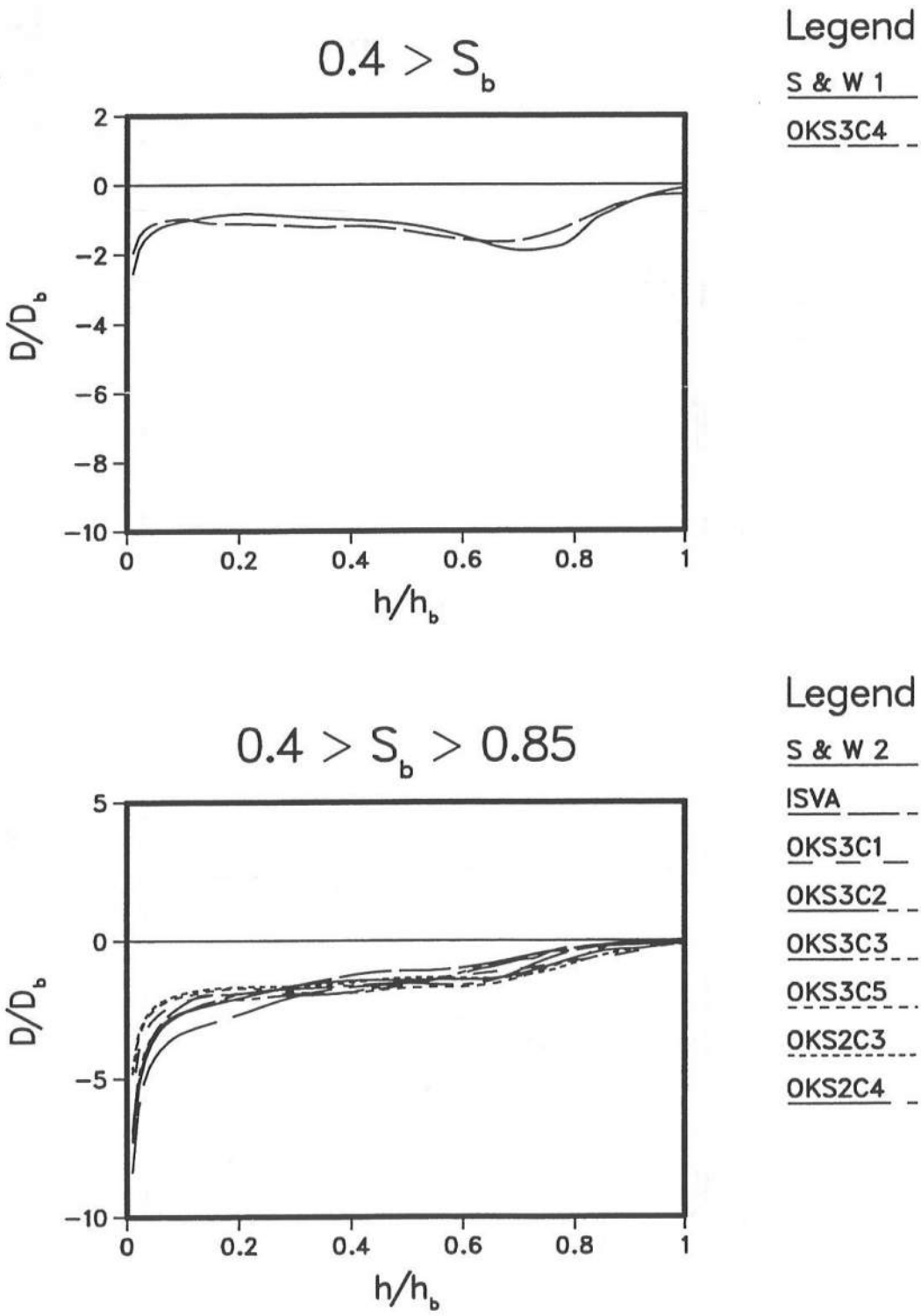

Figure 3.8: Variations of D/D_{bore} for the experiments

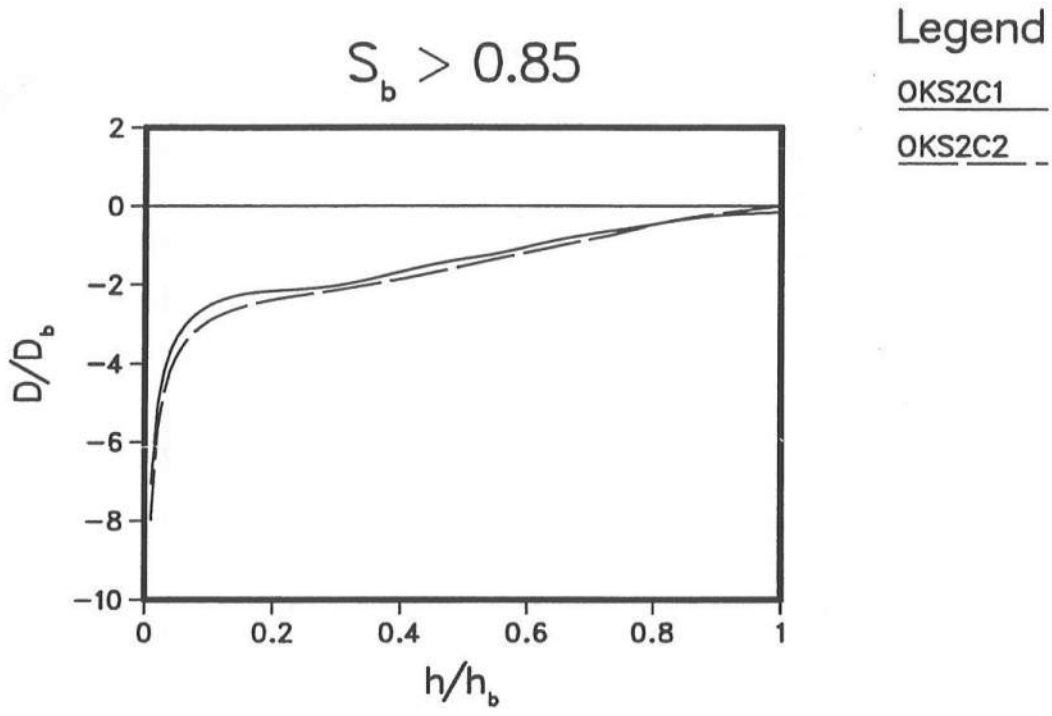

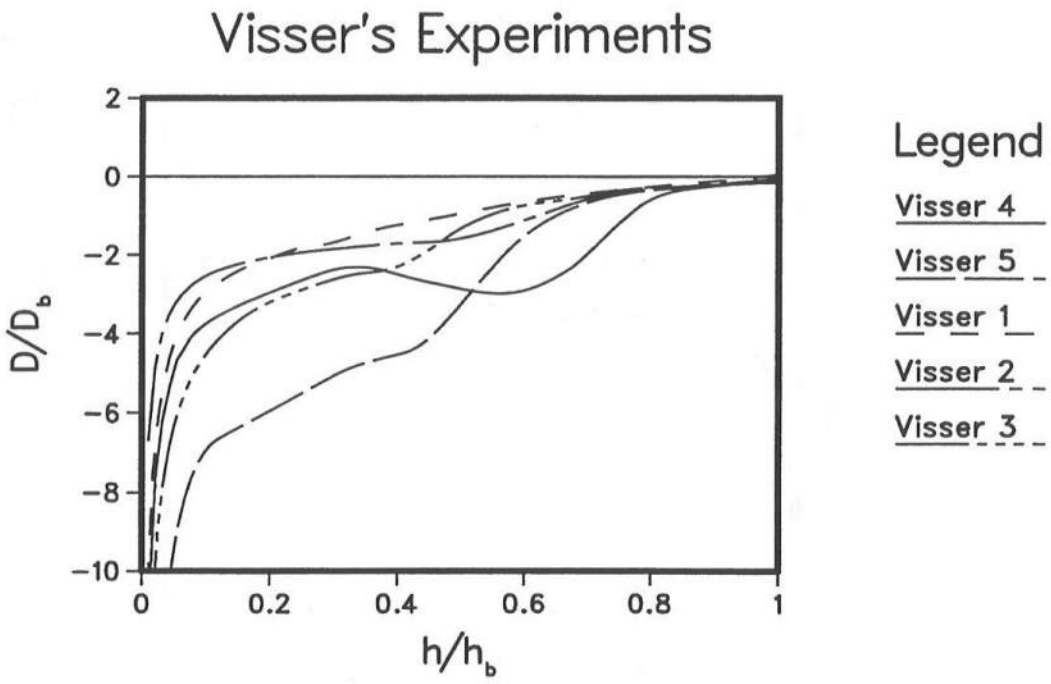

Figure 3.8: Continued

while D_{bore} tends to a constant value in this region D increases (numerically) rapidly making this ratio extremely large. This may be seen from the following argument.

Assume that near the shoreline $H = \gamma h$ and that B is a constant. The energy equation gives

$$\mathtt{D} = -2.5\rho g h\sqrt{gh}\gamma^2 B h_x \tag{3.27}$$

Therefore

$$D = -2.5\rho g h\sqrt{gh}\gamma^2 B h_x \frac{4hL}{\rho g H^3 c} \propto \frac{-1}{\sqrt{h}} \tag{3.28}$$

Therefore, $D \to -\infty$ as $h \to 0$. The implication here is that in this region the nondimensionalization adopted (which is based on bore dissipation) is not a very good one and that the approximation that the actual dissipation is proportional to the dissipation in a bore is not valid near the shoreline.

If the experimental results of Visser are accurate then the extremely high values of P would indicate that Visser's waves are more massive than the broken waves from other sources. In that case, the B_0 variation by Hansen (1990) used in the analysis would almost certainly be too small which then implies that the values determined for B and D are even larger than the already large values shown here.

3.5 Sensitivity of the results

Given some of the uncertainties in particular of the interpretation of the data it is relevant to examine the sensitivity of the results to the variations used and the various approximations made along the way.

3.5.1 Sensitivity to the parameter values used

Assumptions were made earlier regarding the values of the momentum correction factor, α_u, and the quantity B_0. It is evident that these affect the results only for B and D. The sensitivity of the results to inaccuracies in α_u may be assessed by the following

$$\frac{\partial B}{\partial \alpha_u} = \frac{B_0}{2} \tag{3.29}$$

implying that

$$\frac{\Delta B}{B} \approx \frac{B_0}{2B}\Delta\alpha_u \tag{3.30}$$

Since we know that $B_0 \leq B$ we find from the above that a 30% error in the estimation of the momentum correction factor, α_u, produces less than 15% error in the estimation of the dimensionless energy flux, B, which in turn produces a similar error in the calculated dissipation rate. We also know from figure 3.6 that the momentum correction factor used should be accurate to within 30%. We, therefore, conclude that errors in B and D from this source will not exceed 15% (in most cases they are about 7-8%). Figure 3.9 demonstrates this. Shown in this figure are comparisons of results for calculations using $\alpha_u = 1$ and $\alpha_u = 1.3$. This figure shows that, as expected, there is less than 15% difference in the results for the two values of the momentum correction factor.

Similarly the effect of inaccuracies in B_0 are

$$\frac{\Delta B}{B} = \frac{\Delta B_0}{B_0}\frac{B_0}{B}\left(\frac{\alpha_u}{2} - \frac{1}{4}\right) \tag{3.31}$$

Since we expect $B_0 \sim B/2$ and $\alpha_u \sim 1$ we expect that a 20% error in B_0 will produce less than a 5% error in B. So, this is not of significant concern either.

From the above two paragraphs we conclude that the inaccuracies made by using the B_0 variation suggested by Hansen and an $\alpha_u = 1$ will have a maximum of 10% error in the results presented here.

3.5.2 Sensitivity to the data interpretation

We first notice that the formulations are such that inaccuracies in wave height have only local effects for the results for P, B and D whereas the inaccuracies in the set-up have an integrated effect on the variation of these quantities. For P and B the inaccuracies of the set-up turns out to be the most important.

Figure 3.10 shows two plausible interpretations of the set-up data for experiment S2C3 of Okayasu *et al.* In both cases we use the same variation of wave height as shown figure 3.2. We notice from figure 3.10 that both assumed variations may be said to be reasonably accurate and that it is difficult to say which of the two variations is justified on the basis of the measurements. While the variations in b themselves are relatively close to each other there are some differences in db/dx.

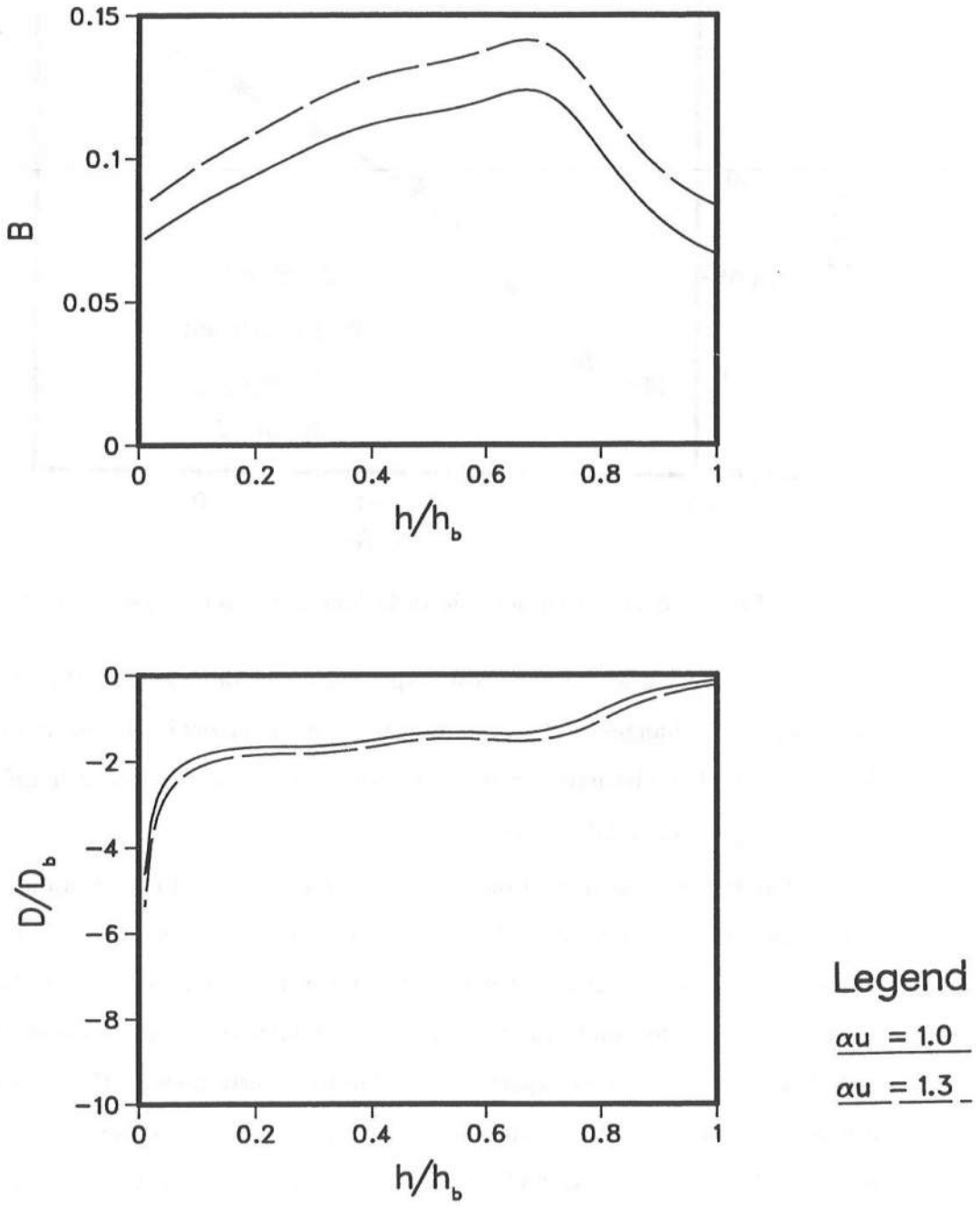

Figure 3.9: Sensitivity to α_u

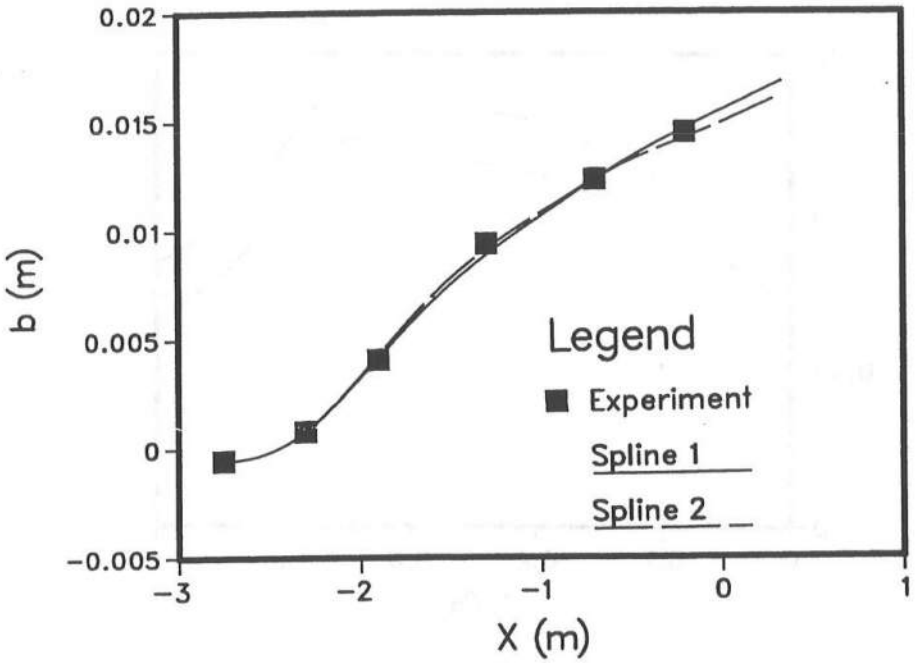

Figure 3.10: Two possible variations of the set-up for OKS2C3 data

Figures 3.11a and 3.11b show respectively the variations of P and D for the two variations. The changes in P suggest that the effect of errors in the set-up on this quantity is significant. The dissipation rate, on the other hand, seems almost indifferent to errors in the set-up as one might expect.

The rather large impact on P of minor inaccuracies of the set-up indicates that we can make rather large errors in this parameter without significantly effecting predictions of set-up. This seems, at a first glance, to be contradictory to what we started out with as the motivation for analyzing the experimental data to determine the forcing. However, note that the inaccuracies expected in P due to uncertainties in the data interpretation are much smaller than the deviation of P from the constant value of $P = 3/16$ that one gets from linear theory. We find that in this region where P is most sensitive to the data interpretations the wave height is less than half that at breaking. A 20% error in the value of P which indicates a 20% error in the value of the radiation stress. When compared with the value of the radiation stress at breaking this difference is relatively small and would be barely discernible on a plot of the radiation stresses for the two variations (see

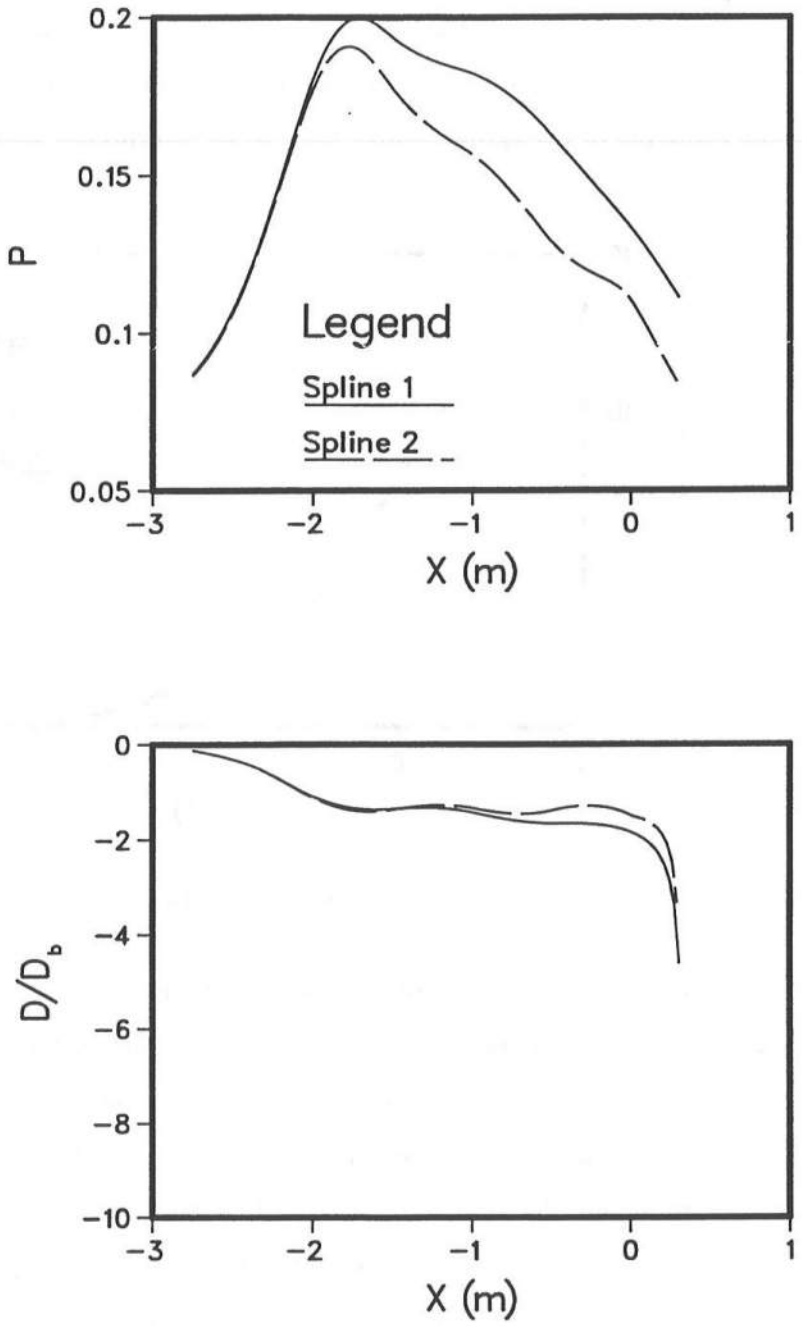

Figure 3.11: Results for the two variations

figure 3.12). The conclusion here is that the important feature is the relatively small value of P at breaking and its subsequent increase through the transition zone. Because data near the shoreline are not available in these experiments, and, because the variations (especially, P) are somewhat sensitive to errors in b we conclude that the variations very near the shoreline of the earlier figures need to be interpreted with caution.

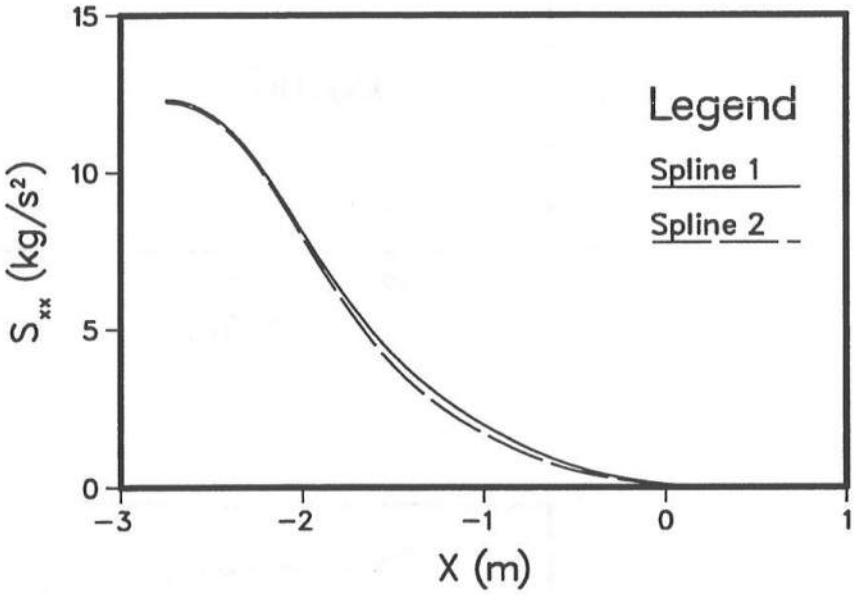

Figure 3.12: S_{xx} for the two variations

This feature may also be responsible for the rather surprising agreement of some models that use linear long wave theory to predict the set-up reasonably if the set-up calculations are started at the transition point. The problem of that approach is that it does not account for the change in radiation stress predicted by linear theory between the break point and the transition point. The approach has the implicit assumption that the radiation stress remains constant between the break point and the transition point. Because there is a significant change in wave height between the break point and the transition point, starting the set-up calculation at the transition point instead of the break point has the assumption that the radiation stress at breaking is significantly smaller than that predicted by linear theory. For models that use the energy equation to calculate

the wave height variation this approach is inconsistent in that the decrease in wave height implies a decrease in the energy flux (according to linear theory) while, at the same time, as discussed above, there is no change in the radiation stress. This inconsistency is of course eliminated if the shape factors are allowed to vary. A similar observation may be made with regard to models that use a constant wave height to water depth ratio and a permanent form theory to calculate the radiation stress if the set-up calculations are begun at the transition point.

3.6 Discussion

The results presented in this chapter showed that relatively simple measurements could be used to determine the variations of the wave averaged quantities in an accurate manner. One of the uncertainties of the analysis can be removed if the quantity B_0 is accurately determined. This quantity may be easily calculated from the measurements as the same gage that measures the wave height provides the information required to calculate this quantity (see equation 3.9).

In the following we discuss some applications of the above. Particularly, we discuss possible improvements in predictions based on the variations found above and extensions to the case we are particularly interested in in this thesis, *viz.*, that of the longshore current case.

3.6.1 Applications of the method

Figures 3.13 and 3.14 present the results of the calculations for the experiments of Visser (experiment 1) and Stive & Wind (experiment 1). The different predictions shown in these figures are based on

1. average value of P and D;
2. average P and correct D and
3. correct P and average D.

where "correct" indicates that the variation of the relevant the dimensionless parameter is as found in section 2.4. Using "correct" P and D and neglecting the bottom friction

will give us back exactly the variation we used. "Average" is defined as the average value computed for the S_b group identified in figures 3.4 and 3.8. For example, the predictions of the variations for Stive & Wind's Experiment 1 use the average values of P and D calculated from figures 3.4a and 3.8a. This exercise is also a form of a sensitivity test. The results show the sensitivity of the predictions to errors in P and D. Not surprisingly, figures 3.13 and 3.14 show that the predictions using the average values are significantly better than the predictions of earlier models. A comparison of the various predictions for Stive & Wind's Experiment 1 shows the inaccuracies entailed by using incorrect values of P. Figure 3.4a shows that the average P is quite different from the variation of P for Stive & Wind's experiment. The results for the set-up show the inaccuracies introduced by using incorrect variations of P. Figure 3.8a shows that the average value of the dissipation rate is extremely close to the actual variation for Stive & Wind's experiment. The predictions of the wave height reflect this feature.

3.6.2 Extension to 2D horizontal situation

The results for P and B can also be used to determine the to estimate the forcing for longshore currents. As shown in the last chapter, we have, to a very good approximation

$$S_{xy} = \left(S_{xx} - \frac{1}{2}\rho g H^2 B_0\right) \sin\alpha \tag{3.32}$$

Thus, with S_{xx}, H and B_0 known we may estimate the longshore component of the radiation stress with reasonable accuracy. It was also shown in the last chapter that to the first approximation the longshore current is governed by

$$\frac{d}{dx}\left(S_{xy} + S'_{xy}\right) + \tau_{by} = 0 \tag{3.33}$$

All previous longshore current models used this equation to predict longshore currents. In these models it was not clear what the sources of the inaccuracies were. The idea of using the present approach to calculating the forcing is that in this way we eliminate one of the uncertainties of the problem. Therefore, incorrect predictions of longshore currents will reflect inaccuracies in the modelling of the other two terms in equation (3.33). The possibility also exists that the interaction term neglected in (3.33) relative to (2.44) is

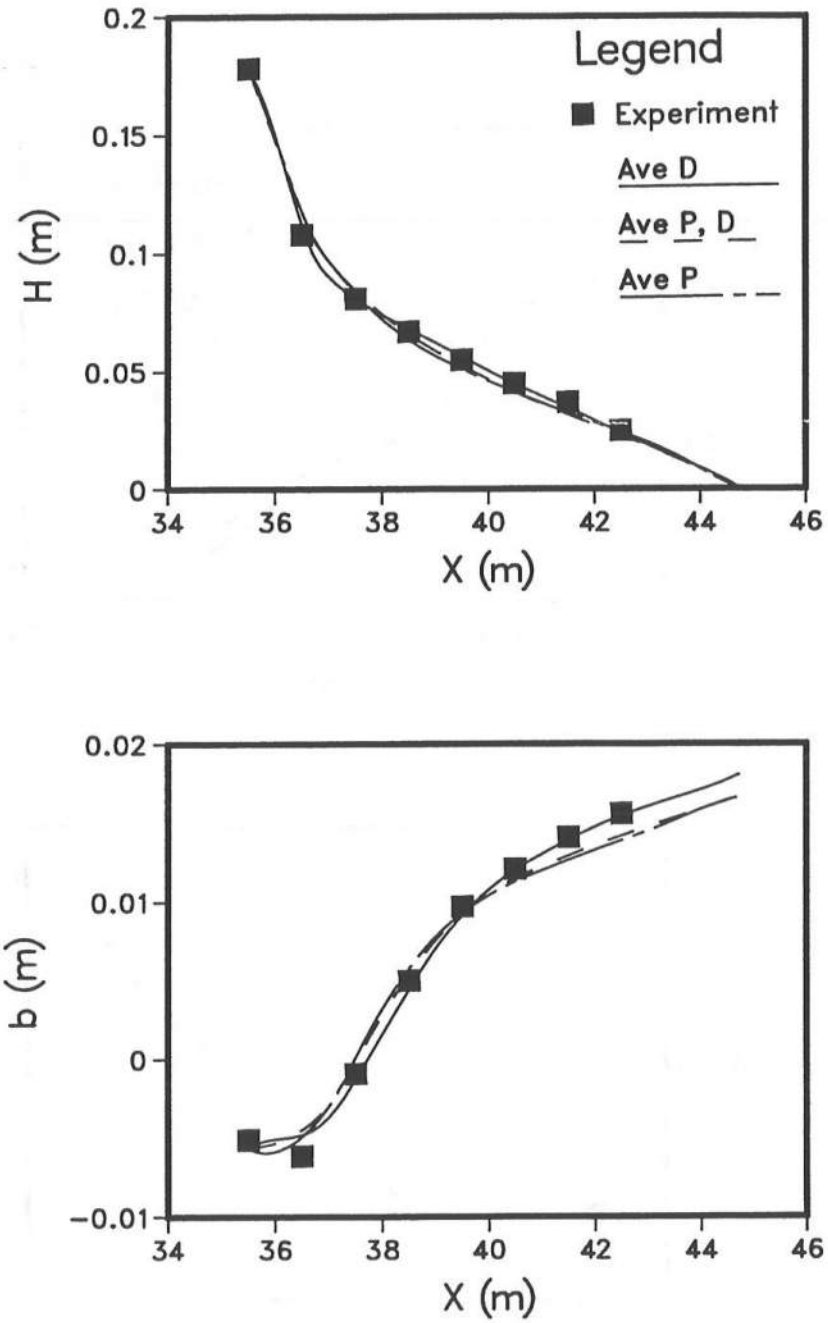

Figure 3.13: Predictions using average parameter values for Stive & Wind Exp. 1

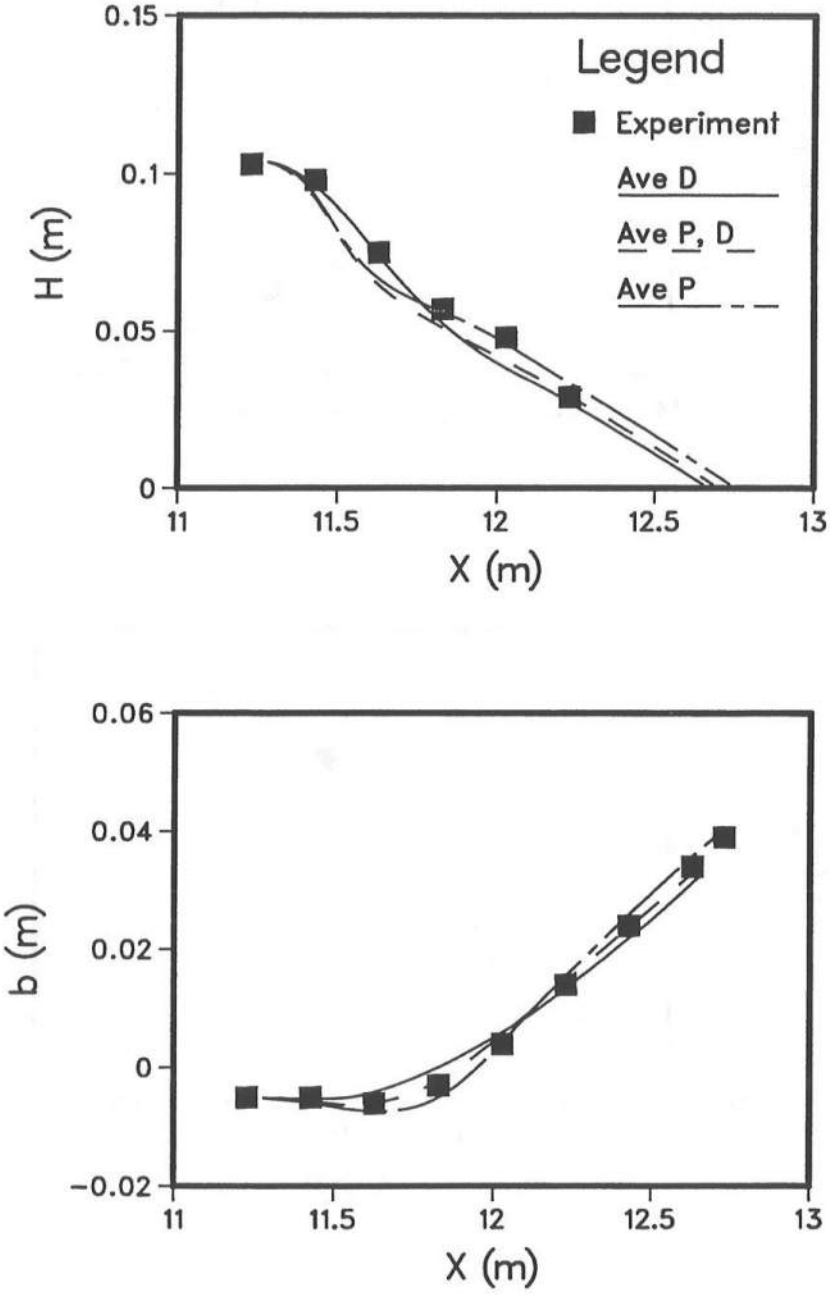

Figure 3.14: Predictions using average parameter values for Visser, Exp. 1

not negligible in comparison to the terms retained. This alternative will be examined in chapter 6.

Figures 3.15 show the variations of S_{xy} for the five Visser experiments. Since the B_0 variation is not known for Visser's experiments, the results are shown for two different variations of B_0. The curve that shows the larger values of S_{xy} is derived using Hansen's variations for B_0. The other curves use a value of B_0 that is one and a half times the value suggested by Hansen. Also, shown on these figures for purposes of comparison is the variation of S_{xy} as predicted by linear long wave theory. These plots show that similar to S_{xx} that the longshore component of the radiation stress at breaking is significantly smaller than the predictions of linear theory and that there is not much change in S_{xy} for a significant fraction of the surf-zone. Near the shoreline the rate of decrease of the radiation stress is significantly larger than the predictions of linear theory. The forcing for the longshore current is given by the gradient of the longshore component of the radiation stress. If the plots under consideration are even approximately correct, they indicate that if linear long wave theory is used to calculate the forcing, (3.33) cannot give accurate predictions of the longshore current if the other terms in that equation are modelled properly.

At this point we have estimated the forcing of the longshore currents. In addition to the forcing, the other two terms of (3.33) need to be modelled to predict longshore currents. Visser's measurements suggest that the longshore currents are rather strong (his measurements show longshore Froude numbers of order 1). We may therefore expect that a linearized bottom friction law may not be a very accurate model and we may need to resort to the more general quadratic law. In the next chapter we discuss a quadratic law that relates the bottom shear stress to the near bottom velocity.

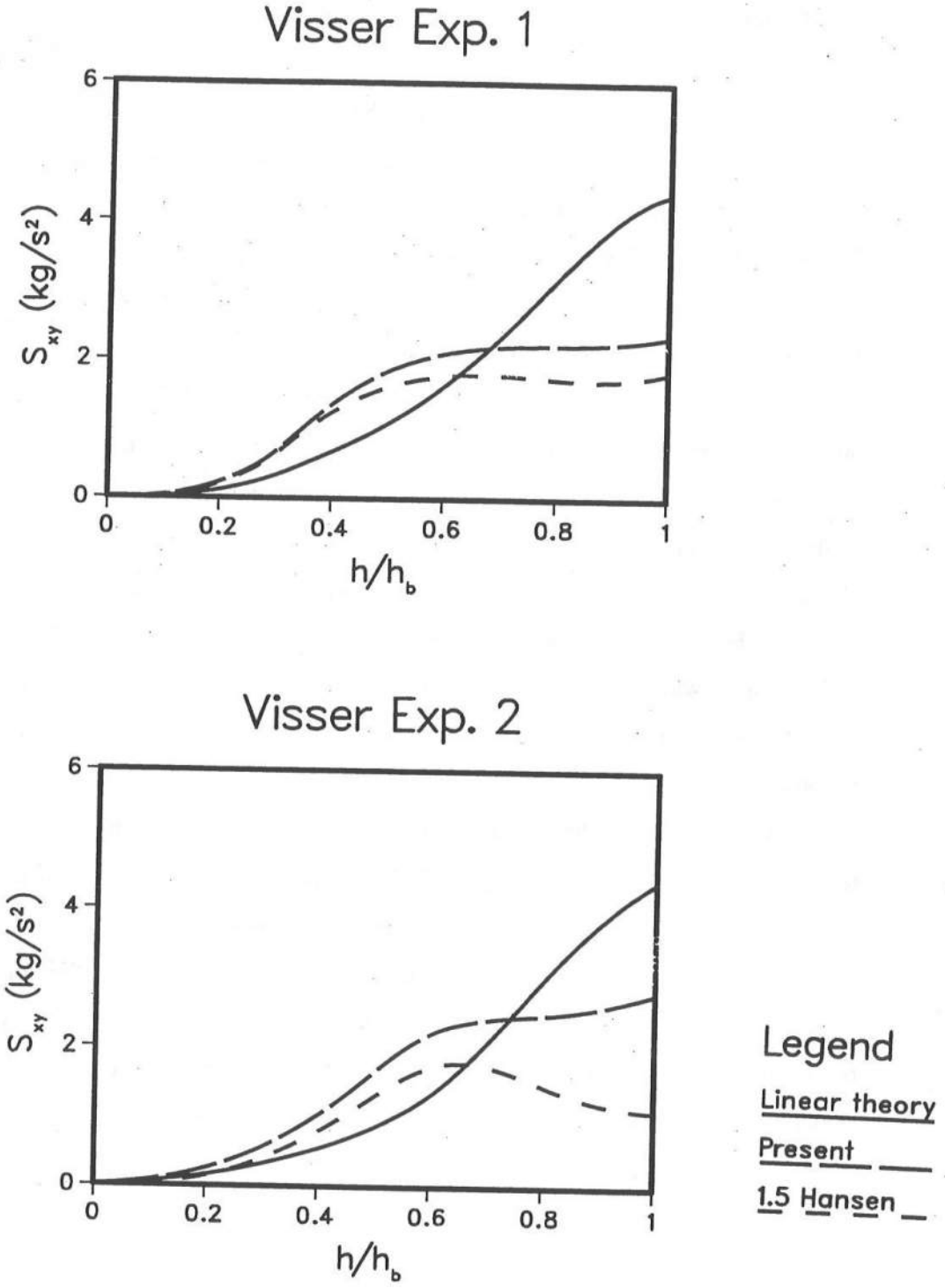

Figure 3.15: Estimates of S_{xy} for Visser's experiments

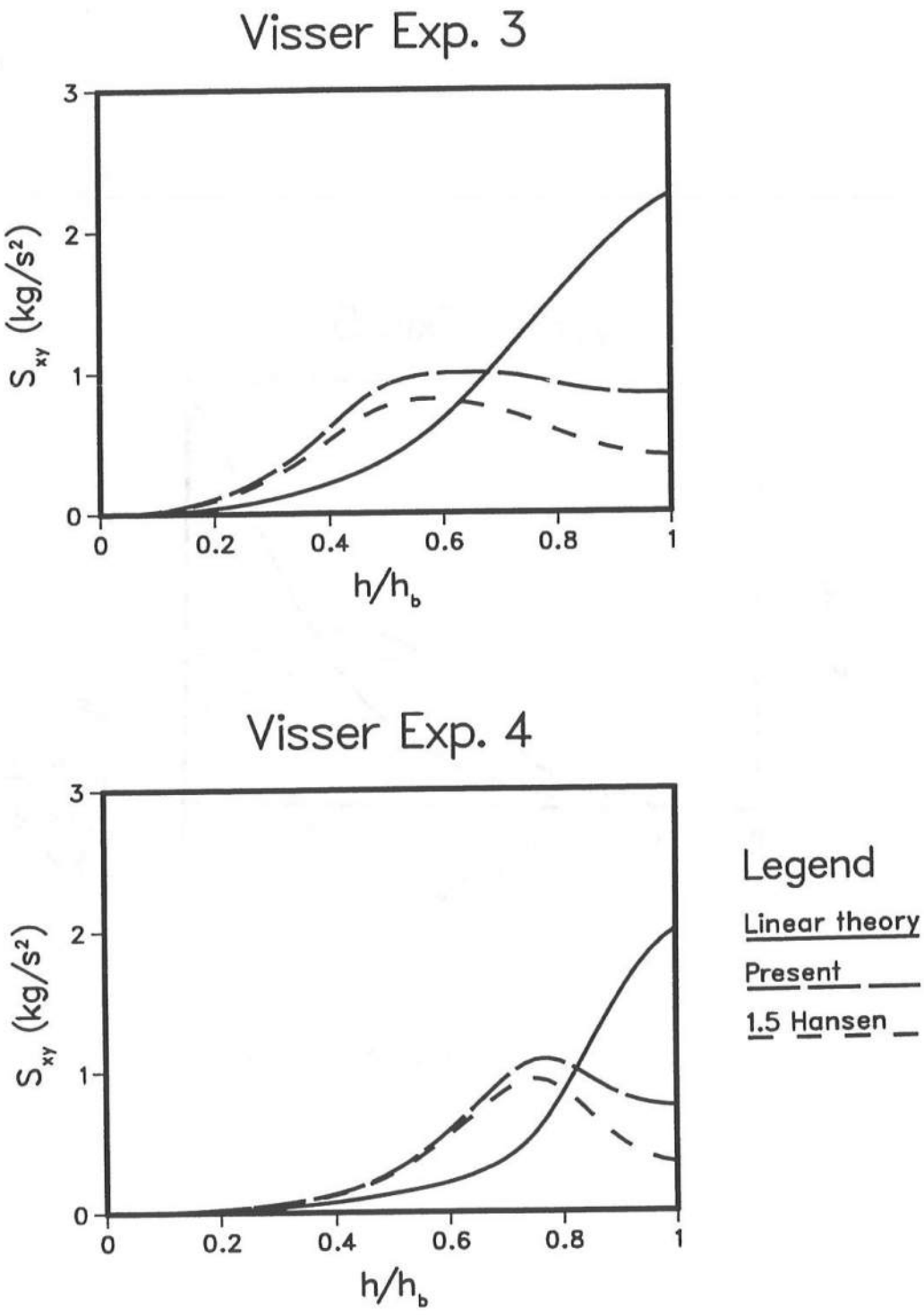

Figure 3.15: Continued

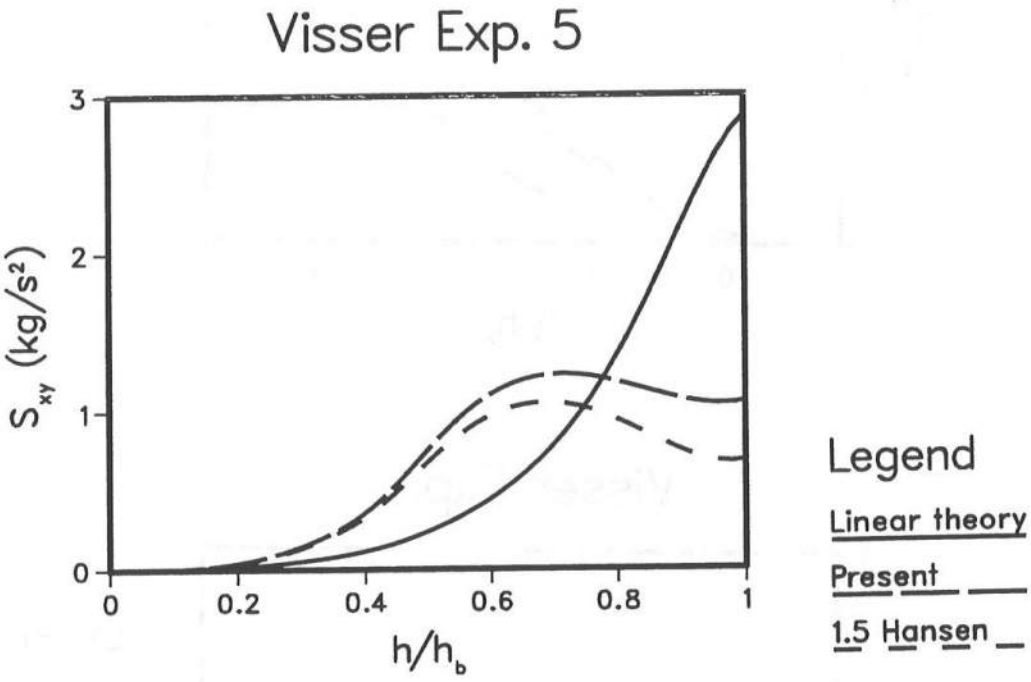

Figure 3.15: Continued

Chapter 4

BOTTOM FRICTION FORMULATION

4.1 Background

In steady, unidirectional flow, the most commonly used relationship between the velocity and the bottom shear stress is a quadratic law typically written in the form (see, *e.g.*, White 1986, p. 303)

$$\tau_b = C\rho f_c u^2 \tag{4.1}$$

where τ_b is the bed shear stress, u is the fluid velocity (typically the mean), f_c is a nondimensional friction factor which depends on the Reynolds' number of the flow and the roughness characteristics of the bed, and C is a dimensionless constant used for historical reasons. The normally used values for C are $1/8$, $1/2$ and 1.

A commonly used extension of (4.1) to oscillatory flow is (see, *e.g.*, Jonsson 1966)

$$\tau_b(t) = \frac{1}{2}\rho f_W u_{wb}(t)|u_{wb}(t)| \tag{4.2}$$

where f_W is a 'wave' friction factor and $u_{wb}(t)$ is the near-bottom velocity of the oscillatory motion. In the presence of currents a formulation similar to (4.2) is normally used with the wave friction factor f_W replaced by a 'wave-current' friction factor f_w and $u_{wb}(t)$ replaced by the instantaneous near-bottom velocity $u_b(t)$ (*e.g.*, Grant and Madsen 1979; referred to hereafter as GM79). The friction factor f_w can only be calculated by means of a detailed boundary layer theory (such as GM79). We use f_w to represent the wave-current friction factor instead of the more common f_{cw} for reasons of typographical simplicity.

In the following we use a quadratic law of the form (4.2) for the case where both waves and currents are present. No assumptions are made regarding the strength of the current relative to the waves. A general formulation is developed that is convenient to use.

We also find that the quadratic law, as it is normally used, has some rather interesting implications. For simplicity, we assume here that the friction factor f_w is known *a priori*. The problem of determining f_w is briefly discussed at the end of the chapter.

4.2 Mathematical formulation

The formulation used here is a generalization of that used by Liu and Dalrymple (1978) to arbitrary wave and current situations. We assume that the near-bottom velocity is given by

$$u_{bi}(t) = U_{bi} + u_{wbi}(t) \tag{4.3}$$

where $i = 1, 2$ and $\vec{U_b}$ is the near-bottom current velocity. For a wave incident at an angle α to the x-axis we have (see figure 4.1 for the definitions)

$$\vec{u}_{wb}(t) = u_o \left[\cos\alpha e_x + \sin\alpha e_y\right] F(t) = u_{oi} F(t) \tag{4.4}$$

where u_o is the magnitude of the near-bottom wave induced velocity, u_{oi} is the amplitude of the wave velocity in the x_i direction, e_x and e_y are the unit vectors in the x and y directions respectively and $F(t)$ is the periodic variation of the wave induced velocity. Typically, $F(t) = \cos(\omega t)$ is used where ω is the frequency of the wave motion. We use this variation here though the extension to other periodic variations is straightforward.

The instantaneous bed shear stress is assumed to be given by the following empirical formulation

$$\tau_{bi} = \frac{1}{2}\rho f_w u_{bi}(t)|\vec{u}_b(t)| \tag{4.5}$$

Such a formulation is commonly used to relate the boundary shear stress to the near bottom velocity (see, *e.g.*, Longuet-Higgins 1970, Jonsson *et al.* 1974, Liu & Dalrymple 1978, Kirby & Dalrymple 1982, Wu *et al.* 1985, Larson & Kraus 1991).

The mean bottom stress is given by the time average of (4.5). Substituting (4.3) and (4.4) into (4.5) and time averaging (after using $F(t) = \cos(\omega t)$) leads to

$$\overline{\tau_{bi}} = \frac{1}{2}\rho f_w \left[\beta_1 U_{bi} + \beta_2 u_{oi}\right] \tag{4.6}$$

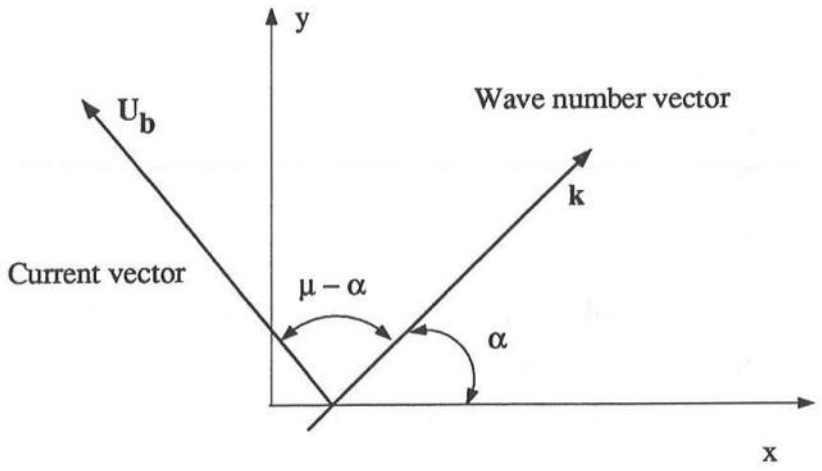

Figure 4.1: Definition sketch for waves and currents

where

$$\beta_1 = \left\{ \left(\frac{\overline{U}}{u_o} \right)^2 + 2 \left(\frac{\overline{U}}{u_o} \right) \cos(\omega t) \cos(\mu - \alpha) + \cos^2(\omega t) \right\}^{1/2} \tag{4.7}$$

$$\beta_2 = \left\{ \left(\frac{\overline{U}}{u_o} \right)^2 + 2 \left(\frac{\overline{U}}{u_o} \right) \cos(\omega t) \cos(\mu - \alpha) + \cos^2(\omega t) \right\}^{1/2} \cos(\omega t) \tag{4.8}$$

In the above μ $(= \tan^{-1} U_{by}/U_{bx})$ is the angle of the current vector with the x-axis and $\overline{U}$ is the magnitude of the current vector $\left(= \sqrt{U_{bx}^2 + U_{by}^2}\right)$.

In (4.6) the first term on the RHS represents the usual bottom friction on the bed due to the current motion. The second term on the RHS represents a contribution to the mean bottom stress from the oscillatory flow.

Figure 4.2 shows the variations of β_1 and β_2 with $\overline{U}/u_o$. The variations are shown for a number of values of $(\mu - \alpha)$. It is easily shown that the β_1 and β_2 have the following limiting values

- $\overline{U}/u_o \to 0$ (Weak current)

$$\beta_1 \to \frac{2}{\pi} \tag{4.9}$$

$$\beta_2 \rightarrow \frac{2}{\pi}\frac{\overline{U}}{u_o}\cos(\mu-\alpha) \tag{4.10}$$

- $\overline{U}/u_o \rightarrow \infty$ (Strong current)

$$\beta_1 \rightarrow \frac{\overline{U}}{u_o} \tag{4.11}$$

$$\beta_2 \rightarrow \frac{1}{2}\cos(\mu-\alpha) \tag{4.12}$$

Liu & Dalrymple considered the special cases of weak and strong currents relative to the wave motion. Special cases of the model presented above have been used in previous longshore current models (see, *e.g.,* Kirby & Dalrymple 1982, Wu *et al.* 1985, Larson & Kraus 1991).

The generalization presented here relative to the earlier works is that the magnitude of the currents and the direction of the coast are not assumed *a priori.* Previous investigators assumed, for example, that the coast was aligned with the y axis *etc.*

4.3 Implications of the mean bottom stress formulation

The quadratic friction law considered above has some interesting implications. Though it is a digression from the central theme of this thesis, it is worthwhile to examine some of these before proceeding to the determination of the mean currents.

4.3.1 Turning of the current vector

As pointed out by GM79, the direction of the mean bottom stress as given by (4.6) is, in the general situation, different from both the direction of the mean current and the direction of wave propagation. This has an interesting nonlinear effect that leads to preferential attenuation of one of the components of the current vector.

To demonstrate this effect, we seek conditions under which (4.6) will yield a bottom stress component on the bed which is in the opposite direction to the component of the current. In other words, we seek conditions under which $\overline{\tau_{bi}} < 0$ with $U_{bi} > 0$. For this to be satisfied we require (no summation implied)

$$\beta_2 < -\beta_1 \frac{u_{oi}}{U_{bi}} \tag{4.13}$$

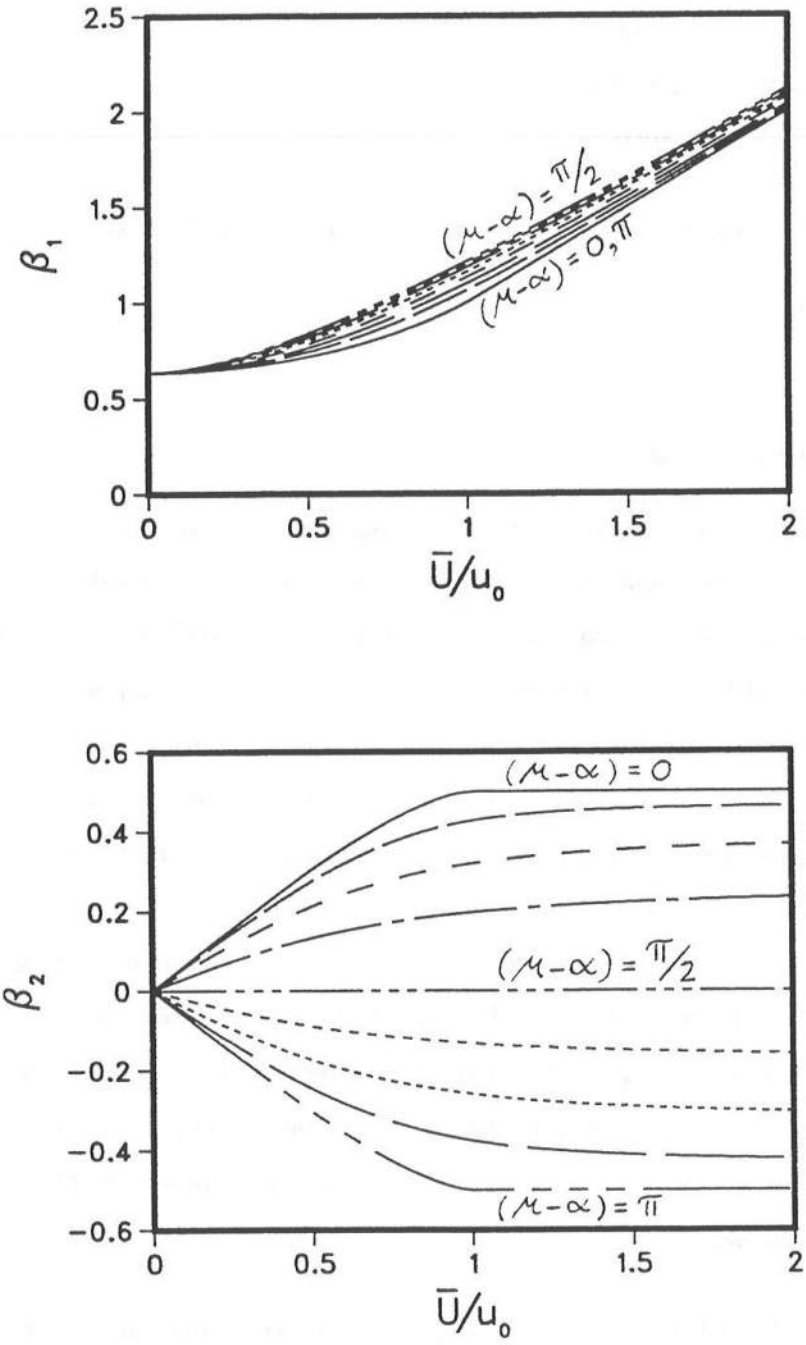

Figure 4.2: Variations of β_1 and β_2

or for the x-component

$$\beta_2 < -\beta_1 \frac{u_o}{U_b} \frac{\cos\alpha}{\cos\mu} \tag{4.14}$$

and for the y-component

$$\beta_2 < -\beta_1 \frac{u_o}{U_b} \frac{\sin\alpha}{\sin\mu} \tag{4.15}$$

Under the weak current assumption the above reduce to

$$\cos\mu > -\cos\alpha\cos(\mu-\alpha) \tag{4.16}$$

and

$$\sin\mu < -\sin\alpha\cos(\mu-\alpha) \tag{4.17}$$

respectively. Figure 4.3 shows the regions in which (4.16) and (4.17) are satisfied.

Let us consider the implication of (4.14) and (4.15). If (4.14) is satisfied then (4.6) shows that the x-component of the mean stress on the bed is in the opposite direction to that of the mean current. This implies that the x-component of the mean bottom stress acting on the fluid is in the direction of the x-component of the current. In other words, the mean bottom stress acts as a forcing that enhances the x-component of the current rather than holding it back. This appears at a first glance to be counter-intuitive since we assume that the bottom stress will always retard the flow. Note, however, that in the present case the y-component of the current, which is much larger than the x-component, is heavily retarded. So, the magnitude of the current decreases while the x-component increases. This leads to a change in direction of the current vector. If x and y are taken to be cross-shore and longshore co-ordinates then, using similar arguments we can find conditions when the longshore component is enhanced at the expense of the cross-shore component.

4.3.2 Effect of current direction on the bottom stress

The presence of the current also affects the mean bottom stress in a perpendicular direction. From the form of (4.6) it is clear that in the present formulation such an effect will be hidden in β_1 and β_2.

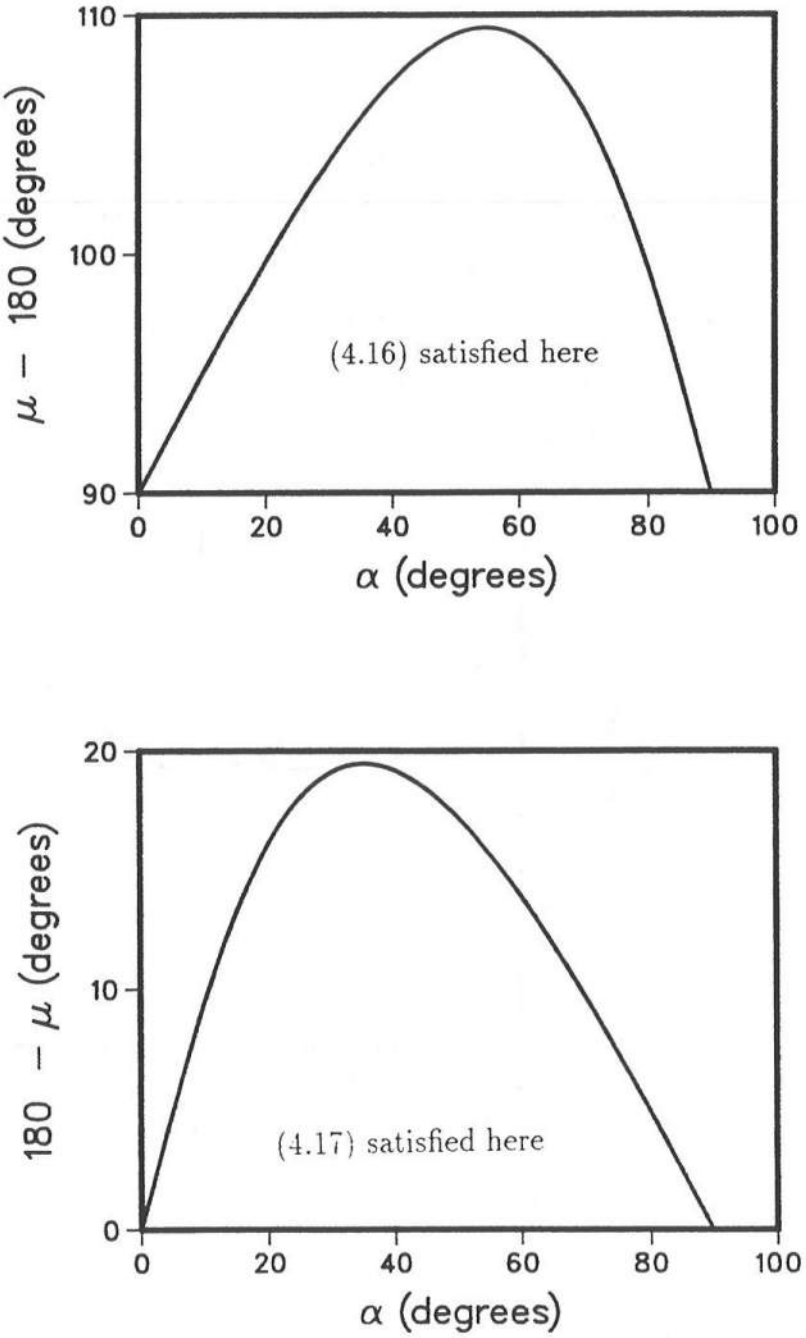

Figure 4.3: Regions in which the bottom friction component is in the direction of the current

Figure 4.4 presents the variation of the cross-shore mean bottom stress $\overline{\tau_{bx}}/\overline{\tau_{bx0}}$ with U_b/u_o for different values of the longshore current. (We have again taken x and y to represent the cross-shore and longshore directions.) In this figure $\overline{\tau_{bx0}}$ is the bottom shear stress calculated by ignoring the presence of the longshore current. This figure shows that for weak cross-shore currents the error made by ignoring the longshore current is not great whereas for strong currents ($U_b/u_o > 1$) the errors made by neglecting the strong longshore current in the calculation of the mean cross-shore bottom stress may be significant. This might become an important consideration for situations in which the bed shear stress is an important parameter.

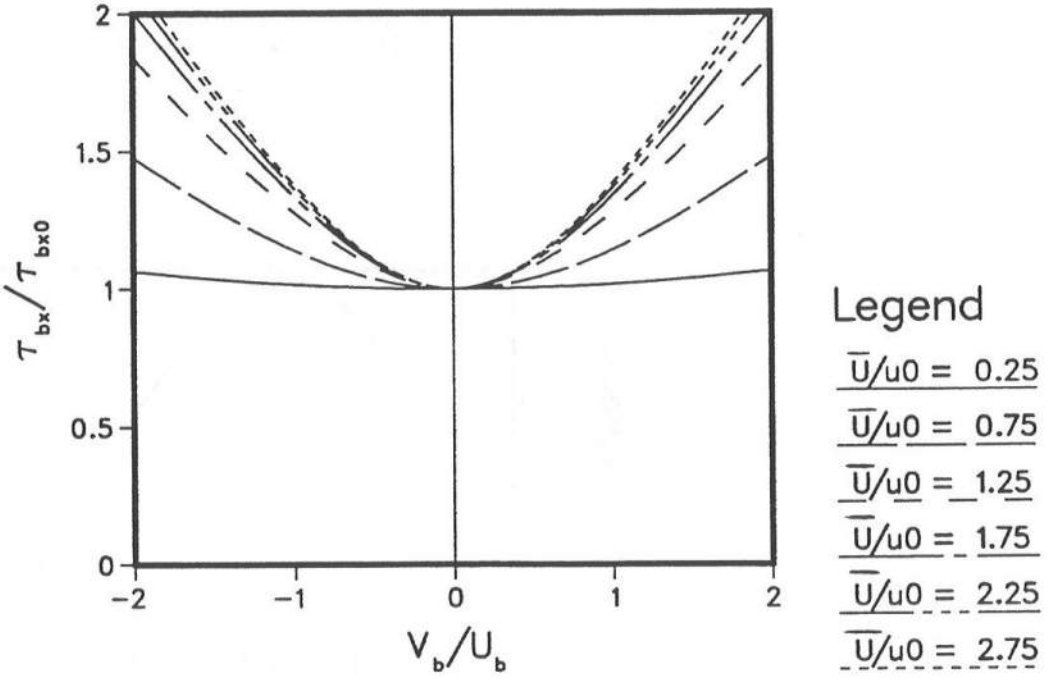

Figure 4.4: Variations of the bottom stress with $\overline{U}/u_0$

4.4 Discussion

We have shown that a commonly used bottom friction formulation has some rather interesting implications. The quadratic law causes a change in direction of the mean current vector and also causes the presence of a strong current to significantly affect the mean bottom stress in a perpendicular direction.

The major shortcoming of (4.5) as it is normally used is that f_w is constant over the entire range of $\overline{U}/u_o$. This assumption, though frequently adopted, is not completely valid. The proper determination of the friction factor requires the modelling of the boundary layer due to waves and currents in the spirit of GM79. It is also not completely clear what value of the current velocity is to be used in (4.3). For example, the theory of GM79 suggests that the appropriate velocity to be used is an "apparent" velocity which is different from the actual velocity.

We note that while the theory of GM79 may give a reasonable estimate of f_w to be used in (4.6) there is no *a priori* reason why it should do so in a general situation. The boundary layer flow in the surf-zone is quite different from the one envisaged by GM79. Inside the surf-zone, the main source of the turbulence is energy dissipated during the wave breaking process and the turbulence generated near the bed is small in comparison. Though it has never been analyzed or measured, this feature will undoubtedly alter the boundary layer flow significantly, and, would therefore affect the variation of f_w.

Wu (1987) calculated the steady streaming in the boundary layer under breaking waves. He ignored the mean pressure gradient arising from the set-up and the turbulence above the boundary layer. He found that the steady streaming was in the opposite direction to the wave propagation near the bed and in the direction of the wave propagation near the outer edge of the boundary layer. He attributes this strange behavior to the neglect of the set-up and suggests that a boundary layer model that combines the approaches of Johns (1983) who developed a model that accounts for a sloping bottom and Svendsen *et al.* (1987) who used a two layer model is required to properly model the boundary layer flow under breaking waves.

At the present time, there are no measurements available for flow in boundary layers under breaking waves. The measurements that come closest to this situation are due to Kirkgoz (1989). Kirkgoz measured velocities in the boundary layer in the very high waves prior to breaking on a slope. However, even in this situation there is hardly any turbulence outside the bottom boundary layer and hence results from these experiments do not directly apply to the surf-zone.

A comprehensive model would require the use of a turbulence model that models the actual physical situation in a realistic manner and the development of a detailed boundary layer theory from which one may predict f_w. This is not undertaken here. The approach commonly used (the present work being an example) assumes that a representation of the instantaneous bottom friction like (4.5) is possible with a known value of f_w. This amounts to a 'black box' approach wherein one assumes that the near-bottom velocity drives a bottom boundary layer whose main effect is to link the bottom shear stress to the near bottom velocity through an appropriate relationship.

Chapter 5

PREDICTION OF 2D HORIZONTAL CURRENTS AND DERIVATION OF THE VERTICAL STRUCTURE OF THE CURRENTS

5.1 Review of previous work on mean circulation on long straight coasts

The mean circulation we deal with in this thesis is composed of a longshore current and the undertow. The longshore currents are forced by gradients of the longshore component of the radiation stress. The undertow is forced by continuity because on a beach there is no net mass flux in the cross-shore direction. This implies that the mass flux due to the waves has to be compensated for by a return current. In this section we summarize the previous work on these phenomena. Longshore currents are dealt with first because work on this phenomenon seems to have begun earlier than work on the undertow.

5.1.1 Longshore currents

Putnam *et al.* (1949) conducted the first systematic study of the longshore current phenomenon. They conducted a series of laboratory and field measurements of the average (across the surf-zone) longshore current. Galvin (1967) reviewed these as well as subsequent measurements of longshore currents and the various empirical formulae available up to that time.

Bowen (1969a) was the first to apply the concept of the radiation stress to the prediction of longshore currents. He showed, using linear theory, that provided there is no dissipation of wave energy outside the surf-zone, the longshore component of the radiation stress is conserved if Snell's law is valid.[7] Inside the surf-zone, he assumed that the wave

[7] This result has been generalized by James (1974a) to apply to the nonlinear case (see appendix B).

height was proportional to the water depth and calculated the corresponding decay in the longshore component of the radiation stress. Using a linearized bottom friction law and a constant eddy viscosity he solved for the cross-shore distribution of the longshore current.

Thornton (1970) and Longuet-Higgins (1970) used the same approach as Bowen with different eddy viscosity formulations. Thornton formulates the problem of longshore currents on beaches with no alongshore variation giving a very useful discussion of the assumptions made along the way. Longuet-Higgins also gives a detailed discussion and summarizes the experimental data available up to that time. Longuet-Higgins' solution for the longshore currents is probably the most well known, perhaps, because of its mathematical simplicity. For this reason as well as because we will be using features of this solution for our discussion here and in the next chapter and also in chapter 7 use this longshore current distribution to study stability characteristics of longshore currents it may be worthwhile at this stage to review essential features of his solution. The first approximation to the longshore current is governed by (2.45)

$$\frac{d}{dx}\left(S_{xy} + S'_{xy}\right) + \tau_{by} = 0 \tag{5.1}$$

Longuet-Higgins assumes that inside the surf-zone $H = \gamma h$ and linearizes the quadratic friction law to get

$$\tau_{by} = \frac{\rho f_w u_0 V}{\pi} \tag{5.2}$$

He uses linear long wave theory to calculate the longshore radiation stress and assumes that $u_0 = \gamma\sqrt{gh}/2$. He further assumes that the turbulent radiation stress may be modelled by

$$S'_{xy} = -\rho N x \sqrt{gh}\frac{dV}{dx} \tag{5.3}$$

where N is a dimensionless constant (between 0 and 0.016). (5.3) will be discussed further below.

Under these assumptions, for the case of a plane beach, $h = h_x x$, (5.1) reduces to

$$P\frac{d}{dX}\left(X^{2.5}\frac{dV}{dX}\right) - X^{1/2}V = -X^{3/2} \tag{5.4}$$

where $X = x/x_b$ and $V = V/V_m$. V_m is the velocity at the breakpoint for $P = 0$ and is given by $V_m = 5\pi\gamma h_x\sqrt{gh_b}\sin\alpha_b/8f_w$. The above equation is then solved by requiring boundedness of the longshore current at $x = 0, \infty$ and continuity of the velocity and its derivative at $x = x_b$. The continuity conditions need to be applied because the forcing (dS_{xy}/dx) changes discontinuously from a non-zero value inside the surf-zone to zero outside the surf-zone. The parameter P is given by

$$P = \frac{2\pi h_x N}{\gamma f_w} \tag{5.5}$$

He finds that this parameter represents the strength of the turbulent mixing and essentially controls the shape of the profile. Smaller values of P lead to higher maximum velocities and larger shears on the seaward face of the longshore current. Measured profiles of longshore currents suggest that reasonable agreement is obtained for P in the range 0.1 to 1.0 (see, *e.g.*, Mei 1983, p. 478). Figure 5.1 shows the variation of Longuet-Higgins' solution for a number of P values.

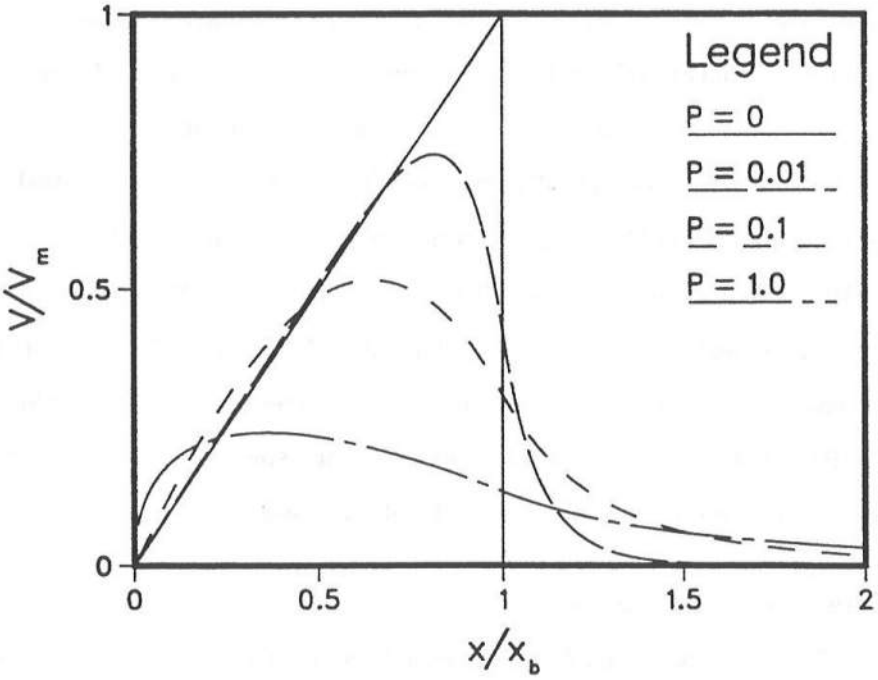

Figure 5.1: Longuet-Higgins' (1970) solution for the longshore currents

James (1974b) calculated longshore currents employing his wave model which was briefly described in chapter 3. He used an eddy viscosity similar to the one used by Longuet-Higgins inside the surf-zone. Outside the surf-zone, he assumed that the eddy viscosity was inversely proportional to the depth. Liu & Dalrymple (1978) studied the effects on the longshore currents of a large angle of incidence and special cases of the quadratic bottom friction law discussed in chapter 4. They neglected lateral mixing. Mizuguchi & Horikawa (1978) measured longshore currents in the laboratory and estimated the vertical structure of the currents. Unfortunately, their experiments did not have alongshore uniformity and hence cannot be used for purposes of comparison here. Kraus & Sasaki (1979) extended Longuet-Higgins' solution for the case of a large angle of incidence. Visser (1982, 1984) measured longshore currents in a laboratory. He measured the longshore current using a dye and also estimated the vertical structure of the currents based on measurements at three depths. McDougal & Hudspeth (1983) extended Longuet-Higgins' solution to non-planar beaches. Svendsen & Lorenz (1989) solved for the local vertical structure of the longshore currents using a perturbation approach. They found that the vertical structure of the longshore current is rather weak. Dong & Anastasiou (1991) also solved for the vertical structure of the longshore currents.

Mizuguchi & Horikawa (1978) reported field measurements of longshore currents. Other field measurements of longshore currents include Thornton & Guza (1981, 1986) and Whitford (1988). Wu *et al.* (1985) published a comparison of the results of a monochromatic numerical model with the data of Thornton & Guza (1981). Thornton & Guza (1986) compared the results of various longshore current models with their field data. Whitford (1988) modified Thornton & Guza's (1986) spectral model and compared the predictions of the modified model to his field observations.

5.1.2 Cross-shore circulation

Dyhr-Nielsen & Sorensen (1970) pointed out that the mean stresses acting on the water column were not evenly distributed over depth and that these imbalances may drive a mean cross-shore flow. Detailed measurements of undertow profiles were carried out by Stive & Wind (1982), Nadaoka & Kondoh (1982), Hansen & Svendsen (1984), Okayasu

et al. (1986, 1988) and Okayasu (1989) in the laboratory. Recent field measurements of the undertow profiles include Wright *et al.* (1982), Guza & Thornton (1985), Haines & Sallenger (1990) and Greenwood & Osborne (1990). Greenwood & Osborne provide an exhaustive list of references for the cross-shore circulation problem.

Dally (1980) and Borecki (1982) presented models for the undertow using linear theory to calculate the radiation stresses. Borecki also gives a very detailed and useful discussion of the various terms that act as forcing for the undertow and their distribution over depth. Svendsen (1984b) modelled the undertow using his roller model briefly described in the previous chapter. The aforementioned authors enforced a near bottom velocity on their undertow solutions. This resulted in predictions of undertow velocities which near the bottom are in the shoreward direction whereas the measurements indicate a seaward velocity near the bed.

To overcome this difficulty Stive & Wind (1986) presented a model for the undertow similar to Svendsen's but specified boundary conditions at trough level instead of at the bottom as Svendsen does. deVriend & Stive (1987) presented a model for the quasi 3D situation which reduces to the model of Stive & Wind for the undertow.

Svendsen *et al.* (1987) used measured quantities to calculate the forcing for the undertow and calculated the resulting undertow profiles by patching the undertow solution with a boundary layer model. In this model they assumed that the turbulence level in the bottom boundary layer is significantly lower than the water column above. They found that while their results for the bottom shear stress were quite sensitive to the assumed thickness of the bottom boundary layer their results for the undertow velocities were quite insensitive to the assumed thickness of the boundary layer. Since the bottom shear stress is the quantity of practical interest this state of affairs is not quite satisfactory. To alleviate this problem, Svendsen & Hansen (1988) used a bottom boundary condition that related the near bottom undertow velocity to the bottom shear stress as calculated by using a friction factor. They also showed that the specification of the surface shear stress as a boundary condition as done by Stive & Wind (1986) is less appropriate than the bottom shear stress condition used by Svendsen *et al.* (1987) or Svendsen & Hansen (1988).

In this work we use an approach similar to that used by Svendsen & Hansen (1988). The friction factor, f_w, becomes one of the parameters of the problem. As remarked in the previous chapter, the proper determination of this factor requires an elaborate boundary layer model which is not pursued here.

Random wave models for the undertow were presented by Stive & Battjes (1984) and Stive & deVriend (1987). Roelvink & Stive (1989) used a slightly modified version of the Stive & deVriend model in their undertow calculations.

5.2 Perturbation solution for the longshore current

Visser's (1984) measurements show very little vertical structure in the longshore current profiles. Svendsen & Lorenz (1989) studied the local depth variation of the longshore current and found no significant vertical structure for the longshore currents. Based on the above we may tentatively assume that the vertical variation of the longshore current is weak and seek a perturbation solution for the longshore current. The perturbation solution used here is quite different from that used by Svendsen & Lorenz (1989). Svendsen & Lorenz did not include the UV and the VW terms in their solution. Of these, the UV terms turn out to be important. Additionally, Svendsen & Lorenz assume that

$$S'_{xy} = -\rho \int_{-h_0}^{b} \nu_{tx} \frac{\partial V}{\partial x} dz \tag{5.6}$$

This is slightly different from the one used here.

To avoid having to refer back to equations in chapter 2 we will reproduce the important equations here. The depth variation of the longshore current is governed by (2.57) (below trough level)

$$\frac{\partial}{\partial z}\left(\nu_{tz}\frac{\partial V}{\partial z}\right) = \frac{\partial}{\partial x}\left(\overline{u_w v_w} + UV\right) + \frac{\partial}{\partial z}\left(\overline{v_w w_w} + VW\right) - \frac{\partial}{\partial x}\left(\nu_{tx}\frac{\partial V}{\partial x}\right) = \alpha_y(x,z) \tag{5.7}$$

and the depth integrated y–momentum equation (2.44) reads

$$\frac{1}{\rho}\left[\frac{d}{dx}\left(S_{xy} + S'_{xy}\right) + \tau_{by}\right] + \frac{\partial}{\partial x}\left[\int_{-h_0}^{\xi_t} UV dz + \overline{\int_{\xi_t}^{\xi} u_w V dz}\right] = 0 \tag{5.8}$$

5.2.1 Order of magnitude analysis

We define the following nondimensional variables

$$\begin{aligned} \mathtt{Z} &= \frac{z}{h_b} \;;\; \mathtt{X} = \frac{x}{x_b} \;;\; \mathtt{n} = \frac{\xi}{h_b} \;;\; \mathtt{h} = \frac{h}{h_b} \;;\; \mathtt{U} = \frac{U}{c_b} \;;\; \mathtt{V} = \frac{V}{c_b} \\ \mathtt{W} &= \frac{W}{c_b} \;;\; \mathtt{u_w} = \frac{u_w}{c_b} \;;\; \mathtt{N_{tx}} = \frac{\nu_{tx}}{h_b c_b} \;;\; \mathtt{N_{tz}} = \frac{\nu_{tz}}{h_b c_b} \;;\; \mathtt{T_b} = \frac{\tau_{by}}{\rho c_b^2} \end{aligned} \tag{5.9}$$

where $c_b = \sqrt{g h_b}$ is the wave celerity at break point. Introducing the nondimensional variables in (5.7) leads to

$$\left(\frac{h_b}{x_b}\right)^2 \frac{\partial}{\partial \mathtt{X}}\left(\mathtt{N_{tx}} \frac{\partial \mathtt{V}}{\partial \mathtt{X}}\right) + \frac{\partial}{\partial \mathtt{Z}}\left(\mathtt{N_{tz}} \frac{\partial \mathtt{V}}{\partial \mathtt{Z}}\right) - \left(\frac{h_b}{x_b}\right) \frac{\partial}{\partial \mathtt{X}}(\mathtt{UV}) - \frac{\partial}{\partial \mathtt{Z}}(\mathtt{VW}) = \frac{\alpha_y}{g} \tag{5.10}$$

When (5.9) is introduced into the properly depth-integrated equation (5.8) it leads to

$$\left(\frac{h_b}{x_b}\right)^2 \frac{\partial}{\partial \mathtt{X}}\left(\mathtt{N_{tx}} \mathtt{h} \frac{\partial \mathtt{V_b}}{\partial \mathtt{X}}\right) - \mathtt{T_b} - \left(\frac{h_b}{x_b}\right) \frac{\partial}{\partial \mathtt{X}} \left\{ \int_{-\mathtt{h_0}}^{\mathtt{n_t}} \mathtt{UV dZ} + \overline{\int_{\mathtt{n_t}}^{\mathtt{n}} \mathtt{u_w V dZ}} \right\} = \frac{1}{\rho c_b^2} \frac{dS_{xy}}{dx} \tag{5.11}$$

where an approximation has been introduced for S'_{xy}. To be consistent with (2.39) the turbulence closure introduced in chapter 2 for modelling the $\overline{u'_i u'_j}$ term, the longshore component of the radiation stress should be given by

$$S'_{xy} = \overline{\int_{-h_0}^{\xi} u'_i u'_j dz} = -\rho \overline{\int_{-h_0}^{\xi} \nu_{tx} \frac{\partial V}{\partial x} dz} \tag{5.12}$$

If the depth variation of the longshore currents were known then the above is easy to evaluate. To properly evaluate the integral we would need to know the current variation above trough level. This is not known. For the present purposes we assume that the integrated Reynolds' stress may be approximated by

$$S'_{xy} = -\rho \nu_{tx} h \frac{dV_b}{dx} \tag{5.13}$$

We prefer to use the bottom velocity instead of the mean (over depth) value because the longshore current does not vary significantly over depth and it is a little more convenient to use the parameterization in terms of the bottom velocity, particularly, in the next chapter. This is because the bottom stress is typically expressed in terms of the bottom velocity. If a velocity different from the bottom value (say the mean value) is used in (5.13) then in order to solve (5.8) for the bottom velocity then the mean velocity would have to be expressed in terms of the mean value. This is not a significant complication and

our calculations indicate that the results are not very different if the mean value is used in (5.13). We will discuss this further in chapter 6 where we will show that the inaccuracy introduced by (5.13) is quite insignificant.

We define

$$\varepsilon = \frac{h_b}{x_b} \ll 1 \tag{5.14}$$

Measurements of the undertow velocities and previous models of undertow suggest that $U/\sqrt{gh} < 0.1$. Therefore, it seems reasonable to assume that

$$\mathtt{U} \sim \varepsilon \tag{5.15}$$

Measurements of longshore currents by Visser indicate that $V/\sqrt{gh} \sim 1$. Therefore we let

$$\mathtt{V} \sim 1 \tag{5.16}$$

The bottom condition (2.60) implies that

$$\mathtt{W} \sim \varepsilon^2 \tag{5.17}$$

Furthermore,

$$\frac{\alpha_y}{g} \simeq \frac{\partial \overline{u_w v_w}}{\partial x} = B_0 \sin\alpha \left(\frac{H}{h}\right)^2 h_x \tag{5.18}$$

Since $B_0 \sim 0.1$ and $\sin\alpha \ll 1$ we will have

$$\sin\alpha B_0 (H/h)^2 h_x \ll h_x \tag{5.19}$$

Therefore, we will have

$$\frac{\alpha_y}{g} \sim \frac{\partial \overline{u_w v_w}}{\partial x} = \sin\alpha B_0 \left(\frac{H}{h}\right)^2 h_x \sim \varepsilon^2 \tag{5.20}$$

or higher. For the rest of this section we will assume that $\alpha_y/g \sim \varepsilon^2$.

Before we proceed any further, we need to estimate the size of the RHS of (5.11). We have

$$\frac{1}{\rho c_b^2}\frac{dS_{xy}}{dx} = \frac{gh}{c_b^2}\left(\frac{H}{h}\right)^2 h_x B_0 \sin\alpha \sim \varepsilon^2 \tag{5.21}$$

This could also have been estimated from the fact that RHS of (5.11) should have the same order as the RHS of (5.10). The T_b term of (5.11) is the term responsible for resisting the forcing and, therefore, we should have

$$T_b \sim \varepsilon^2 \tag{5.22}$$

Furthermore, we have

$$N_{tz}\frac{\partial V}{\partial Z})_{Z=-h_0} = T_b \sim \varepsilon^2 \tag{5.23}$$

Equation 5.23 indicates that there are three possibilities for N_{tz} and $\partial V/\partial Z$, *viz.:*

1. N_{tz} is of order ε^2 and $\partial V/\partial Z$ is of order one or,
2. N_{tz} is of order one and $\partial V/\partial Z$ is of order ε^2 or,
3. both N_{tz} and $\partial V/\partial Z$ are of order ε.

Existing measurements of the vertical structure of longshore currents suggest that the first of these possibilities is not the one that occurs in the nearshore region. The second possibility requires us to have

$$\frac{\nu_{tz}}{h\sqrt{gh}} \sim 1 \tag{5.24}$$

which is in conflict with the value one estimates for ν_{tz} based on measured turbulence levels and predictions of undertow profiles. Therefore, we adopt the third choice above.

$\partial V/\partial Z \sim \varepsilon$ implies that

$$V = V_0(x) + \varepsilon V_1(x,z) \tag{5.25}$$

which shows that

$$\int_{-h_0}^{n_t} UV\,dZ + \overline{\int_{n_t}^{n} u_w V\,dZ} = \int_{-h_0}^{n_t} UV_1\,dZ + \overline{\int_{n_t}^{n} u_w V_1\,dZ} \sim \varepsilon^2 \tag{5.26}$$

Substituting the above in (5.11) we find that the interaction term enters the equation at third order and, therefore, does not contribute to the lowest order solution of the longshore current which is of second order.

So, far we have estimated the size of all the terms of (5.11) except for the first. This term is of order $\varepsilon^2 \mathtt{N_{tx}}$. If we assume that $\mathtt{N_{tx}}$ is of order ε then we find from (5.11) that the lowest order longshore current has no mixing. This is not what observations of longshore current show. Therefore, we choose $\mathtt{N_{tx}} \sim 1$.

An obvious criticism of the above choice is that observations of turbulent eddies (Nadaoka *et al.* 1989) show that these eddies are nearly circular in the surf-zone and hence there is no reason to expect that the eddy viscosity in the vertical direction is significantly smaller than the lateral eddy viscosity. However, we will find later that the lateral eddy viscosity needed to explain measurements of longshore currents is an order of magnitude higher than what turbulence measurements justify. We will suggest there that the lateral mixing is being caused by some mechanism other than turbulence. If this is indeed the case, there is no reason why we can rule out the possibility of the lateral eddy viscosity being significantly larger than the vertical.

An alternative that was not pursued in the above consists of assuming that $\alpha_y/g \sim 1/\left(\rho c_b^2\right)\left(dS_{xy}/dx\right) \sim \varepsilon^3$. This may be justified on the basis that $B_0 \sin\alpha$ is probably much less than h_x and, therefore, it may be reasonable to assume that $\alpha_y/g \sim \sin\alpha B_0 \left(H/h\right)^2 h_x \sim \varepsilon^3$. In this case we could choose $\mathtt{N_{tz}} \sim \varepsilon^2$ and $\partial \mathtt{V}/\partial \mathtt{Z} \sim \varepsilon$. The term that represents the interaction of the longshore currents and the undertow will still be order ε^3. If we let $\mathtt{N_{tx}} \sim \mathtt{N_{tz}}$ or higher we find that the lateral mixing represented by this term will be negligible in the longshore momentum equation. At a first glance, this alternative seems to contradict the findings of Bowen (1969a) and Longuet-Higgins (1970) who found that the lateral mixing needs to be included to get realistic variations of the longshore current. However, note that the present equation has the interaction term that can potentially cause mixing and probably have an effect similar to that represented by the turbulent radiation stresses. This is explored in the next chapter.

In summary, the choices made here are $\mathtt{N_{tz}} \sim \varepsilon$, $\mathtt{N_{tx}} \sim 1$ and $\partial \mathtt{V}/\partial \mathtt{Z} \sim \varepsilon$. The following section uses these to devise a perturbation expansion to solve for the currents.

5.2.2 Perturbation expansion

Reverting back to dimensional variables we find that the arguments of the previous section imply that we may assume

$$V(x,\zeta) = V_0(x) + \epsilon V_1(x,\zeta) \tag{5.27}$$

with

$$\epsilon \ll 1 \tag{5.28}$$

Note that the small parameter ϵ used in this section is not necessarily equal to the parameter ε we used in the previous section. The ε used earlier was explicitly related to the slope. The ϵ used here only represents a small quantity. It need not be related to the slope.

Substituting (5.27) into (5.8) leads to

$$\frac{d}{dx}\left[h\nu_{tx}\frac{d(V_0+\epsilon V_{b1})}{dx}\right] - \left[\frac{\tau_{by}^0 + \epsilon\tau_{by}^1}{\rho}\right] - \frac{d}{dx}\left\{\int_{-h_0}^{\xi_t} \epsilon V_1 U\,dz + \epsilon\overline{\int_{\xi_t}^{\xi} V_1 u_w dz}\right\} = \frac{1}{\rho}\frac{dS_{xy}}{dx} \tag{5.29}$$

Separating the orders we have at order ϵ^0

$$\frac{d}{dx}\left(h\nu_{tx}\frac{dV_0}{dx}\right) - \frac{\tau_{by}^0}{\rho} = \frac{dS_{xy}}{dx} \tag{5.30}$$

This is the equation that has traditionally been used to solve for longshore currents (Bowen 1969a, Thornton 1970, Longuet-Higgins 1970). This is also the equation that Svendsen & Lorenz (1989) find at the lowest order in their perturbation scheme.

At order ϵ^1 we have

$$\frac{d}{dx}\left(h\nu_{tx}\frac{dV_{b1}}{dx}\right) - \frac{\tau_{by}^1}{\rho} - \frac{d}{dx}\left\{\int_{-h_0}^{\xi_t} V_1 U\,dz + \overline{\int_{\xi_t}^{\xi} V_1 u_w dz}\right\} = 0 \tag{5.31}$$

This equation is different from the corresponding equation derived by Svendsen & Lorenz. This difference arises from the fact that these authors neglected the UV terms in the governing equation. These are the terms that are responsible for the last term on the LHS of (5.31).

When (5.27) is substituted into equation 5.7 which governs the vertical structure of the longshore currents it yields

$$\frac{\partial}{\partial z}\left(\nu_{tz}\frac{\partial V_1}{\partial z}\right) = \frac{\partial}{\partial x}\left(\overline{u_w v_w} + UV_0\right) + \frac{\partial}{\partial z}\left(\overline{v_w w_w} + V_0 W\right) - \frac{\partial}{\partial x}\left(\nu_{tx}\frac{\partial V_0}{\partial x}\right) = \alpha_2(x,z) \quad (5.32)$$

The associated boundary conditions are that V_b is determined from (5.31) and using

$$\nu_{tz}\frac{\partial V_1}{\partial z}\Big)_{z=-h_0} = \frac{\tau_{by}^0}{\rho} = \frac{1}{2}f_w u_0\left[\beta_1 V_0 + \beta_2 u_0 \sin\alpha\right] \quad (5.33)$$

The condition as stated above assumes that $\nu_{tx}(\partial U/\partial x)(\partial h_0/\partial x)$ which represents $\tau_{yx}\partial h_0/\partial x$ in (2.35) has a negligible contribution to the bottom stress. Hence the solution to (5.32) becomes

$$V_1(x,\zeta) = \frac{\int_0^\zeta\int_0^\zeta \alpha_2 d\zeta d\zeta}{\nu_{tz}} + \frac{C_1}{\nu_{tz}}\zeta + V_{b1}(x) \quad (5.34)$$

where ζ is the distance from the bed (see figure 2.1). The constant V_{b1} can be solved for, in principle, by substituting (5.34) into (5.31) and solving (5.31) subject to $V_{b1} = 0$ at $x = 0, \to \infty$.

In order to complete the solution for the first order longshore current we need to evaluate the last term of (5.31), *viz.*, $\overline{\int_{\xi_t}^{\xi} V_1 u_w dz}$. This requires making assumptions regarding the current above trough level. For the present, we assume that $V_{b1} \ll V_0$ and that the near-bottom velocity is reasonably well approximated by V_0. The validity of this assumption depends on the magnitude of the last term of (5.31). This term depends on the depth variation of the currents and on how "current" is defined above trough level. If this term is small in comparison to dS_{xy}/dx then (5.31) indicates that V_{b1} is indeed much smaller than V_0 and the approximation made here is reasonable. Chapter 6 is devoted to an evaluation of the effect of the last term of (5.31). Particularly, section 6.5 discusses the impact of the assumptions regarding the current above trough level on the solution for longshore currents.

Under the approximations listed here the longshore current is given by

$$V(x,\zeta) = \frac{\int_0^\zeta\int_0^\zeta \alpha_2 d\zeta d\zeta}{\nu_{tz}} + \frac{C_1}{\nu_{tz}}\zeta + V_0(x) \quad (5.35)$$

where V_0 is given by the solution to (5.30). Substituting for α_2 we find that

$$V(\zeta) = V_b + \frac{\tau_{by}}{\rho\nu_{tz}}\zeta + \frac{\zeta^2}{\nu_{tz}}\left[\frac{1}{2}\frac{\partial}{\partial x}\left(\overline{u_w^2}\cos\alpha\sin\alpha\right) - \frac{\sin\alpha\cos\alpha}{4}\frac{\partial}{\partial x}\left(\overline{u_w^2}\right) + U_0\frac{\partial V_b}{\partial x} - \frac{1}{2}\frac{\partial}{\partial x}\left(\nu_{tx}\frac{\partial V_b}{\partial x}\right)\right] \quad (5.36)$$

where the fact that $v_w = |\mathbf{u_w}|\sin\alpha$ has been used to evaluate the integral of $\overline{v_w w_w}$.

5.3 The undertow solution

The undertow variation with z is governed by ($x-$ component of equation 2.41)

$$\frac{\partial}{\partial z}\left(\nu_{tz}\frac{\partial U}{\partial z}\right) = \frac{\partial}{\partial x}\left(\overline{u_w^2} + U^2\right) + \frac{\partial}{\partial z}\left(\overline{u_w w_w} + UW\right) + g\frac{\partial b}{\partial x} - \frac{\partial}{\partial x}\left(2\nu_{tx}\frac{\partial U}{\partial x}\right) = \alpha_1 \quad (5.37)$$

which may be integrated twice to yield

$$U(x,\zeta) = \frac{\int_0^\zeta \int_0^\zeta \alpha_1 d\zeta}{\nu_{tz}} + \frac{D_1(x)\zeta}{\nu_{tz}} + U_b(x) \quad (5.38)$$

where D_1 and U_b are given by applying the conditions

$$\rho\nu_{tz}\frac{\partial U}{\partial \zeta}\Big)_{\zeta=0} = \tau_{bx} = \rho\frac{f_w u_0}{2}\left\{\beta_1 U_b + \beta_2 u_0 \cos\alpha\right\} \quad (5.39)$$

and

$$\int_{-h_0}^{\xi_t} U dz = -Q_s \quad (5.40)$$

We need to evaluate the integrals of $\overline{u_w w_w}$ and $\overline{v_w w_w}$ in addition to to evaluating the integrals of UW and VW to determine α_1 and complete the solution for the current profiles. For symmetric waves on a a horizontal bottom $\overline{u_w w_w} = \overline{v_w w_w} = 0$. On a sloping bottom the waves can no longer be symmetric and these terms are, in general, non-zero. In the following we make a simple estimate of these terms. The estimates derived below are necessarily crude. Even outside the surf-zone, there are presently no acceptable estimates of these terms. A proper evaluation these terms requires that the problem of steep waves propagating on slopes be solved (see Otta 1992 for some discussions of the state of the art of this problem).

For the purposes of the derivation here we assume that the wave induced horizontal velocity is independent of the depth. We are concerned here with the variations below trough level and Hansen's (1990) analysis of experimental data suggests that in this layer the wave induced velocity is reasonably independent of the depth (this was also the assumption made in chapter 3, see figure 3.5).

We assume further that the effect of the current terms may be represented by the mean value of the undertow and the near bottom longshore current. For the case of the longshore current, this follows from the perturbation scheme devised earlier.

The wave induced vertical velocity can be determined from the continuity equation for the wave motion (this may be derived by subtracting the wave averaged continuity equation from the ensemble averaged continuity equation)

$$\frac{\partial w_w}{\partial z} = -\frac{\partial u_w}{\partial x} \tag{5.41}$$

This implies that

$$w_w(\zeta) = -\int_0^\zeta \frac{\partial u_w}{\partial x} d\zeta + w_w(\zeta = 0) \tag{5.42}$$

From the BBC for the wave motion we have

$$w_w(\zeta = 0) = -u_w \frac{\partial h_0}{\partial x} \tag{5.43}$$

Using the assumption that the wave induced horizontal velocity is independent of the depth below trough level we have

$$\overline{u_w w_w} = -\frac{\partial \overline{u_w^2}}{\partial x}\frac{\zeta}{2} - \overline{u_w^2}\frac{\partial h_0}{\partial x} \tag{5.44}$$

and

$$\int_0^\zeta \overline{u_w w_w} d\zeta = -\frac{\partial \overline{u_w^2}}{\partial x}\frac{\zeta^2}{4} - \overline{u_w^2}\frac{\partial h_0}{\partial x}\zeta \tag{5.45}$$

Returning to the undertow solution (5.38) we find that the undertow may be expressed as follows

$$U(\zeta) = U_b + \frac{\zeta}{\nu_{tz}}\left[D_1 - \frac{\partial h_0}{\partial x}\left(U_0^2 + \overline{u_w^2}\right)\right] + \frac{\zeta^2}{\nu_{tz}}\left[\frac{1}{2}\alpha_1' - \frac{1}{4}\frac{\partial\left(U_0^2 + \overline{u_w^2}\right)}{\partial x}\right] \tag{5.46}$$

where

$$\alpha_1' = \frac{\partial}{\partial x}\left(\overline{u_w^2} + U^2\right) + g\frac{\partial b}{\partial x} - \frac{\partial}{\partial x}\left(2\nu_{tx}\frac{\partial U}{\partial x}\right) \tag{5.47}$$

Using (5.39) the undertow solution may be expressed as

$$U(\zeta) = U_b + \frac{\tau_{bx}}{\rho\nu_{tz}}\zeta + \frac{\zeta^2}{\nu_{tz}}\left[\frac{1}{2}\alpha_1' - \frac{1}{4}\frac{\partial\left(U_0^2 + \overline{u_w^2}\right)}{\partial x}\right] \tag{5.48}$$

Substituting for α_1' we find that

$$U(\zeta) = U_b + \frac{\tau_{bx}}{\rho\nu_{tz}}\zeta + \frac{\zeta^2}{2\nu_{tz}}\left[g\frac{\partial b}{\partial x} + \frac{1}{2}\frac{\partial\left(U_0^2 + \overline{u_w^2}\right)}{\partial x} - \frac{\partial}{\partial x}\left(\nu_{tx}\frac{\partial U_0}{\partial x}\right)\right] \tag{5.49}$$

In terms of the above U_b is given by

$$U_b = -\frac{Q_s + \frac{\alpha_1'' h_t^3}{6\nu_{tz}} + \frac{\beta_2 f_w \sin\alpha (u_0 h_t)^2}{4\nu_{tz}}}{ht\left[1 + \frac{\beta_1 f_w u_0 h_t}{4\nu_{tz}}\right]} \tag{5.50}$$

where

$$\alpha_1'' = g\frac{\partial b}{\partial x} + \frac{1}{2}\frac{\partial\left(U_0^2 + \overline{u_w^2}\right)}{\partial x} - \frac{\partial}{\partial x}\left(\nu_{tx}\frac{\partial U_0}{\partial x}\right) \tag{5.51}$$

The longshore current solution described in an earlier section is derived by following a procedure very similar to the one described here for the undertow. In that derivation, the fact that $v_w = |\mathbf{u_w}| \sin\alpha$ was used.

5.3.1 Effect of the $\overline{u_w w_w}$ term on the undertow profile

In this section we will consider the effect of the $\overline{u_w w_w}$ on the depth variation of the currents. We will consider the undertow case in detail. The considerations for the longshore current are similar and lead to similar results.

Undertow profiles inside the surf-zone typically show rather strong seaward flows near the bed and either a shoreward flow or a weak seaward flow at trough level. Outside the surf-zone, however, the undertow profile shows remarkably different features. Typically it has a small seaward oriented velocity near the bed and a large seaward oriented velocity near the trough. The mean velocity changes direction above this level. This feature is apparent in all the undertow measurements indicated earlier. The measurements of Nadaoka & Kondoh (1982) indicate that this feature extends to some distance shoreward of breaking. Their results are reproduced here as figure 5.2. It turns out that the inclusion of the $\overline{u_w w_w}$ terms may be crucial in modelling this variation. The effect of the $\overline{u_w w_w}$ term is best demonstrated considering the situation seaward of the break point.

As indicated in chapter 3 we do not expect linear theory to provide quantitatively accurate information in the nearshore region. However, we anticipate that the qualitative features are captured by linear theory and since the aim of the following discussion is primarily qualitative we will use linear long wave theory below.

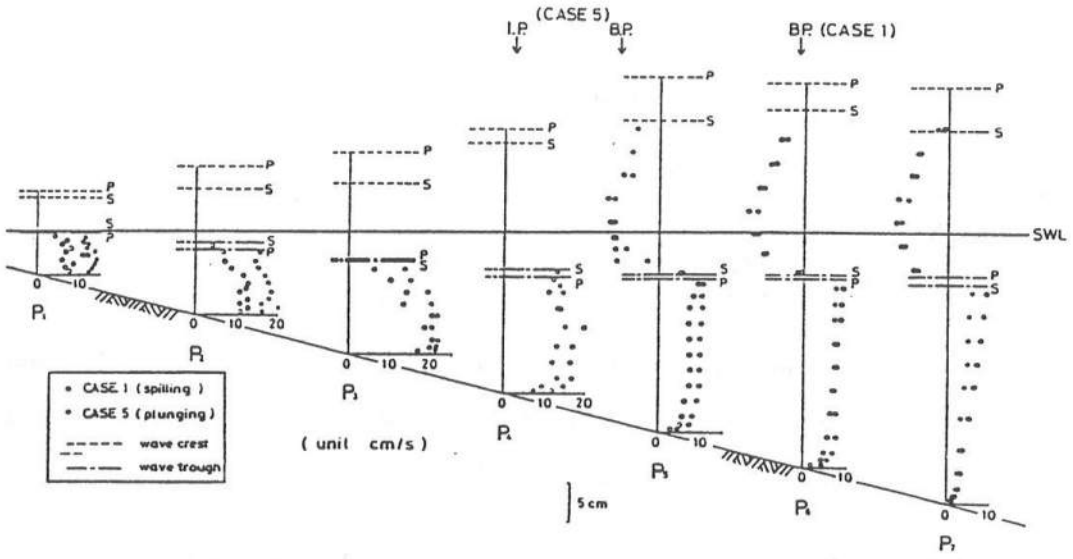

Figure 5.2: Undertow profiles measured by Nadaoka & Kondoh (1982)

Consider the wave averaged cross-shore momentum equation outside the surf-zone. Under the linear long wave approximation it reduces to

$$\frac{db}{dx} = \frac{3}{32}\left(\frac{H}{h}\right)^2 h_x \tag{5.52}$$

where the fact that energy conservation indicates that $H^2\sqrt{gh}$ is constant outside the surf-zone has been used. We also find, using linear long wave theory, that

$$\overline{u_w^2} = c^2\frac{\overline{\eta^2}}{h^2} = \frac{1}{8}gh\left(\frac{H}{h}\right)^2 \tag{5.53}$$

The above implies, after using the fact that $H \propto h^{-1/4}$, that

$$\frac{d}{dx}\overline{u_w^2} = -\frac{3}{16}\left(\frac{H}{h}\right)^2 h_x \tag{5.54}$$

Neglecting the terms arising from the mean velocity contributions the forcing for the undertow α_1 is given by (equation 2.41 suitably simplified)

$$\alpha_1 = \frac{\partial}{\partial x}\left(\overline{u_w^2}\right) + \frac{\partial}{\partial z}\left(\overline{u_w w_w}\right) + g\frac{\partial b}{\partial x} \tag{5.55}$$

We first consider what happens if the $\overline{u_w w_w}$ term is neglected in the above we find, after using (5.53) and (5.54), that

$$\alpha_1 = -\frac{3}{32}\left(\frac{H}{h}\right)^2 h_x \tag{5.56}$$

indicating that the curvature of the undertow profile is negative and therefore the shape of the undertow profile is similar to the undertow profiles one finds well inside the surf-zone which is different from what the observations show.

The derivation of the last section indicates that a reasonable estimate of the wave induced vertical velocity on a horizontal bottom yields

$$\frac{\partial}{\partial z}\left(\overline{u_w w_w}\right) = -\frac{1}{2}\frac{\partial}{\partial x}\left(\overline{u_w^2}\right) \tag{5.57}$$

Substituting this in (5.55) we find that $\alpha_1 = 0$. This indicates that the undertow profile will have no curvature. Using a linearized bottom friction law to relate the bottom stress to the near bottom velocity we find that the near bottom velocity U_b is given by

$$U_b = -\frac{Q_s}{h}\left(\frac{1}{1+\frac{f_w u_0 h_t}{2\pi\nu_{tz}}}\right) \tag{5.58}$$

Because Q_s is shoreward oriented the above indicates that U_b is seaward oriented. The the slope of the profile is given by $\tau_{bx}/(\rho\nu_{tz})[= f_w u_0 U_b/(\pi\nu_{tz})]$. Therefore, we find that the mean velocity at the trough level is seaward oriented and is significantly larger than the near bottom velocity. Above the trough level the mean velocity has to be oriented shorewards. This feature is similar to the observed undertow profiles and is crucially dependent on the inclusion of the $\overline{u_w w_w}$ term. This shows that the $\overline{u_w w_w}$ term plays a very important role in the predictions of the current profiles.

Considerations similar to the above indicate that in the longshore direction the inclusion of the $\overline{v_w w_w}$ reduces the curvature of the profile to a value that is one-fourth the value that one would have if the term is neglected.

Note that the above considerations do not account for changes in wave shape or the forcing arising from the current terms which will modify the forcing and introduce additional complications. The numerical results presented later on in this chapter have these terms included.

5.4 Some unresolved problems related to the longshore current distribution

In spite of all our knowledge about longshore currents – including the results in chapter 3 for the forcing there are still many unresolved questions particularly relating to the mixing mechanisms. In this section we try, by means of selected numerical experiments and comparisons with laboratory data to clarify the nature of the physical inconsistencies. We will restrict ourselves to the lowest order approximation $V_0(x)$ in this section. Some of the features considered here were also reported in Svendsen & Putrevu (1990).

For the purpose of discussion we use, in the next few sections, we will use an S_{xy} variation that corresponds to the P variation of Okayasu-Series 3, Case 1 and a 10° angle of incidence at breaking. This experiment was chosen because its results are typical for a 1/30 slope and we use this value for the slope in most of the examples below. The variation of S_{xy} used in the following is plotted in figure 5.3. In addition, unless otherwise specified, in the following calculations we use the quadratic bottom friction formulation with a constant value of f_w. The near-bottom longshore current is calculated using (5.30). The depth variation of the longshore current is given by (5.36). The undertow is calculated (5.49).

As discussed earlier outside the surf-zone $dS_{xy}/dx = 0$ under the assumptions of irrotational wave motion, energy conservation and validity of Snell's law (see appendix B).

5.4.1 Effect of the eddy viscosity formulation

The eddy viscosity is typically assumed to be the product of a length scale and a velocity scale. In the nearshore region the length scale is typically limited by the local depth and the velocity scale by the local wave speed. The form of the lateral eddy viscosity is, therefore, expected to be

$$\nu_{tx} = c_x h\sqrt{gh} \tag{5.59}$$

and the vertical eddy viscosity is expected to be given by

$$\nu_{tz} = c_z h\sqrt{gh} \tag{5.60}$$

As a model case, consider longshore currents on a 1/30 slope. Measurements of turbulence intensity (on slopes of the order 1/30) and analysis of these measurements show

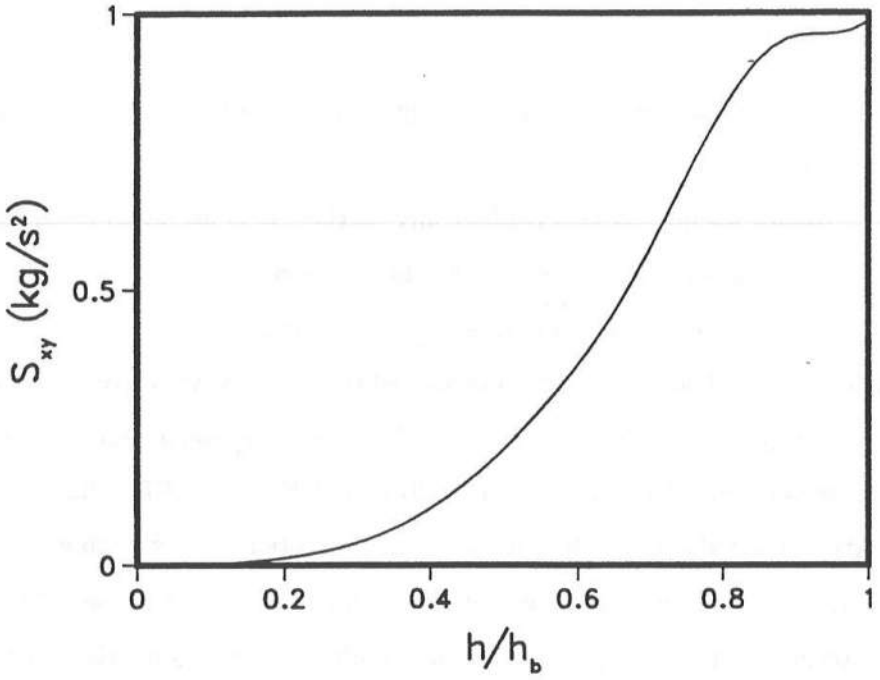

Figure 5.3: Forcing used for longshore current

(Nadaoka & Kondoh 1982; Stive & Wind 1982; Okayasu *et al.* 1986, 1988; Svendsen 1987; see section 6.1 for a brief summary of turbulence measurements and proposed models for mixing in the nearshore region)

$$\nu_{tz} \sim 0.01 h\sqrt{gh} \tag{5.61}$$

inside the surf-zone, *i.e.*, $c_z \sim 0.01$. Outside the surf-zone, the turbulence is much weaker.

Based on the magnitude of the turbulent fluctuations in the horizontal and vertical directions as a first guess one would assume that $\nu_{tx} \simeq \nu_{tz} \simeq 0.01 h\sqrt{gh}$. However, for ν_{tx} Longuet-Higgins (1970) assumes

$$\nu_{tx} = N x\sqrt{gh} \tag{5.62}$$

which for the constant slope considered here reduces to

$$\nu_{tx} = \frac{N}{h_x} h\sqrt{gh} \tag{5.63}$$

i.e., $c_x = N/h_x$. It is well known that using Longuet-Higgins formulation with $P \sim 0.5$ gives reasonable estimates of the longshore currents. In terms of P, N is given by $N = [\gamma f_w/(2\pi h_x)]P$ (see equation 5.5) which when substituted into (5.63) yields

$$\nu_{tx} = \frac{\gamma f_w}{2\pi h_x^2} P h \sqrt{gh} \tag{5.64}$$

which is about fifty times those values given (5.61) for $P = 0.5$ and typical values of the parameters ($\gamma = 0.8$, $f_w = 0.01$).

Before we discuss this conflict any further, it is useful to consider the effect of the variation of the eddy viscosity outside the surf-zone.

Effect of eddy viscosity outside the surf-zone

Outside the surf-zone, one expects the eddy viscosity to decrease rapidly. However, a sudden drop in the eddy viscosity would lead to a sharp increase in the slope of the longshore current. Bowen & Inman (1974) and Battjes (1975) discuss this problem but, to date, no satisfactory solution has been presented to this problem. Therefore, it is of some interest to study the effect of the assumed variation of the eddy viscosity outside the surf-zone on the longshore current prediction. To study the effect we examine the following four variations of eddy viscosity outside the surf-zone (ν_{tb} is the eddy viscosity at breaking)

1. $\nu_{tx} = \nu_{tb}/10 = \text{constant}$
2. $\nu_{tx} = \nu_{tb} = \text{constant}$
3. $\nu_{tx} = \nu_{tb}\,(h_b/h)^2$
4. $\nu_{tx} = \nu_{tb}\,(h_b/h)^4$

In the results presented here the eddy viscosity inside the surf-zone is assumed to be given by $\nu_{tx} = 0.1h\sqrt{gh}$. This high value of the lateral eddy viscosity will be found to be necessary below. Also in these calculations the quadratic bottom friction law was used and current refraction was neglected. We will show later on that the effect of the current refraction on the longshore current predictions is rather weak.

Figure 5.4 shows the longshore current distribution for these cases. The curve for case 1 above shows a sharp drop in the longshore current at break point and the longshore currents outside the surf-zone are much smaller than the other three cases. Longshore currents in cases 2-4 above are not very different from one another in an overall sense

even though the eddy viscosities used are quite different from one another. This indicates that while it is necessary to have a rather large value of eddy viscosity at break point the variation of eddy viscosity away from the break point has relatively little influence on the overall longshore current. The conclusion here is that while it is necessary to have a continuous variation of the eddy viscosity across the breaker line the eddy viscosity can be allowed to decay without significantly altering the overall predictions of longshore currents.

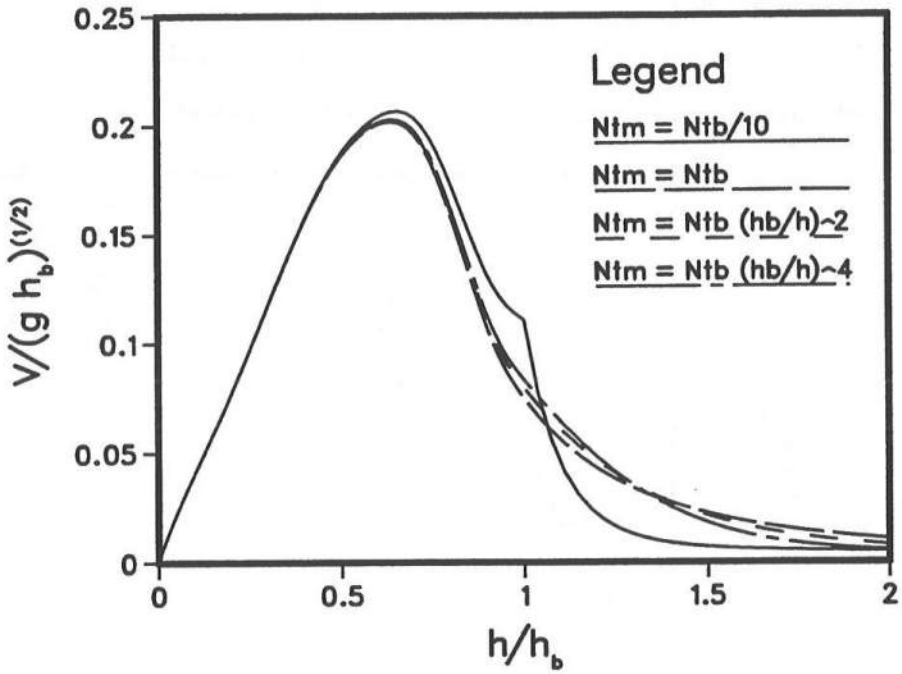

Figure 5.4: Effect of eddy viscosity outside the surf-zone

Effect of eddy viscosity inside the surf-zone

Figure 5.5 shows the variations of the longshore current for eddy-viscosities of $0.1h\sqrt{gh}$ and $0.01h\sqrt{gh}$ inside the surf-zone. These two values are chosen because the second of these gives the variation of the eddy viscosity that is expected based on turbulence characteristics and the first gives eddy viscosities of the order used by previous investigators (*e.g.*, Longuet-Higgins 1970).

Outside the surf-zone, the eddy viscosity is maintained at a constant level (equal to the value at breaking). This value, though high, does not influence the overall results substantially as discussed above. This plot shows essentially the same feature that Longuet-Higgins found with his parameter P. Decreasing the eddy viscosity increases the maximum velocity and makes the offshore gradient much steeper. Measurements of longshore currents show features similar to the higher value of the eddy viscosity (see, *e.g.*, Visser 1982, 1984) whereas measured turbulence levels suggest the lower value. This figure clearly demonstrates that the lateral eddy viscosity is significantly higher than that indicated by measurements of turbulence intensities indicating that the lateral mixing is probably being caused by a mechanism that is different from turbulence.

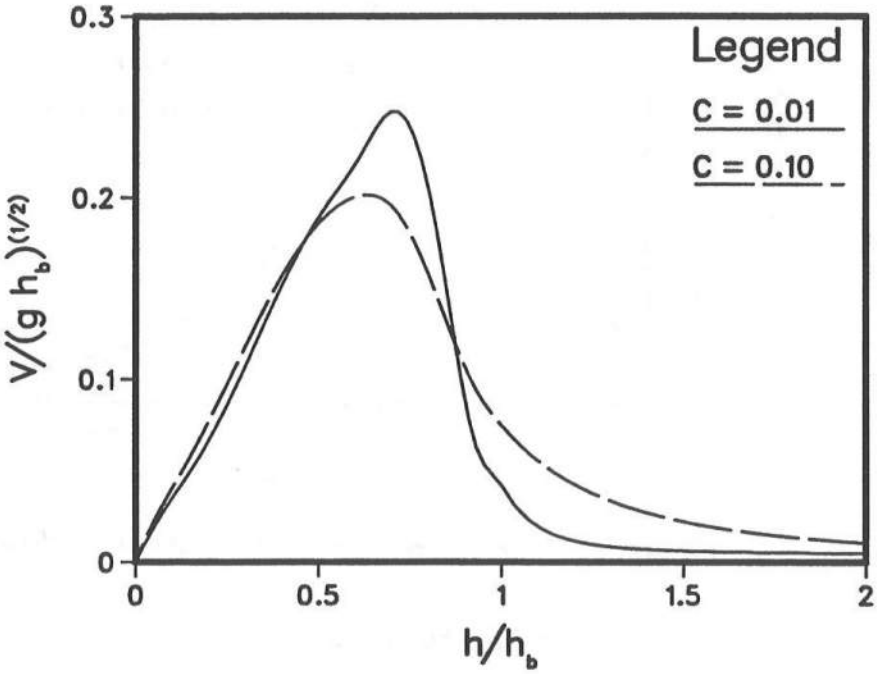

Figure 5.5: Effect of eddy viscosity inside the surf-zone

5.4.2 Effect of slope on the longshore current

At the present time, there is very little experimental evidence of the dependence of the longshore current on the slope. Therefore, it is of some interest to examine the dependence of the longshore current on the slope. Note that the results presented below

are of a speculative nature and require experimental verification before the conclusions can be accepted.

Figure 5.6 shows the variation of the longshore current with h/h_b for different slopes using $\nu_{tx} = 0.1h\sqrt{gh}$ inside the surf-zone and $0.1h_b\sqrt{gh_b}$ outside the surf-zone. For all the curves shown in figure 5.6 the wave height and water depth at breaking are the same (100 mm and 120 mm respectively). Since the slope varies the width of the surf-zone varies. This plot shows that that the milder the slope, the more it tends towards the triangular profile.

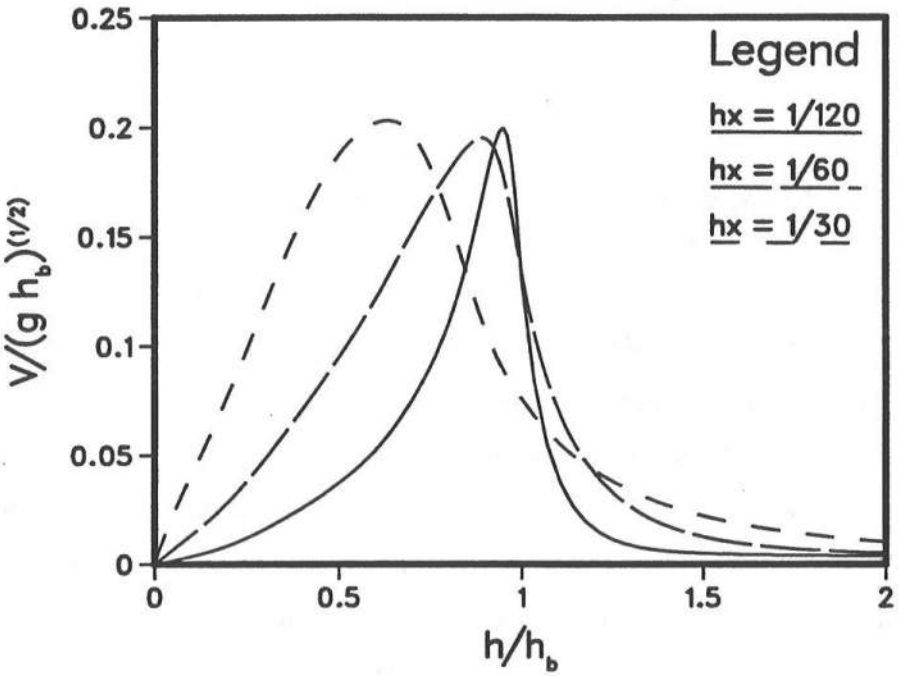

Figure 5.6: Effect of slope on the longshore current distribution

For simplicity, in the above c_x was maintained constant. The eddy viscosity is given by (assuming that the turbulence is the one that is causing the mixing)

$$\nu_t \sim l\sqrt{q^2} \tag{5.65}$$

where l is the length scale of the turbulent eddies and q^2 is the turbulent kinetic energy. If the conditions at breaking are maintained the same then the energy available for dissipation over the surf-zone is the same for all slopes. Since this dissipation is the source of

the turbulent energy, we expect that on steeper slopes the turbulence levels will be higher since the energy is dissipated over a shorter distance. This will lead to higher values of ν_t indicating that c_x should be proportional to the slope. Figure 5.6 indicates that even using a constant value of c_x leads to profiles which show smaller mixing on milder slopes. This result may be further understood by the following argument.

Assume that $h = h_x x$ and $H = \gamma h$. The governing equation for the longshore current reduces to (for a linearized bottom friction formulation)

$$P' \frac{d}{dx}\left(x^{2.5}\frac{dV}{dx}\right) - x^{1/2}V = Fx \tag{5.66}$$

where

$$P' = \frac{2\pi C_x h_x^2}{f_w \gamma} \tag{5.67}$$

$$F = \frac{5\pi}{8}\frac{\gamma h_x}{f_w}\frac{\sin\alpha}{c}h_x \tag{5.68}$$

which is the same equation which Longuet-Higgins (1970) solves and, therefore, will lead will lead to Longuet-Higgins' solution with P (defined by equation 5.5) of his solution replaced by P'. (5.67) indicates that P' decreases quite rapidly as h_x decreases if C_x is constant. The nature of Longuet-Higgins' solution indicates that P' is a measure of the mixing intensity and it decreases as P' decreases. Therefore, we conclude that if the lateral eddy viscosity is related to turbulence then on milder slopes the longshore current profile would lead to longshore current profiles that exhibit weaker mixing. This result is the opposite of what Longuet-Higgins' formulation for the eddy viscosity leads to.

5.5 Effect of current refraction

Kirby & Chen (1989) discussed the dispersion relationship for linear waves riding on a vertically sheared current. The problem of refraction of waves due to shear currents has not been addressed. For our purposes this is not a significant concern since it turns out that the effect of the current refraction is rather weak.

In order to demonstrate this we assume here that the effect of current refraction can be assessed by using a typical value of the current and not accounting for the vertical shear. For waves on currents without a vertical shear, Snell's law reads (see Jonsson 1990)

$$\frac{\sin\alpha}{c + V\sin\alpha + U\cos\alpha} = \frac{1}{C_0} \tag{5.69}$$

where C_0 is the Snell's constant.

In the following we study the effect of the refraction due to longshore currents and undertow. Let us first consider refraction due to the longshore current. Snell's law now reads

$$\frac{\sin\alpha_R}{c_R + V_R\sin\alpha_R} = \frac{\sin\alpha_2}{c_2 + V_2\sin\alpha_2} \tag{5.70}$$

where the subscript R refers to a reference location and the subscript 2 to the location of interest (typically shoreward of the reference location, therefore, typically $h_R > h_2$). The above implies that

$$\sin\alpha_2 = \sqrt{\frac{h_2}{h_R}}\sin\alpha_R \left\{1 + \frac{(V_R - V_2)\sin\alpha_R}{\sqrt{gh_R}}\right\}^{-1} \tag{5.71}$$

The implication of the above is that the depth refraction factor $\sqrt{h_2/h_R}\sin\alpha_R$ is multiplied by a modification factor. The maximum possible effect of current refraction is estimated by using $V_R = 0$. In this case, a 20% modification requires

$$\frac{V_2\sin\alpha_R}{\sqrt{gh_R}} \sim 0.2 \tag{5.72}$$

$$\Rightarrow \frac{V_2}{\sqrt{gh_R}} \sim \frac{0.2}{\sin\alpha_R} \sim 1 \tag{5.73}$$

The above implies that the local longshore Froude number $F_2 = V_2/\sqrt{gh_2}$ has to be significantly greater than one. Even for this rather strong longshore current the effect is quite modest. For most longshore current calculations the effect will be even smaller since typically V_R has the same sign as V_2 thus reducing the effect.

Next, let us consider the effect of the refraction due to the undertow. In this case Snell's law reads

$$\frac{\sin\alpha_R}{c_R + U_R\cos\alpha_R} = \frac{\sin\alpha_2}{c_2 + U_2\cos\alpha_2} = \frac{1}{C_0} \tag{5.74}$$

After a little algebra the above yields

$$\sin\alpha_2 = \frac{\sqrt{gh_2}}{C_0}\left\{\frac{1 + \sqrt{1 - [1 + (U_2/C_0)^2]\,[1 - U_2^2/gh_2]}}{1 + (U_2/C_0)^2}\right\} \tag{5.75}$$

The modification factor in the present case is the term in the parenthesis. It is relatively straightforward to show that the term under the square root sign in the modification factor is always positive and thus the above will always yield real solutions for α_2. The fact that the square root term is positive indicates that

$$\left[1+(U_2/C_0)^2\right]\left[1-U_2^2/gh_2\right] \leq 1 \tag{5.76}$$

$$\Rightarrow 1 \leq 1+(U_2/C_0)^2 \leq \frac{1}{1-U_2^2/gh_2} \tag{5.77}$$

We know that for a typical undertow $U_2/\sqrt{gh_2} \leq 0.2$ which then implies that $U_2^2/gh_2 \ll 1$ which, in turn, implies that $1+(U_2/C_0)^2 \approx 1$ and $1-U_2^2/gh_2 \approx 1$. Taken together, these indicate that the square root term is very small and therefore (5.75) may be approximated by

$$\sin\alpha_2 = \frac{\sqrt{gh_2}}{C_0}\frac{1}{1+(U_2/C_0)^2} \approx \frac{\sqrt{gh_2}}{C_0}\left\{1-\left(\frac{U_2}{C_0}\right)^2\right\} \tag{5.78}$$

Consider U_2/C_0. This quantity is given by

$$\frac{U_2}{C_0} = \frac{F_{u2}\sin\alpha_2}{1+F_{u2}\cos\alpha_2} \tag{5.79}$$

where, $F_{u2} = U_2/\sqrt{gh_2}$ is the local Froude number of the cross-shore current. It is relatively straightforward to show that the extremum of U_2/C_0 is given by

$$\left(\frac{U_2}{C_0}\right)_{ext} = \frac{F_{u2}}{\sqrt{1-F_{u2}}} \tag{5.80}$$

Even with the rather high value of $F_{u2} = 0.2$ we find that $(U_2/C_0)^2$ has a maximum possible value of 0.05. This implies that the maximum possible effect the undertow has on the refraction is about 5% on the wave angle.

Figure 5.7 demonstrates that the above considerations are valid. It compares the results for longshore currents with and without current refraction. A linearized friction formulation is used here in order to enhance the contribution from the longshore current to the refraction. The cases shown here include the case with full current refraction, only the refraction due to the longshore current accounted for and only the refraction due to the undertow accounted for.[8] The corresponding variations of the angle of incidence are shown in figure 5.8.

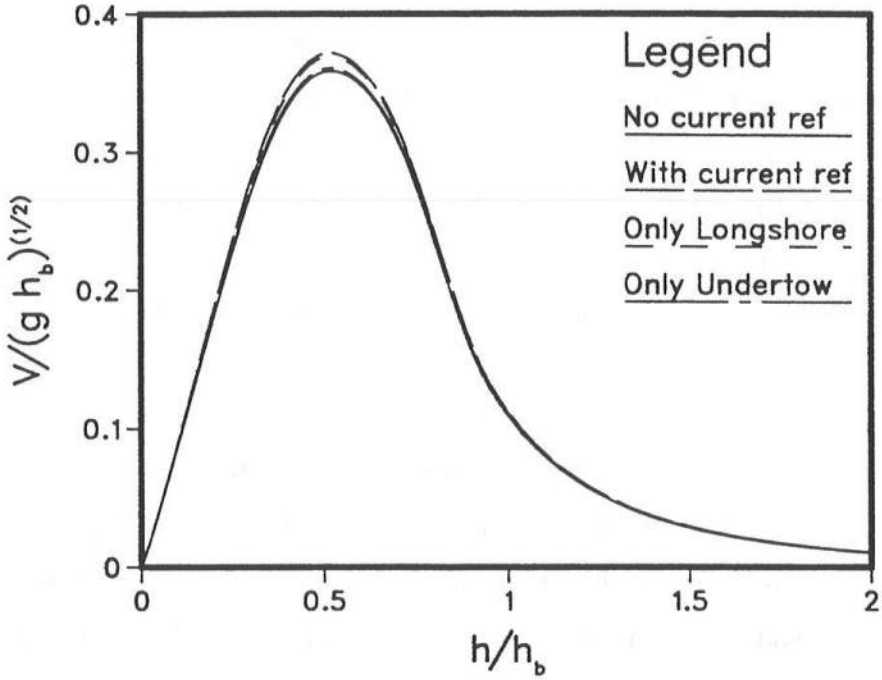

Figure 5.7: Effect of current refraction

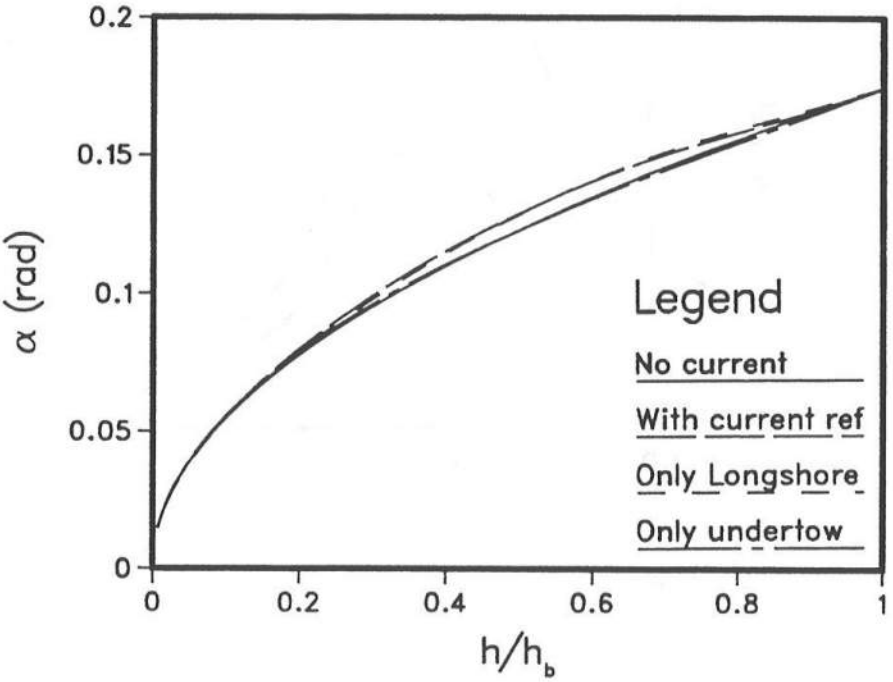

Figure 5.8: Effect of current refraction on the angle of incidence

These figures show that the the effect of the refraction due to the longshore current is modest in comparison with the depth refraction and that the refraction due to the undertow is almost imperceivable. This indicates that the current refraction is extremely small in comparison to the depth refraction. Thornton & Guza (1986) arrived at a similar conclusion while considering the effect of the refraction due to a longshore current.

Based on the above, we may conclude that under typical surf-zone conditions, refraction due to wave generated currents may be neglected without any significant loss of accuracy.

5.6 Comparison of linear and nonlinear friction formulations

Figure 5.9 compares the results for the linear and nonlinear bottom friction formulations. The nonlinear formulation is as described in the previous chapter. The linear formulation is derived by using $\beta_1 = 2/\pi$ and $\beta_2 = 0$ in the nonlinear version.

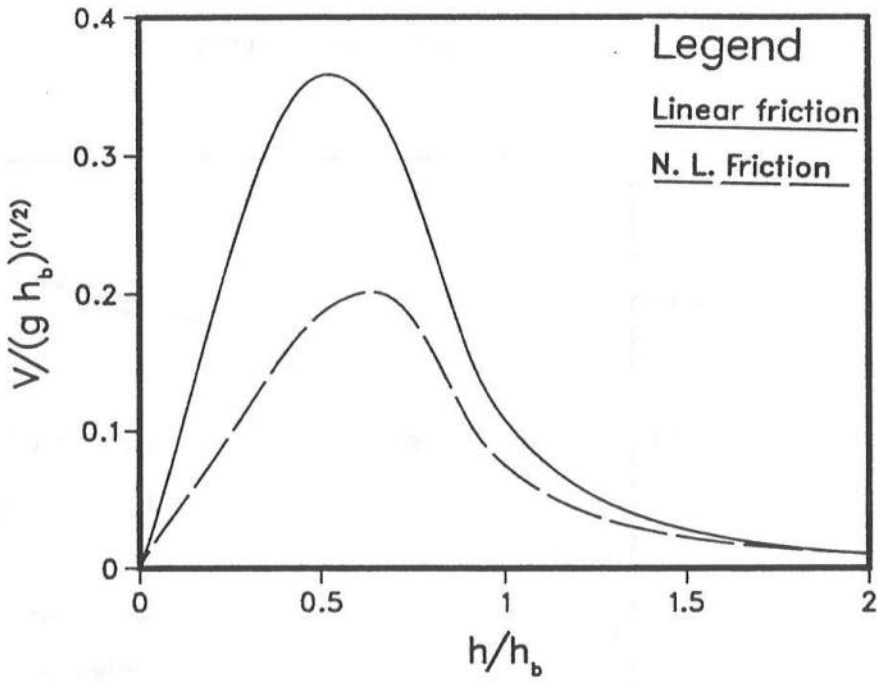

Figure 5.9: Comparison of linear and nonlinear friction

---

[6] The value of the current used for undertow refraction is calculated using $U = -Q_s/h$ where $Q_s = (1.3B_0 + B_r)\,H^2 c/h$. This estimate is based on (3.26) and the roller contribution.

Figure 5.9 shows that, if one uses the same f_w for the two formulations, then using the quadratic law reduces the velocities significantly. Liu & Dalrymple (1978) found a similar result for the case without an eddy viscosity.

5.7 Vertical structure of the currents

As discussed earlier, the undertow and cross-shore current have parabolic depth variations. The current vector at any depth is given by the superposition of the longshore current and undertow at that depth.

Figure 5.10 shows the variation of the dimensionless current vector (nondimensionalized by the local wave speed) with the nondimensional depth across the surf-zone. This figure shows that the current vector varies significantly with the vertical co-ordinate. The direction of the near-bottom current vector is quite different from the direction of the current vector at trough level. Near the break point and the shoreline the longshore current and the undertow have comparable magnitudes. At other locations the longshore current dominates over the undertow. This feature depends crucially on the angle of incidence of the waves. The undertow is relatively insensitive to the angle of incidence. Decreasing the angle of incidence will lead to smaller longshore currents and, therefore, the current vector will show significantly more variation. Increasing the angle of incidence will increase the longshore current and we will have the longshore current dominate over the undertow and the current vectors will show smaller variations.

5.8 Application to Visser's experiments

In this section we compare the results of our numerical computations with the experimental results of Visser (1982, 1984). The forcing in the longshore direction in these experiments was discussed in Chapter 3. As noted there, there is considerable uncertainty with the roller contribution for these experiments. This will of course lead to considerable uncertainty for the undertow calculations. Unfortunately, Visser did not measure the undertow which could have been used to eliminate some of that uncertainty.

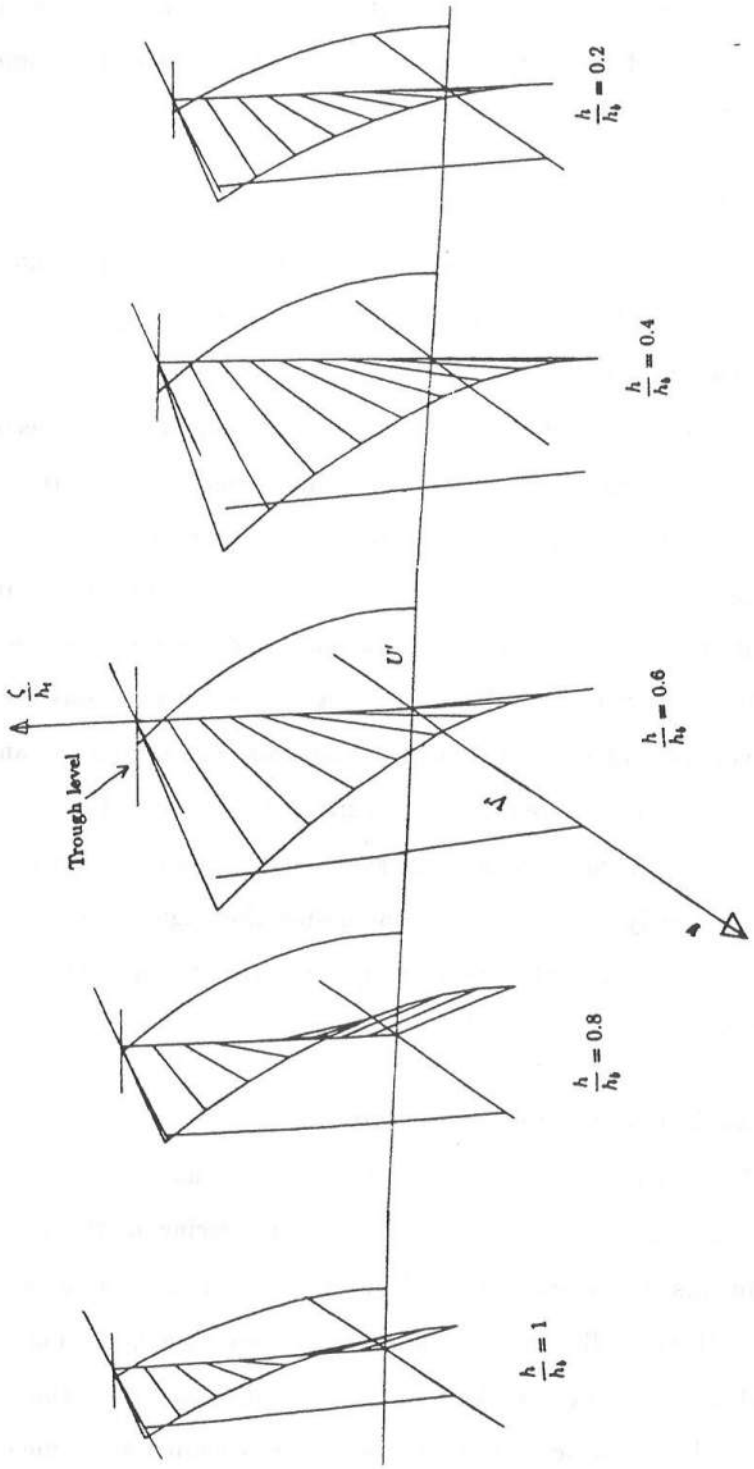

Figure 5.10: Variation of the current vectors across the surf-zone

5.8.1 Description of Visser's experiments

As discussed briefly in chapter 3, Visser conducted measurements of longshore currents in a laboratory wave basin. His experimental layout is presented in figure 5.11.

To maintain uniformity of the longshore current, he pumped water into the basin at one end and sucked it out at the other using a recirculation system. He found that the pumped water induced a "recirculation flow" (a current in the opposite direction of the longshore current seaward of the break point) in a region far seaward of the break point. He found that there was least alongshore nonuniformity for the case when this "recirculation" flow was minimized.

Visser indicates that the wave climate was not completely uniform in the alongshore direction. The wave heights were found to vary $\pm 10\%$ from the mean values. This feature would undoubtedly have contributed to the nonuniformity in the alongshore direction of the longshore current.

The set-up and wave height reported were the average values for two sections (sections 1 and 2). The set-up has to be calculated from the reported value of the mean depth. Visser does not indicate how uniform the set-up was in the alongshore direction.

Table 5.1 lists relevant measurements of Visser. ($x = 0$ corresponds to the mean shoreline.) Note that these experiments have quite a few measurements of local longshore Froude number $V/\sqrt{gh}$ close to or larger than one indicating extremely strong longshore currents. Also, note the extremely strong longshore currents *shoreward* of the mean shoreline in experiments 2 and 3 ($V = 21.7cm/s$ and $19.4cm/s$ at $x = -0.03m$ and $-0.02m$ respectively) and the strong longshore current in experiments 1 and 5 just seaward of the mean shoreline. While the strong longshore currents at other locations may be attributed to the rather large angles of incidence, the measurements near the mean shoreline are probably related to the nonlinear effects of the run-up on steep slopes. These effects are not captured in the present wave averaged model as the present model is not capable of predicting quantities in the swash zone.

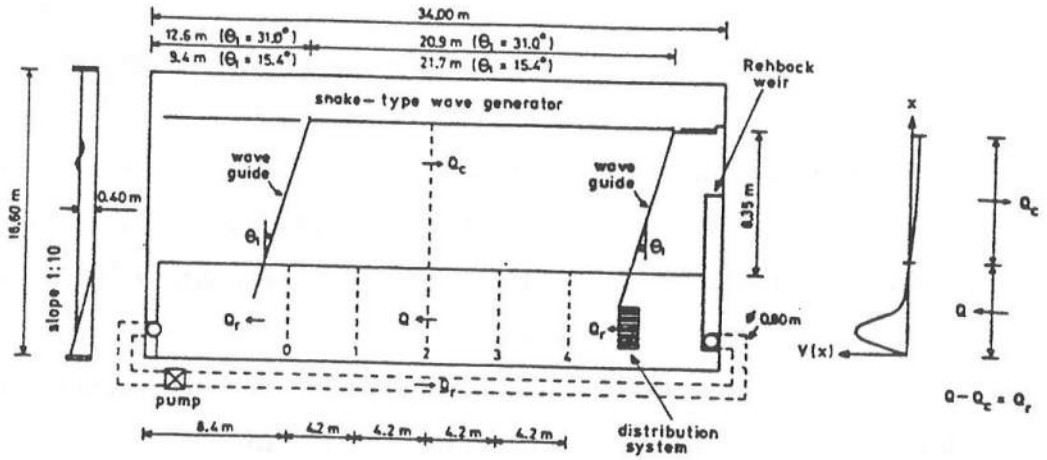

Plan view of wave basin (slope 1 : 10).

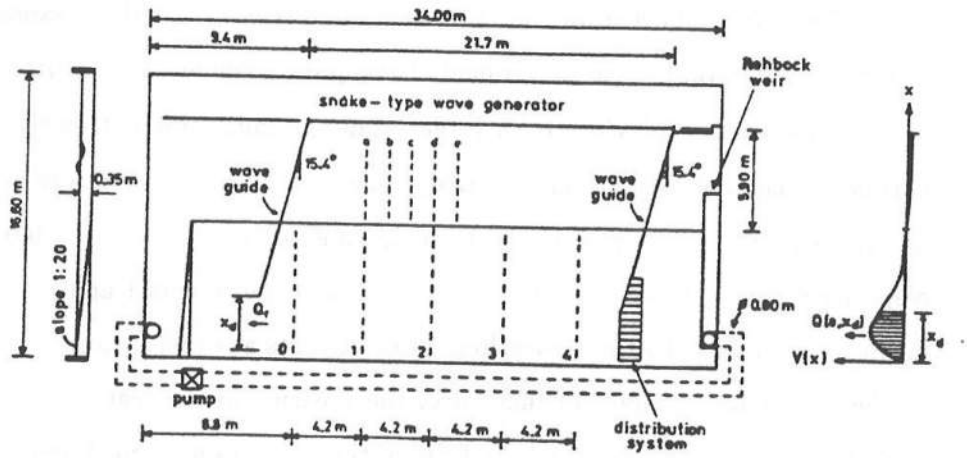

Plan view of wave basin (slope 1 : 20).

Figure 5.11: Visser's experimental layout

Table 5.1: Visser's measurements for experiments 1-5

Experiment 1								
x (m)	0.10	0.30	0.50	0.70	0.90	1.10	1.30	1.50
h (cm)	0.5	1.5	2.5	3.5	4.8	6.5	8.6	10.6
V (cm/s)	39.6	59.4	66.2	65.9	59.2	43.2	28.7	18.8
$V/\sqrt{gh}$	1.79	1.55	1.34	1.12	0.86	0.54	0.31	0.18
x (m)	1.70	1.90	2.10	2.30	2.50	2.70	3.10	
h (cm)	12.7	14.7	16.7	18.7	20.7	22.7	26.7	
V (cm/s)	12.4	8.3	6.0	4.1	2.8	1.9	1.1	
$V/\sqrt{gh}$	0.11	0.07	0.05	0.03	0.02	0.01	-	
Experiment 2								
x (m)	-0.03	0.17	0.37	0.57	0.77	0.97	1.17	1.37
h (cm)	-	1.2	2.6	4.2	5.4	6.8	8.8	10.8
V (cm/s)	21.7	63.1	71.0	72.0	66.2	57.5	43.0	31.6
$V/\sqrt{gh}$	-	1.84	1.40	1.12	0.91	0.70	0.46	0.31
x (m)	1.57	1.77	1.97	2.17	2.37	2.57	2.97	
h (cm)	12.8	14.8	16.8	18.8	20.8	22.8	26.8	
V (cm/s)	23.0	15.8	10.5	6.6	4.2	2.2	0.6	
$V/\sqrt{gh}$	0.21	0.13	0.08	0.05	0.03	0.01	-	
Experiment 3								
x (m)	-0.02	0.18	0.38	0.58	0.78	0.98	1.18	1.38
h (cm)	-	1.2	2.4	3.8	6.1	6.8	8.8	10.8
V (cm/s)	19.4	42.0	45.8	47.1	45.3	41.9	34.8	26.8
$V/\sqrt{gh}$	-	1.22	0.94	0.77	0.64	0.51	0.37	0.26
x (m)	1.58	1.78	1.98	2.18	2.38	2.58	2.98	
h (cm)	12.9	15.0	17.0	19.0	21.0	23.0	27.0	
V (cm/s)	20.3	14.5	9.3	5.8	3.7	2.3	0.8	
$V/\sqrt{gh}$	0.18	0.12	0.07	0.04	0.03	0.02	-	

Table 5.1: Continued

Experiment 4								
x (m)	0.01	0.21	0.41	0.81	1.21	1.61	2.01	2.41
h (cm)	0.2	0.9	1.8	3.6	5.3	6.9	8.5	10.5
V (cm/s)	0	13.3	23.2	35.4	40.4	39.4	30.4	21.1
$V/\sqrt{gh}$	0	0.45	0.55	0.60	0.56	0.48	0.33	0.21
x (m)	2.81	3.21	3.61	4.01	4.41	4.81	5.21	5.61
h (cm)	12.4	14.5	16.6	18.6	20.6	22.6	24.6	26.6
V (cm/s)	13.4	9.1	5.3	2.7	1.1	0.5	-0.1	-
$V/\sqrt{gh}$	0.12	0.08	0.04	0.02	-	-	-	-
Experiment 5								
x (m)	0.12	0.32	0.52	0.92	1.32	1.72	2.12	2.52
h (cm)	0.8	1.5	2.2	3.7	5.1	6.5	8.2	10.3
V (cm/s)	10.3	18.3	26.0	36.8	40.7	40.1	33.9	26.5
$V/\sqrt{gh}$	0.37	0.48	0.56	0.61	0.58	0.50	0.38	0.26
x (m)	2.92	3.32	3.72	4.12	4.52	4.92	5.32	5.72
h (cm)	12.3	14.3	16.4	18.4	20.4	22.4	24.4	26.4
V (cm/s)	18.8	11.3	6.2	2.8	1.2	0.7	0.3	-
$V/\sqrt{gh}$	0.17	0.10	0.05	0.02	-	-	-	-

5.8.2 Numerical results for Visser's experiments

The calculations presented here, have the eddy viscosity outside the surf-zone maintained at the level at breaking. The nonlinear bottom friction formulation has been used. Also, the current refraction has been included although, as discussed earlier, this does not alter the results very much.

The adjustable model parameters in the computation are the eddy viscosity coefficient and the friction factor. There are three possible sources of the error. They are:

1. The forcing;
2. The bottom friction and
3. The mixing.

The forcing for these experiments was already discussed in chapter 3 where it was also shown that the uncertainties involved in the determination of the forcing were expected to be less than about 10-20%.

The principal uncertainty in the bottom friction comes from using a constant value of f_w for all relative magnitudes of wave and current velocities. As indicated in chapter 4, we expect the friction factor to be vary with the relative strength of the wave and current velocities and, therefore, vary with the cross shore location. Another possible source of uncertainty is associated with the use of a sinusoidal time variation for the wave induced velocity.

Using a time variation that is different from a sinusoidal one would lead to a mean bottom friction formulation similar to a mean bottom friction given by an equation similar to (4.6) with $\cos\omega t$ in β_1 and β_2 replaced by $F(t)$, the periodic variation used. It is easy to show that for the weak current case both β_1 and β_2 are proportional to $\overline{|F(t)|}$. Therefore, the error incurred in β_1 and β_2 may be absorbed by redefining the friction factor. Since f_w is unknown and one of the adjustable parameters of the model we conclude that, for a weak current, using a sinusoidal time variation for the wave induced velocity causes no error as far as the model results are concerned.

The situation is somewhat different for the strong current case. In this case we will have $\beta_1 \rightarrow (\overline{U}/u_0)$ and $\beta_2 \rightarrow \overline{F^2}\cos(\mu - \alpha)$. In this case a non-sinusoidal time variation of the wave induced velocity causes an error which cannot be absorbed by a simple redefinition of the friction factor. However, for this case, (4.6) indicates that the contribution from the β_2 term to the mean bottom stress is negligible. Therefore, for the strong current case, the error incurred by using a sinusoidal time variation is negligible.

Based on the above we expect that, in the general case, the error induced by using a sinusoidal time variation for the wave induced velocity will be relatively minor as far as the frictional formulation is concerned.

The frictional resistance when integrated across the extent of the longshore current should equal the total forcing. If the frictional resistance were linear in the velocity the area under the measured velocity profile would be proportional to the total forcing and this could be used to estimate the friction factor. The quadratic law changes the situation somewhat. Nevertheless, we expect that the area under the measured profile gives an estimate of the total frictional resistance.

The mixing term redistributes the velocity profile and has no contribution net contribution when integrated over the entire extent of the longshore current. If the forcing is accurately estimated and the friction is properly formulated then errors in predictions of longshore currents can be attributed to incorrect modelling of the mixing.

Figures 5.12 through 5.16 show the variations predicted by the numerical model. The criterion used for the optimization is a reasonable reproduction of the maximum velocity and an approximate reproduction of the total area under the measured velocity profiles (both based on a visual judgement). The friction factors and eddy viscosity coefficients used are also indicated on the figures.

These figures show that the measurements are fairly well reproduced in experiments 1 and 2. Experiments 4 and 5 show good agreement with the measured values up to the maximum longshore current. Seaward of this location the longshore current is underpredicted by the numerical model. Seaward of the break point the numerical model severely overpredicts the longshore currents in experiments 4 and 5. Results for experiment 3 show

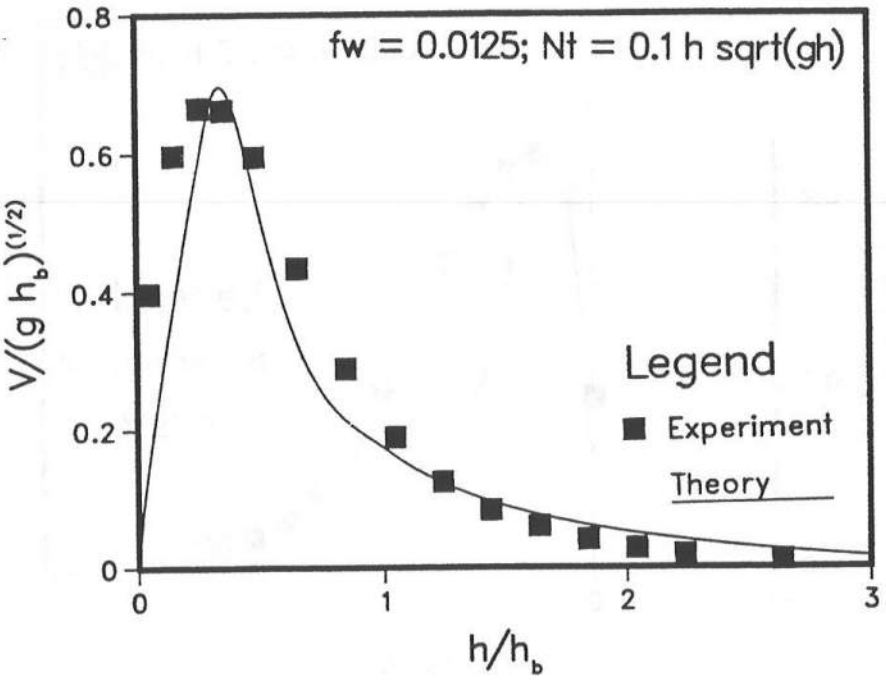

Figure 5.12: Comparison of measured and predicted longshore currents for Visser's experiment 1

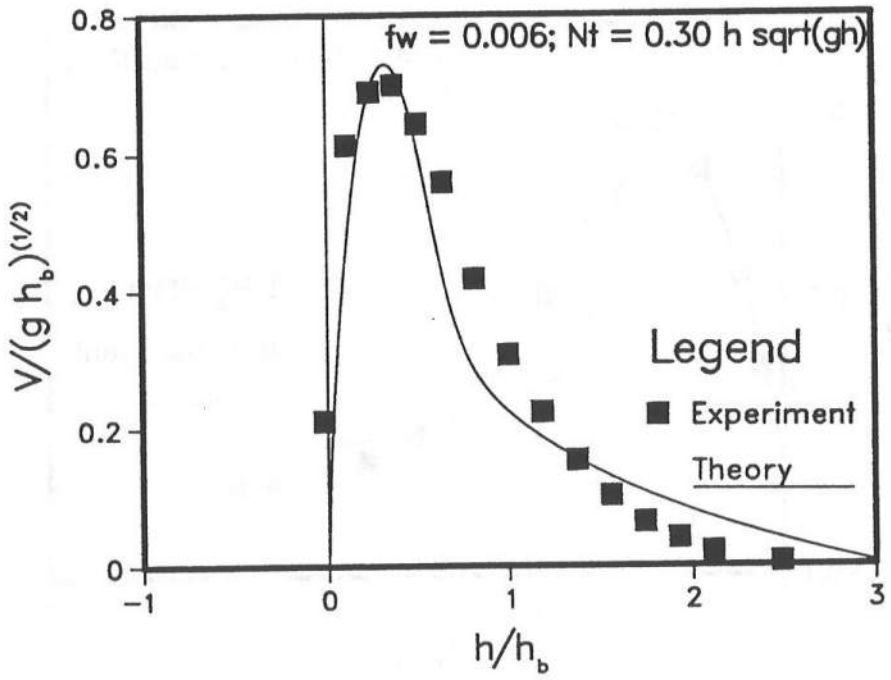

Figure 5.13: Comparison of measured and predicted longshore currents for Visser's experiment 2

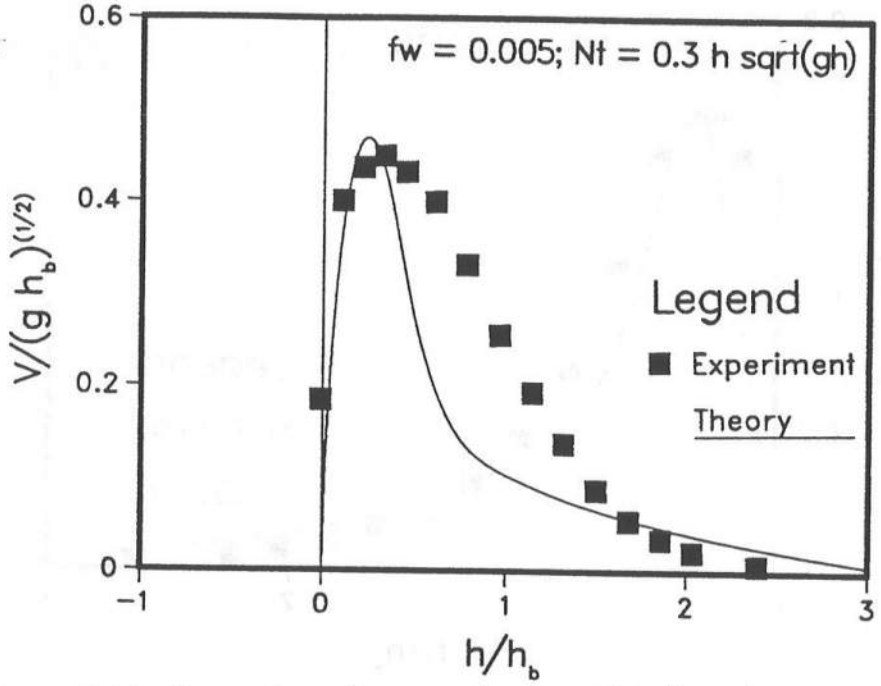

Figure 5.14: Comparison of measured and predicted longshore currents for Visser's experiment 3

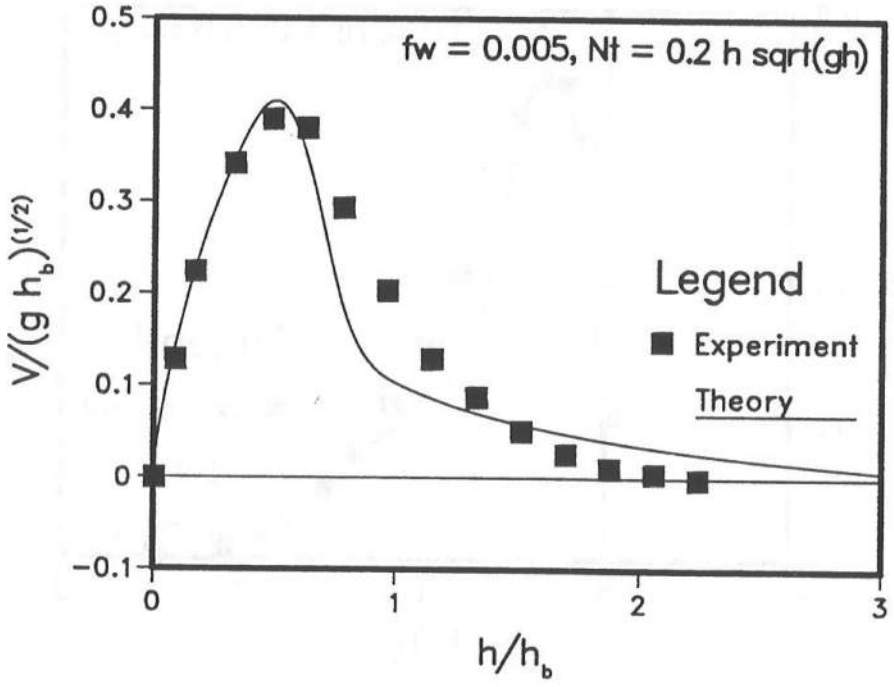

Figure 5.15: Comparison of measured and predicted longshore currents for Visser's experiment 4

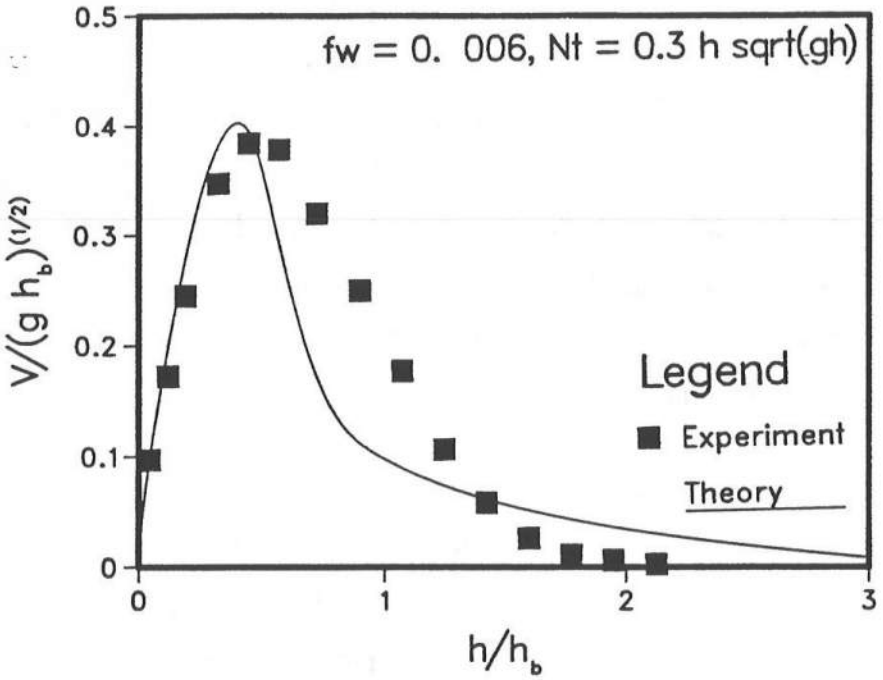

Figure 5.16: Comparison of measured and predicted longshore currents for Visser's experiment 5

similar qualitative features but the quantitative comparison is rather poor. This was also the experiment that showed unusually large values of P in chapter 3.

A general feature in all the comparisons is that seaward of the maximum velocity location the longshore current is underpredicted and seaward of the break point the longshore current is overpredicted by the numerical solution. This indicates that the experiments probably had a larger level of mixing between the maximum velocity location and the breaker line and a smaller value of the mixing further seaward. The second of these is readily understandable since we maintain the mixing level outside the surf-zone at the breaking value. The results presented in figure 5.4 indicate that changing the eddy viscosity outside the surf-zone will not alter the overall results significantly and hence will not improve the overall solution. Furthermore, it is possible that the recirculation flow may have affected the measured velocities in this region.

No effort was made here to fine tune the model parameters so as to get the best fit (say in a least square sense) with the experimental results. The principal aim of the plots

presented here was to demonstrate that very high levels of the eddy viscosity coefficient are required to reasonably predict longshore current profiles. Note that for all the experiments a reasonable prediction of the longshore current requires $c_x \approx 0.1-0.3$. This is, as indicated earlier, a significantly larger value than what the turbulence measurements inside the surf-zone justify. An additional indication of the fact that the lateral eddy viscosity may be caused by a different mechanism than the one that causes the vertical mixing comes from the predictions of the vertical structure of the currents. The prediction of the vertical structure of the currents is dealt with in the following.

5.8.3 Vertical structure of the currents

The predicted depth variations of the longshore currents are shown in figures 5.17 through 5.21. These have been calculated using $\nu_{tz} = 0.02h\sqrt{gh}$. Figure 5.22 shows the variation measured by Visser (1982). Corresponding undertow variations are shown in figure 5.23 through 5.27.

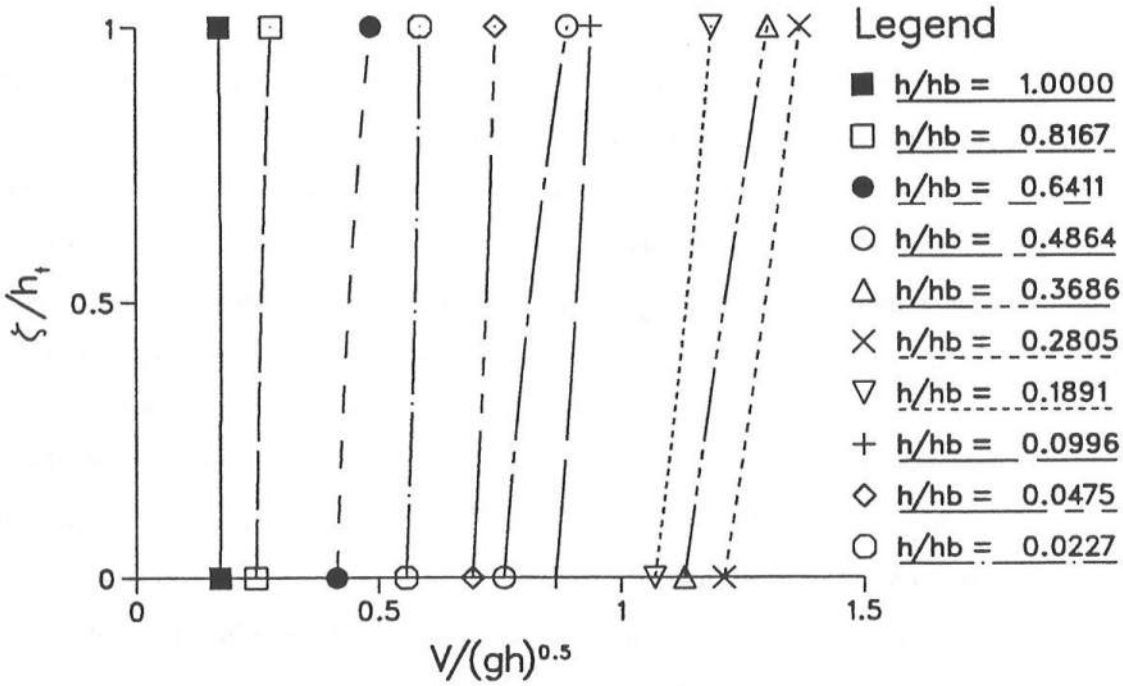

Figure 5.17: Predicted depth variations for Visser's experiment 1

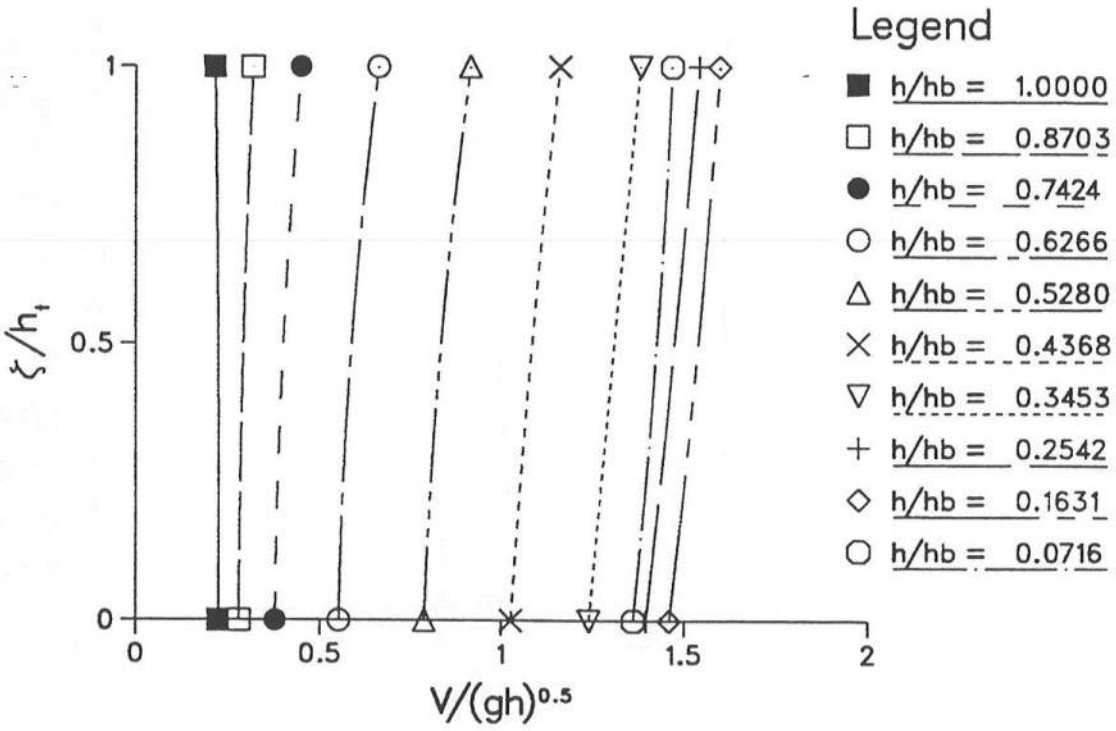

Figure 5.18: Predicted depth variations for Visser's experiment 2

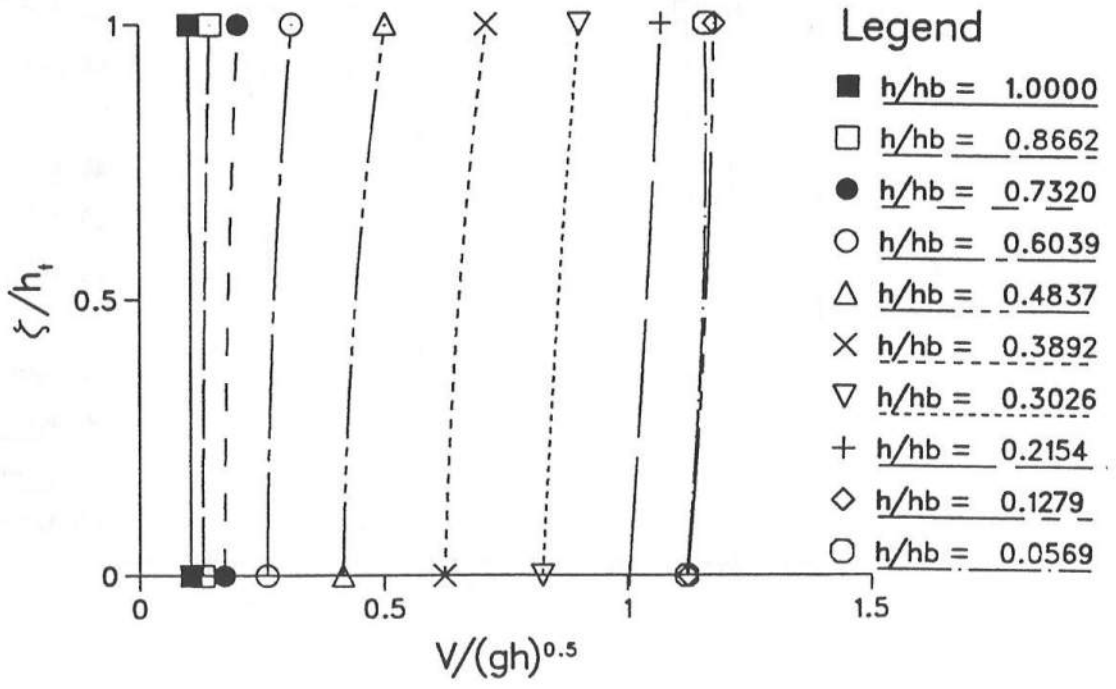

Figure 5.19: Predicted depth variations for Visser's experiment 3

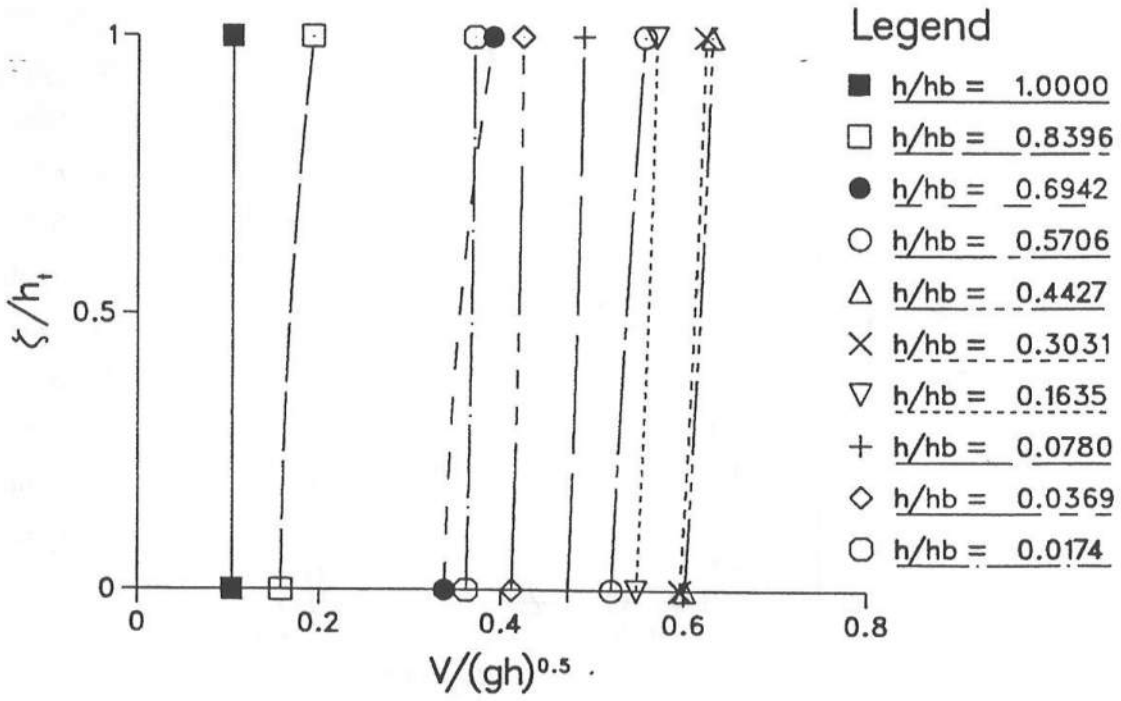

Figure 5.20: Predicted depth variations for Visser's experiment 4

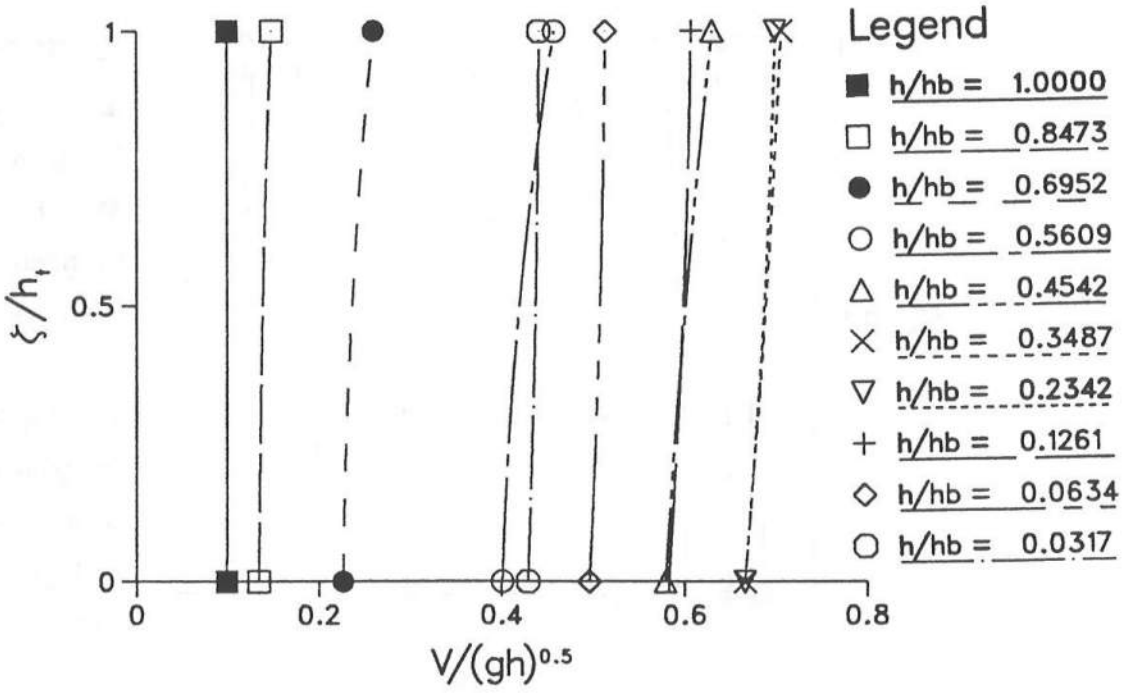

Figure 5.21: Predicted depth variations for Visser's experiment 5

The figures for the longshore currents show relatively small variations over depth. The curvature of the profiles is small. Both these features are consistent with Visser's measurements. The longshore current calculations show that the inclusion of the $\overline{v_w w_w}$ term does reduce the curvature of the profile as anticipated earlier.

The undertow shows more variation in the vertical. In the transition zone (which covers a significant fraction of the surf-zone for these experiments) the undertow profiles show very little curvature and relatively large seaward oriented velocities. In experiments 4 and 5 we see one particular undertow profile ($h/h_b \approx 0.85$) which has a negative curvature and a strong seaward directed cross-shore current. These features are generally consistent with measurements of undertow profiles from other experimental sources.

It is interesting to note that in the inner surf-zone the nondimensional results for the undertow profiles are very close to one another in experiments 1-3. The same is true for undertow profiles close to the shore in experiment 4. Note that in these regions the slope of the mean water surface is constant (see figure 3.2) and that the wave height to water depth ratio does not vary very much in this region (H/h does vary somewhat for experiment 2 in the region under consideration but the variation is less than 15%). The fact that the nondimensional undertow profiles are quite close to one another may be explained in terms of the following argument.

Let us assume that

- h_x = constant
- A linearized bottom friction
- $H/h = \gamma$ = constant
- $Q_s = B_q H^2 \sqrt{gh}/h$

Under these assumptions it is relatively straightforward to show that the nondimensional undertow profile is given by (see appendix C)

$$\frac{U}{\sqrt{gh}} = \epsilon_u + \epsilon_b \frac{\zeta}{h} + \epsilon_a \left(\frac{\zeta}{h}\right)^2 \tag{5.81}$$

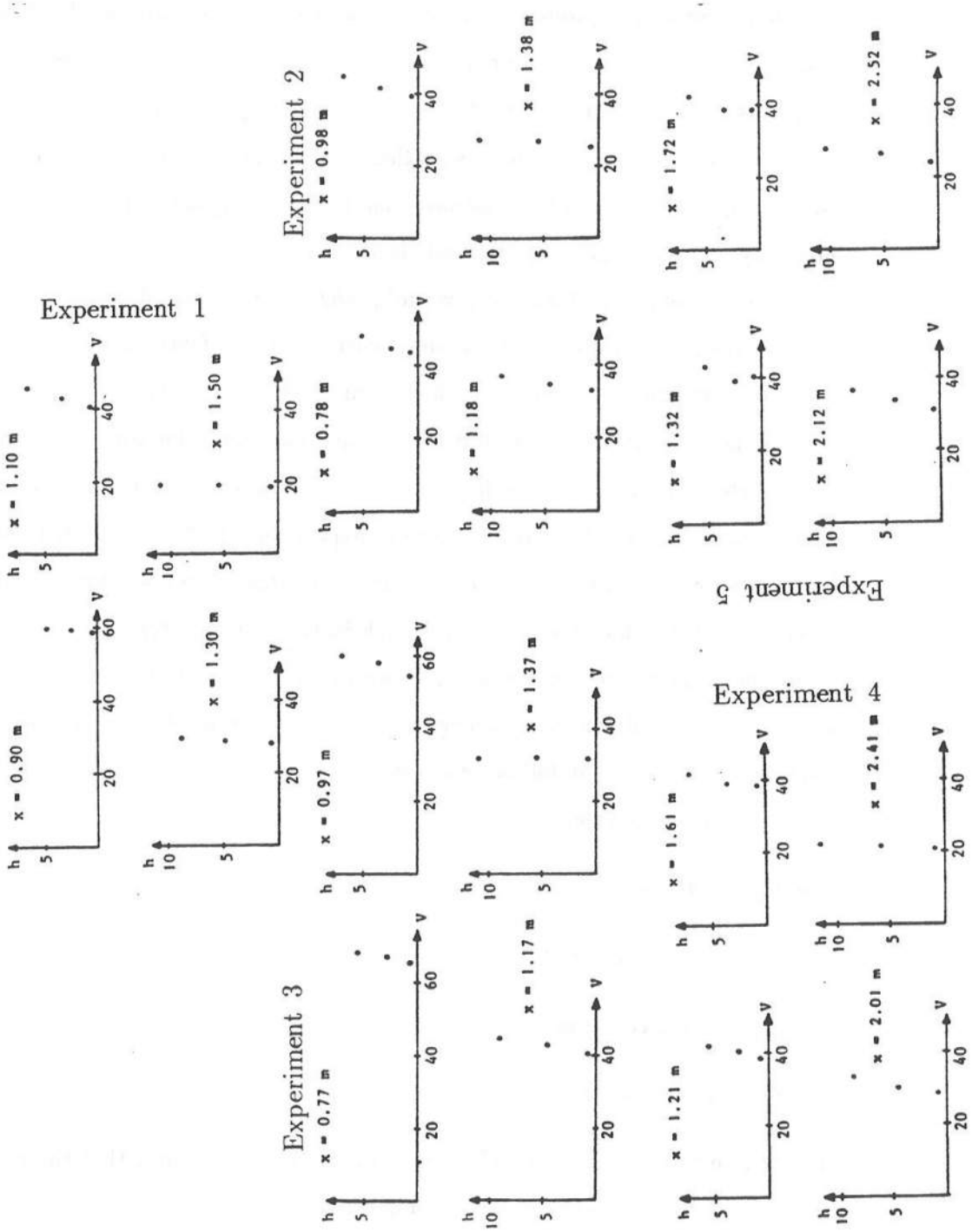

Figure 5.22: Depth variations measured by Visser

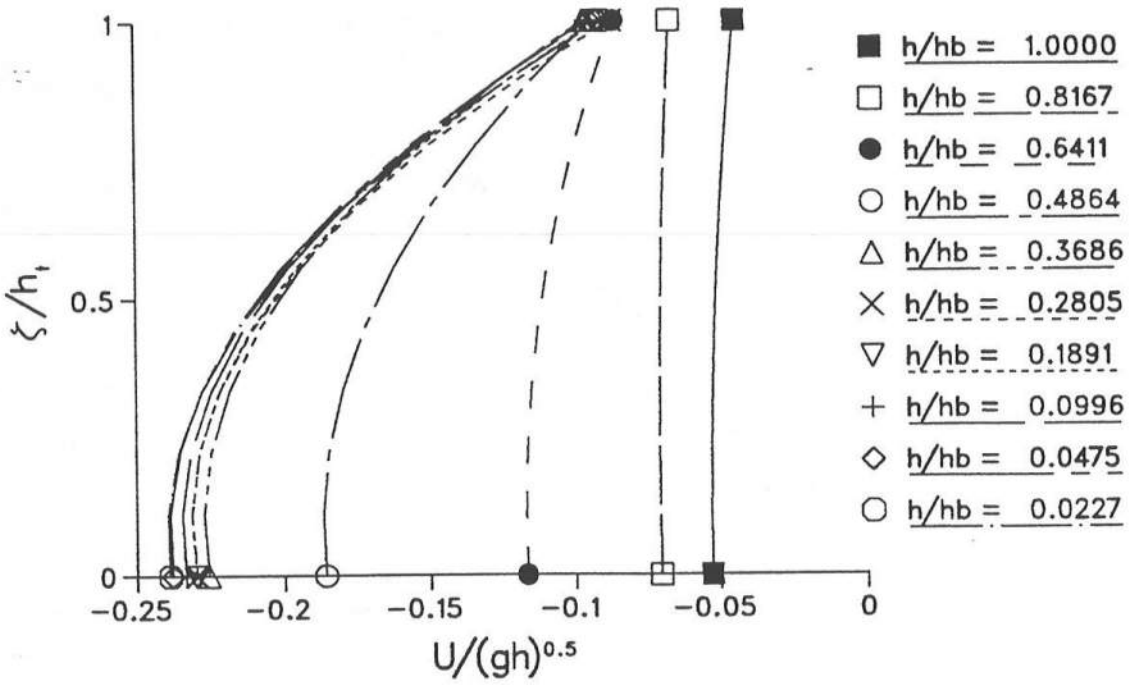

Figure 5.23: Undertow predictions for Visser's Experiment 1

where the ϵ's are as defined in appendix C. This solution shows that if the assumptions are satisfied then the nondimensional undertow solution should be independent of the cross-shore location. The small differences in the solutions at the various locations of the inner surf-zone may be attributed to nonlinearity of the bottom stress, variations in the shape factors, wave height to water depth ratios, *etc.* In experiment 5 we find no region in which b_x stays approximately constant. Therefore, we do not find self-similar undertow profiles in this experiment.

If the vertical eddy viscosity were to be increased by a factor of ten (to match the horizontal value), we would see hardly any variation over depth for both the longshore current and the undertow. Visser's measurements of the vertical structure of the longshore current indicate that the longshore current has some vertical structure. The undertow measurements from other sources indicate that the undertow has significant vertical structure and that the variation we would get by using the larger eddy viscosity would be completely unreasonable.

Note that the vertical values of the eddy viscosity are consistent with the levels

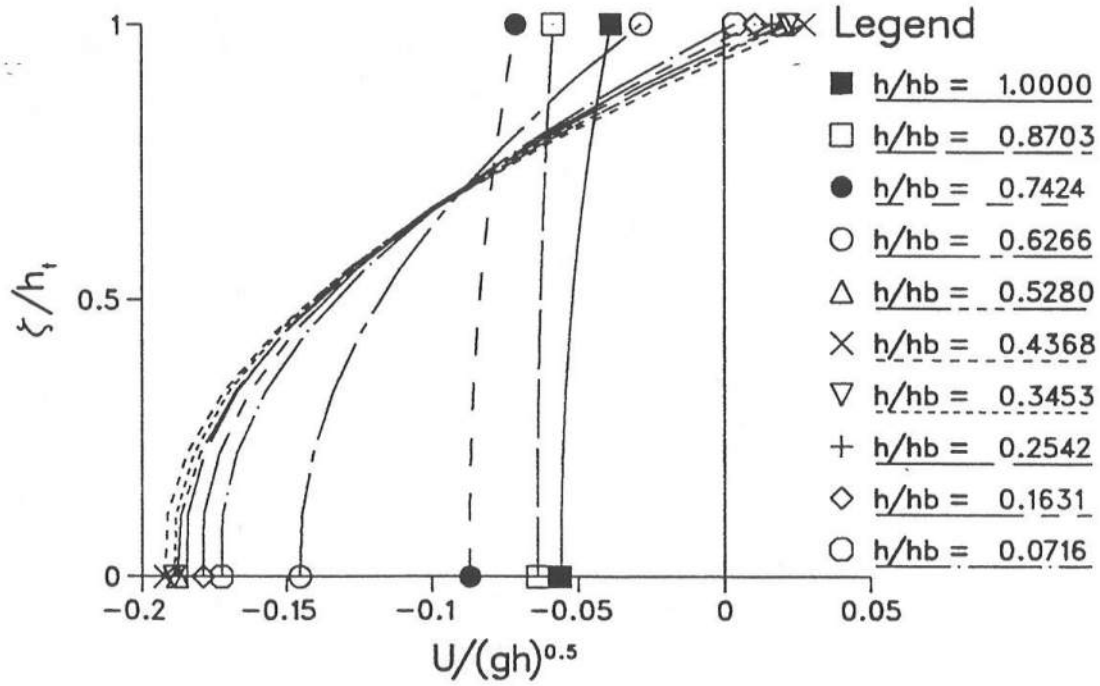

Figure 5.24: Undertow predictions for Visser's Experiment 2

anticipated by the analysis of turbulence intensities referred to earlier (*viz.*, Svendsen 1987, Okayasu 1989). The horizontal eddy viscosity levels are much higher and are consistent with the levels used by earlier investigators (*e.g.*, Longuet-Higgins 1970). We emphasize here that the difference in the lateral and vertical mixing levels does not seem to be compatible with observed turbulence characteristics. This conflict suggests that the lateral mixing may possibly be caused by some mechanism that is not related to turbulence.

As remarked in chapter 2, (5.8) has all the terms required to solve for longshore currents on long, straight beaches. The only difference between (5.1) and (5.8) is the interaction term present in the latter equation. If the contention of the previous paragraph is valid then the possibilities are that 1) The interaction term neglected by (5.1) is responsible for the mixing or 2) There is some external motion that is causing these phenomena.

Note that the derivation of (5.8) assumed that the only type of organized motions in the nearshore region are steady currents and waves. The derivation did not account for the presence of low frequency motions. It is quite possible that Visser's measurements

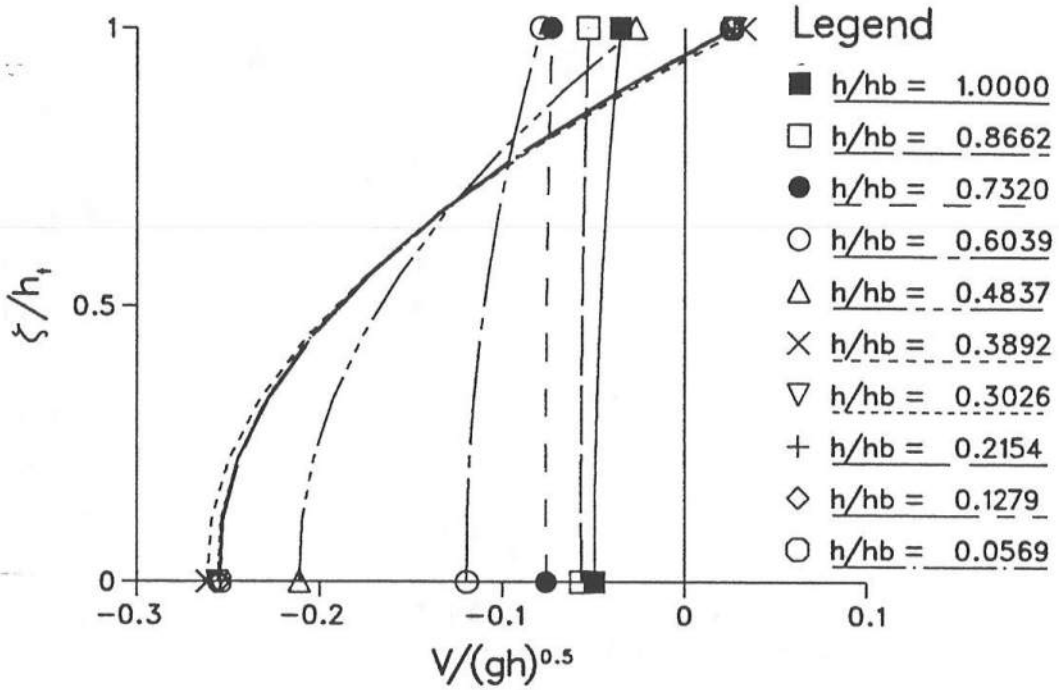

Figure 5.25: Undertow predictions for Visser's Experiment 3

reflect some effect of the low frequency motions and that could be a reason why the measurements are not well predicted. However, Visser does not mention the presence of any such motions. So, if low frequency motions were indeed present they would have been extremely weak.

The next two chapters address some of the questions raised here. The next chapter analyzes the effect of the interaction term. Chapter 7 studies a recently observed extremely low frequency oscillation ("shear waves") in the nearshore region.

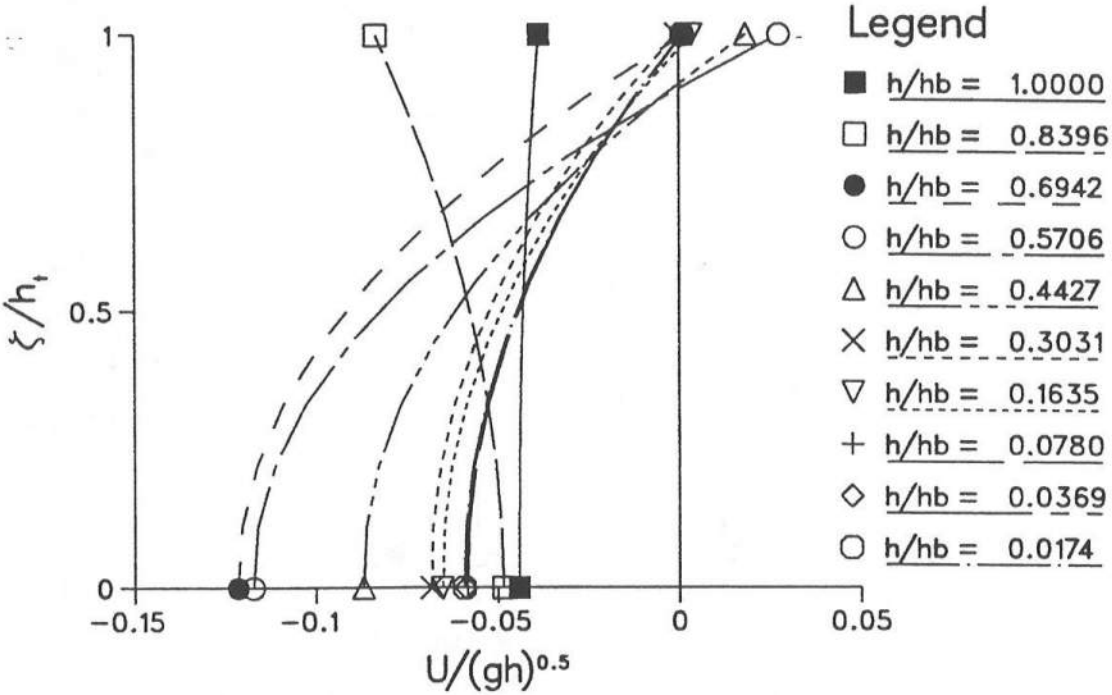

Figure 5.26: Undertow predictions for Visser's Experiment 4

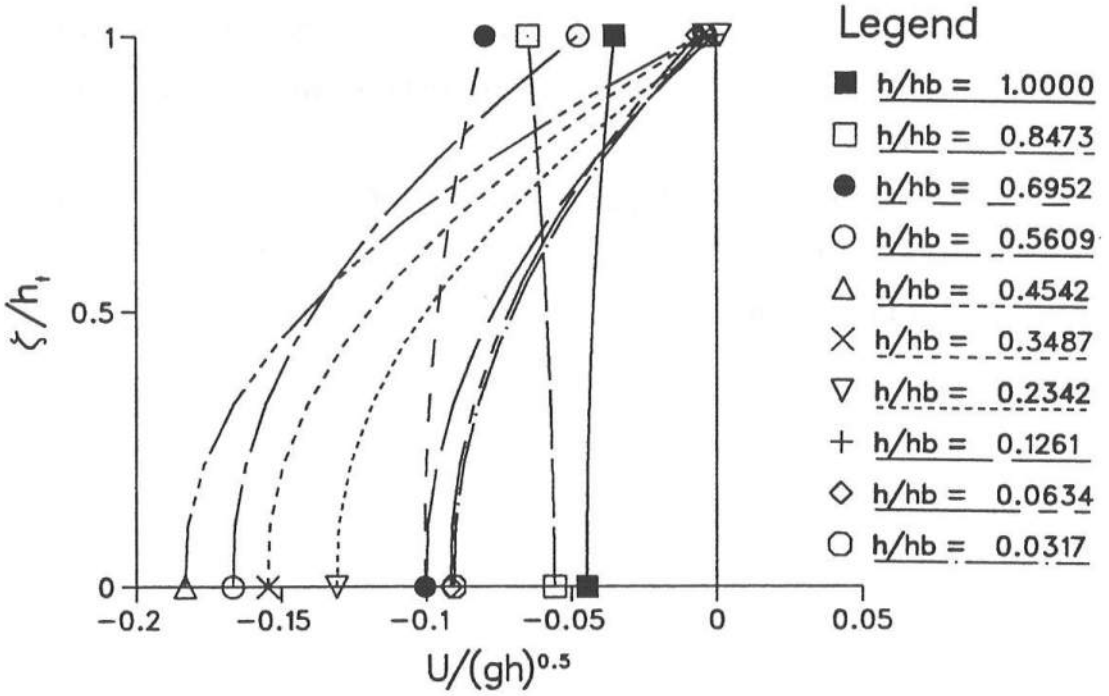

Figure 5.27: Undertow predictions for Visser's Experiment 5

Chapter 6

MIXING DUE TO INTERACTION OF LONGSHORE CURRENT AND UNDERTOW

6.1 Summary of previous mixing models

The earliest attempt to quantify mixing in the nearshore region was made by Harris *et al.* (1963) who conducted field and laboratory studies to measure the intensity of mixing in the nearshore region. They released known amounts of tracer into the surf-zone and estimated the strength of the mixing based on measured concentration of the tracer at later times. They found that the dye dispersed very quickly in the on-offshore direction and that in the absence of rips, the on-offshore mixing was confined largely to the surf-zone. They also found that the mixing in the longshore direction was mainly due to advection by the longshore current.

Bowen (1969a) in his analysis of the longshore current phenomenon used a constant eddy viscosity. To estimate the horizontal eddy viscosity Thornton (1970) assumed that the velocity scale was given by the wave induced velocity and the length scale by the water particle excursion amplitude. Using these he suggested that the horizontal eddy viscosity is given by $\nu_{tx} = H^2\sigma/4\pi(kh)^2$ where H is the wave-height, σ and k are the frequency and wavenumber of the gravity waves and h is the local water depth. Longuet-Higgins (1970) assumed that the velocity scale was proportional to the wave celerity and the length scale was proportional to the distance from the shoreline. Thus his estimates suggested that the eddy-viscosity be modelled by

$$\nu_{tx} = Nx\sqrt{gh} \tag{6.1}$$

where N is a dimensionless constant (less than 0.016). This, with minor modifications, has become one of the most widely used models of mixing in longshore current models.

Inman *et al.* (1971) conducted a field study similar to that of Harris *et al.* and found results similar to the earlier study. Based on their measurements, Inman *et al.* suggested that the horizontal eddy viscosity is roughly given by $\nu_{tx} = H_b x_b / T$ where x_b is the width of the surf-zone, H_b is the wave height at breaking and T is the period of the incident gravity waves.

Bowen & Inman (1974) analyzed the measurements available up to that time and examined the various suggestions for the horizontal mixing coefficient. They found that Longuet-Higgins' suggestion represented the mixing coefficient reasonably well with $N \approx 0.030$.

Battjes (1975) argued that the use of wave orbital parameters to describe turbulence characteristics as done by Thornton is not justifiable because the main source of turbulent energy in the surf-zone is the dissipation of wave energy rather than the energy of the orbital motion of the waves. Using scaling arguments he suggested that the eddy viscosity be given by

$$\nu_{tx} = M\,(D/\rho)^{1/3}\sqrt{gh} \tag{6.2}$$

where M is a dimensionless constant of order one and D is the rate of energy dissipation of wave motion. He showed that for the usually made surf-zone assumption, *viz.*, $H = \gamma h$ (6.2) reduces to

$$\nu_{tx} = M\left[\frac{5}{16}\gamma^2 h_x\right]^{1/3} h\sqrt{gh} \tag{6.3}$$

Comparing this estimate to Longuet-Higgins' suggestion he argued that N rather than being a constant should be a rather strong function of the bottom slope h_x. He also suggested that (6.3) seems reasonable because, all else being equal, the eddy viscosity is expected to increase with bottom slope because of the reduced distance available for the dissipation of the incident wave energy. This trend is predicted by (6.3) and an opposite trend is predicted by the suggestions of Thornton, Longuet-Higgins and Inman *et al.* described above.

Stive & Wind (1982), Nadaoka & Kondoh (1982), Okayasu *et al.* (1986, 1988) and Okayasu (1989) performed a series of laboratory measurements where they measured, among other things, turbulence intensities and undertow profiles. Svendsen (1987) analyzed available turbulence measurements and found that the intensity of turbulent fluctuations, q, is given approximately by

$$q = \sqrt{k_t} \sim 10^{-2}\sqrt{gh} \tag{6.4}$$

where k_t is the turbulent kinetic energy. If the length scale is taken to be the depth h then (6.4) implies that

$$\nu_t \sim 10^{-2} h\sqrt{gh} \tag{6.5}$$

Predictions of the undertow profiles have confirmed that (6.5) gives a fairly good estimate of the vertical eddy viscosity (Svendsen *et al.* 1987, Okayasu 1989).

Clearly, (6.1) and (6.5) are compatible if one assumes that the length scales in the horizontal and vertical directions is given by x and h respectively and that the velocity scale is given by (6.4). However, observations of turbulent eddies (Nadaoka *et al.* 1989, Okayasu 1989) show that in the vertical plane the eddies are very nearly circular and that, therefore, the length scales cannot be very different in the vertical and horizontal directions.

The experimental results results and the analyses quoted in the previous two paragraphs were all for 2D situations. It is conceivable that the presence of a longshore current changes the situation. Turbulence measurements in 2D wave flumes (Stive & Wind 1982, Nadaoka & Kondoh 1982, Nadaoka 1986, Okayasu *et al.* 1988, Okayasu 1989) suggest that the turbulence intensities in the vertical and cross-shore directions are comparable. The fact that the turbulence intensities are comparable even though the currents are quite different emphasizes that, inside the surf-zone, the turbulence intensities are not related to the strength of the currents.

At the present time there are no simultaneous measurements of all three components of the turbulent velocity fluctuations in the nearshore region. In the alongshore

of the turbulent fluctuations in the cross-shore direction in two dimensional experiments. For example, Mizuguchi & Horikawa find $\sqrt{\overline{v'^2}}/\sqrt{gh} \sim 0.06$ and the two dimensional experiments have $\sqrt{\overline{u'^2}}/\sqrt{gh} \sim 0.04$.[9] While these measurements are from different sets of experiments and probably cannot be compared directly without referring to the experimental conditions they do indicate that the intensity of the turbulent fluctuations in the longshore direction is of the same order of magnitude as the intensity in the cross-shore direction even though a strong longshore current may be present. Evidence from a wide class of flows suggests that the turbulent fluctuations in the two horizontal directions are typically of the same order of magnitude. For example, in open channels where the mean flow is in the x direction Townsend (1976, p. 107) gives $\overline{u'^2}/\overline{v'^2} \sim 3$ indicating that the intensity of the velocity fluctuations in a direction perpendicular to that of the mean flow is about 60% of the intensity of the fluctuation in the direction of the main flow. Extrapolating this result to the surf-zone where there may be a strong longshore current on occasion and keeping in mind the evidence that suggests that inside the surf-zone the turbulence intensity does not seem to depend strongly on the current strength we expect $\sqrt{\overline{v'^2}} \sim \sqrt{\overline{u'^2}}$ to be a reasonable assumption.

Even in the case where the turbulent intensities are comparable the mixing could still be larger in the horizontal direction when compared to the vertical direction if the length scale in the horizontal direction were significantly larger than in the horizontal direction. This could be the case if large scale horizontal circulations, like, *e.g.*, rip currents were present. The available experimental evidence (Visser 1982, 1984) do not indicate the

---

[9] These values were derived using the following procedure. Svendsen (1987) reported results for the variation of the turbulent kinetic energy ($= 1/2[\overline{u'^2} + \overline{v'^2} + \overline{w'^2}]$) for 2D experiments. In all the experiments analyzed by him only the cross-shore and vertical components of the turbulent velocity fluctuations were measured. Using results from many different types of turbulent flows Svendsen assumed that $k_t = 1.33k_t'$ where k_t is the TKE and $k_t' = 1/2(\overline{u'^2}+\overline{w'^2})$. He found that $\sqrt{k_t} \approx 0.03\sqrt{gh}$. Assuming that $\overline{u'^2} = \overline{w'^2}$ we find that we may estimate that the intensity of the turbulent fluctuation in the cross-shore direction is given by $\overline{u'^2} \sim k_t/1.33$ which implies that $\sqrt{\overline{u'^2}/gh} \sim 0.04$. Figure 20 of Mizuguchi & Horikawa indicates that $\sqrt{\overline{v'^2}}/v_m \propto \sqrt{h/h_b}$ (v_m is the maximum longshore current velocity). The above implies that $\sqrt{\overline{v'^2}/gh} \propto v_m/\sqrt{gh_b}$. The constant of proportionality may be determined by using the fact that at $h = h_b$ the referred figure indicates that $\sqrt{\overline{v'^2}}/v_m \approx 0.2$. Therefore, we estimate that $\sqrt{\overline{v'^2}/gh} \approx 0.2v_m/\sqrt{gh_b}$. Using the values for v_m and h_b given in their Table 1 we find that $\sqrt{\overline{v'^2}/gh} \approx 0.06, 0.06, 0.07$ and 0.08 for their cases 1 through 4 respectively.

presence of any such large scale circulation features. Therefore, there seems to be no reason to assume that the vertical and horizontal length scales are different from one another in the surf-zone in the presence of a uniform (alongshore), steady longshore current.

In summary, the available experimental evidence seems to suggest that the total horizontal mixing for the longshore currents should be comparable to the estimates of the turbulent mixing based on two dimensional experiments.

Results from the previous chapter as well as the apparent success of various longshore current models based on variations of the Longuet-Higgins' mixing scheme show that a very high level of mixing (relative to measured turbulence intensities) is required to predict the cross-shore structure of the longshore current. The mixing coefficient required to get reasonable predictions of the vertical structure is consistent with the measured turbulence levels as given by (6.4) and is significantly smaller than the horizontal mixing coefficient. Since Visser does not report the presence of any large scale horizontal circulation features or low frequency fluctuations we seek an explanation for the horizontal mixing without having to assume the presence of any such phenomena.

The above discussion suggests that the total mixing in the horizontal direction is very different from the vertical direction. Since this cannot be explained by turbulence measurements, we conclude that the mixing in the horizontal direction is caused by some mechanism other than turbulence.

A further complication seemingly arises from the fact that while a reasonably high level of mixing outside the surf-zone is required for the prediction of longshore currents none of the studies show any mixing outside the surf-zone (see, *e.g.,* Mei 1983, p. 485).

It has been suggested (Battjes 1975, Thornton & Guza 1986) that this mixing may be explained by the time variation of the breaker line due to random waves. That suggestion, however, does not explain the mixing required to predict measurements of longshore currents with regular monochromatic waves (like those of Visser 1982, 1984). Additionally, the method of solution adopted by Thornton & Guza seems to be equivalent to calculating the steady longshore current profiles for individual wave frequencies. The overall longshore current calculated by their model is essentially a weighted average of the

individual steady state profiles. Since their model has no turbulent mixing the longshore current profiles due to individual waves would be equivalent to Longuet-Higgins' triangular profile and since the individual waves break at different locations these profiles would end at different points. When the weighted average of many such profiles is calculated we would find a longshore current that extends all the way to the farthest breaking location. For a random wave field, this location will be significantly seaward of the location where most of the waves break (loosely – the break point). Therefore, the calculated longshore current would extend to a significant distance seaward of the break point thus showing an affect not unlike the one caused by the mixing term.

Mei considers the source of the mixing outside the surf-zone to be one of the outstanding problems of nearshore hydrodynamics. However, this problem may not be as significant as previously believed since our results from the previous chapter show that the variation of the eddy viscosity outside the surf-zone does not significantly influence the longshore current profile as long as the eddy viscosity is continuos across the breaker line.

In this thesis we will consider mixing contributions from two possible mechanisms. The first – to be examined in this chapter – is the interaction of longshore and cross-shore currents. The second, which will be examined in the next chapter, is the recently observed phenomenon of shear motions in the nearshore region.

6.2 A discussion of the effect of the interaction

It was shown in chapter 2 that the longshore current is governed by

$$\frac{d}{dx}\left(\nu_{tx}h\frac{dV_b}{dx}\right) - \frac{\tau_{by}}{\rho} - \frac{d}{dx}\left\{\int_{-h_0}^{\xi_t} VU\,dz + \overline{\int_{\xi_t}^{\xi} Vu_w\,dz}\right\} = \frac{1}{\rho}\frac{dS_{xy}}{dx} \tag{6.6}$$

As remarked in that chapter, this equation has all the terms required to predict steady longshore currents on long straight beaches. If no external influences are present, an incorrect prediction of longshore currents implies that one or more terms of the above equation are not being modelled very well. The last term on the LHS of (6.6) has not been included in any of the previous longshore current models. The idea here is to analyze the

effect of this term and see if it is capable of providing the mixing required for predictions of cross-shore variations of longshore currents.

Before embarking on a mathematical description of the problem it is probably worthwhile to spend some time discussing the physical situation that we are trying to model here.

Below trough level we have the undertow which, for the most part, is directed seawards. Above the trough level, the mass flux due to the wave motion is directed shorewards. The interaction we are after is the effect of these flows on the cross-shore distribution of the longshore current.

Below trough level, the longshore current is pushed seawards by the undertow. Therefore, we expect that the effect of the undertow on the cross-shore distribution of the longshore current is to move the entire distribution seaward. The expected effect of the undertow on the cross-shore distribution of the longshore current is as sketched in figure 6.1a. The line marked "1" represents the distribution in the absence of the undertow and the line marked "2" represents the expected distribution after the undertow has been included.

Above trough level, we expect the opposite of this situation to occur. We expect that the mass flux due to the waves will push the longshore current profile shorewards leading to a situation that is not unlike the one sketched in figure 6.1b. As, before the line marked "1" represents the longshore current distribution in the absence of the interaction term and the line marked "2" denotes the expected effect of the mass flux.

From the rather heuristic discussion above we see that the effect of the term under consideration is unevenly distributed over depth. In a general setting, the contributions from above and below trough level counteract one another – and, in fact, in the special case of a longshore current independent of depth these contributions will exactly cancel one another. However, the longshore current is not constant over depth and this turns out to be important for the interaction terms.

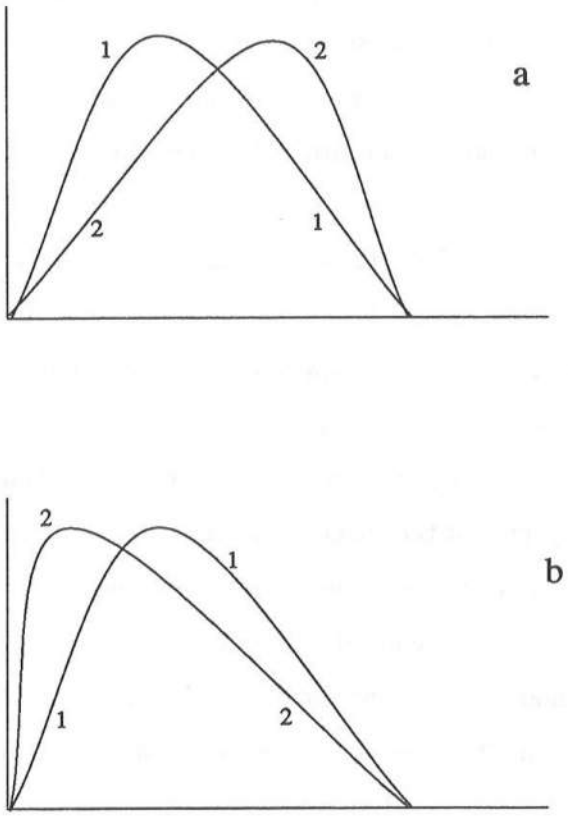

Figure 6.1: Expected effect of the interaction. Curve 1 – Without interaction; Curve 2 – With interaction.

6.3 A simplified mathematical model

To simplify the analysis and clearly demonstrate the effect of the interaction, we will, in this chapter, make several simplifying assumptions. We note that the assumptions made are not absolutely necessary and the effect could equally well be studied using the numerical model employed in the previous chapter.

The following simplifications are made:

1. Use linear shallow water theory for the wave properties;
2. Use H/h constant inside the surf-zone;
3. Use a linearized bottom friction formulation and
4. No net cross-shore flow, so that $Q_s = -\int_{-h_0}^{\xi_t} U(z)dz$.

A benefit of these simplifications is that all terms other than the interaction terms take the simplest possible form.

Under the assumptions listed above the equation governing the longshore currents reduces to

$$\frac{d}{dx}\left(\nu_{tx}h\frac{dV_b}{dx}\right) - \frac{f_w u_0 V_b}{\pi} - \frac{d}{dx}\left\{\int_{-h_0}^{\xi_t} VU\,dz + \overline{\int_{\xi_t}^{\xi} V u_w\,dz}\right\} = \frac{1}{\rho}\frac{dS_{xy}}{dx} \tag{6.7}$$

Clearly, we need to evaluate the last term on the LHS of (6.7) before we proceed any further. The first part of this term is relatively straightforward to evaluate if the depth variation of the currents is known. The second part is the one that is difficult to evaluate.

To properly determine the effect of the interaction term it is necessary to take recourse to the perturbation scheme devised in the previous chapter. The perturbation expansion discussed in the last chapter had the following ordering.

At ϵ^0

$$\frac{d}{dx}\left(h\nu_{tx}\frac{dV_0}{dx}\right) - \frac{\tau_{by}^0}{\rho} = \frac{dS_{xy}}{dx} \tag{6.8}$$

At ϵ^1

$$\frac{d}{dx}\left(h\nu_{tx}\frac{dV_{b1}}{dx}\right) - \frac{\tau_{by}^1}{\rho} - \frac{d}{dx}\left\{\int_{-h_0}^{\xi_t} V_1 U\,dz + \overline{\int_{\xi_t}^{\xi} V_1 u_w\,dz}\right\} = 0 \tag{6.9}$$

The depth variation of the longshore current and undertow are given by (ζ is the distance from the bottom, see figure 2.1)

$$V_1 = V_{b1} + b_v\zeta + a_v\zeta^2 \tag{6.10}$$

and

$$U = U_b + b_u\zeta + a_u\zeta^2 \tag{6.11}$$

where the coefficients a_u, b_u, U_b, a_v and b_v are given by

$$a_u = \frac{1}{2\nu_{tz}}\left[g\frac{\partial b}{\partial x} + \frac{1}{2}\frac{\partial\left(\overline{u_w^2} + U_0^2\right)}{\partial x}\right] \tag{6.12}$$

$$b_u = \frac{f_w u_0 U_b}{\pi\nu_{tz}} \tag{6.13}$$

$$U_b = -\left(\frac{Q_s + b_u\frac{h_t^2}{2} + a_u\frac{h_t^3}{3}}{h_t}\right) \tag{6.14}$$

$$a_v = \frac{1}{\nu_{tz}}\left[\frac{1}{2}\frac{\partial}{\partial x}\left(\overline{u_w^2}\cos\alpha\sin\alpha\right) - \frac{\sin\alpha\cos\alpha}{4}\frac{\partial}{\partial x}\left(\overline{u_w^2}\right) + \frac{U_0}{2}\frac{\partial V_b}{\partial x}\right.$$
$$\left. -\frac{1}{2}\frac{\partial}{\partial x}\left(\nu_{tx}\frac{\partial V_b}{\partial x}\right)\right] \tag{6.15}$$

$$b_v = \frac{f_w u_0}{\pi\nu_{tz}}V_0 \tag{6.16}$$

Equations 6.10 and 6.11 imply that

$$\int_{-h_0}^{\xi_t} V_1 U\,dz = -V_{b1}Q_s + b_v\left[\frac{U_b h_t^2}{2} + \frac{b_u h_t^3}{3} + \frac{a_u h_t^4}{4}\right] + a_v\left[\frac{U_b h_t^3}{3} + \frac{b_u h_t^4}{4} + \frac{a_u h_t^5}{5}\right] \tag{6.17}$$

Now, let us concentrate on evaluating the second part of the term under consideration. To evaluate this term we write

$$\overline{\int_{\xi_t}^{\xi} V u_w dz} = \alpha_s V_e(\bar{\xi})Q_s \tag{6.18}$$

$V_e(\bar{\xi})$ is defined as the velocity obtained by evaluating (6.10) at the mean water surface (recall that equation 6.10 is, strictly speaking, valid only below trough level), *viz.*,

$$V_e(\bar{\xi}) = V_b + b_v h + a_v h^2 \tag{6.19}$$

α_s can be calculated if we know the variations of the longshore current and the wave induced velocity above the trough level. In this analysis, for simplicity, we assume that $\alpha_s = 1$. Later in this chapter we will discuss the sensitivity of the results to this assumption.

Therefore, we have

$$\int_{-h_0}^{\xi_t} UV_1 dz + V_1(\bar{\xi})Q_s = F_{Q1}V_0 + F_{Q2} \tag{6.20}$$

where V_0 is the solution to (6.8) and the F_Q's are given by

$$F_{Q1} = \frac{f_w u_0 h}{\pi\nu_{tz}}\left[Q_s + \frac{U_b h_t^2}{2h} + \frac{b_u h_t^3}{3h} + \frac{a_u h_t^4}{4h}\right] \tag{6.21}$$

and

$$F_{Q2} = a_v h^2\left[Q_s + \frac{U_b h_t^3}{3h^2} + \frac{b_u h_t^4}{4h^2} + \frac{a_u h_t^5}{5h^2}\right] \tag{6.22}$$

The first order longshore current is now governed by

$$\frac{d}{dx}\left(h\nu_{tx}\frac{dV_{b1}}{dx}\right) - \frac{\tau_{by}^{1}}{\rho} = \frac{d}{dx}\left(F_{Q1}V_0 + F_{Q2}\right) \tag{6.23}$$

To complete the solution for the longshore current, the variations of the lateral and vertical eddy viscosities both inside and outside the surf-zone need to be specified. Inside the surf-zone, we may write ν_t as

$$\nu_{tx} = c_x h\sqrt{gh} \tag{6.24}$$

$$\nu_{tz} = c_z h\sqrt{gh} \tag{6.25}$$

Outside the surf-zone, for the present, we let the eddy viscosities remain constant at the breaking value. This means that we assume an unrealistically large value of the horizontal eddy viscosity ν_{tx}, in particular, outside the surf-zone. As will become apparent later this is necessary for the assumed perturbation expansion to be valid. The sensitivity of the results to the variation of the vertical eddy viscosity will be discussed later in this chapter.

The calculation of the zeroth and first order solutions for the longshore current using a numerical procedure is straightforward. The solution correct to first order is obtained by adding the first order correction calculated using (6.23) to the zeroth order solution. As in the previous chapter, the longshore current shown in all the plots is the near bottom value.

Figure 6.2 shows an example of the effect of the interaction on the longshore current distribution calculated using the perturbation scheme. The parameters used in this example are $c_x = 0.1$, $c_z = 0.01$, $f_w = 0.01$, $h_x = 1/30$, $\gamma = 0.6$ and $b_q = -0.1$. V_{max} in figure 6.2 represents the maximum value of the zeroth order longshore current. This figure clearly demonstrates that the interaction term causes significant change in the distribution of $V(x)$ even in a case like the present where ν_{tx} is already very large ($c_x = 0.1$). A comparison of the location of the maximum velocity for the two cases (with and without the UV interaction term) indicates that the mixing caused by the interaction term is roughly equivalent to increasing c_x by a factor of two relative to the already large value.

The predicted depth variations of the longshore currents are shown in figure 6.3. Note that this figure shows that outside the surf-zone the longshore current profiles have

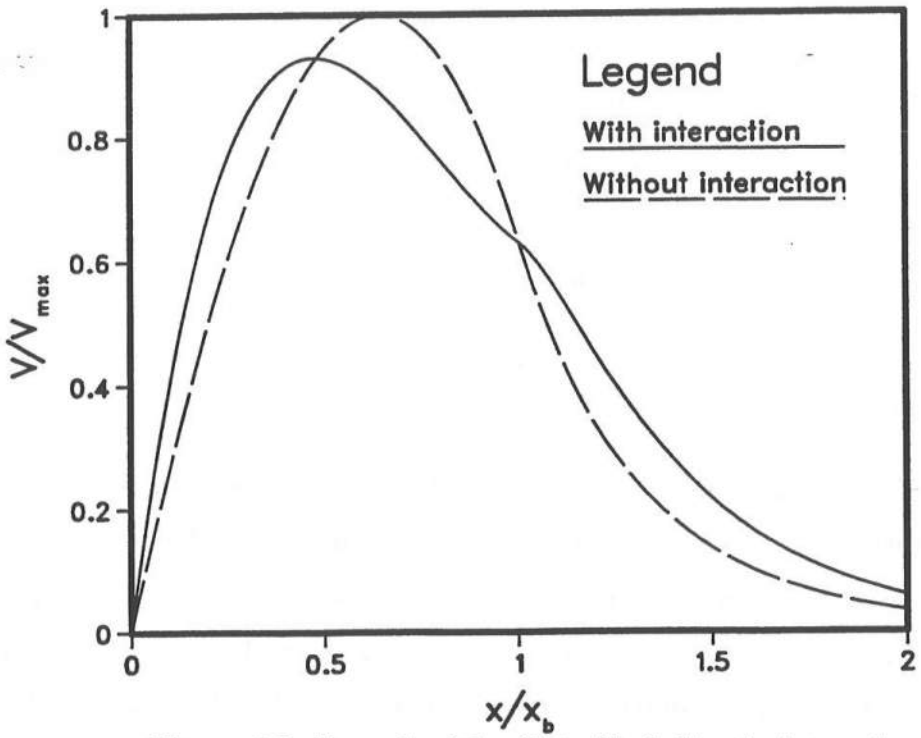

Figure 6.2: Example of the effect of including the interaction

a negative curvature indicating that in this region the current terms in a_v dominate over the wave terms. Some evidence of the decreasing trend above the bed of the longshore current may be found in the measurements of Visser (1984). A representative example of his measured variation is reproduced here as figure 6.4. This figure shows a weak decrease of longshore current with distance from the bed. While this variation is relatively weak and the differences in velocity between the three depth locations probably are comparable to the experimental inaccuracy, it seems significant that a decrease in velocity outside the surf-zone is visible in almost all of Visser's experiments. This suggests that outside the surf-zone the longshore currents do decrease away from the bed. A similar, and somewhat stronger, trend is found in the experimental results of Mizuguchi and Horikawa (1978), though, as indicated in the previous chapter, these experiments had considerable alongshore nonuniformity and therefore the results cannot directly be used in the present work.

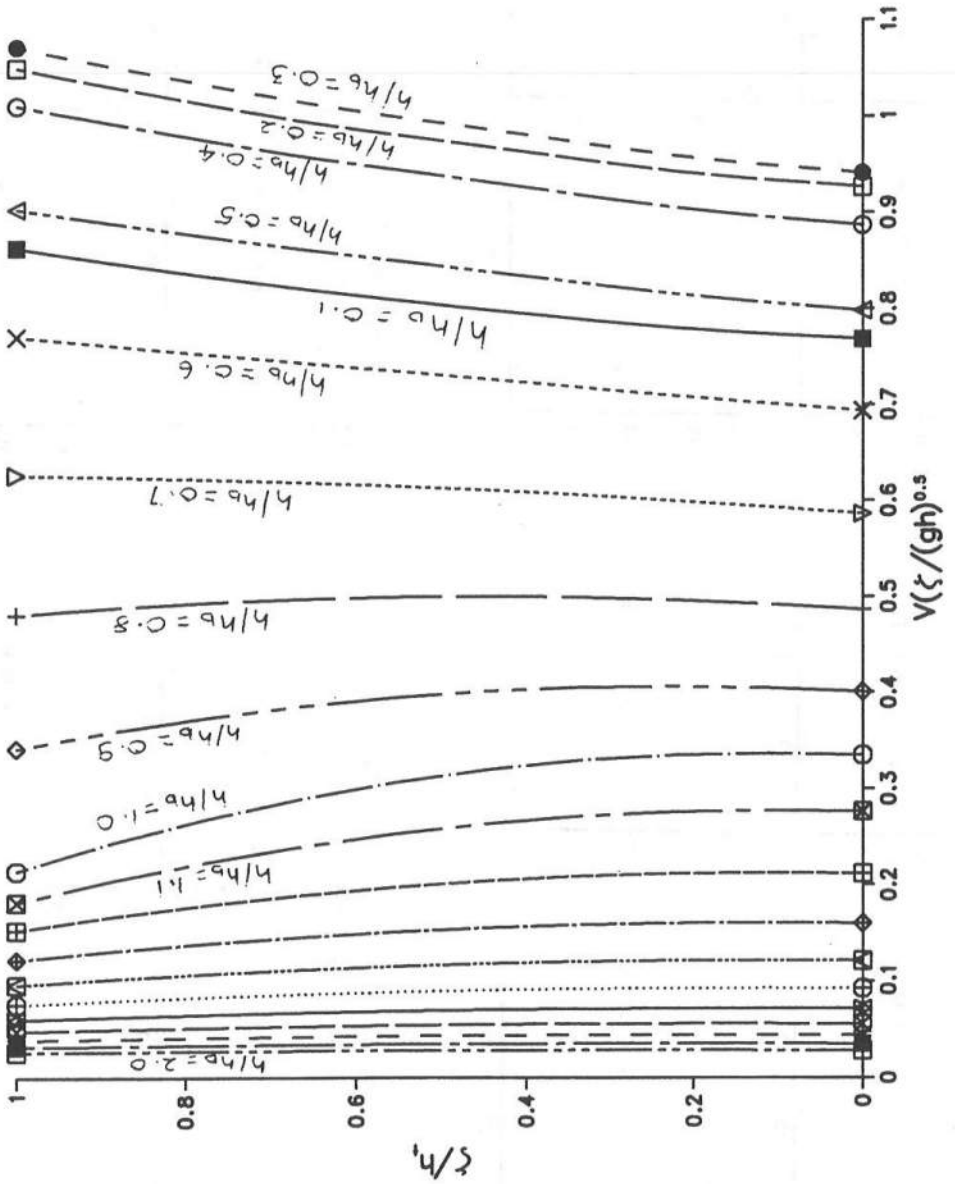

Figure 6.3: Predicted longshore current variations over depth

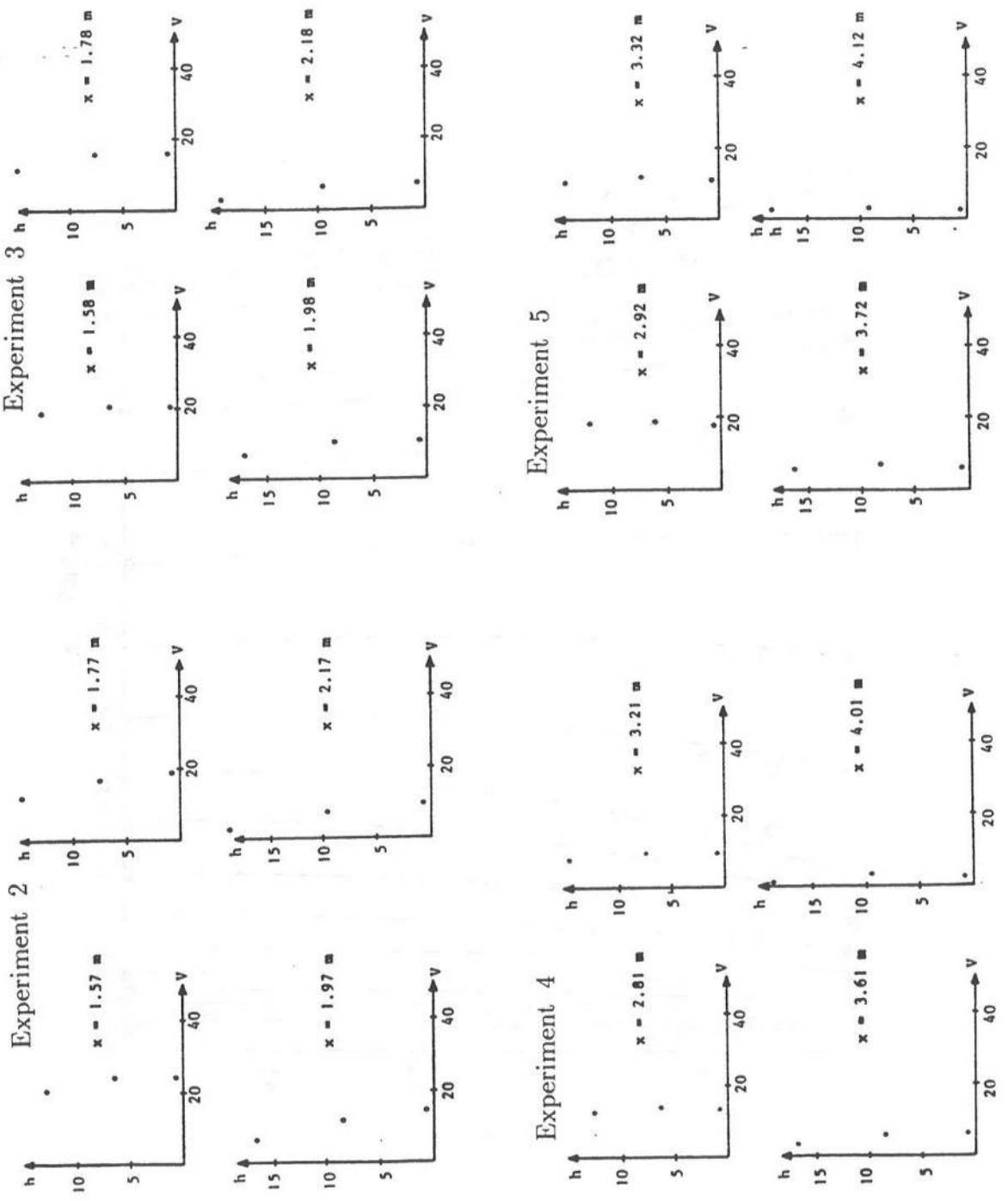

Figure 6.4: Visser's measurement of longshore current variation outside the surf-zone

In the previous chapter we encountered an interesting variation of the longshore current with the slope. We found that keeping c_x constant reduced the level of mixing as the slope was decreased. Here, we examine the slope dependence of the interaction term to see how the slope affects the mixing due to the interaction. Figure 6.5 shows the longshore currents calculated using the perturbation approach for different slopes. In all cases c_x is the same and hence by (5.67) each curve corresponds to a different value of the parameter P'. The appropriate conclusion from this figure is that in the absence of the interaction term the longshore current profile tends towards the triangular one. The inclusion of the interaction term weakens this tendency significantly.

6.4 Discussion

The preliminary analysis presented above used a constant value for both the horizontal and vertical eddy viscosities outside the surf-zone. In reality we would expect both these eddy viscosities to decrease seaward of the break point. Figure 6.6 presents a comparison of three different variations of the vertical eddy viscosity ν_{tz} outside the surf-zone. In all three cases ν_{tz} was the same inside the surf-zone and the ν_{tx} was the same everywhere and given by (6.24) inside the surf-zone and maintained constant outside the surf-zone. The variations shown correspond to: a) $\nu_{tz} = \nu_{tzb}$, $\nu_{tz} = \nu_{tzb}(h_b/h)^2$ and $\nu_{tz} = \nu_{tzb}(h_b/h)^4$ where ν_{tzb} is the value of ν_{tz} at breaking. This plot shows a rather surprising insensitivity of the overall solution to the variation of the vertical eddy viscosity outside the surf-zone.

The above result may be understood on the basis that the most important term in the forcing for the first order longshore current is the $U_0 dV_0/dx$ term (in a_v). This term is significant inside the surf-zone and in a very limited region seaward of the break point. In the region just seaward of breaking the vertical eddy viscosities are not changed significantly. Therefore, the UV forcing for the first order longshore currents and consequently the solution for that current are not altered very much as long as the eddy viscosity varies smoothly across the break point.

A comparison of the undertow and longshore current velocity profiles for two different values of the vertical eddy viscosity are shown in figures 6.7 and 6.8. The solid lines

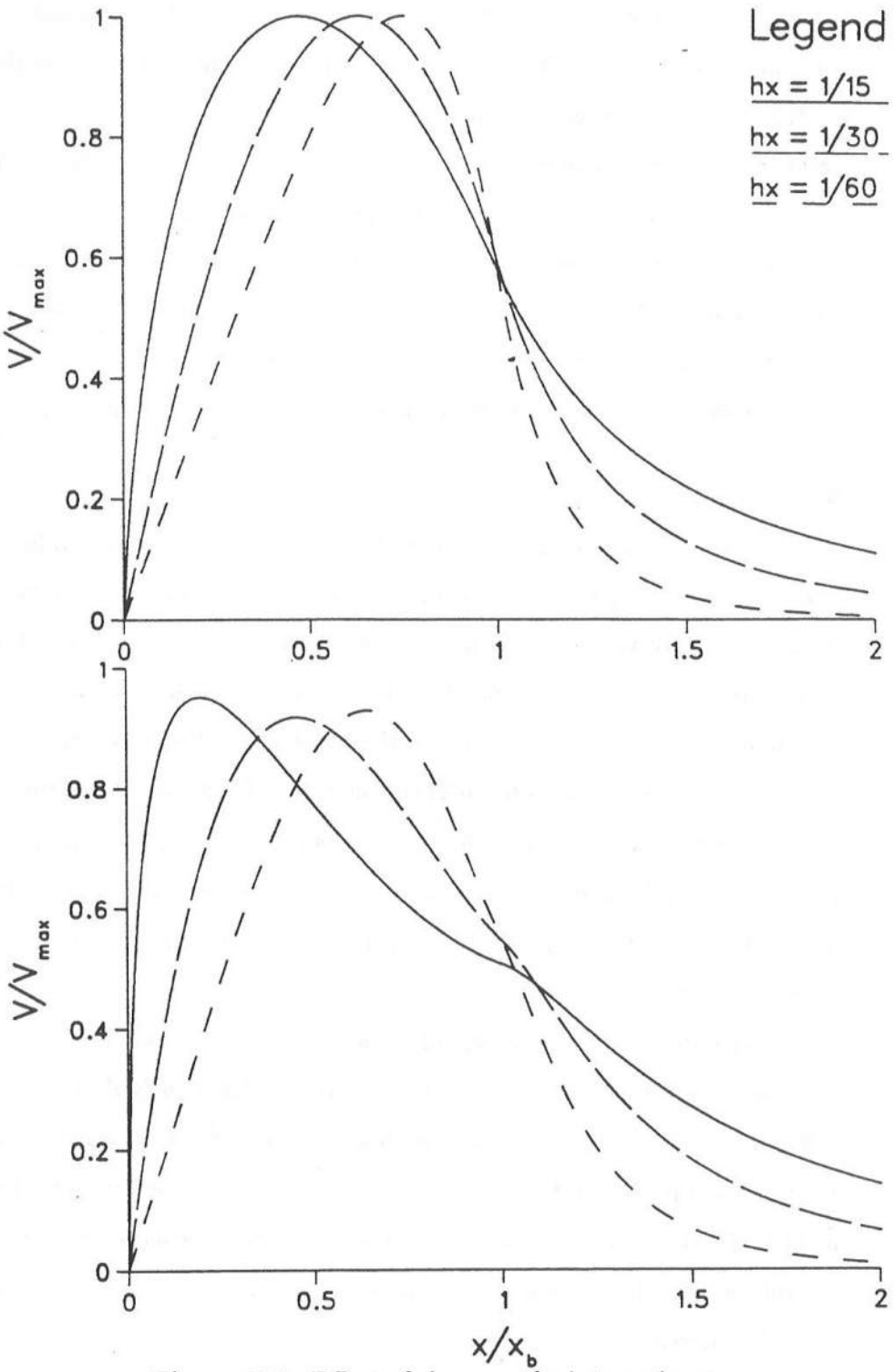

Figure 6.5: Effect of slope on the interaction term

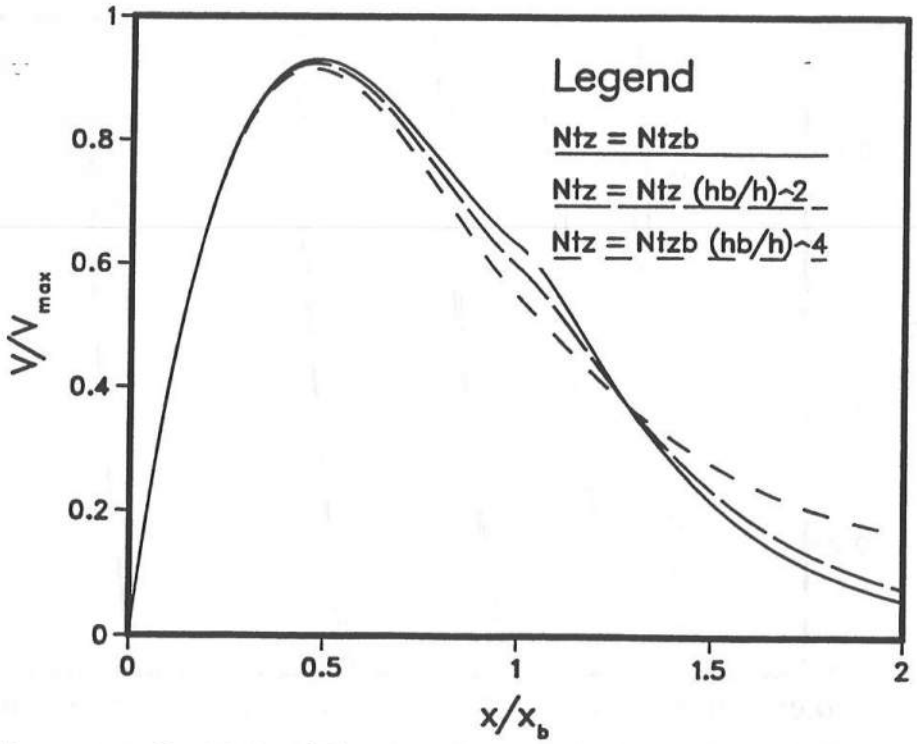

Figure 6.6: Sensitivity of the interaction contribution to the vertical eddy viscosity variation outside the surf-zone

represent the profiles predicted using a constant value of ν_{tz} outside the surf-zone and the dashed lines represent the profiles that have a quadratic decay of the eddy viscosity seaward of the break point. The undertow profiles outside the surf-zone show a surprising lack of sensitivity to the vertical eddy viscosity. The longshore current variations are somewhat more sensitive to the eddy viscosity variations.

The extreme lack of sensitivity of the undertow profile to the eddy viscosity variation may be understood by the following consideration. As shown in the previous chapter the curvature of the undertow profiles outside the surf-zone is quite small. Therefore, to a first approximation we have

$$U_b + \frac{b_u h}{2} = \frac{-Q_s}{h} \tag{6.26}$$

Substituting for b_u in terms of U_b and solving for U_b we have

$$U_b = \frac{-Q_s}{h}\frac{1}{1+y} \tag{6.27}$$

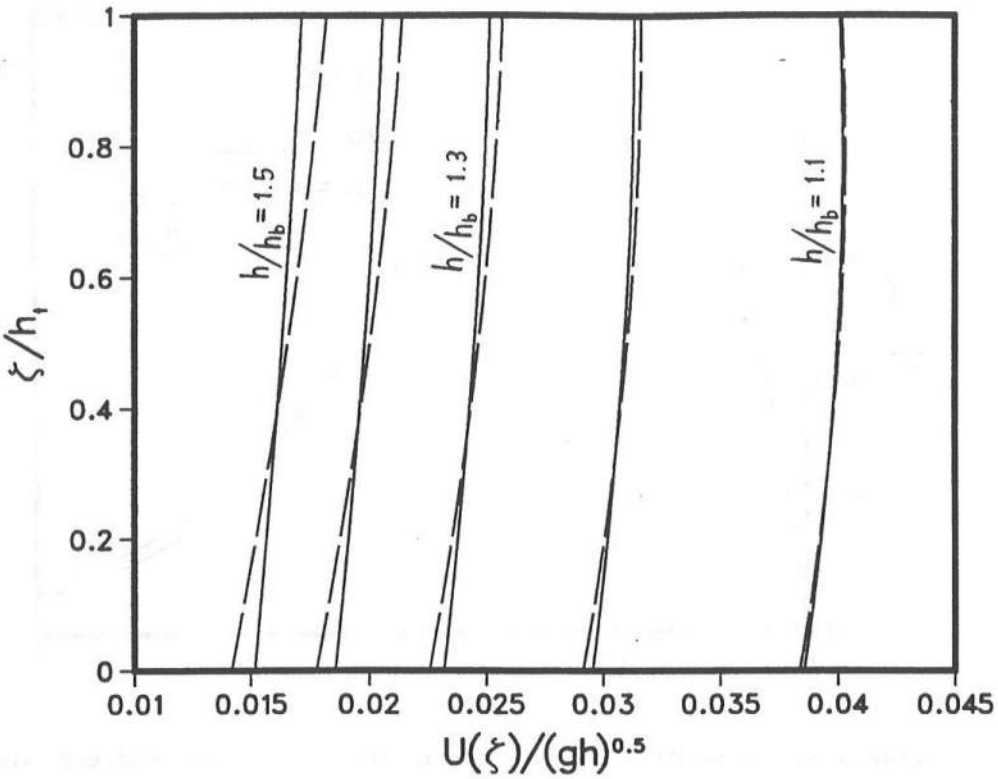

Figure 6.7: Undertow variations for two different assumptions for the vertical eddy viscosity. Solid lines represent ν_{tz} = constant, dashed lines represent quadratic decay of ν_{tz}.

where $y = f_w u_0 h/(2\pi\nu_{tz})$. Using $f_w \sim 0.01$, $u_0 \sim \gamma\sqrt{gh_b}/2$, $\nu_{tz} \sim 0.01 h_b\sqrt{gh_b}$ we find that $y \ll 1$. The sensitivity of U_b to y and, therefore, to ν_{tz} is given by

$$\frac{\Delta U_b}{U_b} \approx \frac{\Delta y}{1+y} \ll 1 \tag{6.28}$$

indicating that the value of the vertical eddy viscosity used does not affect the near bottom cross-shore current significantly.

A comparison of the qualitative features of the predicted undertow velocity outside the surf-zone with the measurements of that quantity by Nadaoka & Kondoh (1982) is encouraging. Figure 5.2 indicates that just seaward of the break point they have undertow velocities of the order $0.1m/s$ and these velocities are directed seaward all the way up to trough level. The two measurements of that figure correspond to one spilling and one plunging breaker. For the plunging breaker case they have $h_b = 0.25m$ and for the spilling

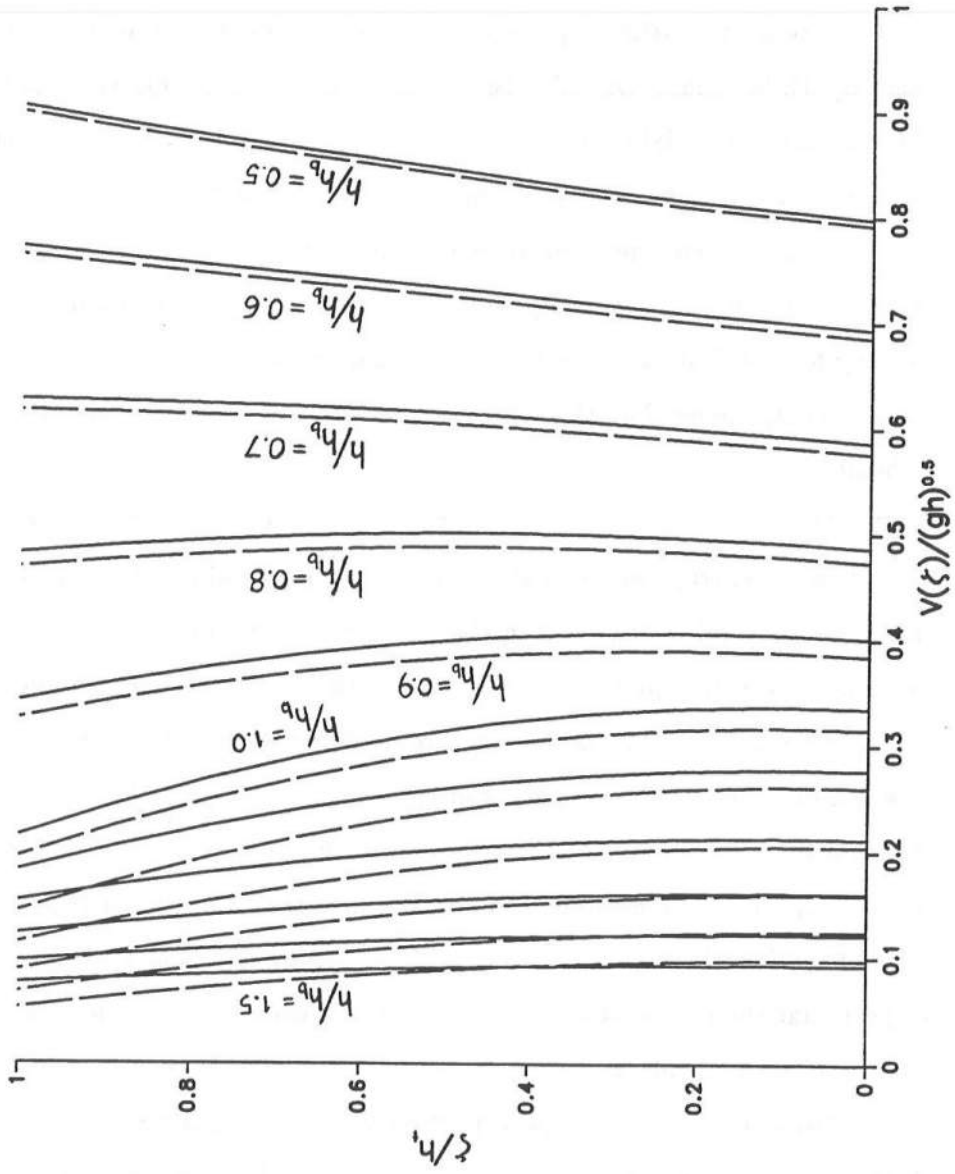

Figure 6.8: Longshore current profiles for two different assumptions for the vertical eddy viscosity. Solid lines represent ν_{tz} = constant, dashed lines represent quadratic decay of ν_{tz}.

breaker case $h_b = 0.50m$ indicating a $U/\sqrt{gh} \sim 0.05$. This value compares favorably with our results (see figure 6.7). Unfortunately, since this value is quite insensitive to the way the eddy viscosity varies seaward of the break point, this comparison cannot be used to determine the nature of that variation.

The perturbation approach used here requires that the correction V_1 to the basic velocity V_0 be small. Outside the surf-zone, the basic profile $V_0(x)$ is generated entirely by the turbulent mixing represented by ν_{tx}. For small ν_{tx} (as we expect in reality) this condition may not be satisfied. This implies that the present method will not work very well for cases where the basic velocities are very small outside the surf-zone. Also, large gradients in the basic velocity profile as we find for small ν_{tx} lead to extremely large forcing for the first order velocity profile and, therefore, to first order velocities that are substantially bigger than the zeroth order velocities thereby invalidating the perturbation scheme.

One way to estimate the results for low (and probably more realistic) values of c_x would be by extrapolation of the results for higher values of c_x. A second – and, more reliable – method is discussed in the next section. Figures 6.9a and 6.9b show the basic and the "complete" solution (the solution with the interaction term included) for the very large values of $c_x = 0.2$ and $c_x = 0.4$ respectively. The other parameters of the problem are not changed relative to the example presented in figure 6.2 which gives the solution for $c_x = 0.1$. A comparison of figures 6.9 with figure 6.2 clearly shows that the interaction of the longshore currents and the undertow increases with increasing shear on the seaward face of the longshore current (which is achieved by decreasing c_x) and, therefore, we can expect that the interaction term will provide enormous mixing for the case of an original profile with small values of c_x.

However, the present perturbation solution cannot be used to solve for that case. It turns out that this problem is easily solved by a slight change in the solution procedure. This is discussed below.

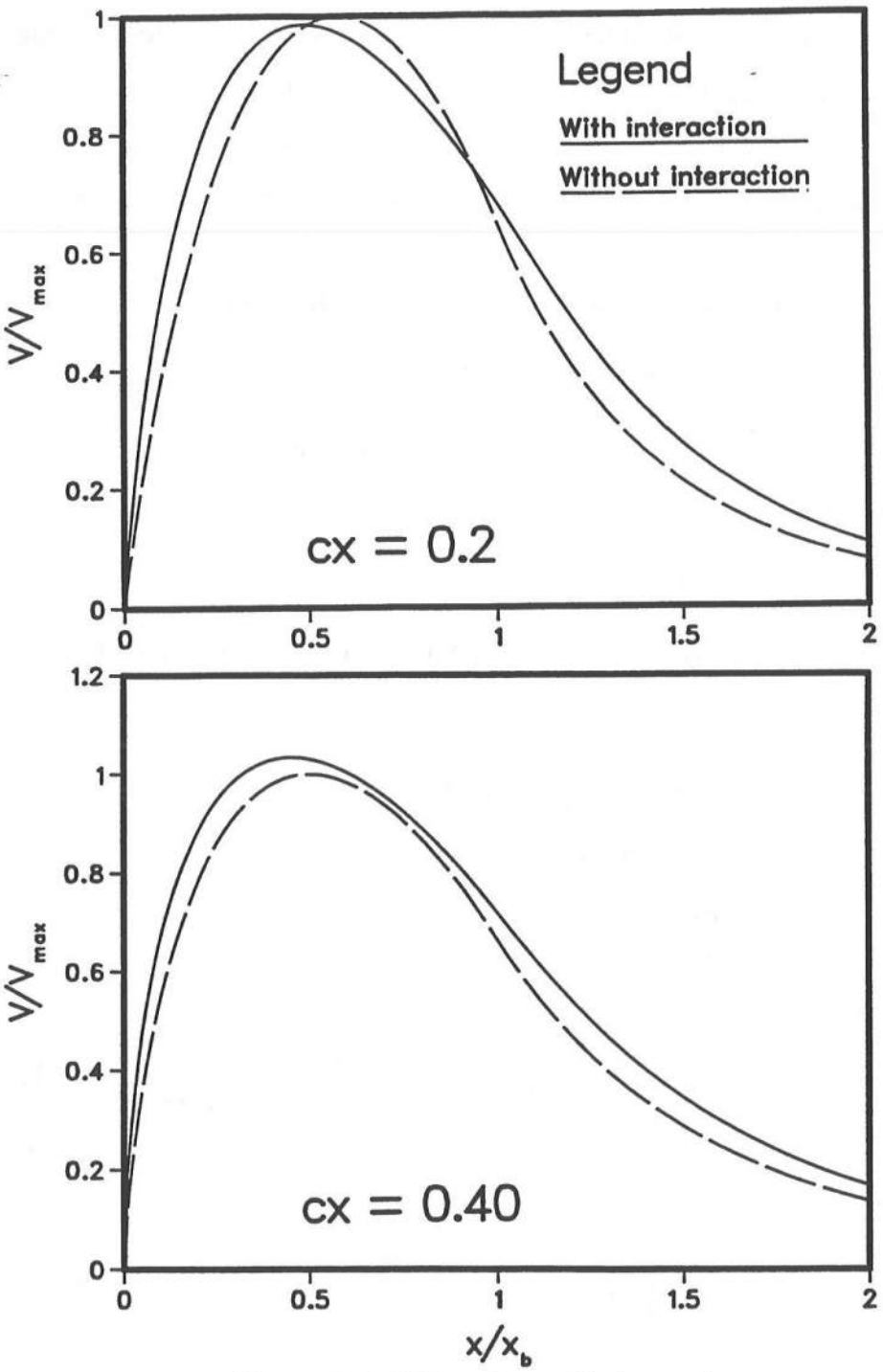

Figure 6.9: Effect of c_x on the interaction

6.5 Effect of interaction for small values of the horizontal eddy viscosity

The principal difficulty of using the perturbation expansion comes from the fact that the $U_0(dV_b/dx)$ is no longer small it is reasonable to expect that rearranging the equation such that this term is accounted for in the first approximation may solve the problem.

We assume that the longshore current is given by

$$V(\zeta) = V_b + b_v\zeta + a_v\zeta^2 \tag{6.29}$$

with $b_v = f_w u_0 V_b/(\pi\nu_{tz})$. Using the above we find that the interaction term may be expressed as

$$\int_{-h_0}^{\xi_t} UV\,dz + V(\bar{\xi})Q_s = F_{Q1}V_b + F_{Q2} \tag{6.30}$$

where F_{Q1} and F_{Q2} are given by (6.21) and (6.22) respectively. The governing equation for the longshore current becomes

$$\frac{d}{dx}\left(\nu_{tx}h\frac{dV_b}{dx}\right) - \frac{f_w u_0 V_b}{\pi} - \frac{d}{dx}\left\{F_{Q1}V_b + F_{Q2}\right\} = \frac{1}{\rho}\frac{dS_{xy}}{dx}$$

Now write a_v in the following form

$$a_v = a_{v1} + \frac{U_0}{2\nu_{tz}}\frac{dV_b}{dx} \tag{6.31}$$

where

$$a_{v1} = \frac{1}{\nu_{tz}}\left[\frac{1}{2}\frac{\partial}{\partial x}\left(\overline{u_w^2}\cos\alpha\sin\alpha\right) - \frac{\sin\alpha\cos\alpha}{4}\frac{\partial}{\partial x}\left(\overline{u_w^2}\right) - \frac{1}{2}\frac{\partial}{\partial x}\left(\nu_{tx}\frac{\partial V_b}{\partial x}\right)\right] \tag{6.32}$$

Using the above, the equation governing the longshore current may be written in the following form

$$\frac{d}{dx}\left\{\left(\nu_{tx} + \nu_{txUV}\right)h\frac{dV_b}{dx}\right\} - \frac{d}{dx}\left(F_{Q1}V_b\right) - \frac{f_w u_0 V_b}{\pi} = \frac{1}{\rho}\frac{dS_{xy}}{dx} + \frac{d}{dx}\left(F_{Q21}\right) \tag{6.33}$$

where

$$\nu_{txUV} = -\frac{U_0 h}{2\nu_{tz}}\left(Q_s + \frac{U_b h_t^3}{3h^2} + \frac{b_u h_t^4}{4h^2} + \frac{a_u h_t^5}{5h^2}\right) \tag{6.34}$$

and

$$F_{Q21} = a_{v1}h^2\left(Q_s + \frac{U_b h_t^3}{3h^2} + \frac{b_u h_t^4}{4h^2} + \frac{a_u h_t^5}{5h^2}\right) \tag{6.35}$$

The ν_{txUV} term in (6.33) clearly demonstrates the mixing nature of the interaction term that is being considered in the present chapter. Before we proceed any further it may be worthwhile to estimate the size of the ν_{txUV} term to see how this compares with the ν_{tx} term.

The size of ν_{txUV} is probably most easily estimated by considering the conditions just seaward of the break point because the term in the parenthesis of (6.34) is most easily estimated at that location. As shown before, seaward of the break point we have $a_u \approx 0$ and $b_u h_t \ll U_b$. Therefore, to a very good approximation, we will have

$$\nu_{txUV} \approx -\frac{U_0 h}{2\nu_{tz}}\left(Q_s + \frac{U_b h_t^3}{3h^2}\right) \sim \frac{1}{3}\frac{Q_s^2}{\nu_{tz}} \tag{6.36}$$

where the fact that $U_0 = -Q_s/h_t$ and $h_t \sim h$ have been used. Reasonable estimates of Q_s and ν_{tz} are

$$Q_s \sim 0.1\frac{H^2}{h}\sqrt{gh} \tag{6.37}$$

$$\nu_{tz} \sim 0.01h\sqrt{gh} \tag{6.38}$$

Using these estimates we find that

$$\nu_{txUV} \sim \frac{1}{3}\gamma^4 h\sqrt{gh} \tag{6.39}$$

indicating that if ν_{txUV} were written in the form $\nu_{txUV} = c_{xUV}h\sqrt{gh}$ we would have $c_{xUV} \sim 0.05$ (using $\gamma = 0.6$). Clearly, this is a very strong mixing. Also, this is perfectly capable of replacing the mixing provided by the overestimated ν_{tx}. In other words: we can now assume ν_{tx} to be as small as we have as we have suspected all along (such as $10^{-2}h\sqrt{gh}$ inside the surf-zone and lower outside).

Equation 6.33 may easily be solved with minor modifications to the numerical procedure developed for (6.8) provided the $\nu_{tx}\partial V_b/\partial x$ term in a_{v1} is known. We find that this term is generally small and is easily handled iteratively. The numerical solution used to generate the results discussed below has this term included in an iterative manner. We find that convergence is achieved within three or four iterations. This modification allows us to solve for the effect of interaction for small (and, we believe, realistic) values of c_x.

Figure 6.10 shows the results of a calculation using such reasonable values of c_x. The specific values used in this example are: $c_x = c_z = 0.01$, $b_q = -0.1$ and $f_w = 0.01$. Furthermore, in accordance with expected turbulence characteristics, we let both the horizontal and vertical eddy viscosities decrease quadratically with distance from the break point seaward of that location. The results clearly demonstrate the strength of the mixing provided by the UV interaction between the longshore currents and the undertow and also shows that the high level of lateral mixing required for predictions of the measured cross-shore distribution of the longshore current can be provided by the interaction under consideration here. This supports our earlier conjecture that the lateral and the vertical mixing in the nearshore region is caused by fundamentally different mechanisms. The results of figure 6.10 also support the alternative ordering scheme proposed in section 5.2.1. This ordering scheme suggested that the turbulent mixing does not enter the lowest order equation governing the depth integrated longshore current and the mixing found necessary to explain the longshore current variations comes from the interaction of the longshore currents with the undertow.

These results also show that the undertow may play a very significant role in the establishment of the cross-shore variation of the longshore current both inside and outside the surf-zone. It is also possible to see now that the effect of using $S'_{xy} = \rho\nu_{tx}h(dV_b/dx)$ in the longshore momentum equation (see equation 5.13) instead of $S'_{xy} = \overline{\rho\int_{-h_0}^{\xi}\nu_{tx}(dV/dx)dz}$ is relatively minor since the S'_{xy} term seems to be quite unimportant.

It is interesting to analyze how well the representation $c_x h\sqrt{gh}$ models the mixing caused by the interaction of longshore currents and undertow. As a criterion for the comparison we use equality of the maximum velocity. Figure 6.11 shows one such comparison. The curve labeled "Interaction mixing" has $c_x = c_z = 0.01$ and the eddy viscosities drop off quadratically seaward of the break-point. The dashed line has $c_x = 0.07$ and a quadratic drop of the decay of the eddy viscosity from the break point. The interaction term is neglected in this calculation. (The solution represented by the dashed line essentially assumes that $S'_{xy} + \rho\left\{\int_{-h_0}^{\xi_t} V_1 U dz + \overline{\int_{\xi_t}^{\xi} V_1 u_w dz}\right\} = -c_x h\sqrt{gh}\ \ \rho h(dV_b/dx)$.) The comparison shows that the mixing caused by the interaction seems to be reasonably well

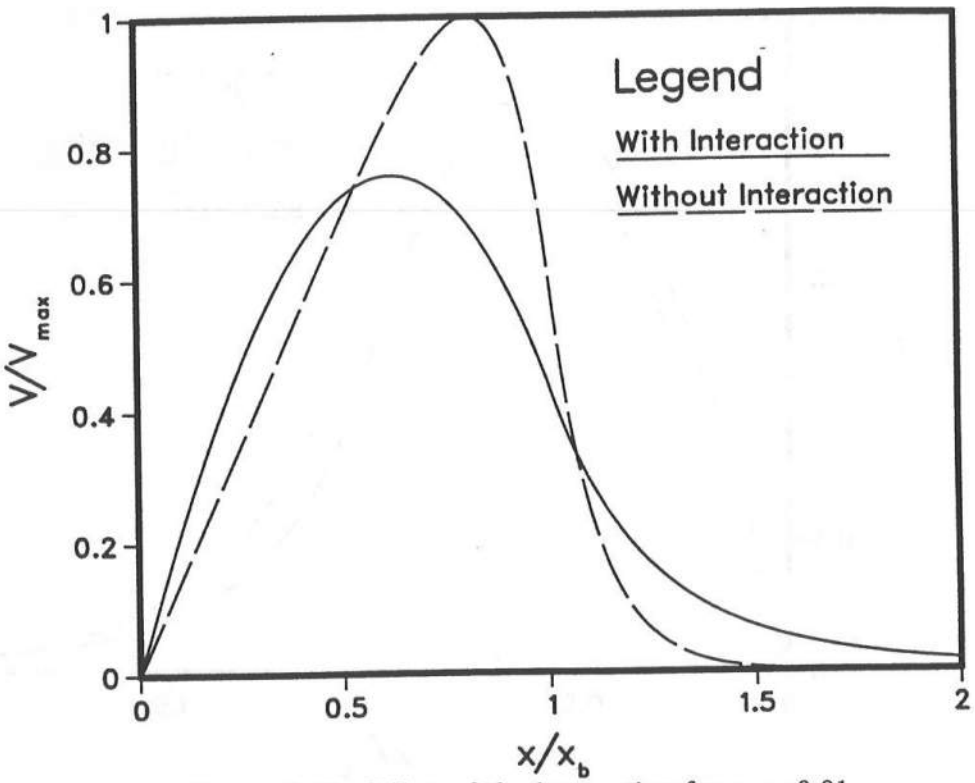

Figure 6.10: Effect of the interaction for $c_x = 0.01$

represented by the formulation adopted. This shows that the mixing found in longshore currents may be caused by the mechanism considered here.

For reasons of clarity, the calculations presented here used very simple variations of wave parameters and a linear friction formulation. It is straightforward to extend the procedure adopted here for more realistic variations of radiation stresses and bottom formulations (like, *e.g.*, the ones used in the previous chapter). The results presented here, we believe, clearly show the large effect of this term.

6.6 Effect of α_s

The most significant assumption made in the results presented in this chapter was assuming that $\alpha_s = 1$ (see equation 6.18). α_s can be calculated if the variations of the longshore current and the wave induced velocity above the trough level were known. However, as remarked before, the specification of the current above trough level is not

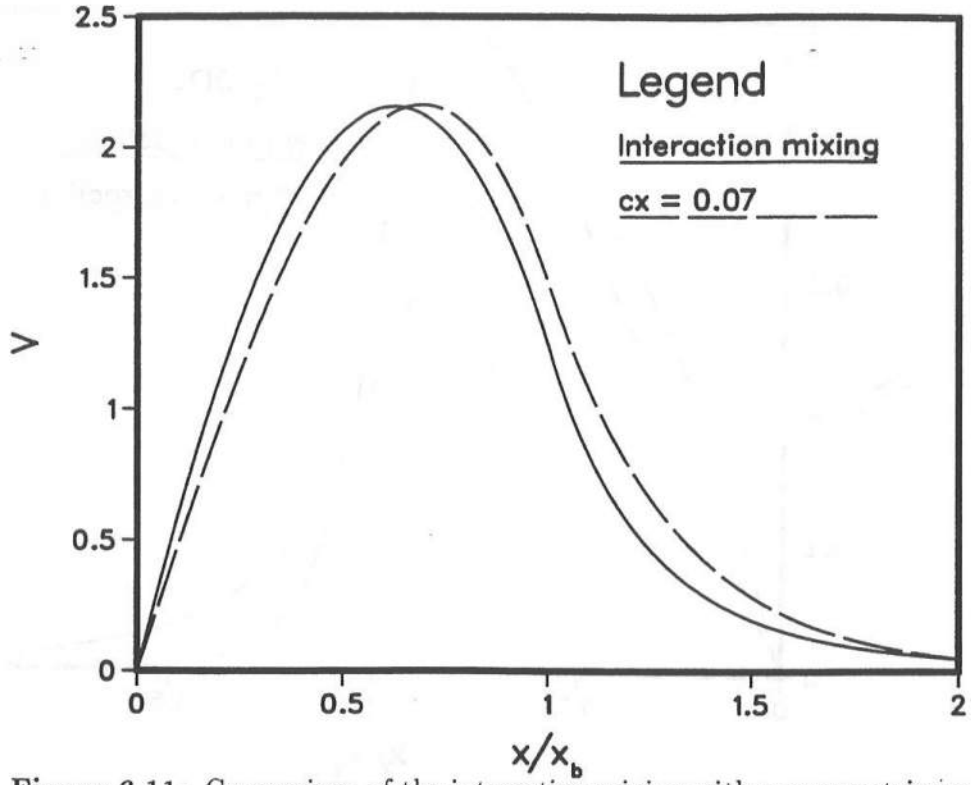

Figure 6.11: Comparison of the interaction mixing with a parametric representation

straightforward. Therefore, there is some uncertainty associated with the contribution to the interaction from above the trough level. To estimate the sensitivity of the results to this contribution we calculate the results using different values of α_s.

Using (6.18) in (6.6) leads to

$$\frac{d}{dx}\left\{h\left(\nu_{txUV1}+\nu_{tx}\right)\frac{dV_b}{dx}\right\}-\frac{\tau^1_{by}}{\rho}-\frac{d}{dx}\left\{F_{q1}V_b+F_{q2}\right\}=\frac{d}{dx}\left(\frac{S_{xy}}{\rho}\right) \tag{6.40}$$

where

$$\nu_{txUV1} = -\frac{U_0 h}{\nu_{tz}}\left(\alpha_s Q_s+\frac{U_b h_t^3}{3h^2}+\frac{b_u h_t^4}{4h^2}+\frac{a_u h_t^5}{5h^2}\right) \tag{6.41}$$

$$F_{q1} = \frac{f_w u_0 h}{\pi \nu_{tz}}\left[\alpha_s Q_s+\frac{U_b h_t^2}{2h}+\frac{b_u h_t^3}{3h}+\frac{a_u h_t^4}{4h}\right] \tag{6.42}$$

and

$$F_{q2}=a_{v1}h^2\left[\alpha_s Q_s+\frac{U_b h_t^3}{3h^2}+\frac{b_u h_t^4}{4h^2}+\frac{a_u h_t^5}{5h^2}\right] \tag{6.43}$$

Figure 6.12 presents the results for different values of α_s. This figure shows that the results depend quite strongly on α_s indicating that the assumed value of $\overline{\int_{\xi_t}^{\xi} V u_w dz}$ has a significant effect on the solution. This figure also shows that it is extremely important to retain the interaction term even if measurements of the longshore current profiles show very little variation over depth below trough level. This is because even if the longshore current is constant over depth below trough level there is the possibility that above trough level the longshore current shows variation with the vertical co-ordinate. The contribution from the interaction term is zero only if the contribution above the trough level completely cancels the contribution from below that level. This happens if the longshore current is the same over the entire water column.[10] Given the importance of the contribution from above the trough level, the difficulty involved in calculating this contribution is particularly disappointing. This presents the most significant uncertainty for a quantification of the mixing caused by the interaction of the longshore currents and the undertow. The results presented here seem encouraging and should provide motivation for an attack on this problem.

In spite of this shortcoming which causes considerable uncertainty in the quantification of the mixing there does seem to be a way to verify the present hypothesis that the mixing in longshore currents is caused by the interaction of the longshore currents and the undertow. This is discussed in the final chapter.

---

[10] It is of course possible to imagine other special variations of the undertow and longshore current that also give zero contribution when integrated over the entire depth.

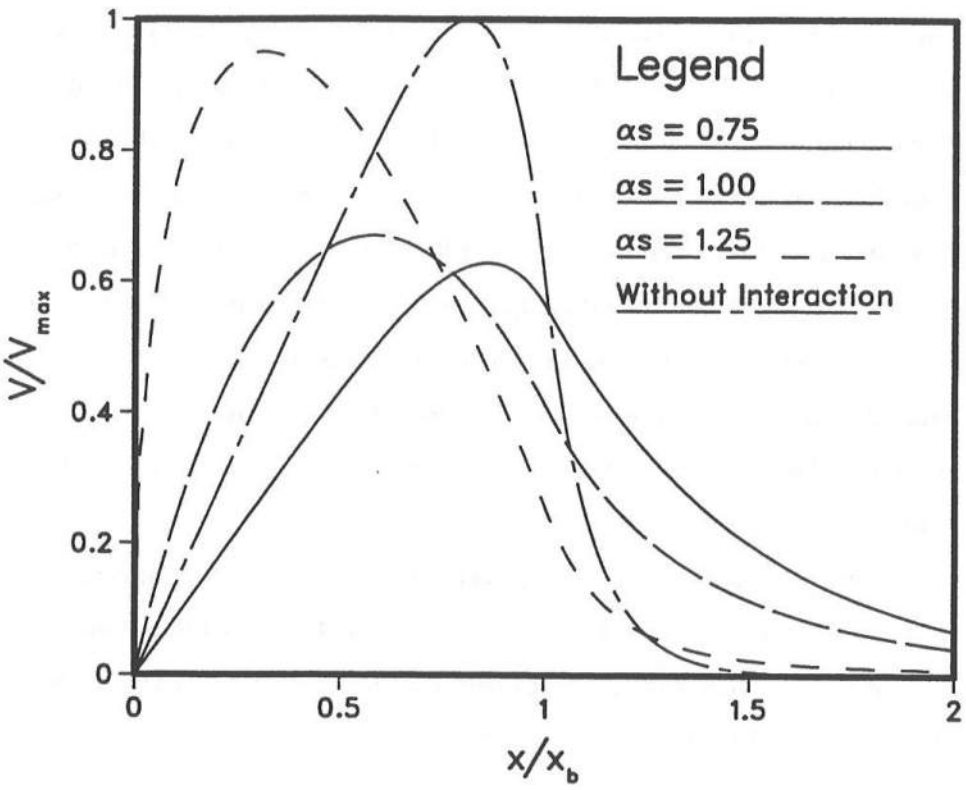

Figure 6.12: Sensitivity to α_s

Chapter 7

SHEAR INSTABILITY OF LONGSHORE CURRENTS

In this chapter we examine the (inviscid) stability of longshore currents to small perturbations of the velocity field. This work was motivated by the recent finding of Bowen & Holman (1989; referred to hereafter as BH89) that under certain conditions steady longshore currents may be unstable to perturbations of the velocity field. BH89 examined the stability characteristics of an extremely simplified longshore current profile. We extend the analysis here to more general profiles. BH89 also suggest that the instability of the longshore currents is responsible for the recently observed extremely low frequency motions in the nearshore region (Oltman-Shay *et al.* 1989). We also study the characteristics of the motion resulting from the instability of the longshore current to determine whether these motions could contribute to the mixing in the nearshore region and whether this contribution could explain the high level of mixing needed for longshore currents.

7.1 Summary of previous work

Tang & Dalrymple (1988) and Oltman-Shay *et al.* (1989) identified extremely low frequency motions in the nearshore region. Oltman-Shay *et al.* showed these motions were a new class of oscillations in the nearshore region. These oscillations were shown to be distinct from gravity waves. They are shorter in length and have longer periods than gravity waves. Frequencies typically range from 10^{-2} to 10^{-3} Hz on natural beaches. This band of frequencies has been called the FIG (Far Infra Gravity) band by Oltman-Shay *et al.* (1989), and the term shear waves has also been used to denote these oscillations. (Since gravity seems to play no part in the generation of these motions it seems more appropriate to use the term "shear waves" as opposed to FIG waves.) Oltman-Shay *et al.* plotted the observed dispersion relationship of the shear waves and compared the same to

the dispersion relationship of traditional infra-gravity motions in the nearshore. A typical plot of the observed dispersion relationship is sketched in figure 7:1. As this figure shows, the frequency of the shear wave for a given wave number is significantly smaller than the frequency of the zero mode edge wave of the same wave number. Zero mode edge wave (the so-called Stokes' mode edge wave) has the lowest frequency for a given wave number among all traditional infra-gravity oscillations.

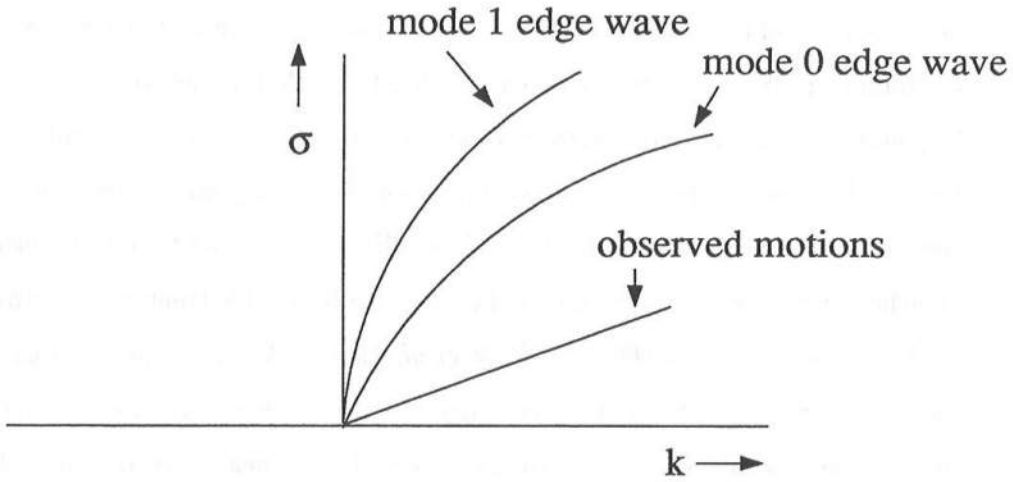

Figure 7.1: Sketch of a typical observed dispersion relationship

Kinematics of shear waves were found to be closely linked to the strength of the mean longshore current. BH89 showed that these observations are consistent with a model based on a shear instability of a steady longshore current.

BH89 solve the instability equation analytically for a horizontal bottom and assuming a triangular velocity profile (this combination of velocity profile and bottom topography is plotted in figure 7.2a). They find that this velocity profile is linearly unstable for a range of longshore wave numbers. Dodd & Thornton (1990) extended the stability analysis to a velocity profile that increases from zero to its maximum value quadratically and then drops off to zero linearly over a bottom topography that consists of a combination of sloping and horizontal regions (see figure 7.2b). Their results for the stability

characteristics are not very different from those found by BH89.

The general problem, that of finding the linear stability of an arbitrary longshore current profile over an arbitrary bottom topography, is far too complex to be amenable to an analytical solution. Therefore, in this chapter we solve the equation of instability numerically. This allows us to study a general range of beach and longshore current velocity profiles.

As a model for the velocity profile, in most cases, we use the longshore current variation given by Longuet-Higgins (1970). Our results for the characteristics of shear waves are qualitatively consistent observations of Oltman-Shay *et al.* This confirms that shear waves are a plausible explanation for the observed temporal and spatial oscillations.

Alternative mechanisms to explain these oscillations have been proposed by Fowler & Dalrymple (1990) and Shemer *et al.* (1991). The first of these essentially consists of the interaction of two wave trains of slightly different frequencies. They show that such an interaction produces a migrating rip-current which has a low frequency signature in the wavenumber-frequency space that is similar to the shear waves. This was also the explanation originally suggested by Tang & Dalrymple to explain their observations. Shemer *et al.* show that a sideband instability of the incident gravity waves leads to a slow modulation of the radiation stress which, in turn, causes a modulation in the longshore currents similar to the observations of shear motions.

7.2 Mathematical formulation

Neglecting the bottom friction and variation of radiation stresses and assuming a gently sloping bottom so that the pressure driving the currents is hydrostatic the depth integrated and wave averaged momentum equation reads

$$\mathbf{u}_t + \mathbf{u} \cdot \nabla \mathbf{u} = -g \nabla \eta \tag{7.1}$$

where $\mathbf{u}(x, y, t)$ is the depth averaged velocity field. The instability equation is derived from (7.1). Following BH89 we assume that the flow field consists of a steady longshore current $V(x)$ and an infinitesimal perturbation $\vec{u}(x, y, t)$. Substituting this into (7.1) and retaining only terms linear in the perturbation leads to

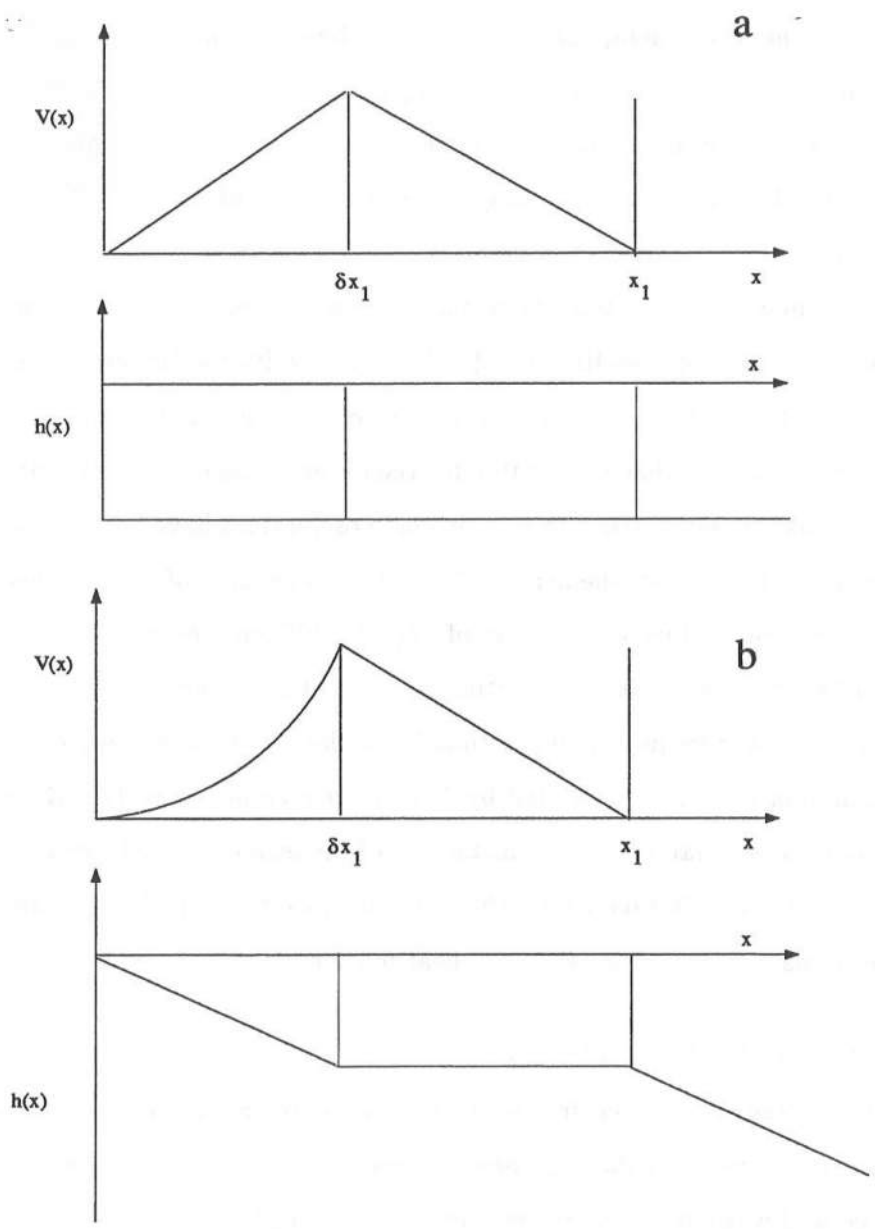

Figure 7.2: Velocity profiles and depth variations used by Bowen & Holman (1989) and Dodd & Thornton (1990)

$$u_t + V u_y = -g\eta_x \tag{7.2}$$

$$v_t + uV_x + V v_y = -g\eta_y \tag{7.3}$$

where u and v are the x and y components respectively of $\vec{u}(x,y)$. Next, we assume that the time rate of change of the surface elevation is small in comparison to the other terms in the continuity equation. This approximation is sometimes referred to as the "rigid lid" approximation though the "lid" is only applied to the conservation of mass. This reduces the continuity equation to

$$\nabla \cdot (h\vec{u}) = 0 \tag{7.4}$$

where h is the undisturbed depth of the fluid column. This form of the continuity equation allows the introduction of a transport stream function, Ψ, such that $\Psi_x = hv$ and $\Psi_y = -hu$. Furthermore, the perturbation may be assumed to be of the form

$$\Psi(x,y,t) = \psi(x) \exp i(ky - \sigma t) \tag{7.5}$$

Elimination of η between (7.2) and (7.3) by cross differentiation and introducing Ψ yields

$$(V-c)(\psi_{xx} - k^2\psi - \frac{\psi_x h_x}{h}) - h\psi(\frac{V_x}{h})_x = 0 \tag{7.6}$$

where $c = \sigma/k$. This is the equation governing the instability. Solutions will be progressive waves with phase velocity equal to the real part of c which is the speed with which the entire perturbation pattern moves in the longshore direction. For those values of the wavenumber where c has a negative imaginary component, the solution has an exponentially growing amplitude which, basically, indicates that the longshore velocity profile, $V(x)$, is unstable to perturbations of the velocity field with that wavenumber.

Equation 7.6 is a modified Rayleigh equation and the eigenvalues occur in complex conjugate pairs similar to the well known result for the Rayleigh equation (Drazin and Reid 1982, p. 131). With this in mind, in all the plots we show in the following we indicate only the magnitude of the imaginary part of σ – the sign is understood to be negative.

For the situations studied, the boundary conditions associated with (7.6) are

$$\psi = 0 \quad @ \quad x = 0, x \to \infty \tag{7.7}$$

Equation 7.6 is difficult to solve analytically for a general velocity distribution, $V(x)$, and/or bottom profile. Hence, we resort to a numerical solution. Before proceeding to the numerical solution, however, it is probably worthwhile to spend some time deriving some general conditions that are necessary for the existence of an instability.

7.2.1 Necessary conditions for the existence of an instability

We now proceed to derive some necessary conditions for the existence of an instability. Mainly, we will derive the modified forms of the Rayleigh and Fjortoft conditions. The derivation here closely follows the derivation of these conditions for the Rayleigh equation in Drazin & Reid (1982, pp. 131-132) and is a minor extension of those results. To derive the modified conditions rewrite (7.6) in the form (for $V \neq c$)

$$\left(\frac{\psi_x}{h}\right)_x - \frac{k^2\psi}{h} - \left(\frac{V_x}{h}\right)_x \frac{\psi}{V-c} = 0 \tag{7.8}$$

Multiplying (7.8) by ψ^*, the complex conjugate of ψ, and integrating from $x = 0$ to $x = \infty$ we get, after applying the boundary conditions,

$$\int_0^\infty \left[\frac{|\psi_x|^2}{h} + \frac{k^2|\psi|^2}{h}\right] dx + \int_0^\infty \frac{|\psi|^2}{V-c}\left(\frac{V_x}{h}\right)_x dx = 0 \tag{7.9}$$

The fact that $\Psi_x = hv$ implies that ψ_x/h is bounded at the shoreline has been used above. The real and imaginary parts of (7.9) are:

Real

$$\int_0^\infty \left[\frac{|\psi_x|^2}{h} + \frac{k^2|\psi|^2}{h}\right] dx + \int_0^\infty \frac{|\psi|^2 (V-c_{re})}{(V-c_{re})^2 + c_{im}^2}\left(\frac{V_x}{h}\right)_x dx = 0 \tag{7.10}$$

Imaginary

$$c_{im}\int_0^\infty \frac{|\psi|^2}{(V-c_{re})^2 + c_{im}^2}\left(\frac{V_x}{h}\right)_x dx = 0 \tag{7.11}$$

(7.11) leads to the Rayleigh condition stated by BH89, *viz.*, that V_x/h must have an extremum in the domain for the existence of an instability ($c_{im} \neq 0$). Adding

$$(c_{re} - V_s)\int_0^\infty \frac{|\psi|^2}{(V-c_{re})^2 + c_{im}^2}\left(\frac{V_x}{h}\right)_x dx = 0$$

to (7.10) we get (V_s is the value of V where $(V_x/h)_x = 0$)

$$\int_0^\infty \frac{|\psi|^2 (V - V_s)}{(V - c_{re})^2 + c_{im}^2} \left(\frac{V_x}{h}\right)_x dx = -\int_0^\infty \left[\frac{|\psi_x|^2}{h} + \frac{k^2|\psi|^2}{h}\right] dx < 0 \tag{7.12}$$

which shows that $(V_x/h)_x(V - V_s) < 0$ in some part of the domain for an instability to exist. Note that the modified forms of the Rayleigh and Fjortoft conditions are not sufficient conditions and, therefore, do not guarantee the presence of an instability.

7.3 Numerical formulation

To obtain ample numerical accuracy, we use a fourth order finite difference scheme to represent the derivatives in (7.6) and solve for the eigenvalues and eigenfunctions of the governing equation. The details of the numerical scheme are shown in appendix D. When the governing equation (7.6) is discretized using the finite difference approximations given in appendix D the following matrix equation results

$$[A]\{\psi\} = c[B]\{\psi\} \tag{7.13}$$

Here A and B are N by N matrices and $\{\psi\}$ is a vector of size N where N is the number of points used across the flow region. For the prescribed boundary conditions this equation can be solved only for certain values of c – the eigenvalues. These eigenvalues of the matrix equation are equivalent to the eigenvalues of the governing equation (7.6). For each value of the wave number k, (7.13) will yield N eigenvalues. We are particularly interested in values of k where the eigenvalue has an imaginary component. In cases where more than one such eigenvalue is present, it is assumed that the one with the largest imaginary component will dominate the instability of that wavenumber. If, for a particular value of k, all the eigenvalues are real then the longshore current is neutrally stable to disturbances with wave number k.

The solution of the generalized eigenvalue problem defined by (7.13) is quite standard and use may be made of well established mathematical routines. The routine used here is based on the algorithm of Moler and Stewart (1973) and is capable of handling the case where one of the two matrices A or B is singular.

7.4 Numerical results

The numerical model is used to investigate the stability of various longshore current profiles on arbitrary bottom topographies. This implies that for a given velocity profile and bottom topography, we solve (7.13) for various values of k and, for each k, the eigenvalues are determined. Figure 7.3 shows a comparison of the numerical and analytical solutions for the growth rate for the situation studied by BH89. The comparison presented is for $\delta = 0.5$. 400 nodes were used in the numerical solution and the seaward boundary condition was applied at $x = 2x_1$ (x_1 and δ are defined in figure 7.2). Figure 7.3 shows that the numerical solution is fairly accurate.[11]

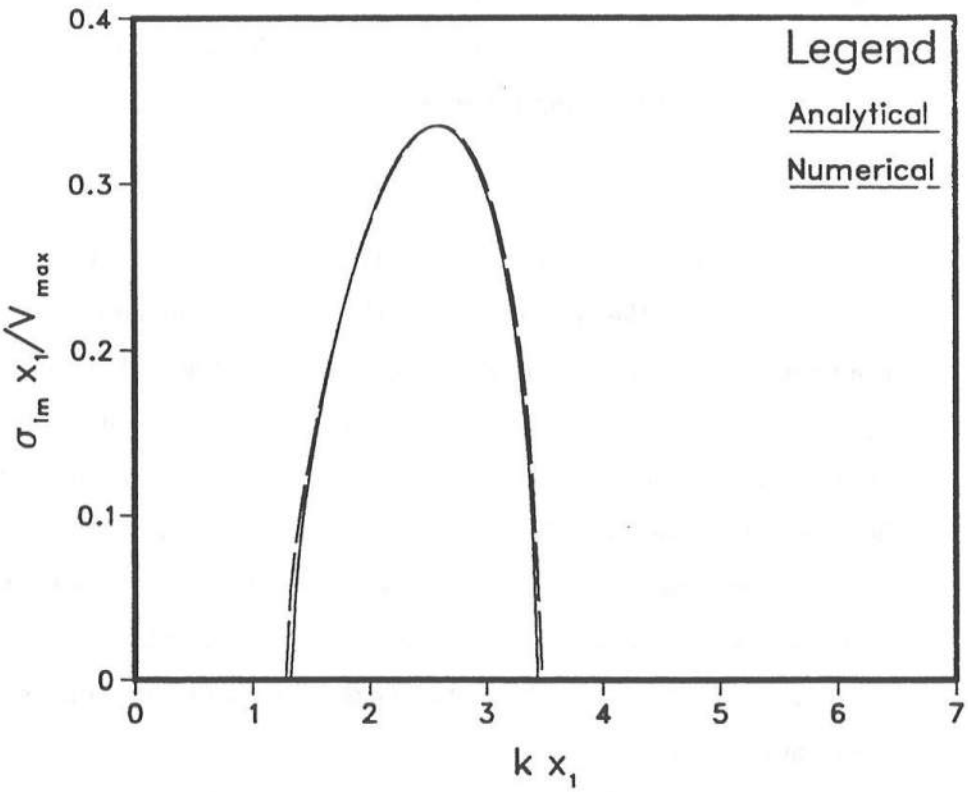

Figure 7.3: Comparison of numerical solution with the analytical result of BH89 ($\delta = 0.5$)

[11] Note that a slight modification of the numerical procedure is required to handle the BH89 case. This is because of the discontinuity of V_x at $x = \delta x_1$ and x_1. The solution has to be matched at these points. The matching conditions used are continuity of η and ψ at these points. As far as the numerical procedure is concerned, this translates into replacing the differenced form of the governing equation by the matching conditions at these points in the overall matrix equation (D.8) of appendix D.

The real part of σ is much greater than the imaginary part shown in figure 7.3. The absolute inaccuracies in the calculation of the real part of σ are of the same magnitude as those seen in figure 7.3. Inaccuracies of such small magnitude are not discernible on a plot similar to figure 7.3 for the variation of σ_{re} vs k.

The longshore current distribution has a substantial influence on the occurrence of the instabilities and the distribution used by BH89 is quite unrealistic. We wish to study the stability of more realistic longshore current distributions. As a characteristic example, we choose to use the distribution given by Longuet-Higgins (1970). As discussed in chapter 4, these are one parameter profiles are given by

$$\frac{V}{V_m} = f(\frac{x}{x_b}, P) \tag{7.14}$$

with a shape that depends on the parameter P which is a dimensionless parameter depending on the strength of turbulent mixing. In (7.14) x_b is the width of the surf-zone, V_m is the longshore current velocity at x_n for $P = 0$. For the present purposes it suffices to note that higher values of P reduce the maximum velocity, shift the point of maximum velocity closer to the shoreline and lead to smoother velocity profiles. The profiles were plotted in figure 5.1 for different values of P.

7.4.1 Effect of bottom topography

To get a first estimate of the effect of the bottom topography consider the form of (7.6) for the special case of a beach profile given by

$$h = ax^n \tag{7.15}$$

Here a is a function of the ratio, h_b/x_b, breaker depth to surf-zone width (a measure of the overall beach steepness in cases where $n \neq 0$). This class of profiles includes the constant depth case studied by BH89 ($n = 0$), the plane beach case ($n = 1$) and the equilibrium beach profile ($n = 2/3$) (Bruun 1954 and Dean 1977). Substituting into (7.6) leads to

$$(V - c)(\psi_{xx} - k^2\psi - \frac{n\psi_x}{x}) - \psi V_{xx} + \frac{n\psi V_x}{x} = 0 \tag{7.16}$$

Since a does not occur explicitly in (7.16) or the corresponding boundary conditions we conclude that the eigenvalues, c, of (7.16) are independent of a and hence of the overall

beach steepness. c, however, may still depend noticeably on the configuration of the depth variation and also vary implicitly with other factors such as the beach steepness and wave conditions via the way these factors influence $V(x)$.

In this section we further limit the discussions to the study of four characteristic topographies (figure 7.4). These are:

1. $h(x)$ constant - Horizontal bottom
2. $h(x) = x^{2/3}$ - 'Equilibrium' profile (Brunn 1954 and Dean 1977)
3. $h(x) = x$ - Plane beach
4. $h(x) = x - \frac{x_b}{2} \exp\left[-30\left(\frac{x-x_b}{x_b}\right)^2\right]$ - 'Barred' profile with bar crest at break point

Figure 7.5 shows overall results for the variations of σ (fig. 7.5a the real part and fig. 7.5b the imaginary part) with k for these topographies. For simplicity, we keep the longshore current distribution the same for all four topographies by letting P be fixed at 0.5.

In figure 7.5 we see that the real part of σ is quite insensitive to the bottom topography. Since the magnitude of the imaginary part is generally very small in comparison with the real part, the absolute value of σ is essentially determined from the real part. These results suggest that not only is the magnitude of c independent of the overall beach steepness but it is also quite insensitive to the shape of the beach profile.

The imaginary part of σ gives the growth rate of the instability and figure 5a shows that σ_{im} varies significantly with the shape of the beach profile. The higher the growth rate, the more likely it is that the instability will overcome the threshold of stabilizing frictional forces (neglected here) and become observable. The results of figure 7.5 therefore indicate that a barred bottom topography is much more conducive to the development of shear waves.

It is also interesting to see that there is a significant difference in the growth rates for the horizontal bottom and the plane beach cases. On a plane slope, the maximum σ_{im} is both much smaller and occurs at a somewhat smaller kx_b than on the horizontal bottom. This result is in direct contrast to the results of Dodd & Thornton (1990) who found no

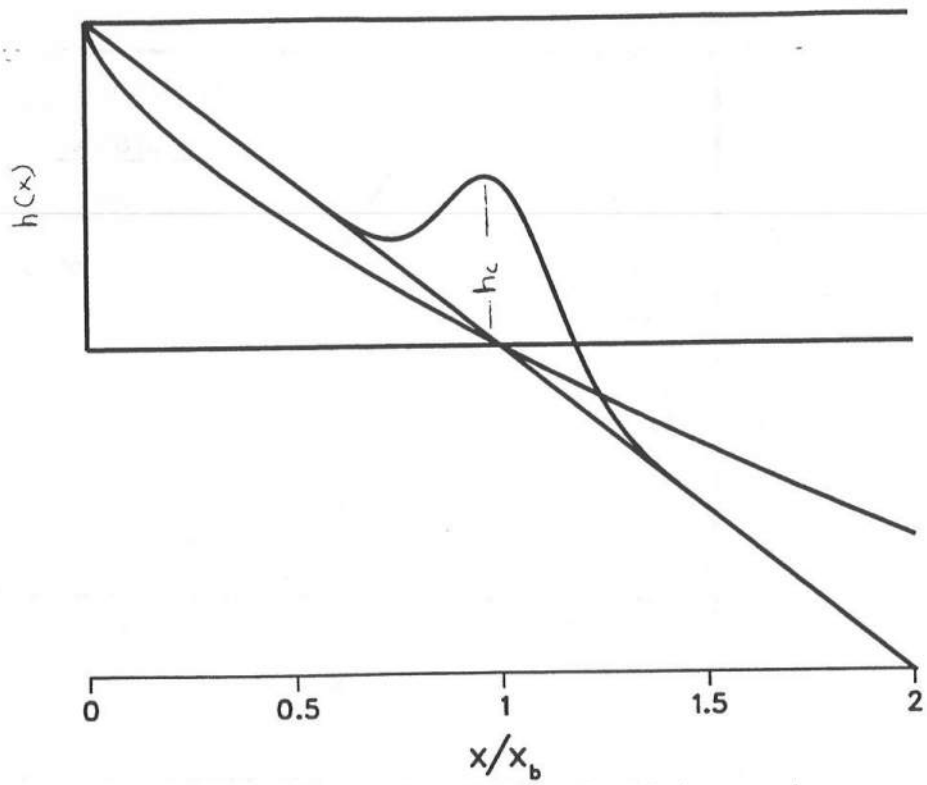

Figure 7.4: The depth variations used

such effect although part of beach profile was a plane slope. This is probably because their combination of current distribution and beach profile actually have a constant depth on the seaward face of the longshore current distribution similar to BH89. Our results and the results of BH89 suggest that this is the important region for the instability mechanism. This is also the region where typically $(V_x/h)_x(V - V_s) < 0$ (V_s is the value of V where $(V_x/h)_x = 0$) which is a necessary condition for the the existence of an instability according to the slightly modified form of Fjortoft's theorem derived earlier. This is the likely reason why the results of Dodd and Thornton do not show the strong effect of the slope. Notice that for the profiles used by BH89 and Dodd and Thornton $(V_x/h)_x$ is zero everywhere except at $x = \delta x_1$ where it is undefined.

Some of the curves in figure 7.5a show irregular humps at the higher values of k. The eigenvalues in that region are highly dependent on the number of nodes used in the computation indicating that for these values of k convergence has not been achieved with

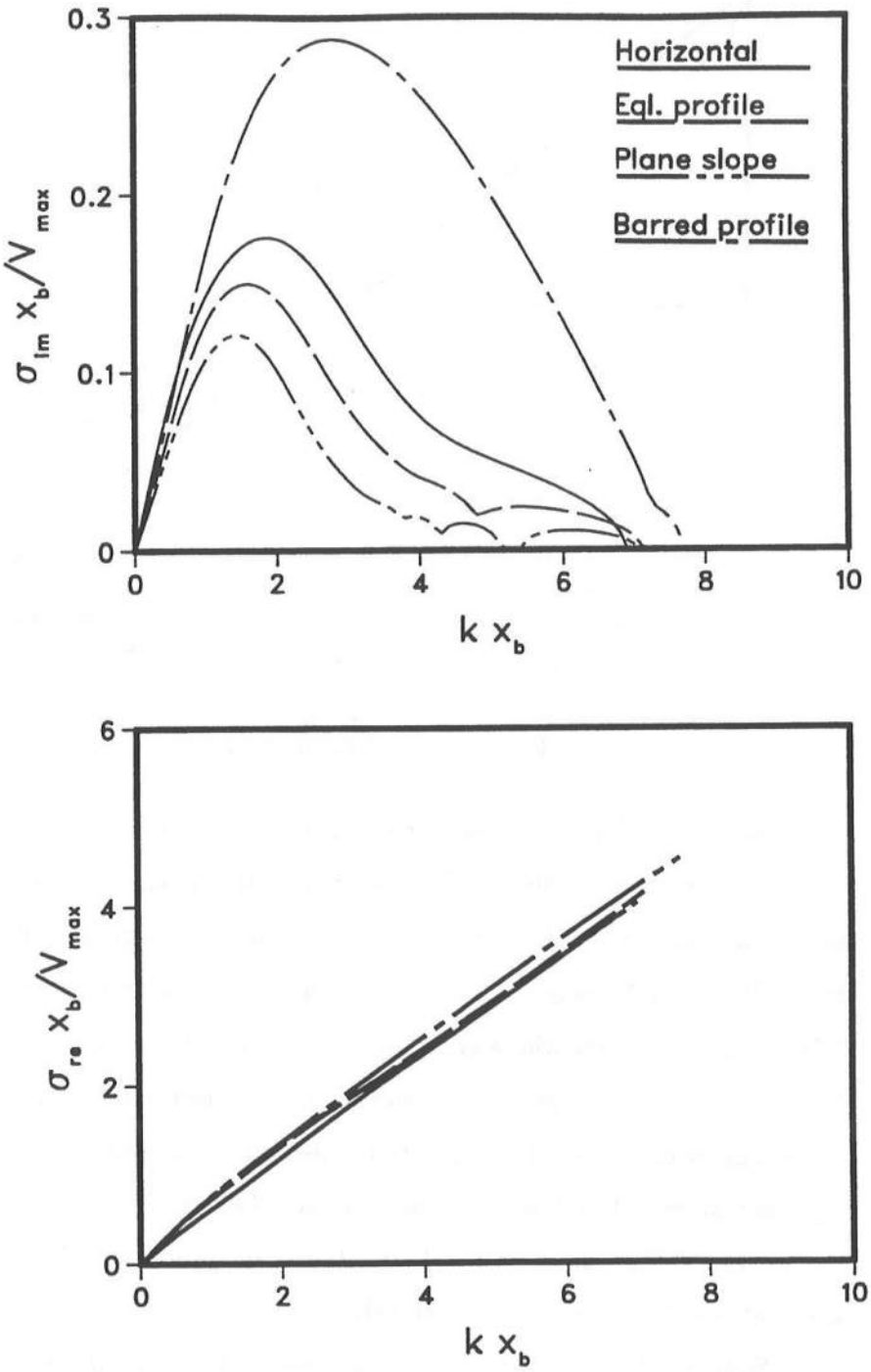

Figure 7.5: Variation of σ for bottom topographies considered

the number of nodes used in the computation. However, these are not of great concern because we have found that the maximum value of σ_{im} (which is the quantity of interest) is well defined and does not depend on N for sufficiently large N. We will discuss this problem further in section 7.8.

In the same region of large k values intervals occur where σ is purely real. In such cases there is no instability and we cannot define a unique eigenvalue. The gaps (not clearly visible in these plots, but gaps are present at relatively large values of k) in the dispersion relationship for the sloping bottom situation correspond to k values for which there is no imaginary part of the frequency, σ, for the number of nodes used in the computation.

7.4.2 Effect of the location of the bar crest

Since figure 7.5 shows that the presence of a bar significantly influences the stability characteristics of the longshore current profile, it is of interest to investigate this effect more closely.

It turns out that on barred beaches one of the important parameters for the instability is the position of the maximum of the current relative to the bar crest. On a given beach profile the variation in wave conditions may change this position substantially. Field data of Sallenger & Howd (1989) shows that the bar crest is not always located at or near the break point. Hence, it is relevant to examine the effect of the location of the bar crest relative to the break point. We have, for simplicity of discussion, chosen to illustrate this effect by letting the position of the current maximum and bar crest be independent parameters and have performed a parametric study using (7.14) for a range of P values.[12]

To do this we model the bottom variation by

$$h(x) = x - h_c x_c \exp\left[-30\left(\frac{x - x_c}{x_c}\right)^2\right] \tag{7.17}$$

[12] A direct computation of the actual longshore current profiles could easily be made for different depth profiles, for example, using the numerical solution of chapter 5. However, that would only introduce discussions regarding the various assumptions involved in the modelling of longshore currents and which value of P to be used. Such discussions will only detract from the clarity of the present discussion. Furthermore, the effects of bottom and velocity profiles on the stability characteristics can no longer be separated.

where x_c is the location of the crest of the bar and h_c is the dimensionless height of the bar relative to the local plane beach depth (see figure 7.4). In all the results presented here $h_c = 0.5$ has been used.

Figure 7.6 shows the variations of σ_{im} and σ_{re} with k for some characteristic values of x_c compared to the case of no bar (plane beach). For $x_c = 0.46x_b$ (the crest location coinciding with the location of the maximum velocity when $P = 0.5$) the imaginary part follows quite closely the curve for the case without a bar.

The curve for $x_c = 0.6x_b$ (bar crest seaward of the current maximum) on the other hand, has values of σ_{im} that are significantly lower than that in the case of no bar. Also, for this case, there is a local minimum in the value of σ_{im} at $kx_b \approx 3.5$. The values of σ_{im} for the higher values of k are not insignificant.

The curve for $x_c = 0.65x_b$ has a maximum value comparable to that for $x_c = 0.6x_b$. However, this maximum occurs at $kx_b \approx 5$ as opposed to $kx_b \approx 1.5$ for the former case. Also, with $x_c = 0.65x_b$ there are two relative minima of σ_{im}.

The plot of the real part shows that the curve for $x_c = 0.6x_b$ has a discontinuity at $kx_b \approx 3.5$. Also, the slope of σ_{re} vs k changes considerably at this point. The curve for $x_c = 0.65x_b$ starts out with a relatively high value of the slope (relative to the case without a bar) which jumps to a value comparable to the case without a bar around $kx_b \approx 1.5$ as marked by the discontinuity in the value of σ_{re} at that point. This process is reversed at $kx_b \approx 2$ where there is another discontinuity in σ_{re} similar to the case of $x_c = 0.6x_b$.

The curve for $x_c = 0.7x_b$ shows that σ_{re} varies almost linearly with k with a slope that is comparable to the higher of the slopes for the $x_c = 0.6x_b$, $0.65x_b$ cases and no discontinuities occur. Comparison of figures 7.6a and 7.6b reveal that the locations of the discontinuities in the dispersion relationship coincide with the locations of the relative minima of the σ_{im} curves indicating that these two phenomenon may be linked. Closer inspection reveals that this is indeed the case.

The mechanism responsible for this behavior is illustrated in figure 7.7. Essentially what happens is the following: For all the cases in the absence of the bar there is one

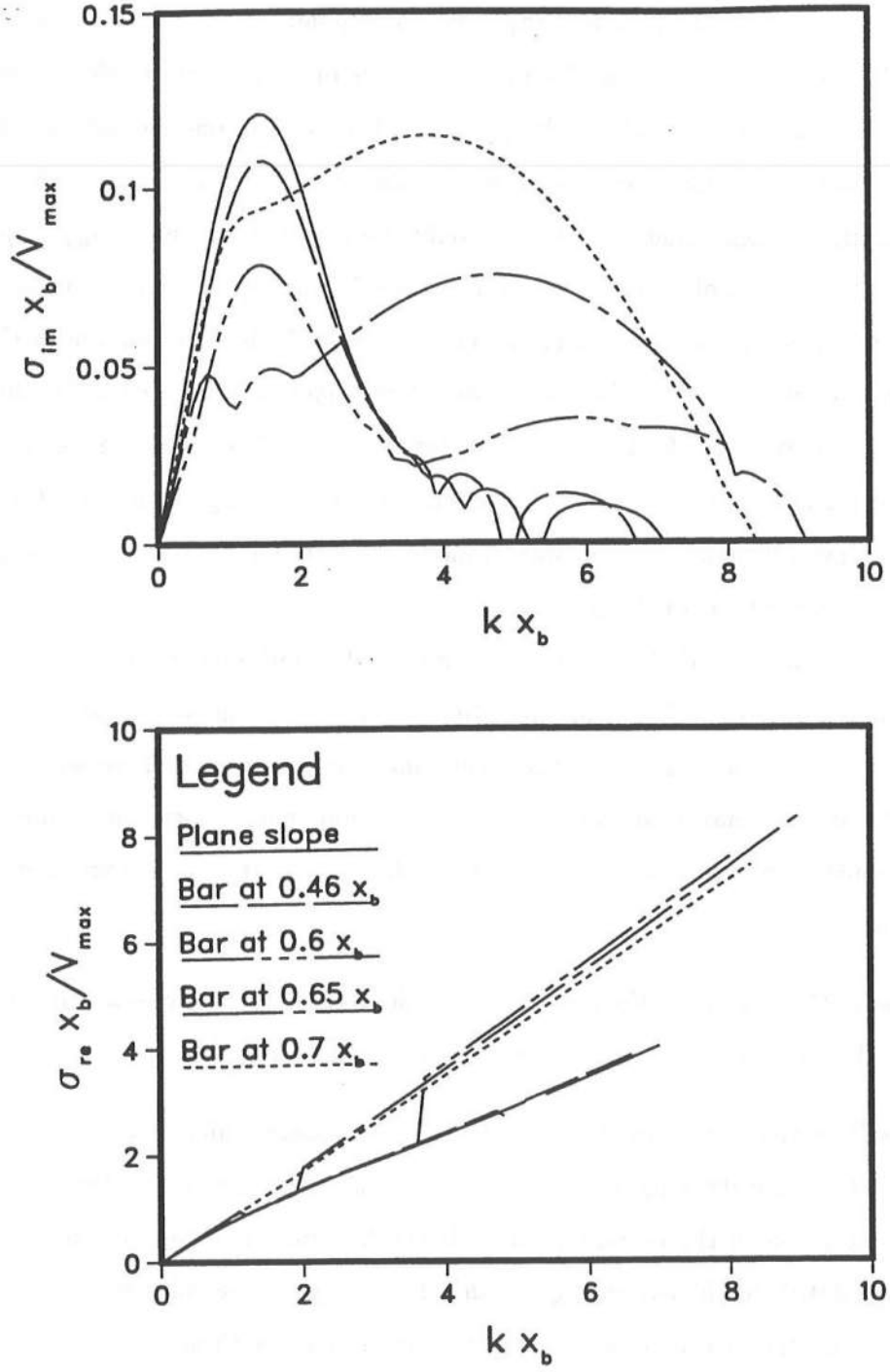

Figure 7.6: Variation of σ for different bar crest locations

eigenvalue with a dominant imaginary part for a given k (indicated by "dominant eigenvalue" on the sketch of figure 7.7a). This corresponds to one dominant mode of instability in this case. The presence of a bar introduces other possible modes of instability. This is indicated in figure 7.7b by the presence of more than one eigenvalue with comparable imaginary components. In fact, several modes of motion are theoretically possible for this case. If, for each value of k, we plot only the maximum value of σ_{im} as per section 7.3, the intersections of two of these modes would show up as local minima in the plots of σ_{im} provided the situation is as sketched in figure 7.7b. The minima in the plots of σ_{im} therefore separate intervals of k where different modes of the instability dominate.

The real part for the various modes may be as sketched in figure 7.7c. Since a swap from one mode to another is also associated with a change in propagation speed for the whole instability pattern the swap of modes corresponds to discontinuities in the real part at the intersections of the modes.

We have carried out extensive numerical experiments with various locations of the bar crest, different velocity profiles, different basic bottom configurations (like, *e.g.*, a bar on a horizontal bottom), *etc.* The results indicate that a general sequence of events occurs as the bar crest moves seaward from the maximum velocity location. Some elements of this sequence have been alluded to in the preceding paragraphs. The sequence is essentially as follows:

- In the absence of the bar (the plane slope case) there is one well defined mode which has a growth rate that is significantly higher than the others.

- The presence of the bar introduces other modes which have non-zero growth rates. The important parameter is the position of the bar crest relative to the maximum location of the current profile. If the bar crest is shoreward of a certain position relative to the current maximum (depending on the value of P and the bar height) then the instability is essentially as on a beach with no bar.

- As the bar moves seaward relative to the current distribution the instability of the mode that occurs in the absence of the bar gets weaker. At the same time, the

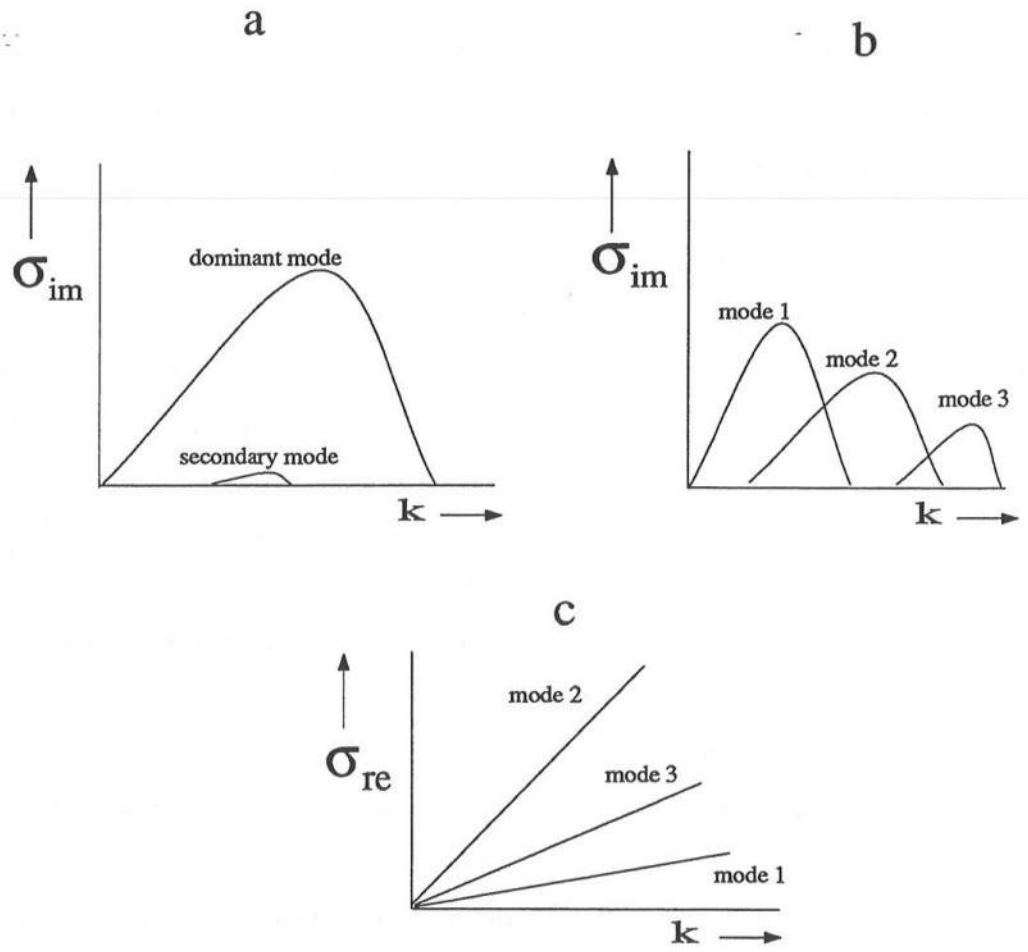

Figure 7.7: Sketch of the jump mechanism

strength of the instability of the mode(s) induced by the bar increases.

- As the bar moves further seaward, all the modes that are excited due to the presence of the bar combine to give one mode with a dominant imaginary component. This mode is quite different from that excited in the absence of the bar: a mode swap occurs.

- If the bar is sufficiently seaward of the maximum of the current profile the bar ceases to influence the stability and we simply return to the solution for the case with no

bar, and with the instability the same as that with a constant beach slope. The entire instability is located shoreward of the bar.

A very similar effect and sequence of events occur if the location of the bar crest is maintained a constant and the height of the bar is varied.

7.4.2.1 The flow pattern

To more clearly demonstrate the difference between the two characteristic modes described above figures 7.8 and 7.9 show the particle velocities induced by the shear wave instability for $kx_b = 3.5$ and $kx_b = 3.6$ for $P = 0.5$ and bar crest located at $0.6x_b$. (We will discuss the spatial structure and the determination of the induced velocities in a later section.) We choose these two values of kx_b because although the two values are very close the mode interchange occurs between these values of kx_b. The first of the plots ($kx_b = 3.5$) shows that there is a significant induced velocity seaward of the bar crest at $0.6x_b$. The induced velocity distribution is in fact very similar to that due to a shear wave generated on a plane beach, which indicates that it is essentially the same mode of motion. In Figure 7.9 ($kx_b = 3.6$) the motion is almost entirely confined to a region shoreward of the bar. Hence, this is a mode that is virtually trapped by the bar. Our numerical experiments indicate that the essential effect of the bar is to trap the shear wave shoreward of the bar even when there are significant longshore current velocities seaward of the bar crest.

7.4.3 Effect of longshore current velocity profile

In this section we examine the the effect of varying P in the longshore current distribution (7.14). As noted earlier, decreasing P is equivalent to increasing the maximum velocity and shifting the position of the maximum velocity closer to the break point thus increasing δ and therefore increasing the shear on the seaward face of the velocity profile. Figure 7.10 shows the variation of σ_{im} and σ_{re} with k for $P = 0.1, 1.0$ (see figure 7.5 for results corresponding to $P = 0.5$). Results for horizontal bottom, sloping bottom and a sloping bottom with a bar crest at breakpoint are shown. It is clear that decreasing P (*i.e.*, increasing the shear) increases the maximum unstable frequency, $\sigma_{im,max}$, and also increases the range of wavenumbers over which the instability occurs. This implies that

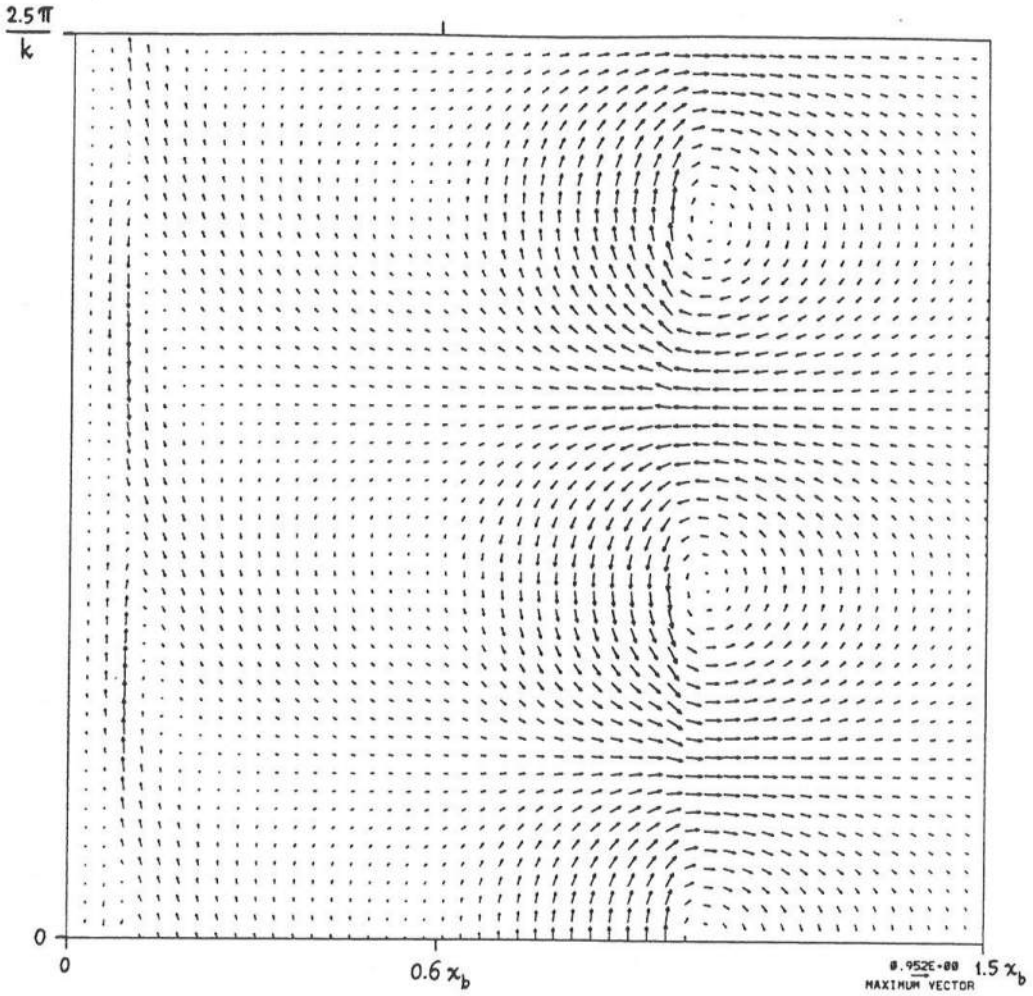

Figure 7.8: Plot of the distribution of the shear-wave induced velocity for $P = 0.5$, bar crest located at $0.6x_b$, $kx_b = 3.5$

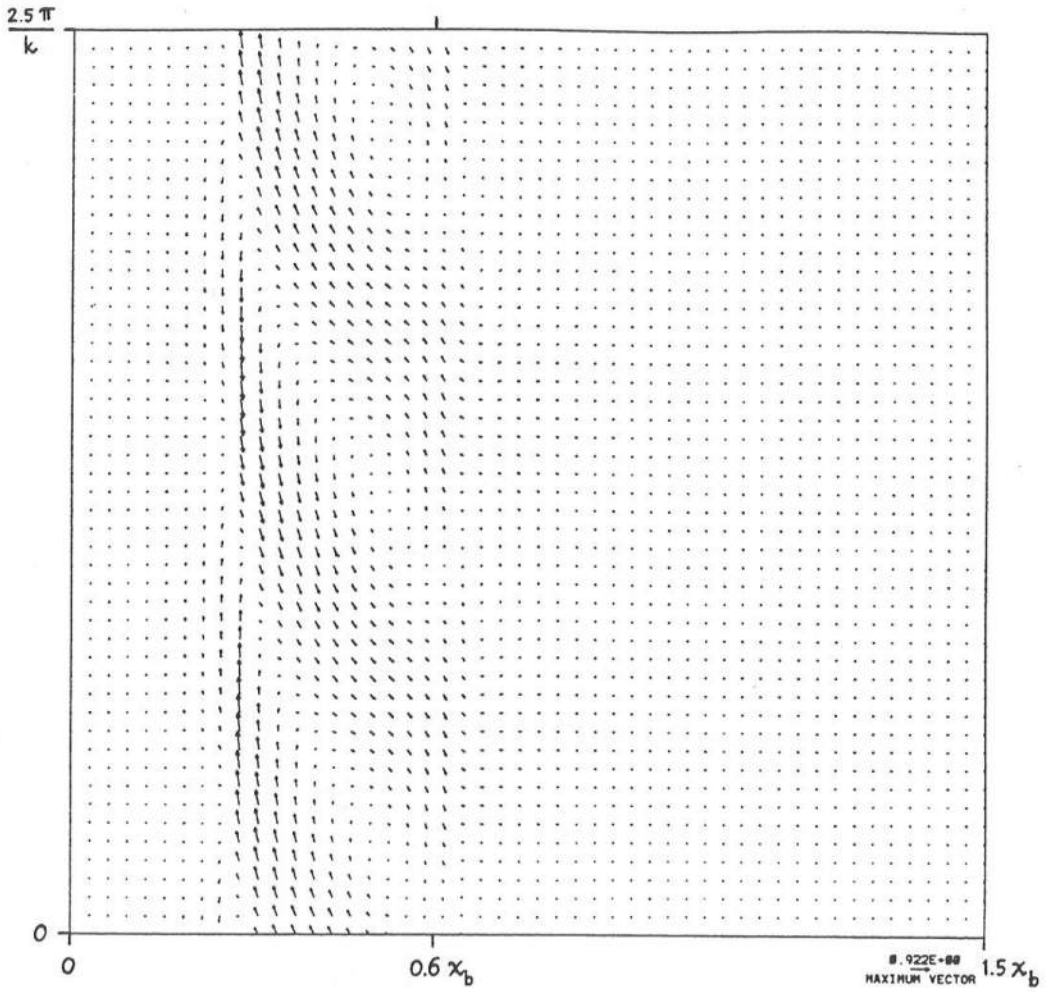

Figure 7.9: Plot of the distribution of the shear-wave induced velocity for $P = 0.5$, bar crest located at $0.6x_b$, $kx_b = 3.6$

the strength of the instability increases with increasing shear on the seaward face. We also note that the higher the value of P the more dramatic is the difference between the flat bottom and slope situations and that in all cases the barred topography is significantly more unstable than the other two situations. The variation of σ_{re} with k (figure 7.10b) shows that that quantity and hence the propagation speed of the instability is much less sensitive to the backshear.

Also, we have performed a similar analysis for the velocity profile used by BH89. Not surprisingly, similar behavior occurs for the BH89 profile and hence confirms the result of BH89 that the shear on the seaward face is one of the more important parameters of the problem.

7.5 Spatial structure of shear waves

Once the eigenvalues of (7.13) are known, the corresponding eigenvectors may be calculated in a straightforward manner. As usual, the eigenvectors are can only be determined correct to an arbitrary multiplicative constant.

The strict mathematical formulation requires the imposition of $\psi = 0$ as $x \to \infty$. Obviously, this condition has to be applied at a finite distance in a numerical solution. Numerical experiments indicate that $\sigma_{im,max}$ is quite insensitive to the location of application of the seaward boundary condition (some evidence of this will be given in section 7.9). The same is true, though to a lesser extent, of the stream function.

Figures 7.11a and 7.11b show respectively the variations of the real and imaginary parts of the stream function for the horizontal bottom, sloping bottom and barred profile (with bar crest at break-point) cases. These correspond to values of the wavenumber, k, which has the highest growth rate ($kx_b = 1.9$ [horizontal bottom], $kx_b = 1.4$ [plane beach], $kx_b = 2.8$ [barred profile] for the conditions considered here [$P = 0.5$]; see figure 7.5a for the variation of σ_{im} with k). The stream function has been normalized such that it has a value of $1 + 0i$ (in arbitrary units) at $x = x_b$. These plots show that up to about $0.75x_b$ the stream functions for the plane and barred beach situations are reasonably close to one another. Since in this region the depths of these two situations have more or less the same variation it follows that the induced velocities will be similar for these cases in this

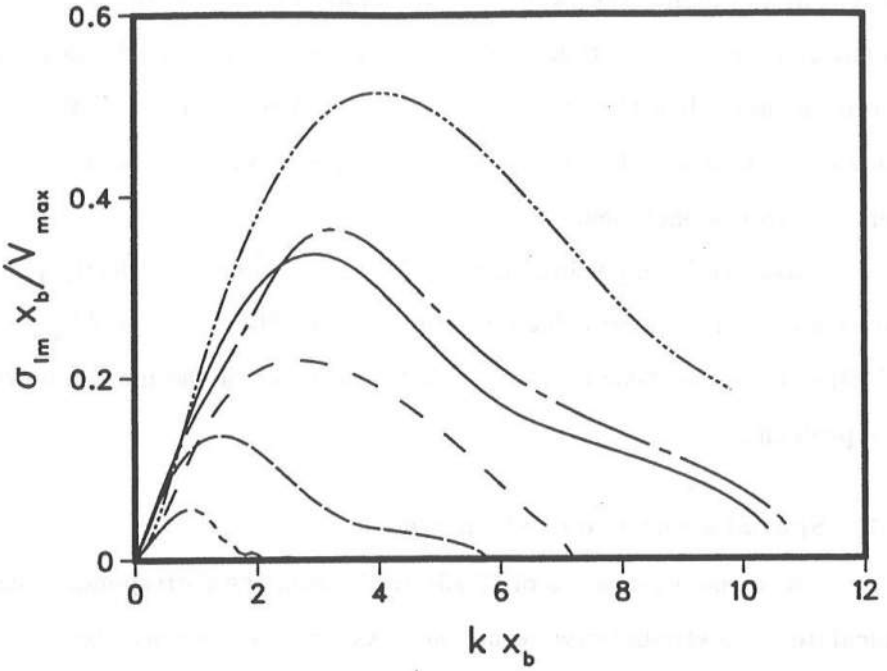

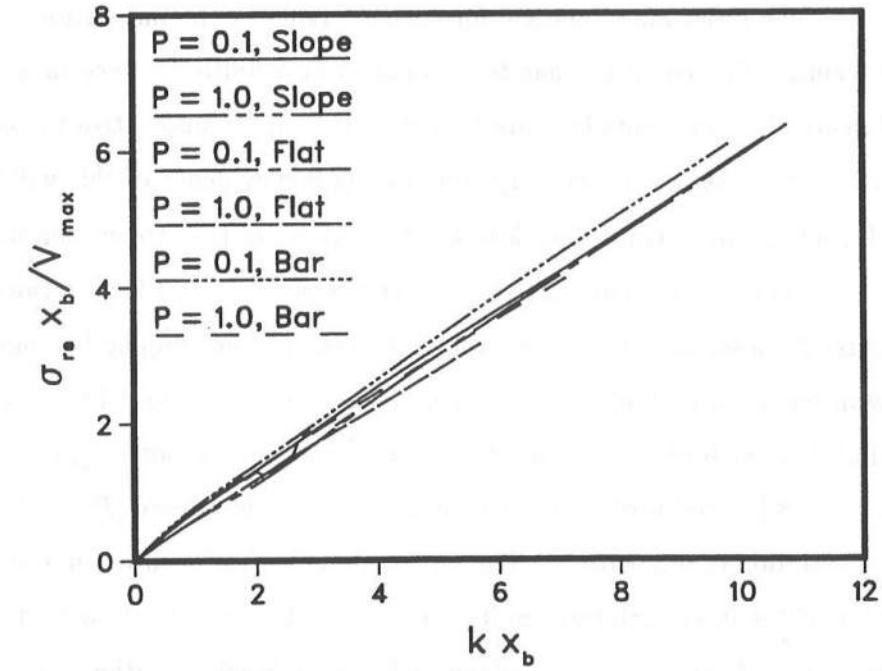

Figure 7.10: Variation of σ for $P = 0.1, 1.0$

region. Around the break point the stream function for the barred beach shows extremely rapid variation in comparison with the other two cases indicating that the induced velocity in this region would be much higher for this case than in the other two cases. Seaward of the break point the decay of the stream function for the barred profile case is much weaker than the variation near the break point which indicates small induced velocities in comparison with values at break point. This indicates that the induced velocities for the barred profile case are mainly concentrated near the breaker line which coincides with the location of the bar crest in this case. A plot of the induced velocity for this case shows that the velocity distribution is very similar to that presented in figure 7.9 except for the fact that in the present case the region of high induced velocities is around x_b as opposed to around $0.6x_b$ in figure 7.9.

Similar plots of the shear wave induced velocities demonstrates that the horizontal bottom solution has circulation cells extending much further offshore than the sloping bottom case. This can be readily understood by noticing that before substituting (7.5) the equation for Ψ can be written (neglecting small terms)

$$\frac{D\gamma}{Dt} = \Psi_y \left(\frac{V_x}{h}\right)_x \tag{7.18}$$

where $D/Dt = \partial/\partial t + V\partial/\partial y$ and $\gamma = \Psi_{yy}/h + (\Psi_x/h)_x$ is the potential vorticity of the shear wave. Thus for a given $V(x)$ the rate of growth of potential vorticity of the shear wave decreases much faster seawards on a slope than on a constant depth topography.

Figures 7.12, 7.13 and 7.14 show the total velocity distributions of the shear waves superposed on the longshore current for the horizontal bottom, plane beach and barred profile cases respectively. These have been scaled such that the maximum y component of the velocity induced by the shear wave is the same as the maximum longshore current velocity. The plots show that the instability creates a meandering of the longshore current about its mean location.

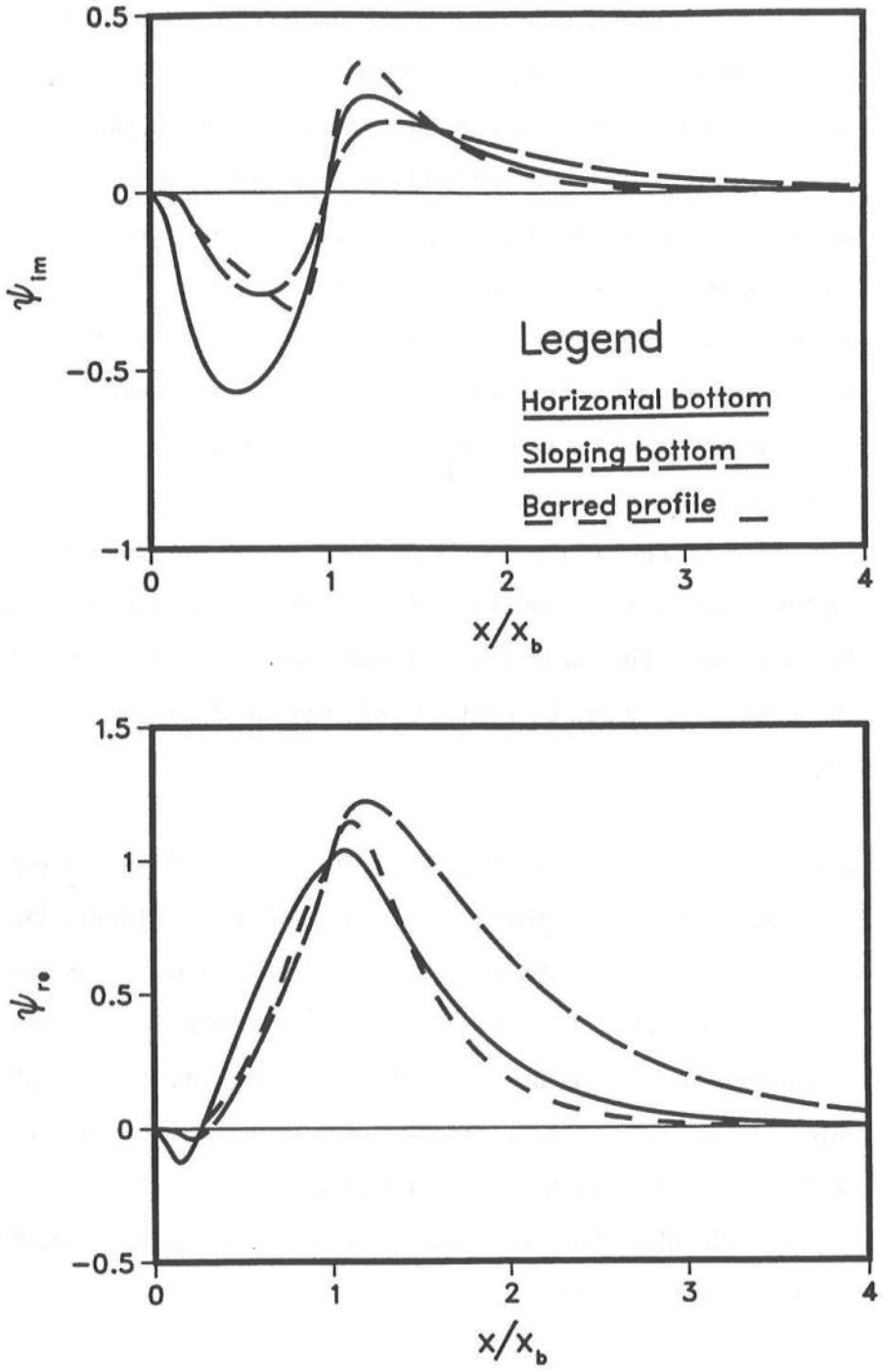

Figure 7.11: Plot of the stream function for horizontal bottom, sloping bottom and barred profile cases ($P = 0.5$)

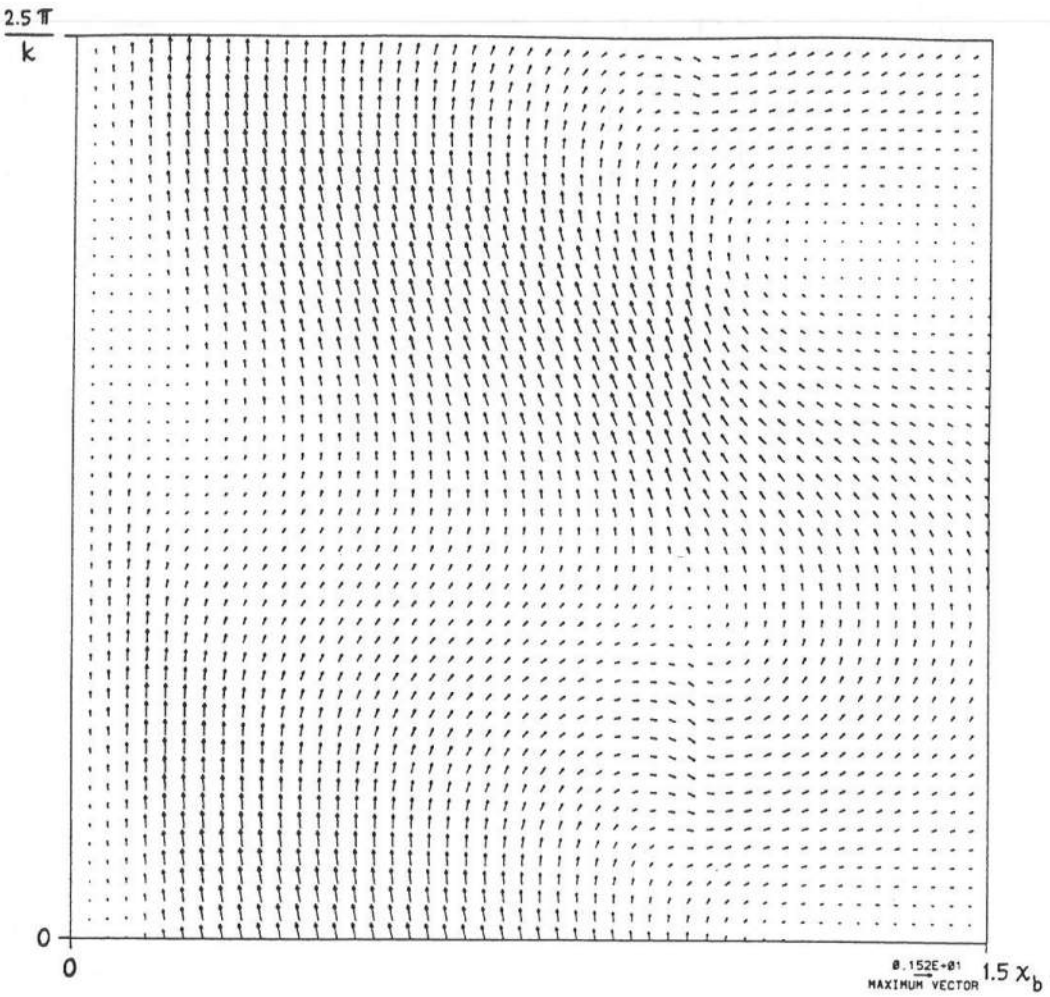

Figure 7.12: Plot of the shear wave velocity superposed on the longshore current on a horizontal bottom ($P = 0.5$)

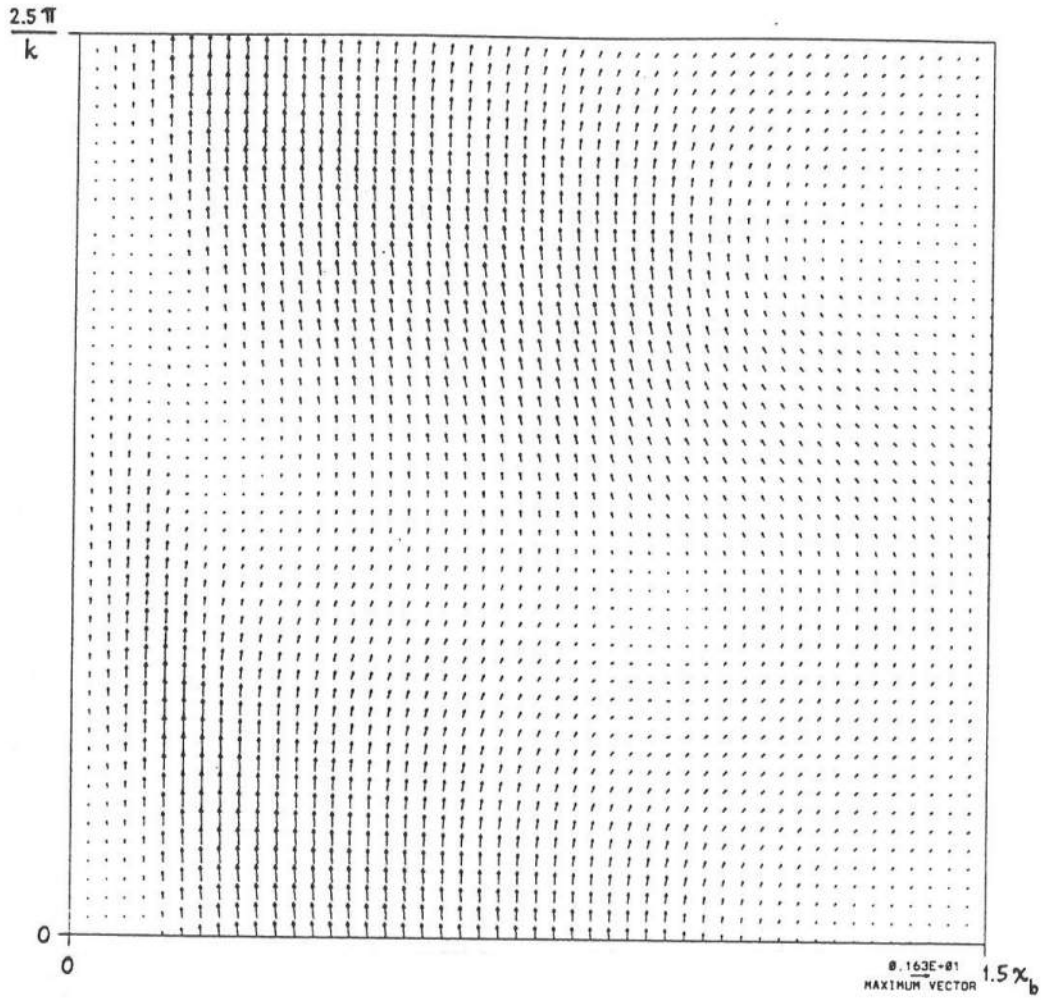

Figure 7.13: Plot of the shear wave velocity superposed on the longshore current on a sloping bottom ($P = 0.5$)

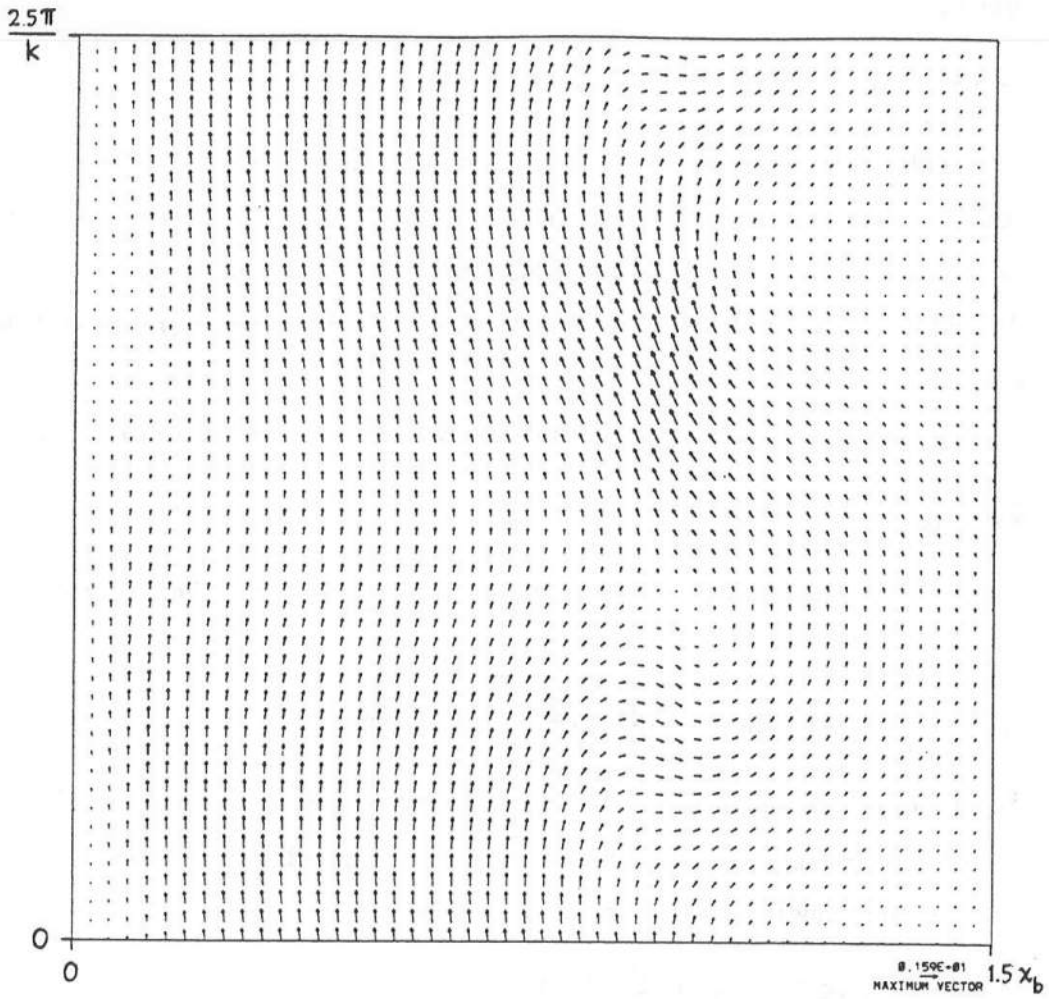

Figure 7.14: Plot of the shear wave velocity superposed on the longshore current on a barred bottom profile. Bar crest located at breakpoint. ($P = 0.5$)

7.6 Mixing due to shear waves

As shown in chapter 2 and discussed in chapter 5, on a beach with no alongshore variations of bottom topography, the first approximation to the longshore velocity is governed by

$$\frac{d}{dx}\left(S_{xy} + S'_{xy}\right) + \tau_{by} = 0 \tag{7.19}$$

The following question naturally arises at this point: Will the shear waves, as described above, contribute to S'_{xy} the excess momentum flux. Based on figures similar to 7.12-7.14, BH89 conjectured that this is indeed the case. In the following we estimate the mixing produced by shear waves and the level of eddy viscosity required if this mixing were parametrized by an eddy viscosity.

Without loss of generality, Ψ may be written as follows (recall that $\sigma_{im} < 0$)

$$\Psi = A_1(x)\cos(ky - \sigma_{re}t + \theta)\exp(-\sigma_{im}t) \tag{7.20}$$

where θ is a phase angle. Substituting for u and v in terms of the stream function leads to

$$uv = -\frac{A_1 k}{h^2}\left(A_1\frac{d\theta}{dx}\sin^2\phi - \frac{dA_1}{dx}\sin\phi\cos\phi\right)\exp(-2\sigma_{im}t) \tag{7.21}$$

where ϕ is defined to be $ky - \sigma_{re}t + \theta$. Averaging the above over a time $2\pi/\sigma_{re}$ and using the fact that $-\sigma_{im} \ll \sigma_{re}$ to argue that the factor $\exp(-2\sigma_{im}t)$ may be taken to be unity over the averaging interval in the above leads to

$$\frac{dS'_{xy}}{dx} = \frac{d}{dx}\left(\rho h\overline{uv}\right) = -\frac{d}{dx}\left(\rho\frac{A_1^2 k}{2h}\frac{d\theta}{dx}\right) \tag{7.22}$$

which shows that shear waves may produce mixing only if the phase, θ, is a function of x. This happens if the wave celerity c has an imaginary part (*i.e.*, whenever there is an instability). Dodd & Thornton (1990) arrive at the same general conclusion using an energy argument.[13] The present method also supplies the magnitude of the mixing by (7.22).

---

[13] There seems to be a misprint in their paper. The RHS of their equation 21 should read $\int_0^\infty V(\overline{uv})_x dx$ instead of $-\int_0^\infty V_x\overline{uv}dx$.

Figure 7.15 shows the variation of θ with x for the bottom topographies considered here (these have been calculated for $P = 0.5$ and the value of k that is most unstable for each of the topographies). This plot clearly shows that θ is indeed a function of x but only inside the surf-zone. Outside the surf-zone, the value of θ rapidly approaches a constant. This means that although mixing occurs due to the growth of the shear waves the mixing produced will be confined to the surf-zone. Outside the breaker zone, there is only weak mixing and only in a region very close to the break point.

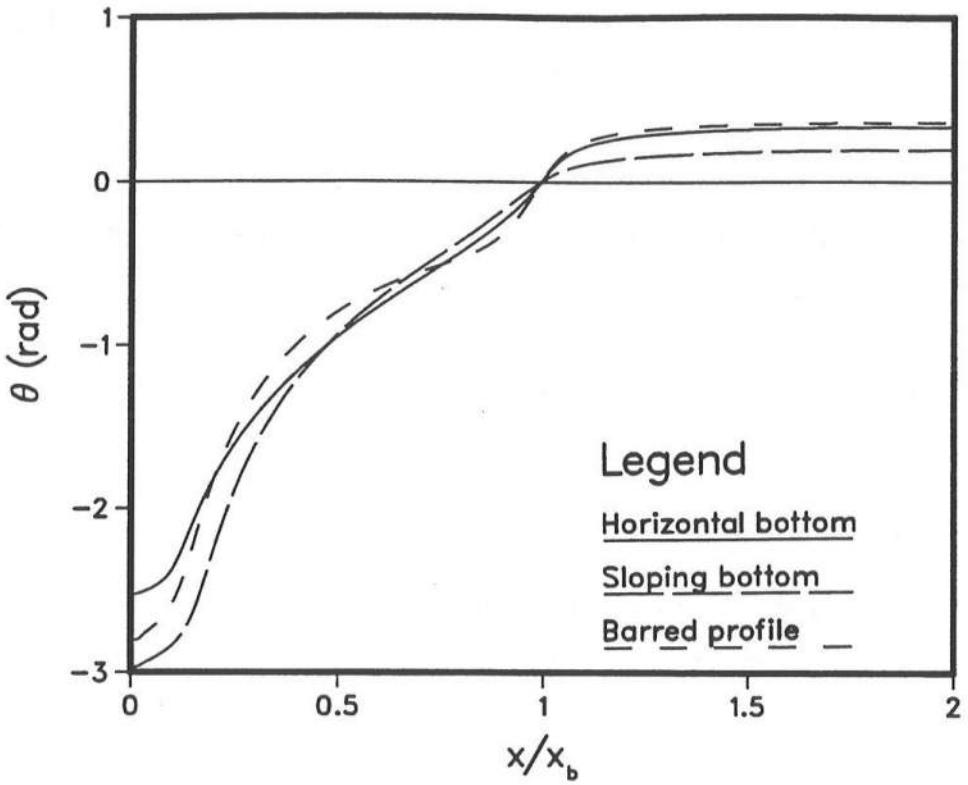

Figure 7.15: Variation of the phase for the different topographies used ($P = 0.5$)

The strength of the mixing will obviously depend on the strength of the instability. We therefore proceed to estimate the required strength of the shear wave (or strength of the instability) for it to be a plausible mechanism of mixing in the nearshore region. We will perform a simple order of magnitude analysis to determine this.

7.6.1 Order of magnitude analysis of the mixing

The following orders of magnitude may be written down

$$x \sim x_b \tag{7.23}$$

$$\frac{d\theta}{dx} \sim \frac{1}{x_b} \tag{7.24}$$

$$A_1 \sim \psi \sim h_s v_f x_b \tag{7.25}$$

where v_f is a typical particle velocity induced by the shear-wave and h_s is a typical depth. Substituting the above into (7.22) leads to

$$\frac{dS'_{xy}}{dx} \sim \frac{\rho h_s (k x_b) v_f^2}{x_b} \tag{7.26}$$

If instead, we parametrize S'_{xy} in terms of an eddy viscosity, ν_t, then

$$\frac{dS'_{xy}}{dx} = \frac{d}{dx}\left(\rho \nu_t h_s \frac{dV}{dx}\right) \tag{7.27}$$

We saw in chapter 5 that the eddy viscosity required for the prediction of longshore currents was given by

$$\nu_t \sim 10^{-1} h_s \sqrt{g h_s} \tag{7.28}$$

If the shear wave growth should account for this mixing (7.26) and (7.27) should be of the same order. Therefore, we can estimate the required order of magnitude of the shear-wave velocity, v_f, by equating (7.26) and (7.27). Doing this leads to

$$v_f^2 \sim \frac{10^{-1}}{k x_b} \frac{h_s}{x_b} V_0 \sqrt{g h_s} \tag{7.29}$$

Typically, $h_s/x_b \ll 1, k x_b \sim 1$ and $V_0 \sim \sqrt{g h_s}/(4 \text{ or } 5)$.

Therefore (7.29) is equivalent to

$$v_f^2 \sim \frac{10^{-1}}{k x_b} \frac{h_s}{x_b} \left(V_0 \sqrt{g h_s}\right) \ll V_0^2, g h_s \tag{7.30}$$

which shows that even an extremely weak shear-wave may be capable of providing sufficient mixing provided the phase, θ, is a function of the cross-shore distance. Therefore, we conclude that this mechanism may possibly provide the high level of mixing required

inside the surf-zone. Outside the surf-zone, the shear waves seem to provide very little mixing. However, as discussed in chapter 5, the variation of the mixing outside the surf-zone is not very critical to the longshore current predictions as long as the variation of the mixing is continuous across the breaker line. The conclusion, therefore, is that shear waves are a valid mechanism for lateral mixing in the nearshore region.

At this point, it seems appropriate to mention that BH89 compare mixing mechanisms in incident gravity waves and shear waves assuming that gravity waves exhibit mixing that can be described an eddy viscosity ν_t given by

$$\nu_t = UX \tag{7.31}$$

where U is a typical particle orbital velocity and X a characteristic excursion amplitude. Such a parametrization has frequently been adopted. However, since mixing is caused by the time average of the convective acceleration terms (integrated over depth in the present case) we find that regular incoming gravity waves cause no mixing.

7.7 Relevance to laboratory experiments

Most of the laboratory measurements of longshore currents have been conducted on a sloping bottom. Therefore, while discussing possible shear wave instabilities in laboratory measurements, it is appropriate to consider scales corresponding to this topography. These are:

- Length scale: $kx_b \simeq 1.5 \Rightarrow L \sim 4x_b$
- Time scale : $c/V_{max} \sim 0.5 \Rightarrow T = L/c \sim 8x_b/V_{max}$

As discussed earlier, Visser (1982) measured longshore currents on relatively steep slopes (1/10 and 1/20) in a reasonably wide tank ($\sim 21m$). Typical measurements are $V_{max} \sim 0.75m/s$ and $x_b \sim 2m$. Using these to estimate scales of shear-wave motion in the laboratory leads to $L \sim 8m$ and $T \sim 20s$. These scales indicate that shear wave motions could be detectable in a laboratory although in this particular case the length of the tank may have been too small to allow motion to develop freely. At least Visser does not give

any indication of the temporal variations of the longshore current. The relatively long length scale could be one reason why shear waves had not been detected in the laboratory.

Another reason why shear waves have not been detected could be the damping effect of bottom friction. On a straight coast the steady part of the bottom friction is balanced by the longshore radiation stress component. Thus including those two contributions and introducing the friction effect on the shear wave as a perturbation relative to the equilibrium value leads to the same principal result as found by BH89 who simply introduced a linearized bottom friction neglecting the radiation stress.

The resulting stability equation takes the form

$$(V - c - \frac{i\lambda}{kh})(\psi_{xx} - k^2\psi - \frac{\psi_x h_x}{h}) - h\psi(\frac{V_x}{h})_x = 0 \tag{7.32}$$

Here λ is determined from the quadratic relationship for the bottom stress of the form

$$\vec{\tau_b} = \frac{1}{2}\rho f \mathbf{u}|\mathbf{u}| \tag{7.33}$$

where $\mathbf{u}$ is the total velocity (*i.e.*, the shear wave velocity plus the longshore current velocity as in section 7.2). For small perturbations $\vec{u}$ from the mean longshore currents we get

$$\vec{\tau_b} = \overline{\tau_b}\vec{e_y} + \vec{\tau_b'} = \frac{1}{2}\rho f V^2 \vec{e_y} + \rho f V \vec{u} \tag{7.34}$$

where $\vec{e_y}$ is the unit vector in the y direction. The linearization of the deviations from the equilibrium of a steady current means that $\lambda = fV$.

The presence of the $i\lambda$ term equation 7.32 indicates the presence of a stabilizing threshold that must be overcome for the instability to develop ($-\sigma_{im} > \lambda/h = \sigma_{thresh}$) and the threshold, $\sigma_{thresh} = fV/h$, depends on the steady longshore current V.

For Visser's experiments a crude estimate of the threshold is (using $V_{max}/2$ as a representative value for the velocity)

$$\sigma_{thresh} = \frac{\lambda}{h} = \frac{fV_{max}}{2h} \sim \frac{(0.02)(0.75)}{2(0.1)} = 0.075 \ \ Hz \tag{7.35}$$

From figure 7.5a we get

$$-\sigma_{im} \sim 0.1\frac{V_{max}}{x_b} \sim (0.1)(0.75)/(2) \simeq 0.04 \ \ Hz \tag{7.36}$$

This value is below the viscous threshold estimated by (7.35) indicating that the viscous threshold is probably not overcome for this case, that is the viscous damping has probably suppressed the instability in Visser's experiment.

Using a barred bottom topography should be more conducive to the development of shear motions. Not only does the bar make the longshore current profile more unstable thus making it easier to overcome the viscous threshold it also reduces the length scale relative to the plane beach case thus making it more likely that the instabilities have more room to develop in a laboratory wave basin.

Results presented in section 7.4 indicate that for certain crest locations it was possible to have more than one local maxima of σ_{im}. In such cases the mode with the largest value of the growth rate among the local maxima would get excited. If two or more of the modes have growth rates that are equal to the maximum growth rate then, in the absence of an externally imposed length scale, there is the potential for the excitation of more than one mode of motion. However, we note that we have only found such behavior at a transition from one dominant mode to another and in such cases, the growth rate during the transition is substantially smaller than the growth rate of the two dominant modes (see section 7.4). So, it is quite likely that the viscous threshold is not reached in the transition process. If this is the case, then the actual swap of modes may never be observed in practice.

7.8 Discussion

The observations of Oltman-Shay *et al.* (1989) suggest the following characteristics of shear-waves

1. They propagate in the direction of the longshore current;
2. The variation of the observed frequency (σ_{re}) with observed wave number (k) is almost linear with a 0, 0 intercept;
3. The speed of propagation is in the range $0.5V_m$ - V_m where V_m is the mean longshore current magnitude;

4. Cross-shore and longshore velocity components are in quadrature phase and
5. The range of observed wave numbers is independent of the magnitude of the longshore current.

The last observation clearly suggests that phenomenon is linear – provided, of course, that the phenomenon is linked in some way to the longshore current. This means that the model of BH89, and the extension presented here, may be acceptable approximations to the actual situation.

In the model the assumption that the stream function may be assumed to be given by (7.5) ensures that, if σ_{im} is zero, the relative phase between the velocity components will always agree with point 4 in the list of characteristics above.

Figures 7.5 and 7.10 show variations of σ_{re} with k for the different bottom topographies and velocity profiles. First of all, we notice that the slope of the "dispersion" relationship is positive indicating that the waves are propagating in the direction of the longshore current (positive y direction). Secondly, we note that given the average beach slope the dispersion relationship is relatively insensitive to bottom topography. Finally, the dispersion relationship is remarkably linear with a slope which in our nondimensional variables is about 0.5 and has a 0, 0 intercept. In physical variables a slope of 0.5 corresponds to $c/V_{max} = 0.5$. Clearly, this is in good agreement with observation three above.

The observations show that shear motions span a range of wave numbers. The instability theory predicts that the shear motions will be dominated by a single wave number. The range of observed wave numbers cannot be explained by the instability theory.

It is clear from the results that the shape of the beach profile has a strong effect on the stability characteristics. As mentioned earlier, the higher the strength of the instability the higher the likelihood that the motion would overcome the viscous threshold and be discernible. Thus, based on the results presented here we would anticipate shear motions to be more predominant on beaches with bars.

The result that longshore current profiles with high backshears are extremely unstable leads to an interesting speculation regarding the development of longshore currents. As has been pointed out many times in this thesis, observed longshore currents show cross-shore distributions that indicate a level of mixing that is much higher than what measurements of turbulence levels indicate. The speculation is this: As gravity waves begin to approach the shore obliquely, they set up a longshore current distribution with large backshears (consistent with observed turbulence levels). According to the present theory such current profiles would be extremely unstable and generate shear motions which enhance the level of mixing. This enhanced level of mixing then sets up a longshore current with a lower value of backshear. Such a profile is more stable and is probably what is observed. If this mechanism is valid then the longshore current would approach the steady value in an oscillatory fashion because the extremely unstable initial current profile would generate strong shear motions which provide strong mixing and set up longshore currents with very weak backshears. Because these profiles have small growth rates the viscous threshold will probably not be exceeded and shear motions will be absent which means that the available level of mixing would no longer be able to sustain a weak backshear. The oscillatory process would probably continue (with decreasing amplitude) till a longshore current is generated whose instability has a growth rate that balances the viscous threshold. Of course, all this is extremely speculative since we are using the results of a steady situation to try and understand a fundamentally unsteady problem, *viz.*, the development of longshore current profiles. The above speculation assumes that the mixing is not caused by the interaction of the longshore current and the undertow described in the previous chapter.

We note that the frequencies encountered in these examples are indeed much smaller than those normally associated with infra-gravity motions in the nearshore region (edge waves). The slowest edge wave (Stokes' or zero mode edge wave) travels with a speed of gh_x/σ. The motions encountered here have a speed of approximately $0.5V_{max}$. For a shear wave to travel with the speed of an edge wave we would need

$$\frac{gh_x}{\sigma} \simeq \frac{1}{2}V_{max} \tag{7.37}$$

or using $\sigma = kc \simeq 0.5kV_{max}$ and $h_x = h_b/x_b$ (h_b is the depth at breaking) we get

$$1 \sim \frac{kx_b}{4}\frac{V_{max}^2}{gh_b} \tag{7.38}$$

For this to hold we would need a longshore current velocity corresponding to $V_{max}^2/gh_b \sim 2$ since the maximum instability on a plane beach occurs at $kx_b \sim 2$. This is clearly not very realistic. For $V_{max}^2/gh_b < 1$ we would have the shear wave traveling much slower than the slowest infragravity motion for a given wave number. This implies that, for a given wave number, the frequency of the shear wave is much smaller than the lowest frequency of all possible traditional infragravity motions, which is precisely what was observed by Oltman-Shay *et al.* (1989).

At this juncture, it is appropriate to discuss the validity of neglecting the $\partial\eta/\partial t$ term in the continuity equation. This term is of order c_{re}^2/gh times the terms retained.

$$\frac{\partial\eta}{\partial t} \sim \left(\frac{c_{re}}{V_{max}}\right)^2 \left(\frac{V_{max}^2}{gh_b}\right) \left[\frac{\partial(hu)}{\partial x}, \frac{\partial(hv)}{\partial y}\right] \tag{7.39}$$

For the rather high $V_{max}^2/gh_b \sim 0.5$ we get

$$\frac{\partial\eta}{\partial t} \sim 0.1 \left[\frac{\partial(hu)}{\partial x}, \frac{\partial(hv)}{\partial y}\right] \tag{7.40}$$

using $c_{re}/V_{max} \simeq 0.5$. Thus, we may conclude that the vertical acceleration terms would indeed be small and that it is justified to neglect the surface elevation in the continuity equation.

Finally, concurrent with the present work, Dodd *et al.* (1991) added a friction term and solved the instability equation numerically using longshore current velocity profiles generated from a numerical model and found that the wavenumbers and frequencies of the most unstable modes agreed with the experimental observations re-confirming that the mechanism is a plausible one.

7.9 An observation on the numerical resolution of the eigenvalues

An interesting feature was encountered while developing the numerical results shown in the previous sections. An indication of the problem may be found in figure 7.5. An examination of the variation of σ_{im} with the number of nodes used in the computation N for the larger values of k ($kx_b > 4$) for the sloping bottom situation shows that

σ_{im} is highly dependent on N indicating that the eigenvalues have not converged at the number of nodes used in the computation for these values of k.

It was analyzed whether this is a problem with the accuracy of the solution and if the problem could be alleviated by using a more accurate numerical procedure. To examine this we conducted the following numerical experiment. We compared the results for the eigenvalues on a plane beach for the following cases ($\Delta x = x_b/50$)

1. 200 nodes, Δx spacing, 2^{nd} order finite difference scheme;
2. 200 nodes, Δx spacing, 4^{th} order finite difference scheme;
3. 400 nodes, $\Delta x/2$ spacing, 2^{nd} order finite difference scheme;
4. 400 nodes, $\Delta x/2$ spacing, 4^{th} order finite difference scheme and
5. 200 nodes, $2\Delta x$ spacing, 2^{nd} order finite difference scheme.

where the second order scheme referred to above is the usual central difference scheme.

Clearly, if the order of the numerical scheme were important, there should be a noticeable difference in the solution for 1 and 2 above, whereas the solutions of 2 and 3 above should be roughly the same and the solution for 4 should be much better than the solution for 3. The results are plotted in figure 7.16. It is evident from that figure that the expectations listed above are not completely met. The solution seems only dependent on N virtually independent of the overall order of accuracy of the scheme. Thus, we conclude that the most important parameter is the number of nodes, N.

The matrix equation (7.13) has at most N distinct eigenvalues. The governing differential equation has many more. Since the phenomenon under consideration seems to be dependent mainly on N, it is our conjecture that it has some connection with not resolving all the eigenvalues of the differential equation using the matrix approximation.

Note that in all the cases above the quantity that we are normally interested in, *viz.*, the maximum growth rate, $\sigma_{im,max}$, is very well defined.

Also note that in cases 1 through 4 above the seaward boundary condition is applied at $x = 4x_b$. In case 5 the seaward boundary condition is applied at $x = 8x_b$. The fact

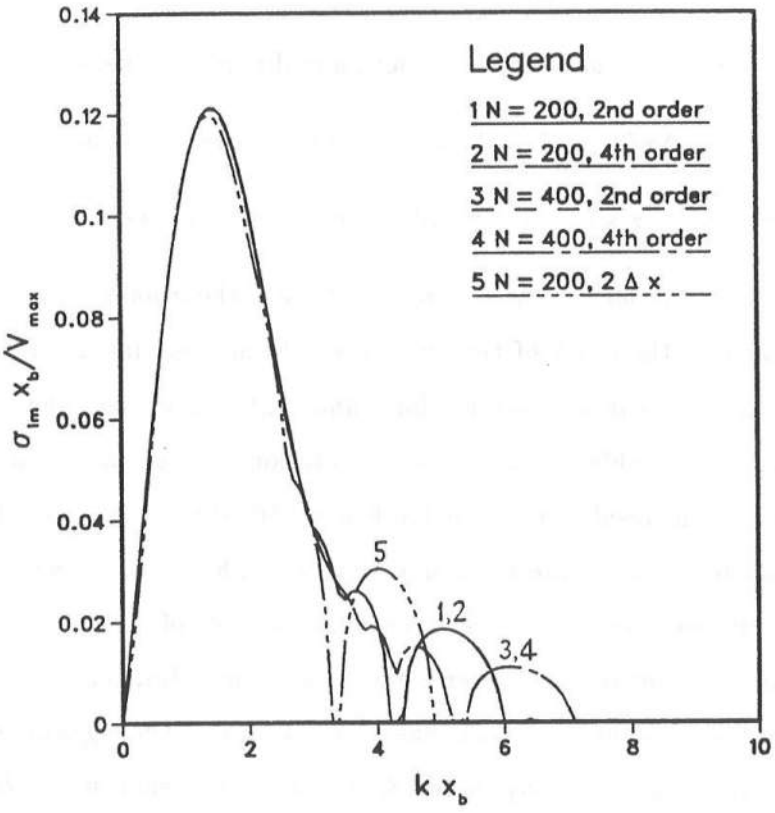

Figure 7.16: Variation of σ_{im} for different values of N and Δx

that the results of case 5 above compare favorably with the others for $\sigma_{im,max}$ indicates that the size of the computational domain does not affect $\sigma_{im,max}$, consistent with what we claimed in section 7.5.

Chapter 8

CONCLUDING REMARKS

8.1 Summary and conclusions

The work presented in this thesis was an effort aimed at understanding some of the basic mechanisms governing the mean circulation in the nearshore region. To simplify the analysis we focussed on the case of a long straight beach. We particularly concentrated on the various factors involved in the prediction of longshore currents.

Chapter 2 discussed the derivation of the equations governing the steady quantities in the nearshore region. The equations derived in that chapter are valid for currents that have a depth variation. These equations were then simplified for the case of a long, straight beach and the simplifications afforded by the choice of this topography were also discussed in some detail.

Existing laboratory measurements of the wave heights and set-up were analyzed in chapter 3 in order to determine the variations of the radiation stress and energy dissipation rate across the surf-zone. We showed in this chapter that the assumptions normally made in surf-zone models (use of linear theory, bore dissipation model, *etc.*) require reevaluation. We also showed in this chapter that the forcing for the longshore currents may be overestimated by as much as a factor of two if linear theory is used.

Chapter 4 discussed a formulation of the quadratic law. We demonstrated in that chapter that the quadratic law may be written in a convenient form. Some interesting implications of the quadratic law were also discussed in that chapter.

In chapter 5 we first developed a perturbation solution for the longshore currents. The perturbation scheme indicated that the equation normally solved for the prediction of the longshore currents gives only the first approximation to the actual prediction of

the longshore currents. We also found in this chapter that the lateral mixing needed to explain the measurements of longshore currents while being consistent with the lateral mixing level used in earlier models of longshore currents, is much higher than what the turbulence measurements justify. Furthermore, predictions of the vertical structure of the undertow and longshore currents required the use of mixing coefficients that are consistent with turbulence measurements. This indicated that the vertical and horizontal mixing processes may be controlled by different processes.

Chapter 6 analyzed the effect of the interaction of the undertow and longshore currents in an effort to see if this interaction could provide the required mixing. We demonstrated in this chapter that this interaction is extremely important and could significantly increase the level of mixing and therefore easily account for the high level of mixing. However, the strength of this mixing is significantly dependent on the evaluation of the time average of the longshore current and the wave induced velocity above the trough level. This quantity is not easy to evaluate because, as discussed in chapter 2, the determination of the longshore current above trough level is probably not possible using a wave averaged model.

Chapter 7 discussed the inviscid stability of longshore currents. A numerical solution procedure was used to solve the stability equation for general longshore current and depth profiles. We showed in this chapter that that the bottom topography plays an extremely important role in the stability characteristics of longshore currents. We found that the presence of a longshore bar significantly increases the strength of the instability. It was also shown that the bar tends to trap motions shoreward of the bar. We demonstrated here that the characteristics of the motions resulting from the instability are consistent with the characteristics of the observations of low frequency motions in the nearshore region (Oltman-Shay *et al.* 1989) thus indicating that the instability mechanism is a plausible explanation for these motions as suggested by Bowen & Holman (1989). We also found here that the viscous threshold probably suppresses the instability on plane beaches and may possibly be one of the reasons why these motions have not been encountered in a laboratory so far. The shear waves were also found to be a plausible source of

mixing in the nearshore region.

8.2 Suggestions for future work

The work presented here has clearly demonstrated the need for new and detailed experimental data. An experiment in the spirit of Visser's would be extremely useful especially if detailed measurements can be made. We found in chapter 3 that measurements of set-up and wave height could be used to accurately estimate the variation of the cross-shore component of the radiation stress. If measurements of instantaneous surface elevation are available to the extent that quantities of the type $\left(\overline{\eta^2}/H^2\right)$ can be calculated then the longshore component of the radiation stress can be accurately estimated from the measurements of the set-up and wave height. Also, such an experiment could be used to check the dependence of the longshore current on the slope. Such an experiment would need to be carefully designed and monitored to ensure alongshore uniformity. Based on our estimates of the strength of the instability in chapter 7 we would expect the longshore currents to be stable if the beach has a monotonic depth variation. If the aim is to measure shear waves in the laboratory then it would be extremely conducive to introduce a longshore bar. In fact, this feature could probably be used as a test for the instability theory of shear waves. According to the instability theory shear motions are more likely to develop on barred beaches than on plane beaches. The fact the shear motions seemed to be more prevalent at SUPERDUCK where the beach profile is characterized by a bar system in comparison with the rather weak evidence in the earlier observations at Torrey Pines lends credence to this feature but a laboratory verification is necessary before one can be convinced that the observations of the low frequency motions are a result of the instability of longshore current. Successful verification of the predictions of the instability theory would indicate that a new class of oscillations is present in the nearshore region with potentially significant implications for the nearshore circulation.

Another application of such an experiment could be to test the hypothesis of chapter 6, *viz.*, that the mixing required for longshore current predictions is controlled by the interaction of the longshore currents and the undertow rather than the turbulence. If this does turn out to be the mechanism that controls the mixing, the implication is that

the presence of an undertow plays an extremely significant part in the establishment of longshore currents. It is clear from the nature of the interaction that it is strongly dependent on the mass flux due to the waves. Therefore, if the mechanism is a valid one, a longshore current generated by waves with a higher value of the mass flux should exhibit more mixing than longshore currents generated using waves that have a smaller value of the mass flux. Since the mass flux in waves is strongly dependent on the wave height this implies that longshore currents generated by using higher waves will exhibit more mixing if the interaction mechanism controls the mixing. The level of turbulent mixing will also increase with the wave height. The increase in the turbulent mixing can probably be estimated by comparing vertical profiles of the horizontal currents for different wave heights. Therefore, it seems possible that an experiment of the Visser type could be used to test this hypothesis. There is, however, the drawback that in order to quantify the mixing caused by the interaction the contribution from above trough level has to estimated accurately. The proper evaluation of this contribution would probably require the use of a depth and time dependent circulation model. None of the models known to the present authors have both time and depth dependency. Currently available computational resources probably make such models impractical. Therefore, until this problem is resolved experiments can only provide qualitative verification of the hypothesis that the mixing is controlled by the interaction of the longshore currents and the undertow.

It would be interesting to use a highly nonlinear numerical wave theory to calculate the radiation stresses just prior to breaking and compare these results with those of analyses similar to those carried out in chapter 3 and also with the radiation stresses calculated from the basic definitions using direct measurements of velocities and pressures. It is conceivable that for this purpose use could be made of one of the boundary element models that have been developed in recent years for computations of highly nonlinear waves (like, *e.g.*, Otta 1992). Though such models cannot be used inside the surf-zone they could , for example, be used to investigate the importance of the $\overline{u_w w_w}$ term outside the surf-zone. A first step in this direction was undertaken by Otta who calculated the velocities under very steep solitary waves.

There is also a need for a development of a boundary layer solution under surf-zone conditions. As discussed in chapter 4, there are no measurements that are available at the present time for boundary layer flows inside the surf-zone. While the lack of experimental results will necessarily limit the theoretical efforts, the results from a theory that uses realistic turbulence characteristics and wave conditions would aid in the planning of experiments by suggesting quantities that are important and probably also indicating whether these quantities are measurable using available measurement techniques.

The stability analysis performed here is linear and inviscid. Though estimates of the viscous threshold were developed in chapter 7, a nonlinear viscous stability analysis is required in order to completely address the stability of longshore currents. Such an analysis could, for example, be carried out by using a two dimensional circulation model (like, *e.g.,* Ebersole & Dalrymple 1982, Vemulakonda 1984) and studying the evolution of an arbitrary perturbation to the longshore current.

Appendix A

FIGURES SHOWING THE EXERIMENTAL DATA AND THE VARIATIONS ADOPTED

In this appendix we show the measurements of the wave height and set-up along with the variations adopted for the analysis in chapter 3. We also show here the variations of the wave height to water depth ratio.

A.1 Variations of set-up and wave height

This section contains the variations of the set-up and wave height. The corresponding variations for Okayasu S2C3 were presented in figure 3.2. In the figures that follow the data points represent the measurements and the continuous curves represent the spline variations used.

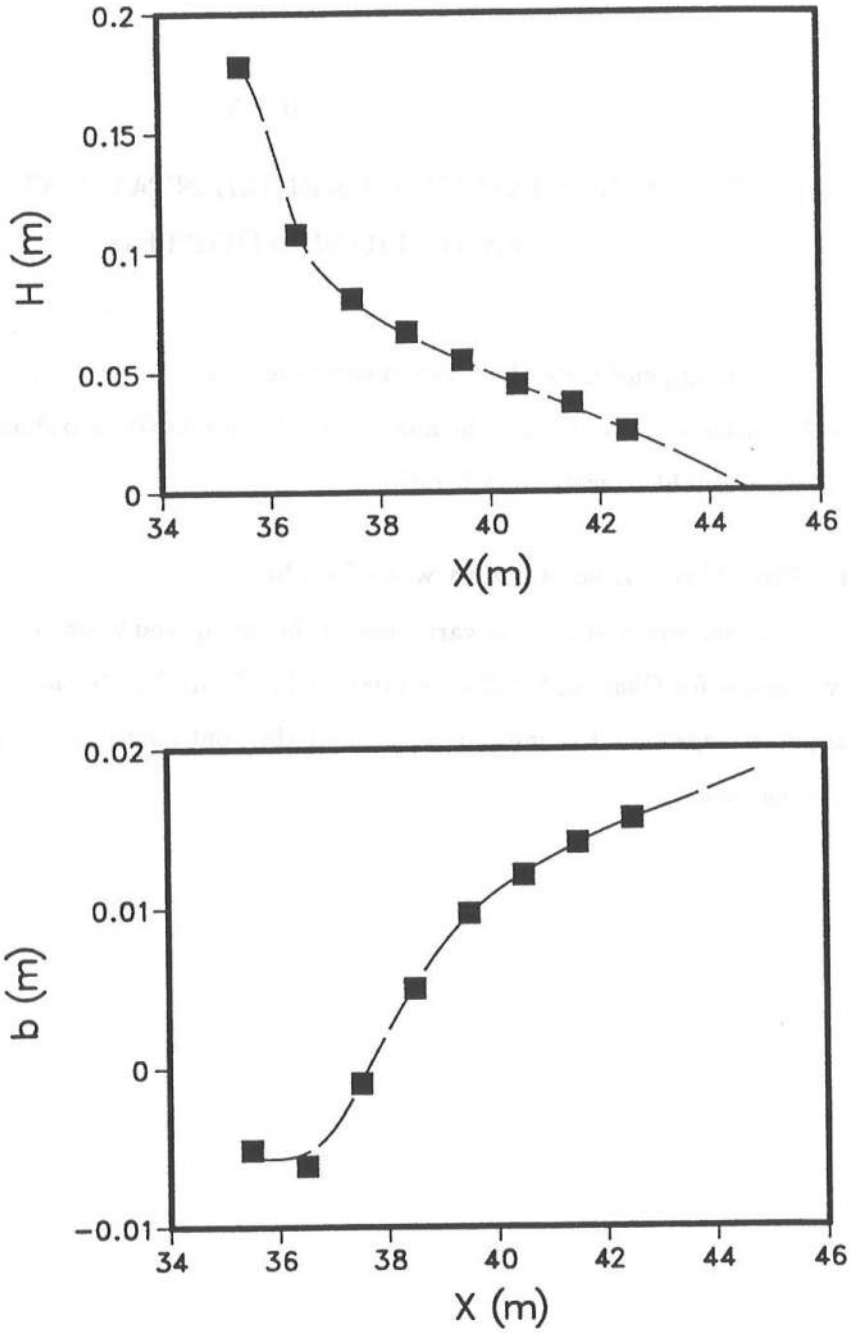

Figure A.1: Spline variations used for Stive & Wind Experiment 1

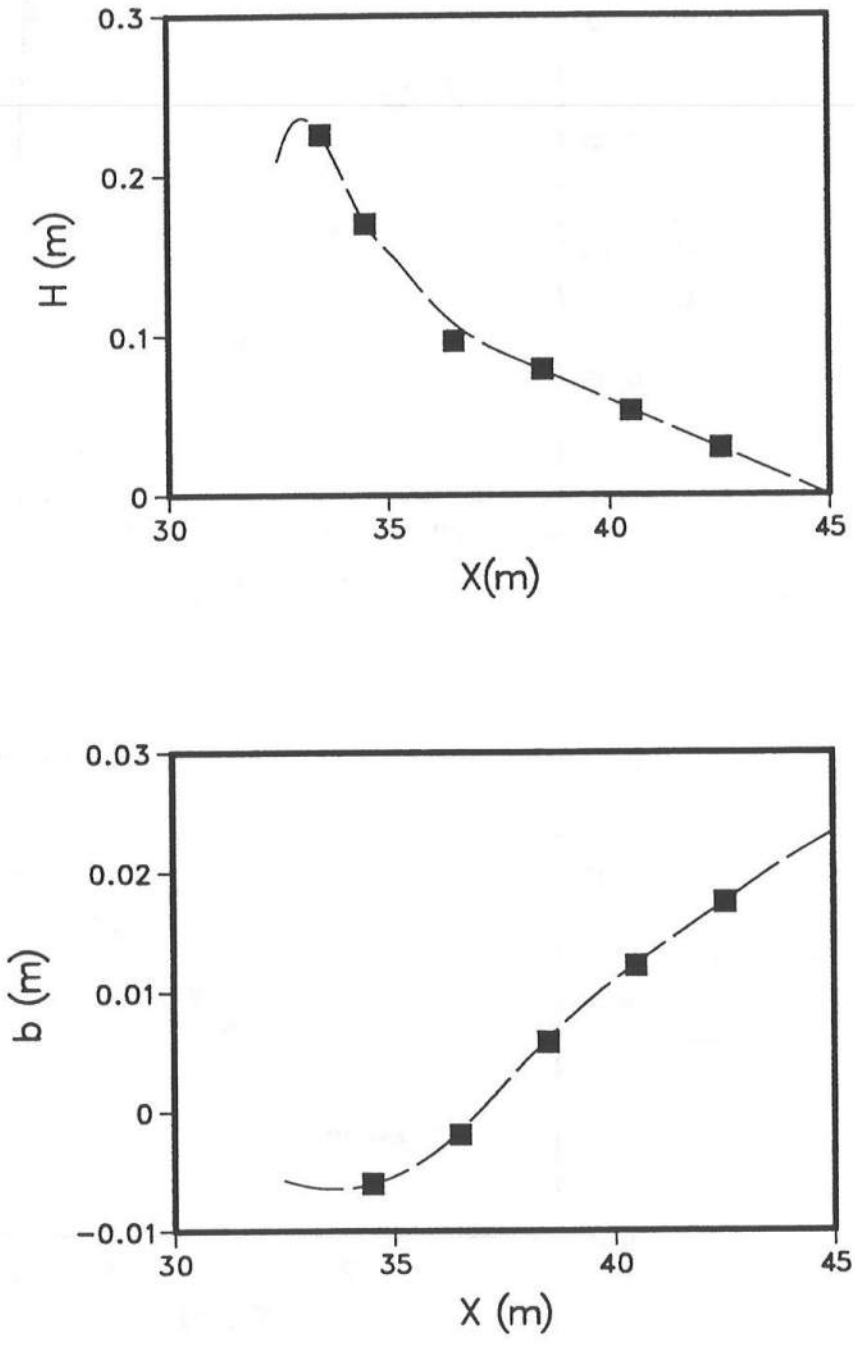

Figure A.2: Spline variations used for Stive & Wind Experiment 2

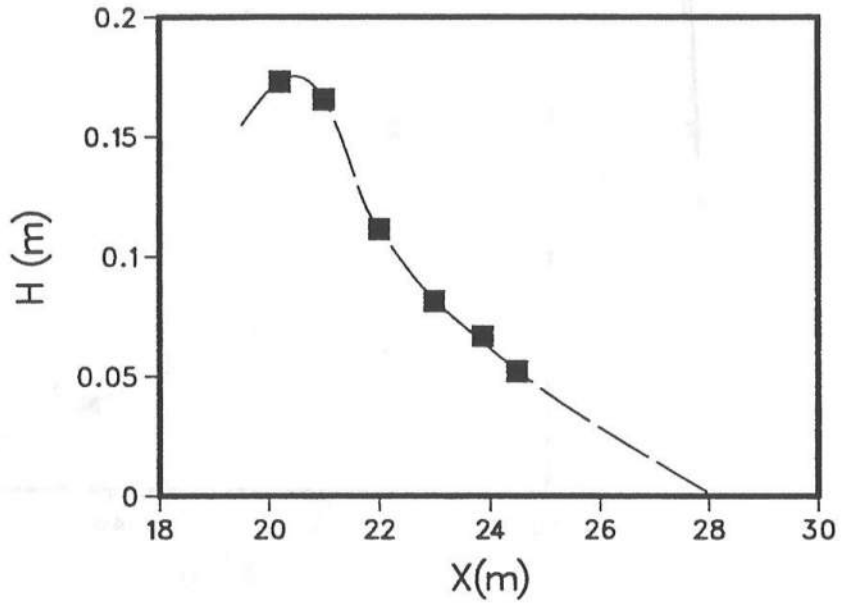

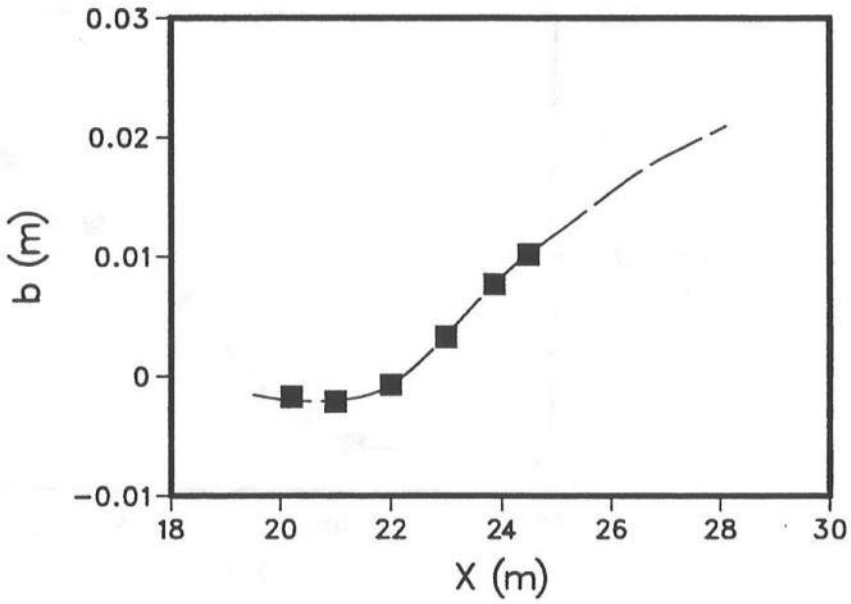

Figure A.3: Spline variations used for ISVA

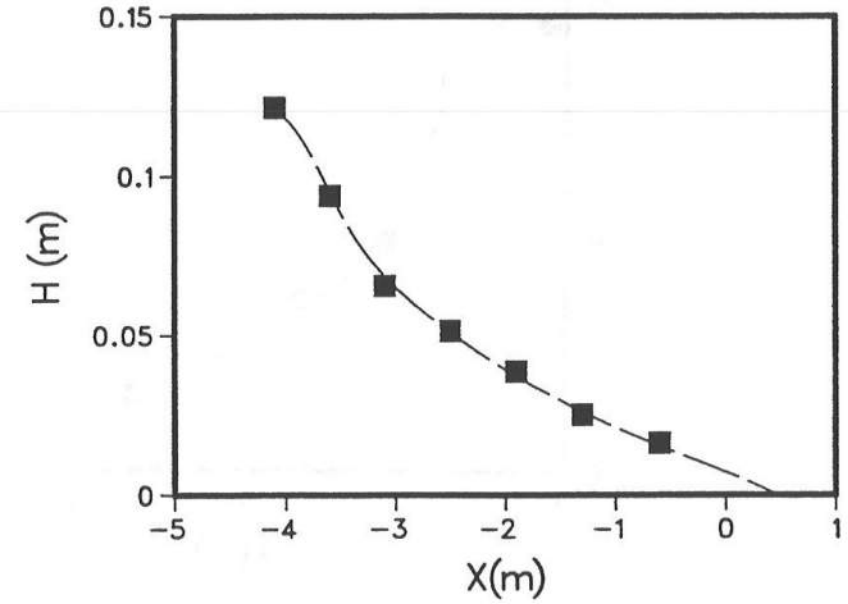

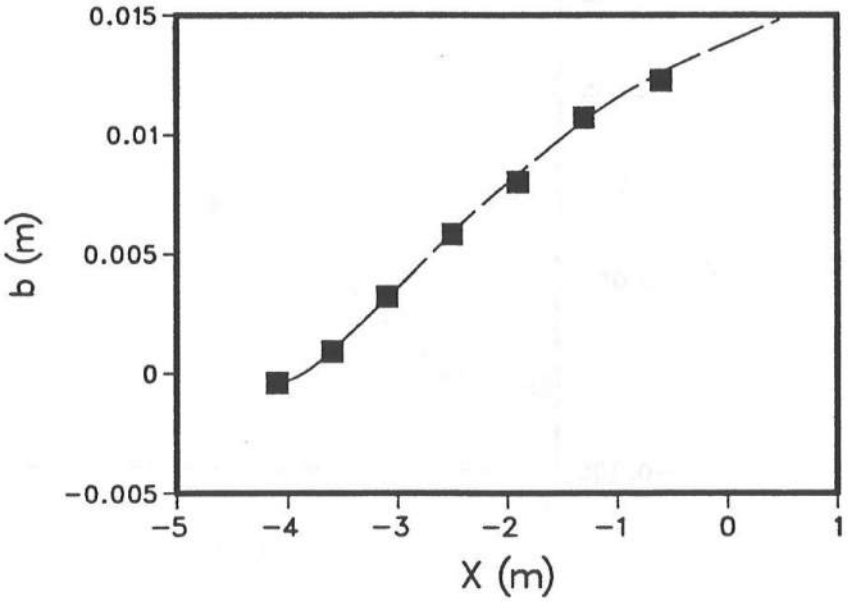

Figure A.4: Spline variations used for Okayasu S3C1

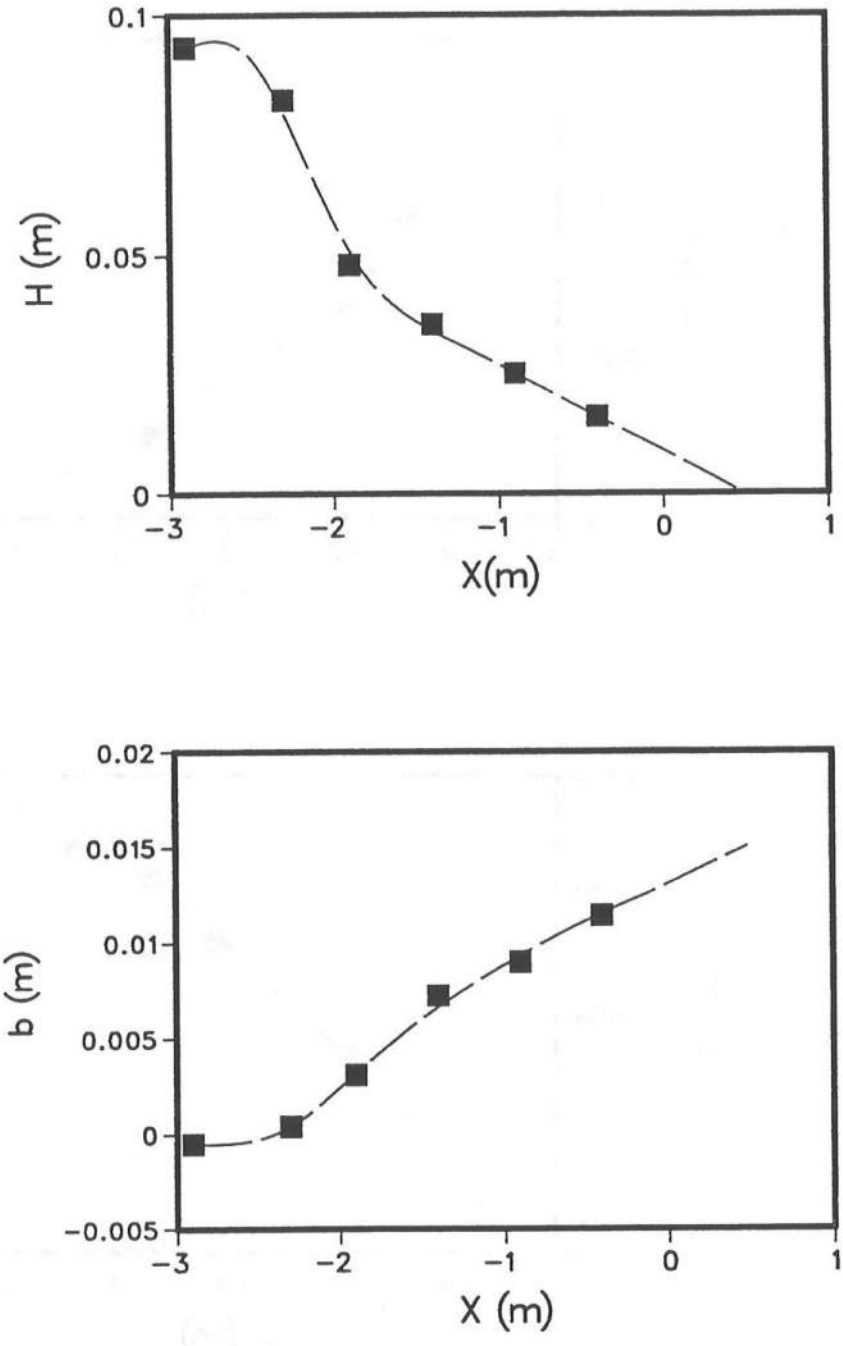

Figure A.5: Spline variations used for Okayasu S3C2

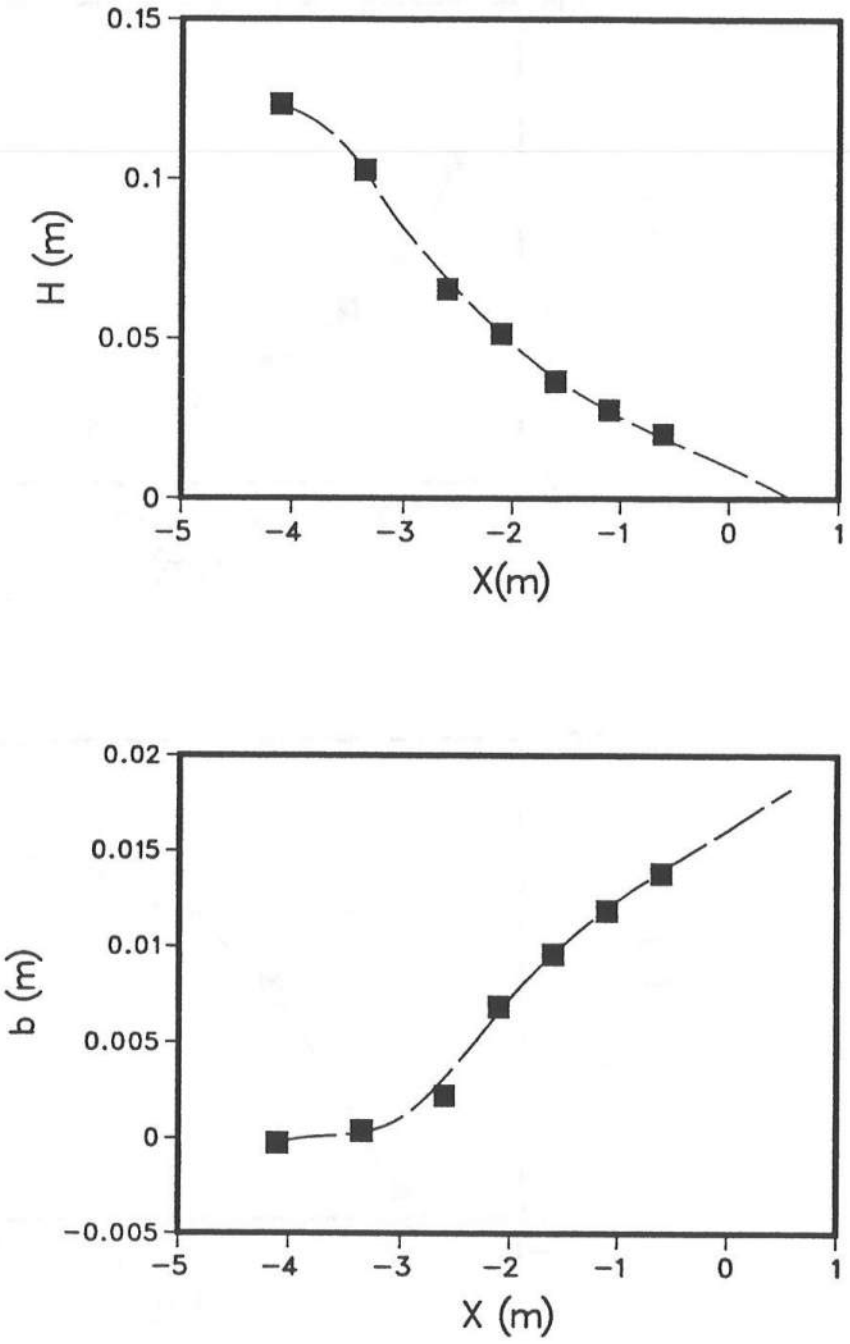

Figure A.6: Spline variations used for Okayasu S3C3

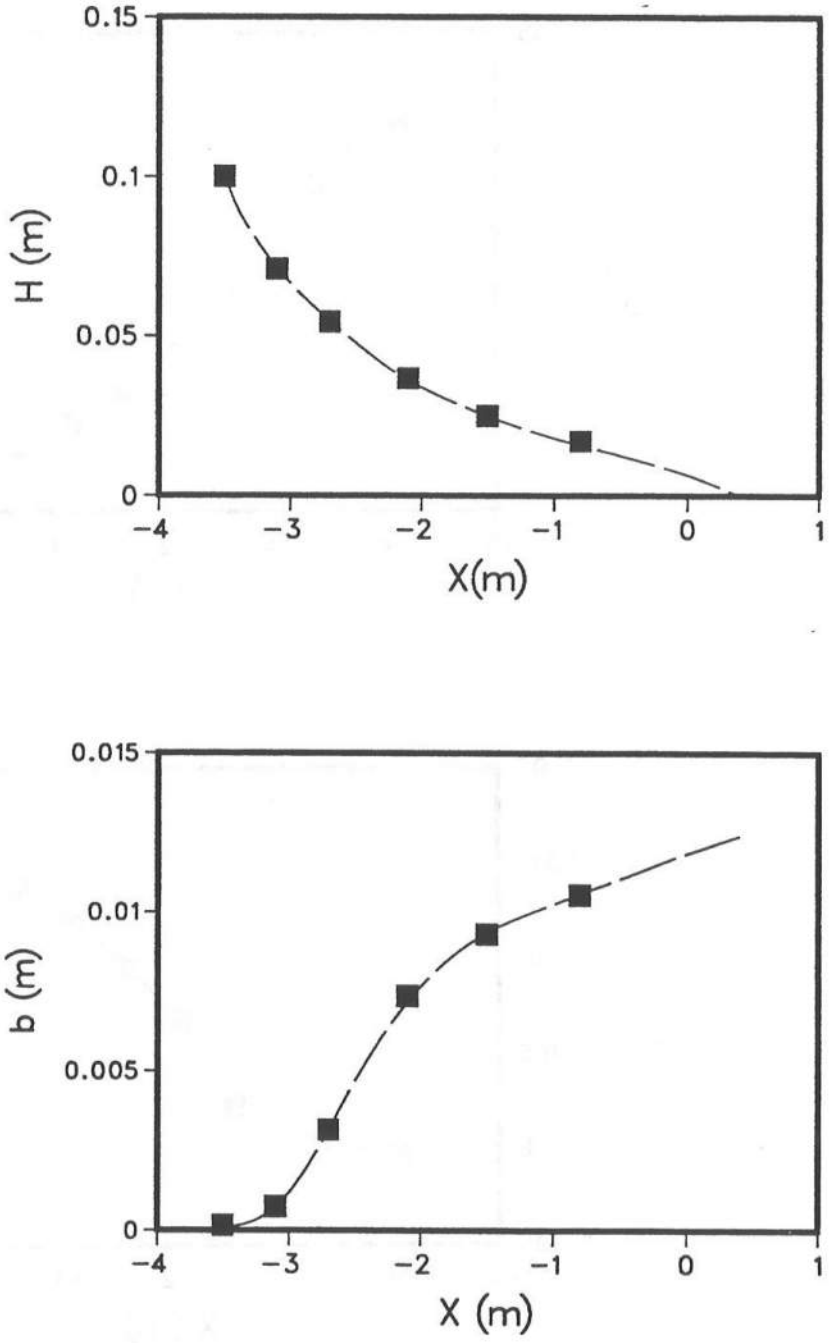

Figure A.7: Spline variations used for Okayasu S3C4

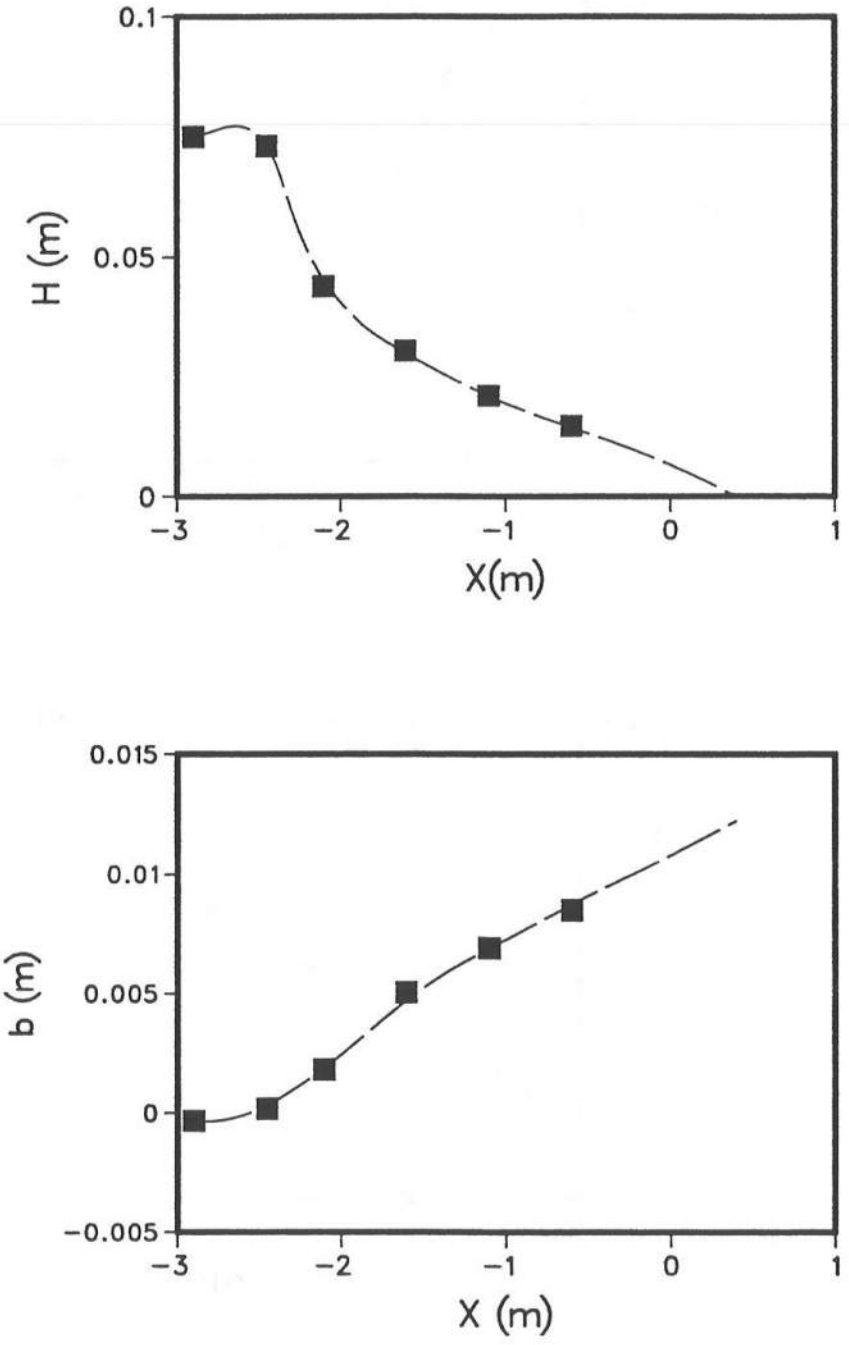

Figure A.8: Spline variations used for Okayasu S3C5

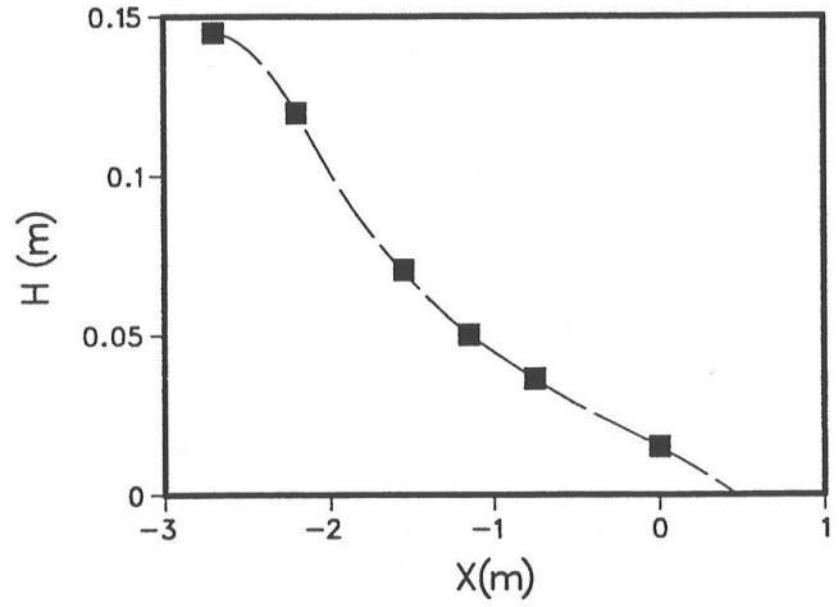

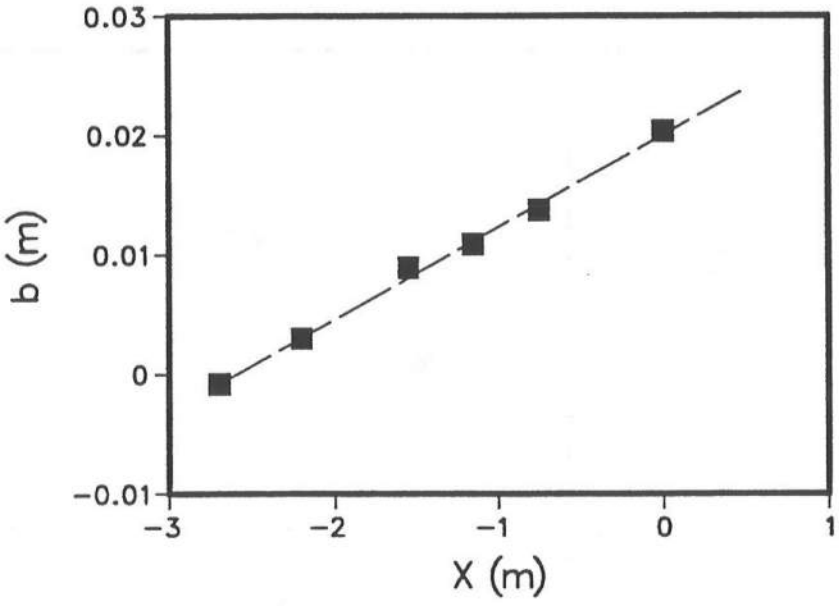

Figure A.9: Spline variations used for Okayasu S2C1

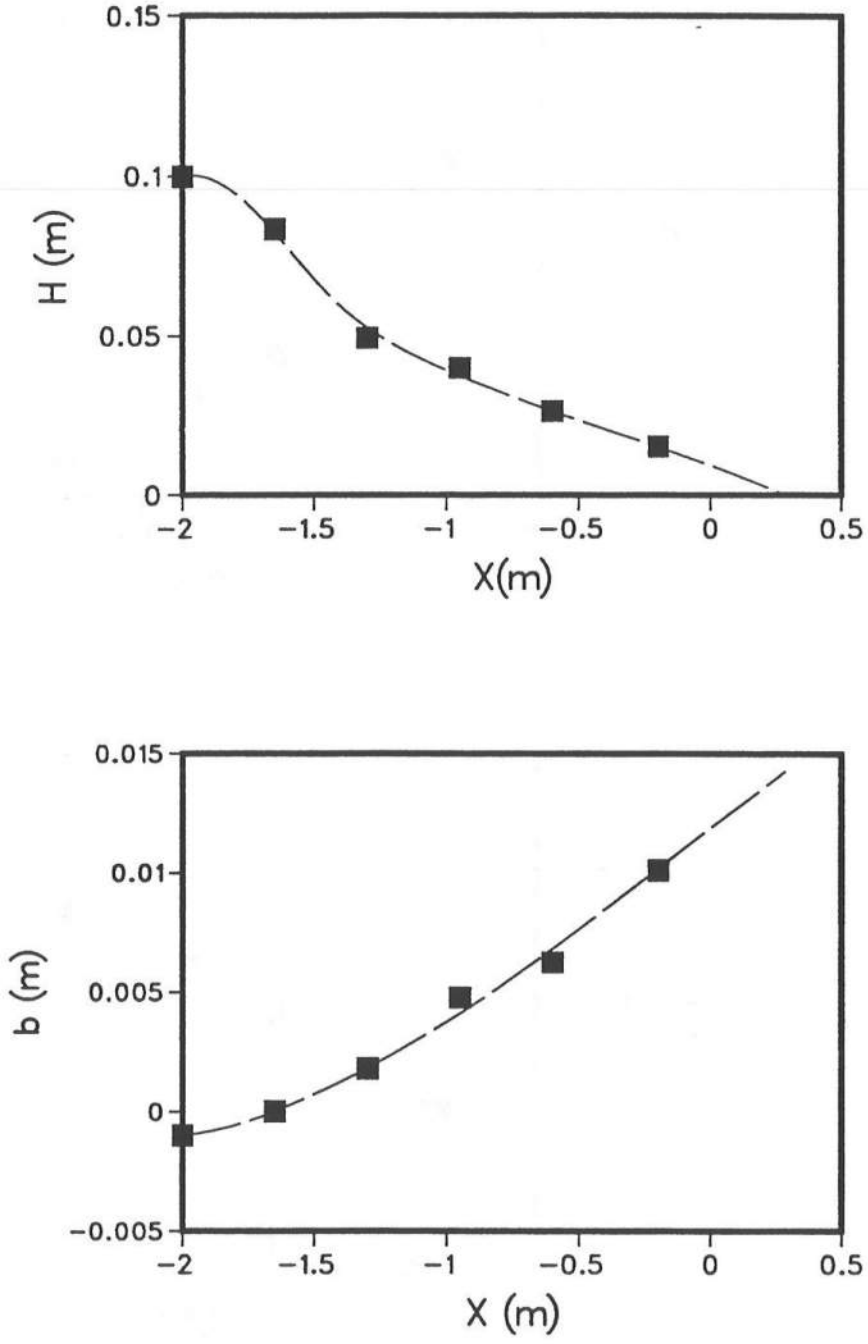

Figure A.10: Spline variations used for Okayasu S2C2

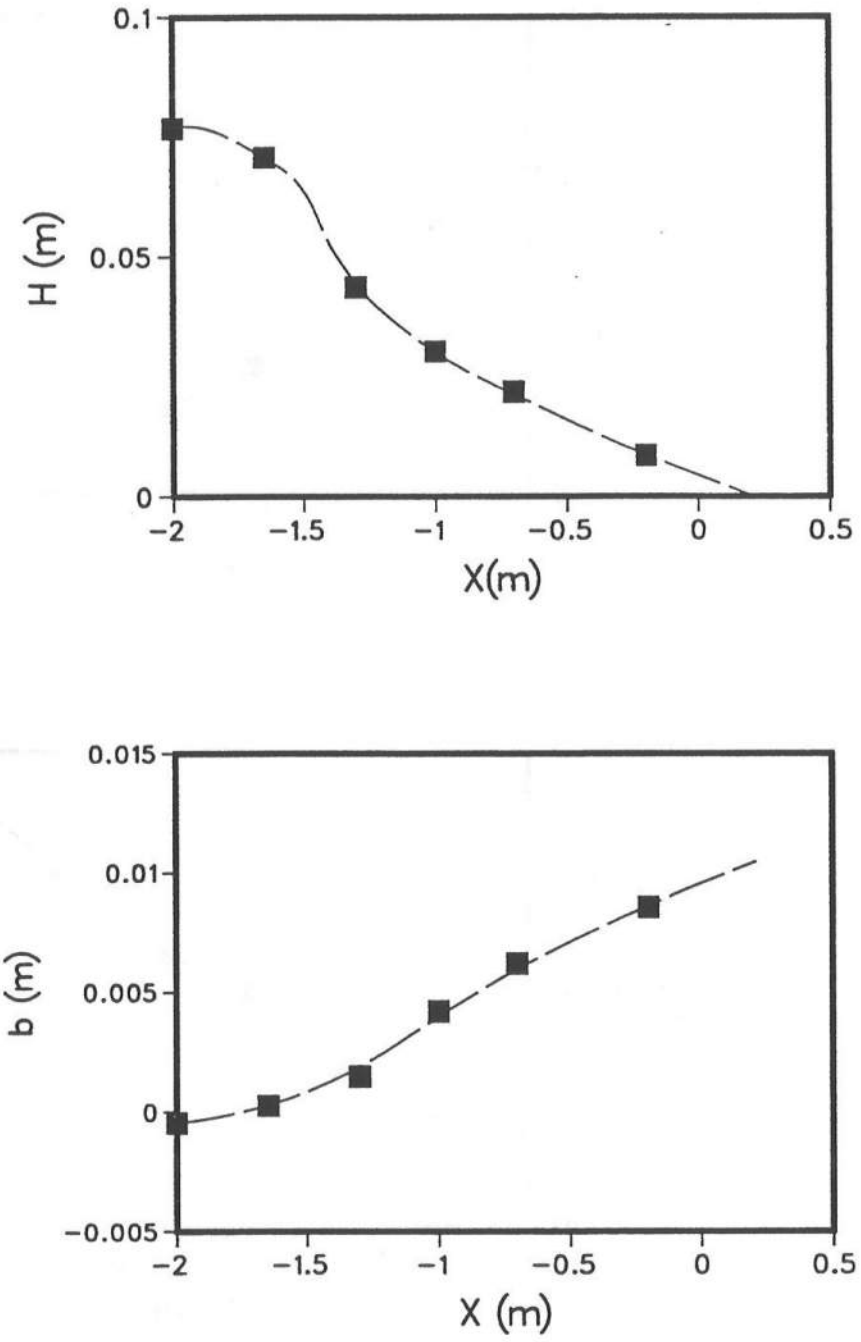

Figure A.11: Spline variations used for Okayasu S2C4

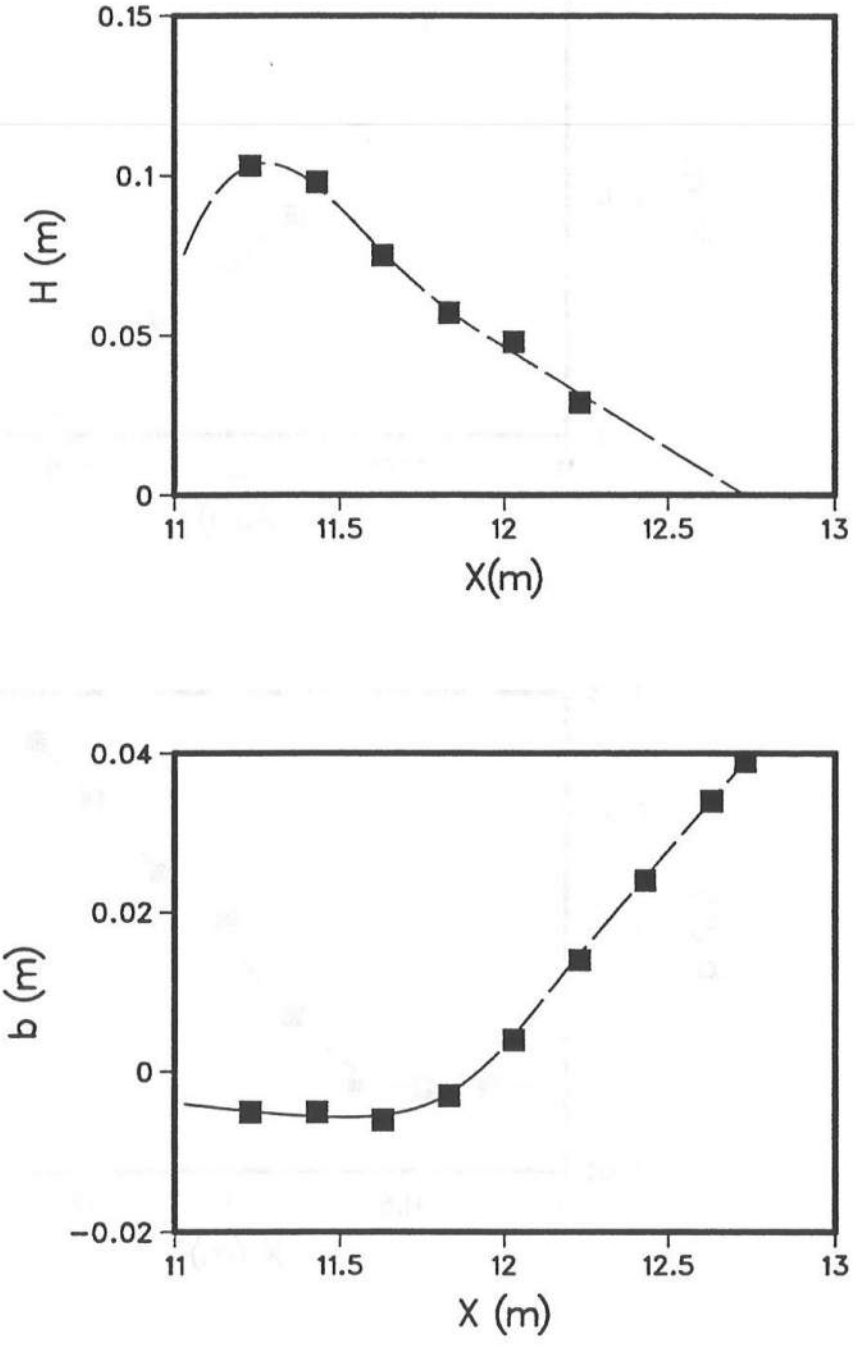

Figure A.12: Spline variations used for Visser Experiment 1

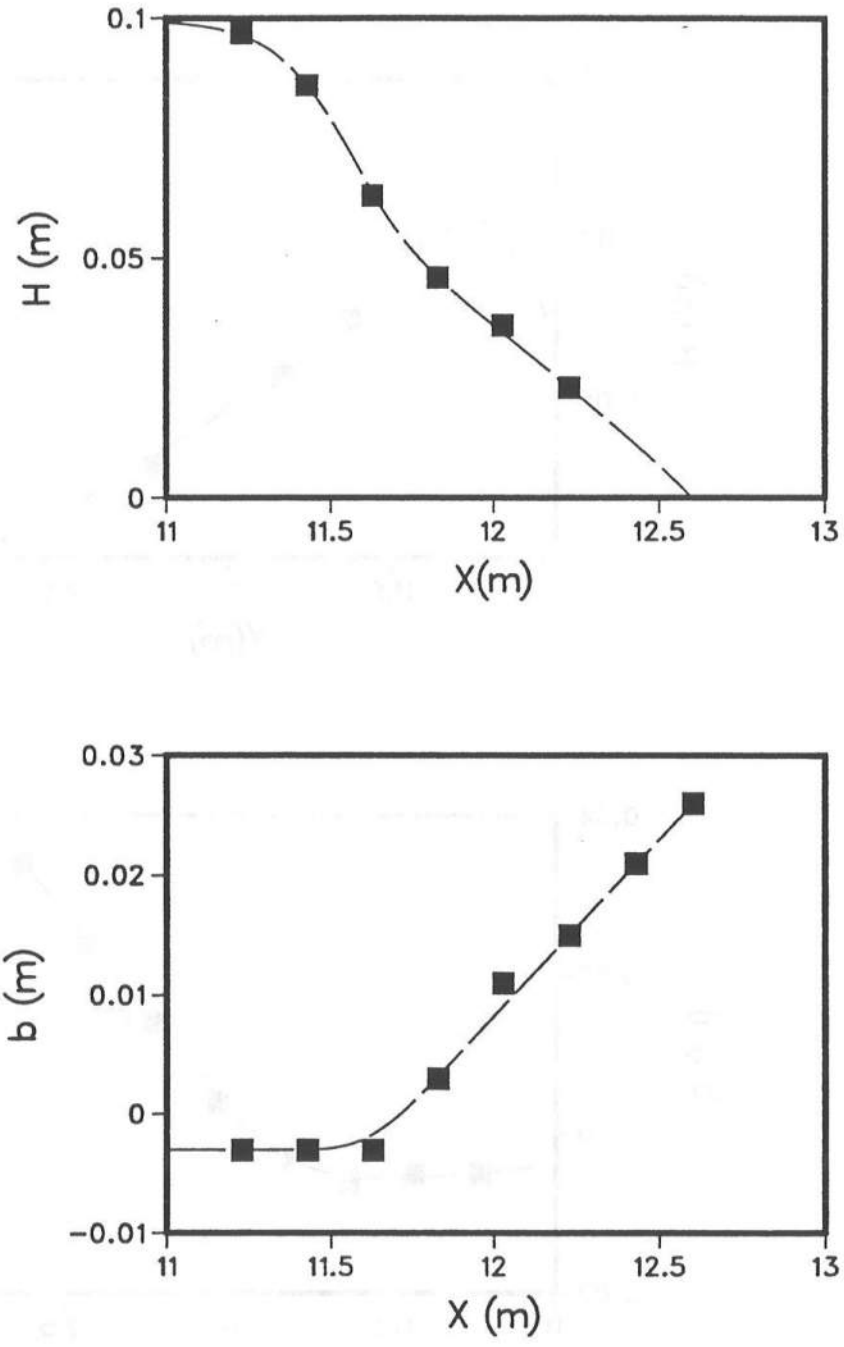

Figure A.13: Spline variations used for Visser Experiment 2

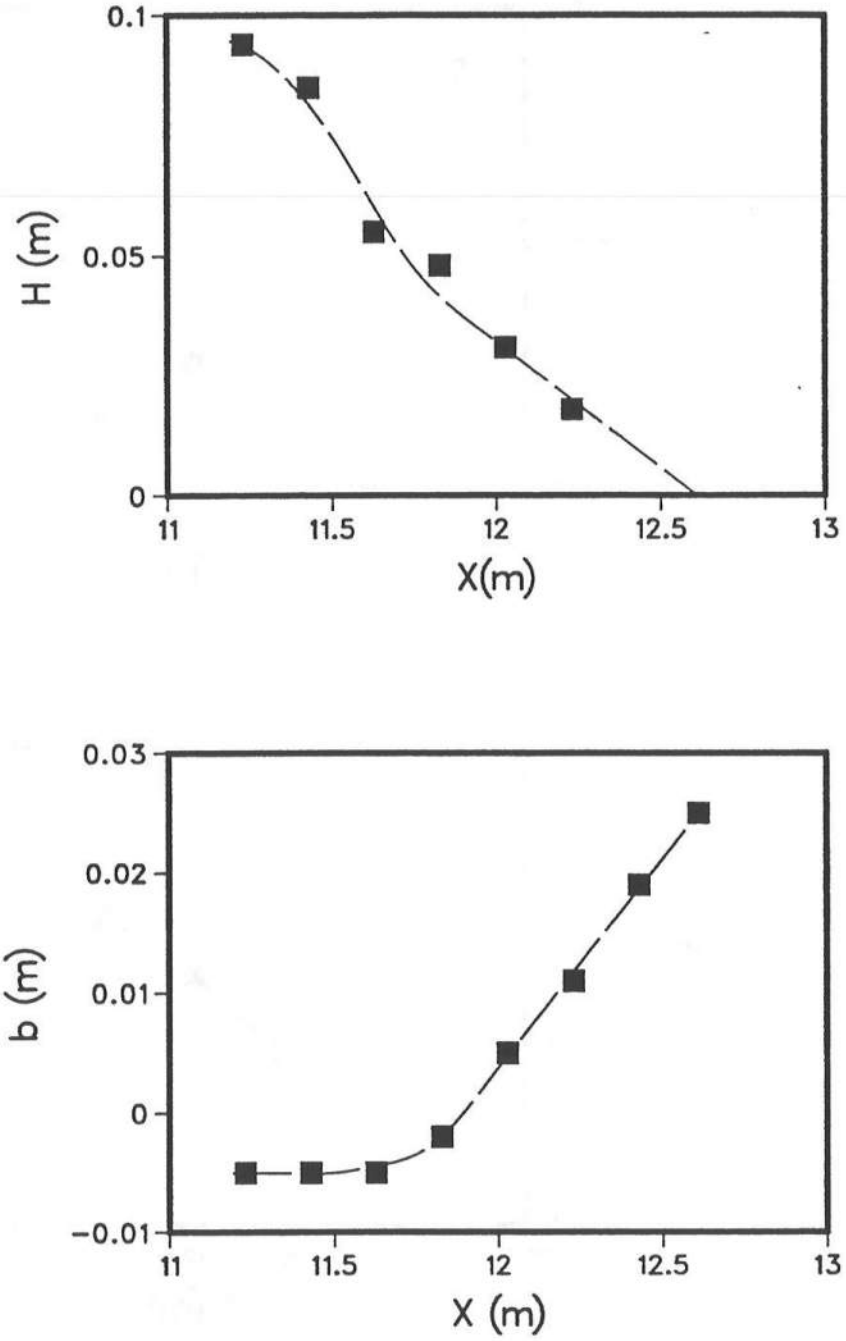

Figure A.14: Spline variations used for Visser Experiment 3

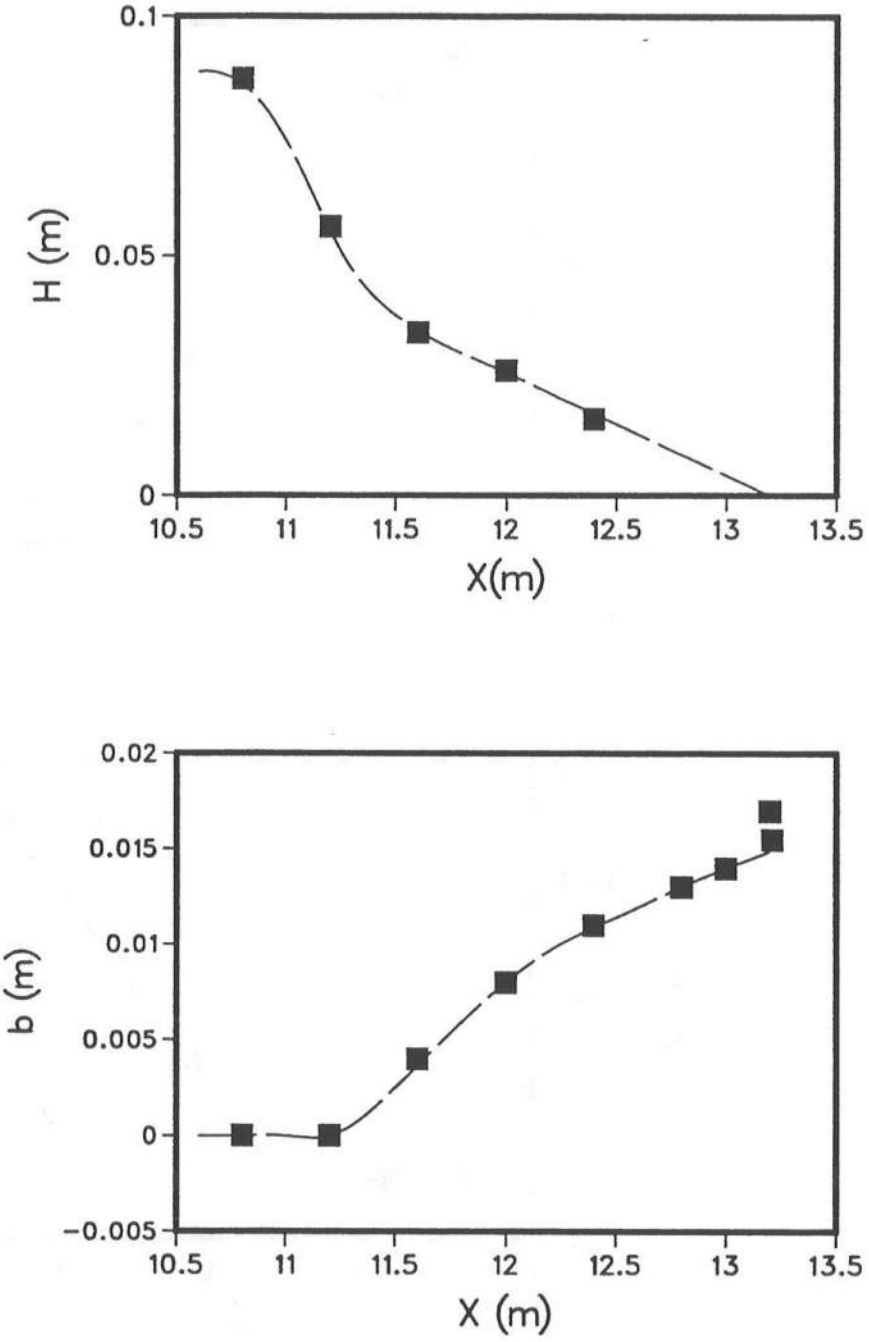

Figure A.15: Spline variations used for Visser Experiment 4

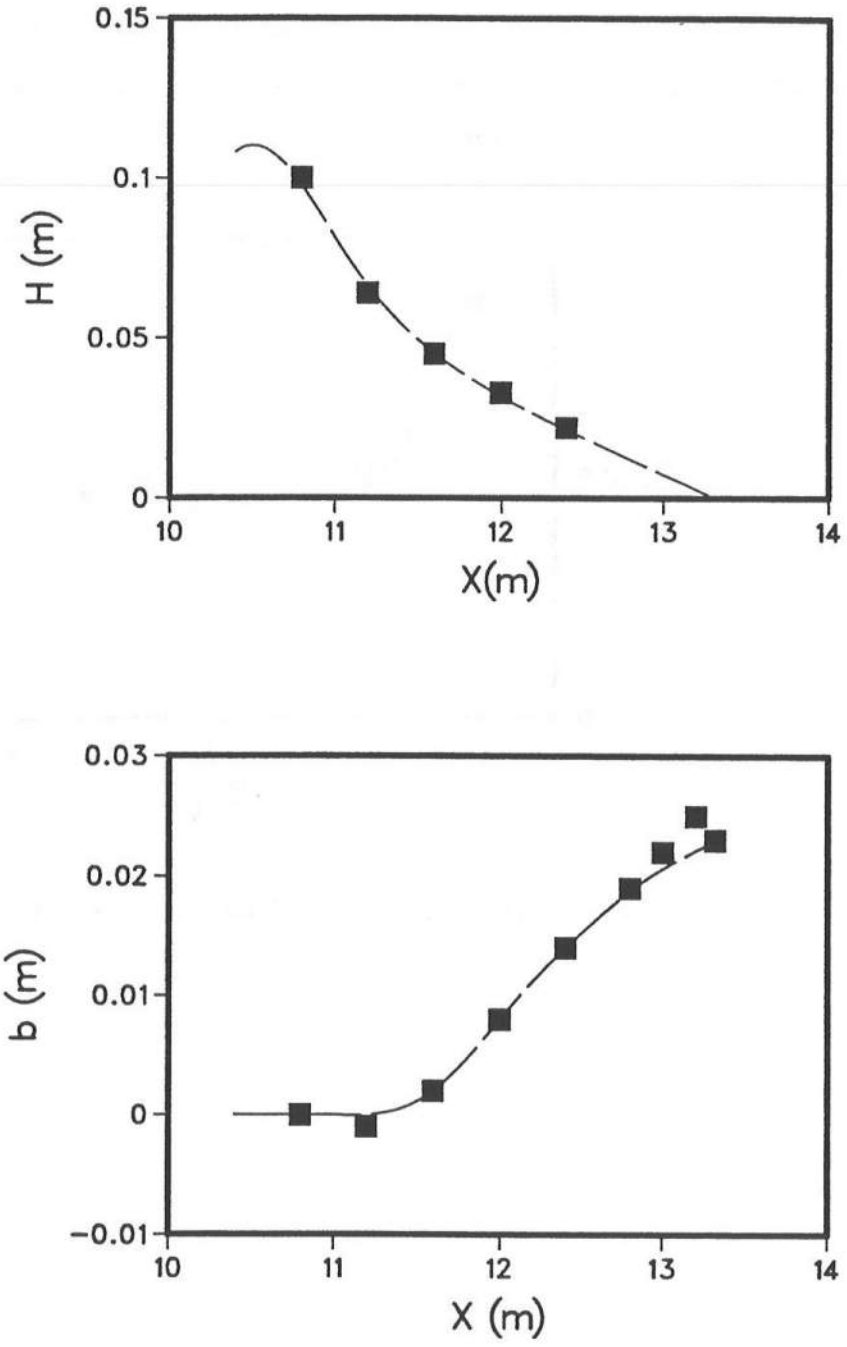

Figure A.16: Spline variations used for Visser Experiment 5

A.2 Variations of H/h

This section contains the variations of the "measured" value of the wave height to water depth ratio and the interpretation of the same. Figure 3.3 contains the variation of this quantity for Okayasu S2C3.

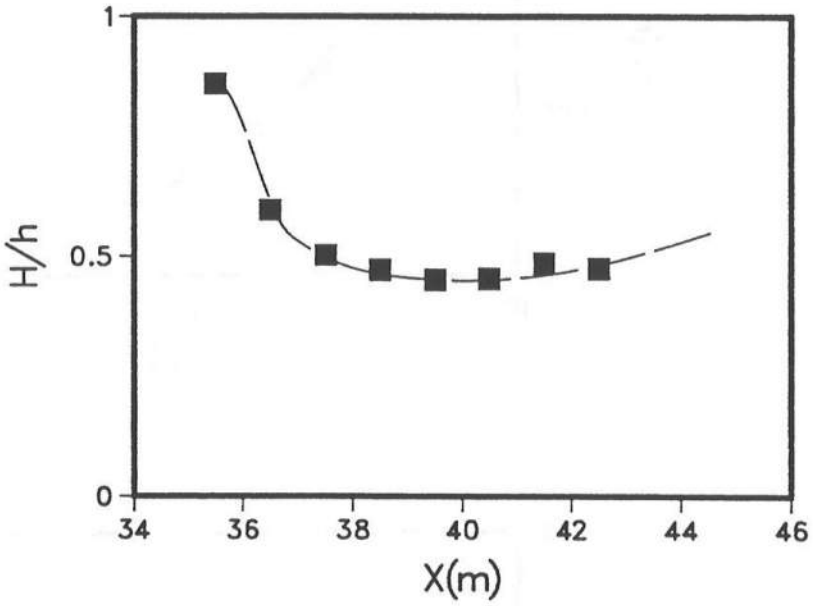

Figure A.17: Variation of H/h for Stive & Wind Experiment 1

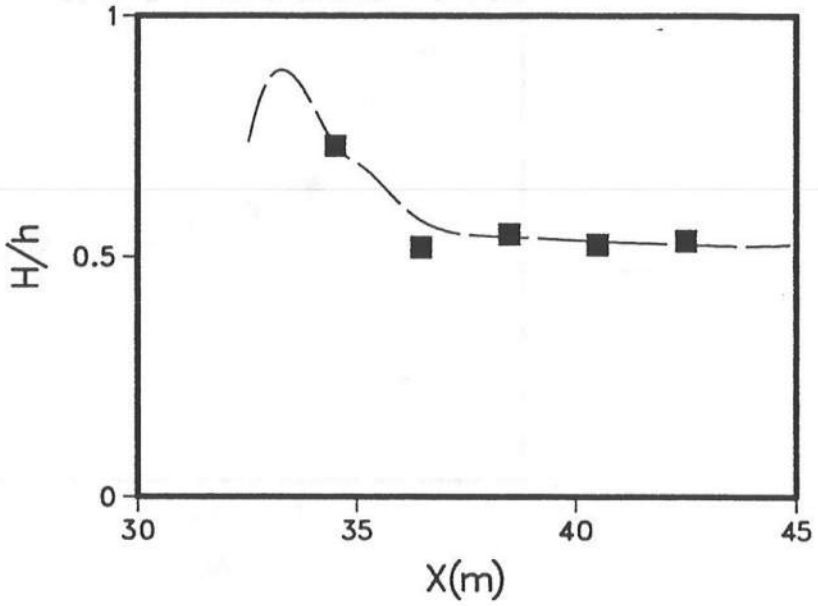

Figure A.18: Variation of H/h for Stive & Wind Experiment 2

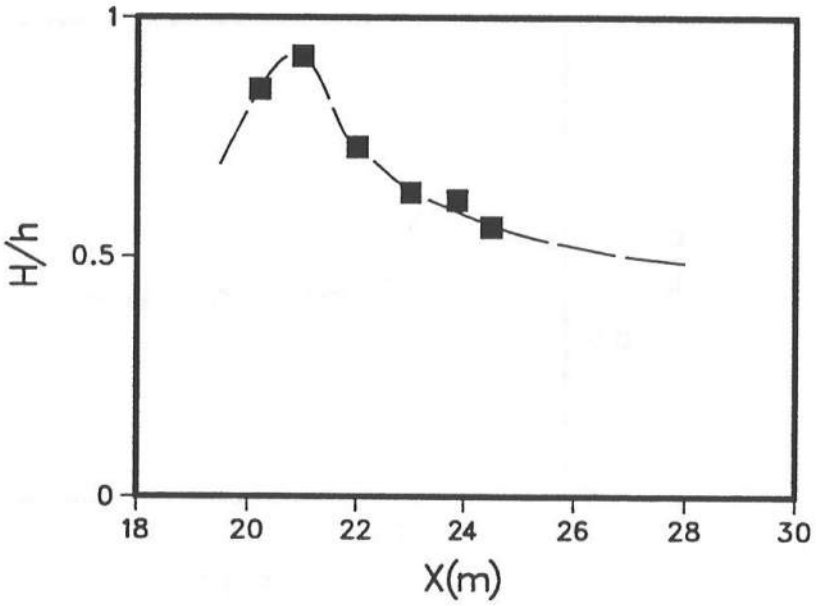

Figure A.19: Variation of H/h for ISVA

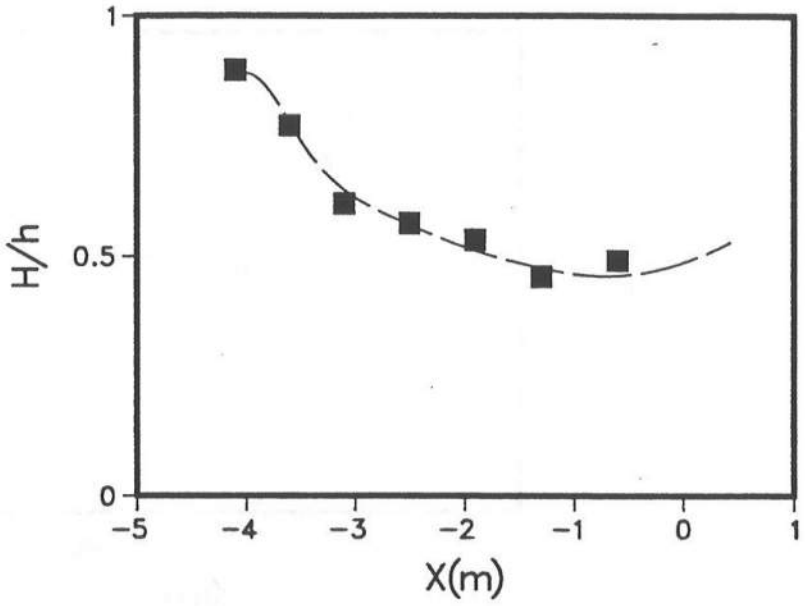

Figure A.20: Variation of H/h for Okayasu S3C1

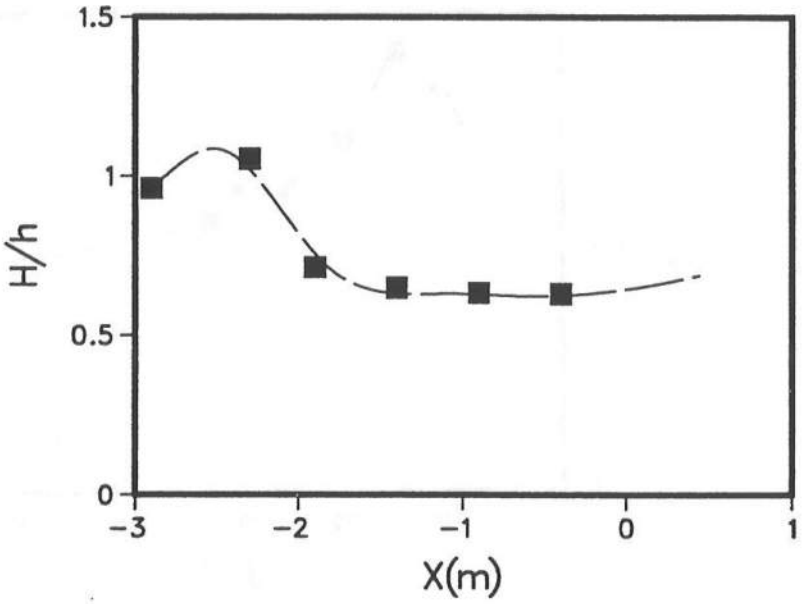

Figure A.21: Variation of H/h for Okayasu S3C2

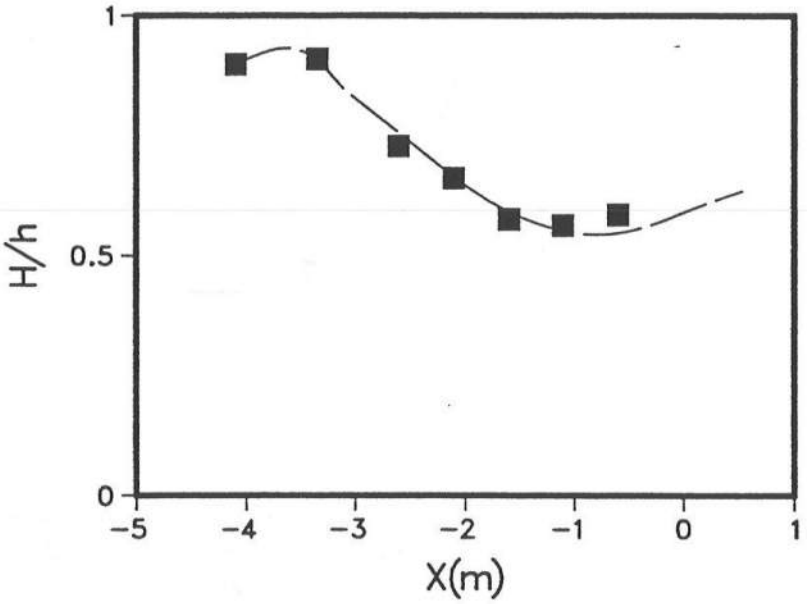

Figure A.22: Variation of H/h for Okayasu S3C3

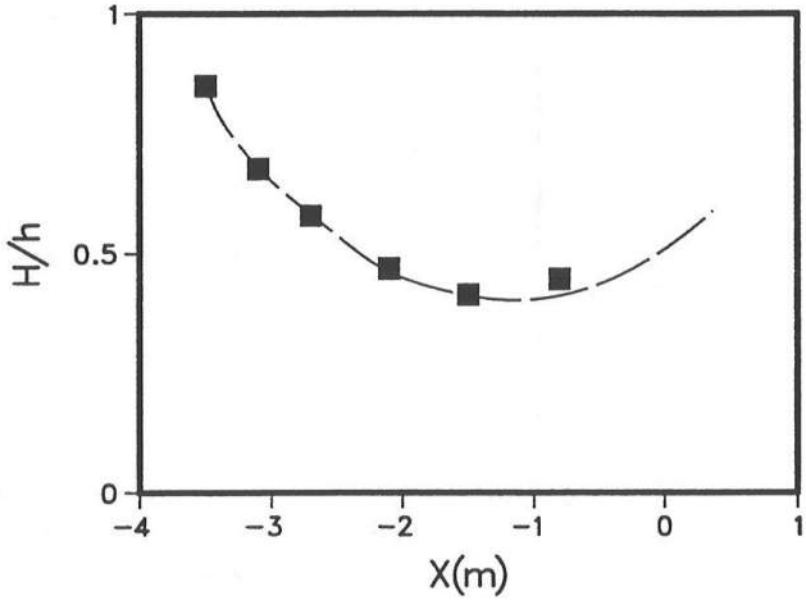

Figure A.23: Variation of H/h for Okayasu S3C4

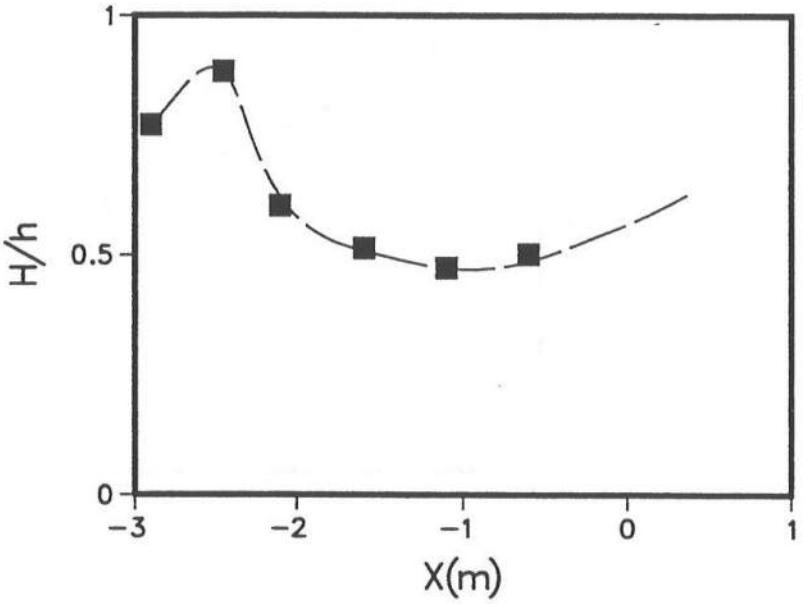

Figure A.24: Variation of H/h for Okayasu S3C5

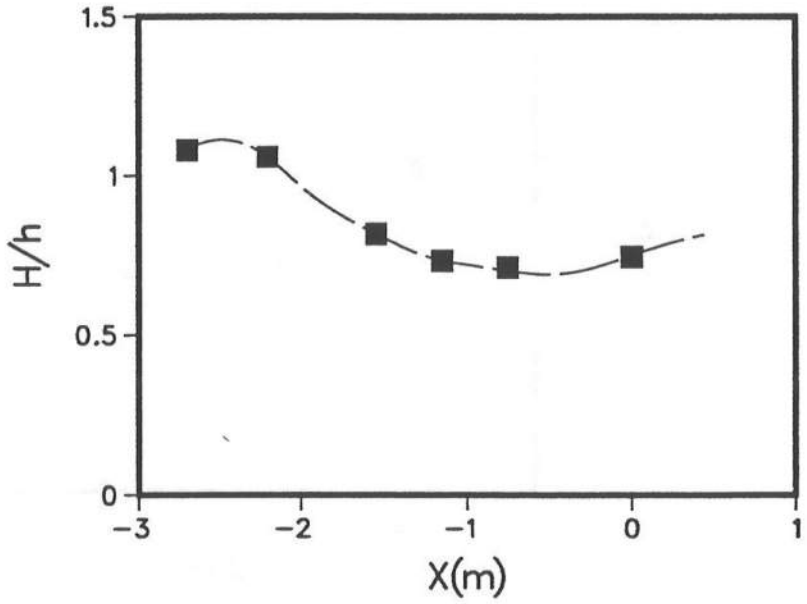

Figure A.25: Variation of H/h for Okayasu S2C1

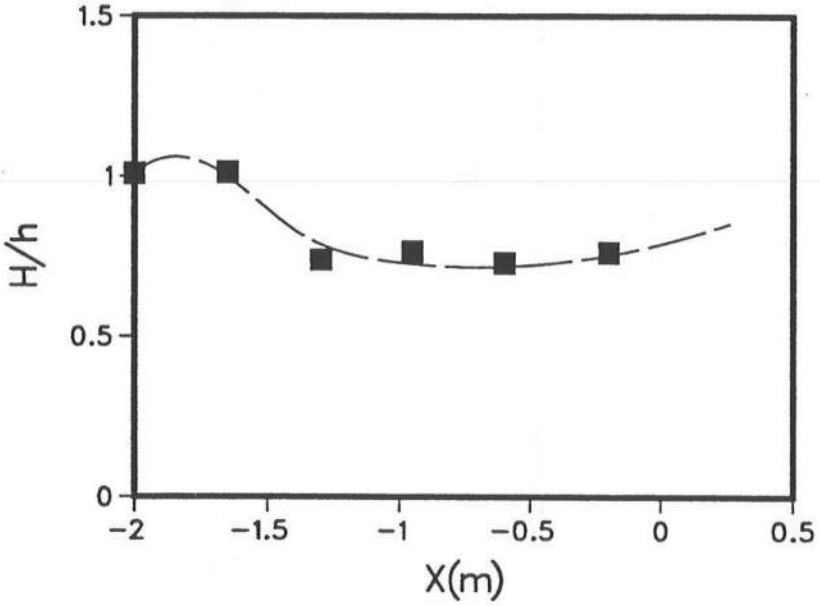

Figure A.26: Variation of H/h for Okayasu S2C2

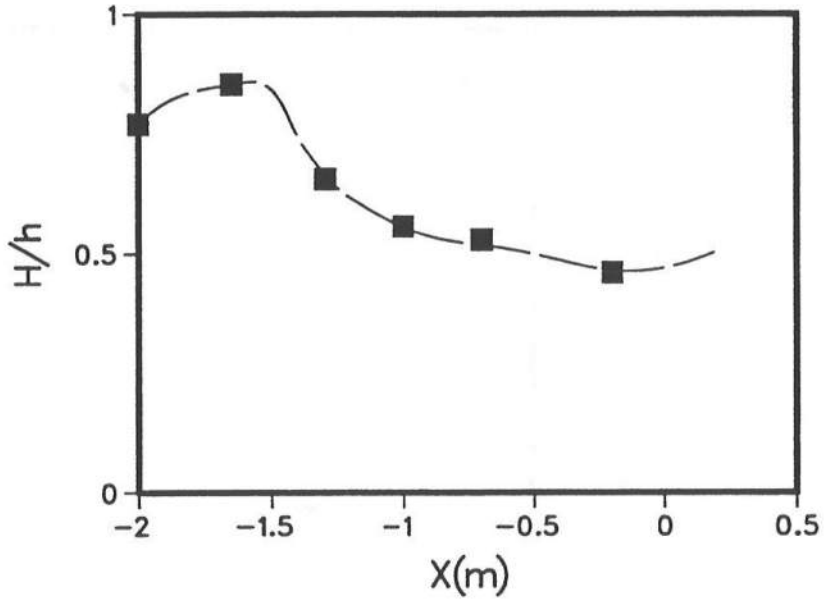

Figure A.27: Variation of H/h for Okayasu S2C4

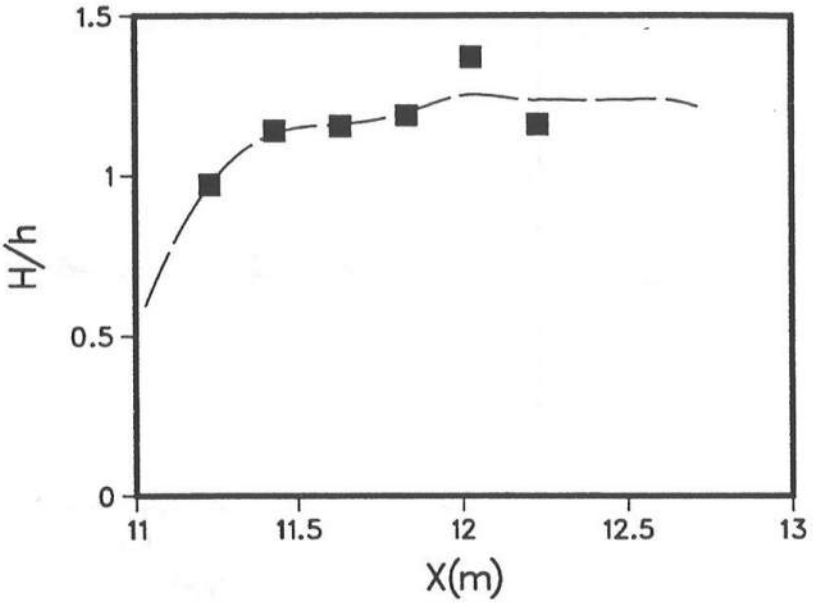

Figure A.28: Variation of H/h for Visser Experiment 1

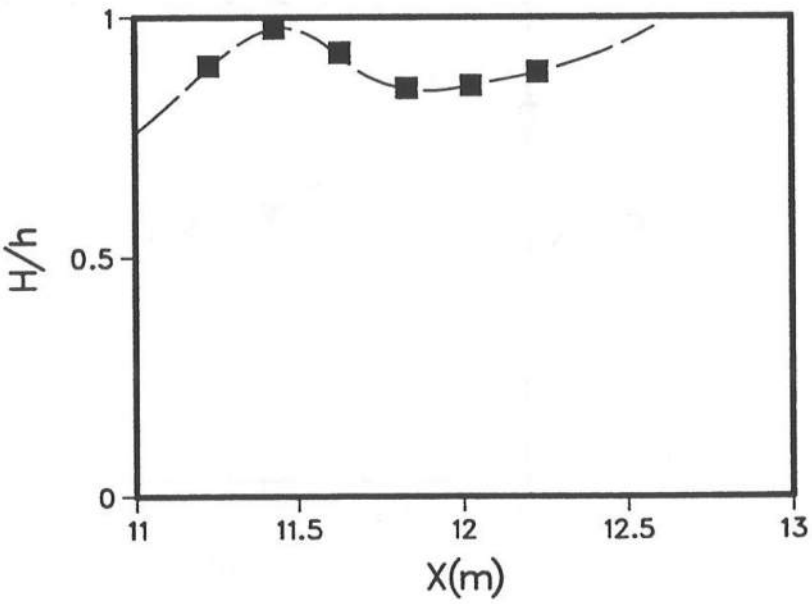

Figure A.29: Variation of H/h for Visser Experiment 2

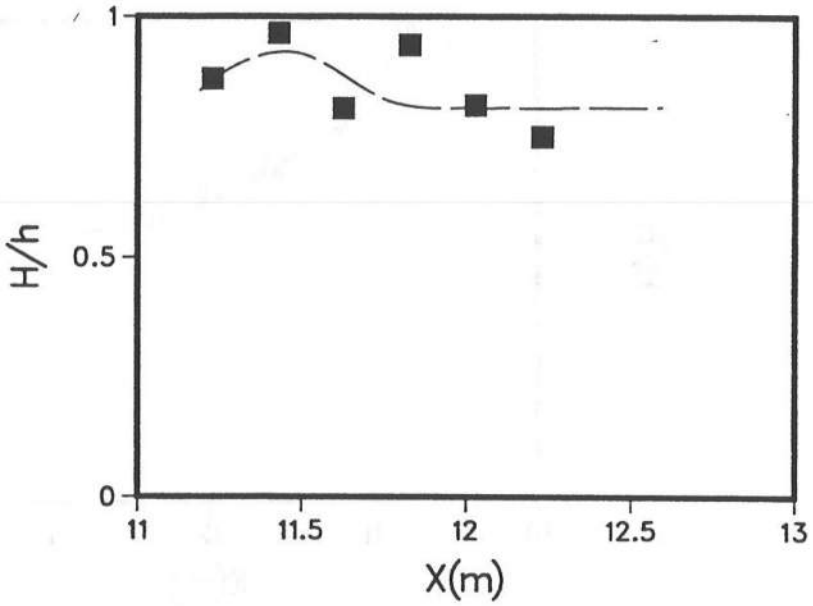

Figure A.30: Variation of H/h for Visser Experiment 3

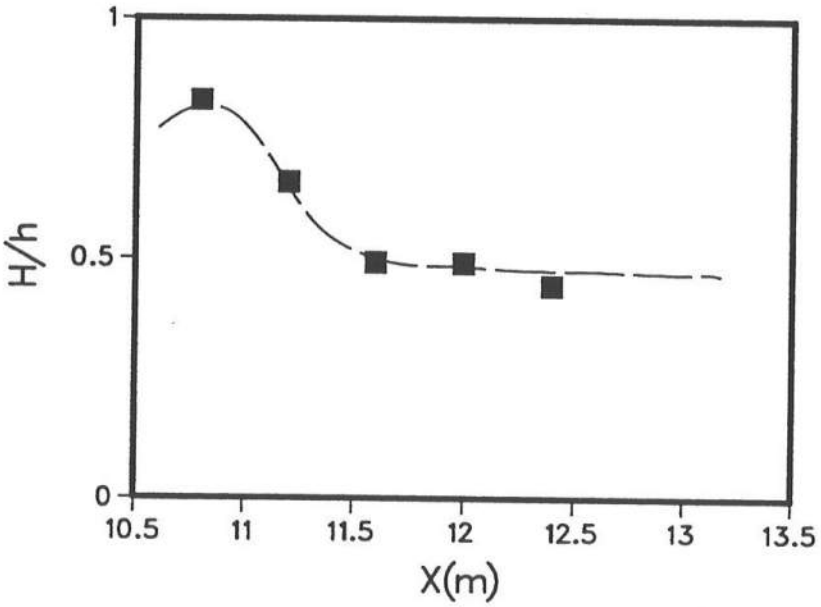

Figure A.31: Variation of H/h for Visser Experiment 4

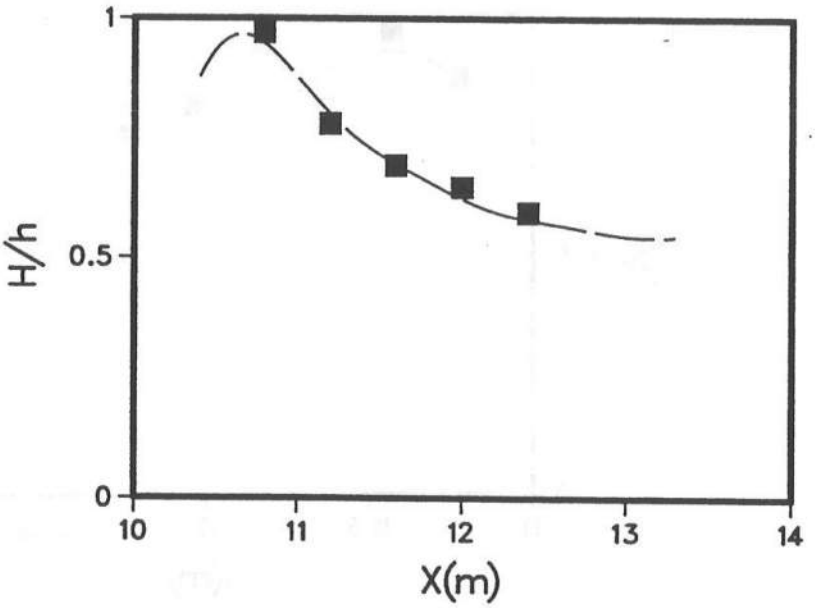

Figure A.32: Variation of H/h for Visser Experiment 5

Appendix B

CONSERVATION OF THE LONGSHORE COMPONENT OF THE RADIATION STRESS OUTSIDE THE SURF-ZONE

In this appendix we derive the condition that $dS_{xy}/dx = 0$ outside the surf-zone. The assumptions required for this derivation are also stated so that the applicability of the result may be readily assessed. The derivation given here follows from James (1974a).

We assume that outside the surf-zone the wave motion is irrotational and may be described by a velocity potential ϕ. The Bernoulli equation states that

$$\frac{\partial \phi}{\partial t} + \frac{p_d}{\rho} + \frac{1}{2}\left(u^2 + v^2 + w^2\right) = 0 \tag{B.1}$$

where p_d is the dynamic pressure ($= p + \rho g z$). The energy flux in the x direction, E_{fx}, is given by

$$E_{fx} = \overline{\int_{-h_0}^{\eta} \left[p_d + \frac{\rho}{2}(u^2 + v^2 + w^2)\right] u dz} \tag{B.2}$$

Substituting (B.1) into (B.2) leads to

$$E_{fx} = -\overline{\int_{-h_0}^{\eta} \frac{\partial \phi}{\partial t} u dz} \tag{B.3}$$

We now assume that the velocity potential is given by

$$\phi(x, y, t) = \phi(k_x x + k_y y - \omega t) \tag{B.4}$$

Therefore we will have

$$\frac{\partial \phi}{\partial t} = \frac{-\omega}{k_y}\frac{\partial \phi}{\partial y} = \frac{-c}{\sin\alpha}\frac{\partial \phi}{\partial y} \tag{B.5}$$

where α is the angle of incidence of the wave. Substituting (B.5) into (B.3) leads to

$$E_{fx} = \frac{c}{\sin\alpha}\overline{\int_{-h_0}^{\eta} \frac{\partial \phi}{\partial y}\frac{\partial \phi}{\partial x} dz} = \frac{c}{\sin\alpha} S_{xy} \tag{B.6}$$

The second of the equalities above follows from the definition of the radiation stress. The result relating the energy flux and the radiation stress was first proved Longuet-Higgins (1970) for the linear case. The extension presented here is due to James (1974a).

By Snell's law we have $c/\sin\alpha$ cosntant. This implies that if the energy flux is conserved then

$$\frac{\partial E_{fx}}{\partial x} = \frac{c}{\sin\alpha}\frac{\partial S_{xy}}{\partial x} = 0 \tag{B.7}$$

Thus, outsude the surf-zone we have conservation of the longshore component of the radiation stress.

Bowen (1969a) points out that the result that $\partial S_{xy}/\partial x = 0$ outside the surf-zone is a consequence of the fact that in this region the wave motion is assumed irrotational and hence cannot provide any forcing for a current of non-zero vorticity.

Appendix C

DERIVATION OF THE VARIATIONS INSIDE THE SURF-ZONE FOR SIMPLIFIED CONDITIONS

In this appendix we show the details that lead to (5.81). Under the assumptions of chapter 6 (which are the same as those listed before equation 5.81) we have

$$Q_s = b_q \frac{H^2}{h}\sqrt{gh} = b_q \gamma^2 h \sqrt{gh} \tag{C.1}$$

$$a_u = \frac{1}{2\nu_{tz}}\left[g\frac{\partial b}{\partial x} + \frac{1}{2}\frac{\partial \overline{u_w^2}}{\partial x}\right] \tag{C.2}$$

Therefore, we have after combining (6.13) and (6.14)

$$U_b = \epsilon_u \sqrt{gh} \tag{C.3}$$

where

$$\epsilon_u = \frac{-b_q\gamma^2\left(\frac{h}{h_t}\right) - \frac{\alpha_1}{6c_z g}\left(\frac{h}{h_t}\right)^2}{1 + \frac{f_w \gamma}{4\pi c_z}\left(\frac{h}{h_t}\right)} \tag{C.4}$$

Substituting (C.3) into (6.13) leads to

$$b_u = \epsilon_b \frac{\sqrt{gh}}{h} \tag{C.5}$$

with

$$\epsilon_b = \frac{f_w \gamma}{2\pi c_z}\epsilon_u \tag{C.6}$$

Similarly, we find that

$$a_u = \epsilon_a \frac{\sqrt{gh}}{h^2} \tag{C.7}$$

where

$$\epsilon_a = \frac{\alpha_1}{2c_z g} \tag{C.8}$$

Subsituting these results into (6.11) we find that the nondimensional undertow is given by

$$\frac{U(\zeta)}{\sqrt{gh}} = \epsilon_u + \epsilon_b \left(\frac{\zeta}{h}\right) + \epsilon_a \left(\frac{\zeta}{h}\right)^2 \tag{C.9}$$

Equation 5.81 may be derived from the above after using the fact that under the assumptions made here h_t/h is a constant. This equation indicates that the nondimensional undertow profiles inside the surf-zone are self-similar.

Appendix D

NUMERICAL FORMULATION FOR THE SOLUTION OF THE INSTABILITY EQUATION

In this appendix we show the details of the numerical scheme used. We approximate the derivatives by the following finite difference approximations which are correct to order $(\Delta x)^4$ (see, for example, Andersen *et al.* 1984, p. 45)

$$\frac{df}{dx} = \frac{f_{n-2} - 8f_{n-1} + 8f_{n+1} - f_{n+2}}{12\Delta x} \tag{D.1}$$

$$\frac{d^2f}{dx^2} = \frac{-f_{n-2} + 16f_{n-1} - 30f_n + 16f_{n+1} - f_{n+2}}{12(\Delta x)^2} \tag{D.2}$$

where $f_p = f(x_p)$. With this scheme, the grid points $n = 2, N-1$ (N is the number of nodes in the finite difference scheme) have to be handled in a special manner (see Orszag and Israeli 1974). We derive a fourth order scheme for approximating the derivatives at these points based on a Taylor series expansion. This derivation is given below.

The idea is this: We expand the function in a Taylor series about the point where the derivatives are desired and then solve for the derivatives in terms of the values of the function at various points. Let the function be given by $f(x)$. The values of the function at $x = x_0 - \Delta x, x_0 + \Delta x, x_0 + 2\Delta x, x = x_0 + 3\Delta x, x = x_0 + 4\Delta x, x = x_0 + 5\Delta x$ are given in terms of quantities at x_0 correct to order $(\Delta x)^6$ by

$$\begin{aligned}
f_{-1} &= f_0 - \Delta x f' + (\Delta x)^2\frac{f''}{2!} - (\Delta x)^3\frac{f'''}{3!} + (\Delta x)^4\frac{f''''}{4!} - (\Delta x)^5\frac{f'''''}{5!} \\
f_1 &= f_0 + \Delta x f' + (\Delta x)^2\frac{f''}{2!} + (\Delta x)^3\frac{f'''}{3!} + (\Delta x)^4\frac{f''''}{4!} + (\Delta x)^5\frac{f'''''}{5!} \\
f_2 &= f_0 + 2\Delta x f' + (2\Delta x)^2\frac{f''}{2!} + (2\Delta x)^3\frac{f'''}{3!} + (2\Delta x)^4\frac{f''''}{4!} + (2\Delta x)^5\frac{f'''''}{5!} \\
f_3 &= f_0 + 3\Delta x f' + (3\Delta x)^2\frac{f''}{2!} + (3\Delta x)^3\frac{f'''}{3!} + (3\Delta x)^4\frac{f''''}{4!} + (3\Delta x)^5\frac{f'''''}{5!} \\
f_4 &= f_0 + 4\Delta x f' + (4\Delta x)^2\frac{f''}{2!} + (4\Delta x)^3\frac{f'''}{3!} + (4\Delta x)^4\frac{f''''}{4!} + (4\Delta x)^5\frac{f'''''}{5!}
\end{aligned} \tag{D.3}$$

$$f_5 = f_0 + 5\Delta x f' + (5\Delta x)^2\frac{f''}{2!} + (5\Delta x)^3\frac{f'''}{3!} + (5\Delta x)^4\frac{f''''}{4!} + (5\Delta x)^5\frac{f'''''}{5!}$$

where $f_p = f(x_0 + p\Delta x)$ and the primes denote the value of the derivatives at $x = x_0$. The system of equations (D.3) can be solved for the derivatives. This yields

$$f' = \frac{-12f_{-1} - 65f_0 + 120f_1 - 60f_2 + 20f_3 - 3f_4}{60\Delta x} \tag{D.4}$$

$$f'' = \frac{10f_{-1} - 15f_0 - 4f_1 + 14f_2 - 6f_3 + f_4}{12(\Delta x)^2} \tag{D.5}$$

The equation for f' is correct to order $(\Delta x)^5$ and the equation for f'' is correct to order $(\Delta x)^4$. The corresponding finite difference approximations for $n = N - 1$ can be derived by a trivial change of notation. An equation for f' correct to order $(\Delta x)^4$ may be derived by solving the first five equations of (35) with the order $(\Delta x)^5$ terms neglected. Doing this leads to

$$f' = \frac{-3f_{-1} - 10f_0 + 18f_1 - 6f_2 + f_3}{12\Delta x} \tag{D.6}$$

This is the equation that that has been used to approximate the first derivative at $n = 2, N - 1$ since this is correct to order $(\Delta x)^4$ consistent with the finite difference approximations used for expressing the other derivatives.

The boundary conditions in discretized form are

$$\psi^{(1)} = \psi^{(N)} = 0 \tag{D.7}$$

When (7.6) is discretized using the finite difference approximations given above and the boundary conditions applied we get the following system of equations

$$\psi^{(1)} = 0$$

$$\begin{aligned}
&\frac{V}{\Delta x}\left(\frac{5}{6\Delta x} + \frac{h_x}{4h}\right)\psi^{(1)} + \left[V\left(\frac{-15}{12\Delta x^2} - k^2 + \frac{5h_x}{6h\Delta x}\right) - V_{xx} + \frac{V_x h_x}{h}\right]\psi^{(2)} - \\
&\frac{V}{\Delta x}\left(\frac{1}{3\Delta x} + \frac{3h_x}{2h}\right)\psi^{(3)} + \frac{V}{\Delta x}\left(\frac{7}{6\Delta x} + \frac{h_x}{2h}\right)\psi^{(4)} - \frac{V}{2\Delta x}\left(\frac{1}{\Delta x} + \frac{h_x}{6h}\right)\psi^{(5)} + \frac{V}{12(\Delta x)^2}\psi^{(6)} \\
&= c\left(\frac{1}{\Delta x}\left(\frac{5}{6\Delta x} + \frac{h_x}{4h}\right)\psi^{(1)} + \left(\frac{-15}{12\Delta x^2} - k^2 + \frac{5h_x}{6h\Delta x}\right)\psi^{(2)} - \frac{1}{\Delta x}\left(\frac{1}{3\Delta x} + \frac{3h_x}{2h}\right)\psi^{(3)}\right. \\
&\qquad \left. + \frac{1}{\Delta x}\left(\frac{7}{6\Delta x} + \frac{h_x}{2h}\right)\psi^{(4)} + \frac{1}{2\Delta x}\left(\frac{1}{\Delta x} + \frac{h_x}{6h}\right)\psi^{(5)} + \frac{1}{12(\Delta x)^2}\psi^{(6)}\right)
\end{aligned}$$

$$-\frac{V}{12\Delta x}(\frac{1}{\Delta x}+\frac{h_x}{h})\psi^{(n-2)}+\frac{V}{3\Delta x}(\frac{4}{\Delta x}+\frac{2h_x}{h})\psi^{(n-1)}-[V(\frac{30}{12\Delta x^2}+k^2)+(V_{xx}-\frac{V_xh_x}{h})]\psi^{(n)}$$
$$+\frac{V}{3\Delta x}(\frac{4}{\Delta x}-\frac{2h_x}{h})\psi^{(n+1)}-\frac{V}{12\Delta x}(\frac{1}{\Delta x}-\frac{h_x}{h})\psi^{(n+2)}$$
$$=c\left(\frac{-1}{12\Delta x}(\frac{1}{\Delta x}+\frac{h_x}{h})\psi^{(n-2)}+\frac{1}{3\Delta x}(\frac{4}{\Delta x}+\frac{2h_x}{h})\psi^{(n-1)}-(\frac{30}{12\Delta x^2}+k^2)\psi^{(n)}\right.$$
$$\left.+\frac{1}{3\Delta x}(\frac{4}{\Delta x}-\frac{2h_x}{h})\psi^{(n+1)}-\frac{1}{12\Delta x}(\frac{1}{\Delta x}-\frac{h_x}{h})\psi^{(n+2)}\right) \quad \text{(D.8)}$$

$$\frac{V}{12(\Delta x)^2}\psi^{(N-5)}-\frac{V}{2\Delta x}(\frac{1}{\Delta x}-\frac{h_x}{6h})\psi^{(N-4)}+\frac{V}{\Delta x}(\frac{7}{6\Delta x}-\frac{h_x}{2h})\psi^{(N-3)}-\frac{V}{\Delta x}(\frac{1}{3\Delta x}-\frac{3h_x}{2h})\psi^{(N-2)}$$
$$+[V(\frac{-15}{12\Delta x^2}-k^2-\frac{5h_x}{6h\Delta x})-V_{xx}+\frac{V_xh_x}{h}]\psi^{(N-1)}+\frac{V}{\Delta x}(\frac{5}{6\Delta x}-\frac{h_x}{4h})\psi^{(N)}$$
$$=c\left(\frac{1}{12(\Delta x)^2}\psi^{(N-5)}-\frac{1}{2\Delta x}(\frac{1}{\Delta x}-\frac{h_x}{6h})\psi^{(N-4)}+\frac{1}{\Delta x}(\frac{7}{6\Delta x}-\frac{h_x}{2h})\psi^{(N-3)}-\right.$$
$$\left.\frac{1}{\Delta x}(\frac{1}{3\Delta x}-\frac{3h_x}{2h})\psi^{(N-2)}+(\frac{-15}{12\Delta x^2}-k^2-\frac{5h_x}{6h\Delta x})\psi^{(N-1)}+\frac{1}{\Delta x}(\frac{5}{6\Delta x}-\frac{h_x}{4h})\psi^{(N)}\right)$$

$$\psi^{(N)}=0$$

In the above $3 \leq n \leq N-2$. The system of equations (D.8) may be concisely expressed in matrix form as follows

$$[A]\{\psi\}=c[B]\{\psi\}$$

This is equation 7.13 of chapter 7.

Finally, we note that there may be some question regarding the formal accuracy of the system of equations (D.3). For example, because of the large value of 5^6 there is some doubt whether the last equation in (D.3) can be considered correct to order $(\Delta x)^6$. Consequently, it may be questioned whether (D.5) and (D.6) are actually correct to order $(\Delta x)^4$. However, according to Orszag and Israeli (1974) it is sufficient to have the boundary approximations correct to third order to ensure that the overall scheme is of fourth order accuracy which the form of (D.3) used should satisfy with reasonable accuracy.

REFERENCES

Andersen, D. A., J. C. Tannehill and R. H. Pletcher, 1984. Computational fluid mechanics and heat transfer. Hemisphere Publishing Corp., New York, 599 pp.

Battjes, J. A., 1974. Surf similarity. Proceedings of the 14th Coastal Engineering Conference, pp. 466-480.

Battjes, J. A., 1975. Modelling of turbulence in the surf-zone. Proceedings of a Symposium on Modelling Techniques, ASCE, San Francisco, pp. 1050-61.

Battjes, J. A., 1983. Surf-zone turbulence. Proceedings of 20th IAHR Congress, Seminar on Hydrodynamics of the Coastal Zone, Moscow, pp. 137-40.

Battjes, J. A., 1988. Surf-zone dynamics. Annual Review of Fluid Mechanics, 20, pp. 257-293.

Borecki, O. S., 1982. Distribution of wave induced momentum fluxes over depth and application within the surf zone. Doctoral dissertation, Department of Civil Engineering, University of Delaware. 108 pp.

Bowen, A. J., 1969a. The generation of longshore currents on a plane beach. Journal of Marine Research, 27, pp. 206-215.

Bowen, A. J., 1969b. Rip currents, Part 1: Theoretical investigations. Journal of Geophysical Research, 74, pp. 5467-78.

Bowen, A. J. and R. A. Holman, 1989. Shear instabilities in the mean longshore current 1: Theory. Journal of Geophysical Research 94: 18,023-030.

Bowen, A. J. and D. L. Inman, 1974. Nearshore mixing due to waves and wave induced currents. Rapp. P.-v. Reun. Cons. Int., 167, pp. 6-12.

Bowen, A. J., D. L. Inman and V. P. Simmons, 1968, Wave 'set-down' and set-up. Journal of Geophysical Research, 73, pp. 2569-2577

Bruun, P., 1954. Coast erosion and the development of beach profiles. Technical memo # 44, Beach Erosion Board.

Cokelet, E. D., 1977. Steep gravity waves in water of arbitrary uniform depth. Philosophical Transactions of the Royal Society of London, 286, pp. 183-230.

Dally, W. R., 1980. A numerical model for beach profile evolution. Master's thesis, Department of Civil Engineering, University of Delaware. 122 pp.

Dally, W. R., R. G. Dean and R. A. Dalrymple, 1985. Wave height variation across beaches of arbitrary profile. Journal of Geophysical Research, 90, pp. 11,917-27.

Dalrymple, R. A., 1980. Longshore currents with wave current interaction. Journal of Waterway, Port, Coastal, and Ocean Engineering. Vol. 106, No. WW3, pp. 414-420.

Dalrymple, R. A. and C. J. Lozano, 1978. Wave-current interaction models for rip currents. Journal of Geophysical Research, 83, pp. 6063-6071.

Davies, A. M., 1987. On extracting current profiles from vertically integrated numerical models. Coastal Engineering, 11, pp. 445-477.

Dean, R. G., 1977. Equilibrium beach profiles: U. S. Atlantic and Gulf coasts. Ocean Engineering report no. 12, Department of Civil Engineering, University of Delaware, 45 pp.

deVriend, H. J. and N. Kitou, 1990. Incorporation of wave effects in a 3D hydrostatic mean current model. Proceedings of the 22nd Coastal Engineering Conference.

deVriend, H. J. and M. J. F. Stive, 1987. Quasi-3D modelling of nearshore currents. Coastal Engineering, 11, pp. 565-601.

Divoky, D., B. LeMehaute and A. Lin, 1970, Breaking Waves on gentle slopes. Journal of Geophysical Research, 75, pp. 1681-1692.

Dodd, N., J. Oltman-Shay and E. B. Thornton, 1991. Shear instabilities in the longshore current: A comparison of observation and theory. Journal of Physical Oceanography. In Press.

Dodd, N. and E. B. Thornton, 1990. Growth and energetics of shear waves in the nearshore. Journal of Geophysical Research, 95, 16,075-083.

Dong, P. and K. Anastasiou, 1991. The vertical distribution of longshore currents on a plane beach. Coastal Engineering, 15.

Drazin, P. G. and Reid, W. H. 1982. Hydrodynamic stability. Cambridge University Press, Cambridge, 527 pp.

Duncan, J. H., 1981. An experimental investigation of wave breaking produced by a towed hydrofoil. Proceedings of the Royal Society of London, Series A, 377, pp. 331-348.

Dyhr-Nielsen, M. and T. Sorensen, 1970. Some sand transport phenomena on coasts with bars. Proceedings of the 12th Coastal Engineering Conference, pp. 855-66.

Ebersole, B. and R. A. Dalrymple, 1979. A numerical model for nearshore circulation including convective accelerations and lateral mixing. Ocean Engineering Report # 21, Department of Civil Engineering, University of Delaware, 87 pp.

Fowler, R. E. and R. A. Dalrymple, 1990. Wave group forced nearshore circulation. Proceedings of the 22nd Coastal Engineering Conference, pp. 729-742.

Galvin, C. J., 1967. Longshore current velocity: A review of theory and data. Reviews of Geophysics, 5, pp. 287-304.

Grant, W. D. and O. S. Madsen, 1979. Combined wave and current interaction with a rough bottom. J. Geophysical Research, 84 , 1797-1808.

Greenwood, B. and P. D. Osborne, 1990. Vertical and horizontal structure in cross-shore flows: An example of undertow and wave set-up on a barred beach. Coastal Engineering, 14, pp. 543-580.

Haines, J. and A. Sallenger, 1990. Vertical structure of cross-shore currents across a barred surface. Transactions of the American Geophysical Union, vol. 71, no. 43, p. 1355.

Hansen, J. B., 1990. Periodic waves in the surf-zone: Analysis of experimental data. Coastal Engineering, 14, pp. 19-41.

Hansen, J. B., 1991. Surf zone parameters on a parabolic bottom. Progress report # 72, Institue of Hydrodynamics and Hydraulic Engineering, Technical University of Denmark, pp. 17-26.

Hansen, J. B. and I. A. Svendsen, 1979. Regular waves in shoaling water, experimental data. Series paper # 21, Institue of Hydrodynamics and Hydraulic Engineering, Technical University of Denmark, 243 pp.

Hansen, J. B. and I. A. Svendsen, 1984. A theoretical and experimental study of the undertow. Proceedings of the 19th Coastal Engineering Conference, Houston. pp. 2246-2262.

Harris, T. F. W., J. M. Jordan, W. R. McMurray, C. J. Verwey and F. P. Anderson, 1963. Mixing in the surf zone. International Journal of Air and Water Pollution, 7, pp. 649-667.

Horikawa, K. and C. T. Kuo, 1966. A study of wave transformation inside the surf-zone. Proceedings of the 10th Coastal Engineering Conference, pp. 217-233.

Hwang, L.-S. and D. Divoky, 1970, Breaking wave setup and decay on gentle slopes. Proceedings of the 12th Coastal Engineering Conference, pp. 347-389.

Inman, D. L., R. J. Tait and C. E. Nordstrom, 1971. Mixing in the surf zone. Journal of Geophysical Research, 76, pp. 3493-3514.

James, I. D., 1974a. Nonlinear waves in the nearshore region: Shoaling and set-up. Estuarine and Coastal Marine Science, 2, pp. 207-234.

James, I. D., 1974b. A nonlinear theory of longshore currents. Estuarine and Coastal Marine Science, 2, pp. 235-249.

Johns, B., 1983. Turbulence modelling beneath waves over beaches. Physical Oceanography of Coastal and Shelf Seas, B. Johns, ed., Elsevier Scientific, pp. 111-133.

Jonsson, I. G., 1966. Wave boundary layers and friction factors. Proceedings of the 10th Coastal Engineering Conference, pp. 127-148.

Jonsson, I. G., 1990. Wave-current interactions. The Sea, Volume 9, LeMehaute ed., John Wiley & Sons, pp. 65-120.

Jonsson, I. G., O. Skovgaard and P. S. Jacobsen, 1974. Computation of longshore currents. Proceedings of the 14th Coastal Engineering Conference, pp. 699-714.

Kirby, J. T. and T.-M. Chen, 1989. Surface waves on vertically sheared flows: Approximate dispersion relations. Journal of Geophysical Research, 94, pp. 1013-1027.

Kirby, J. T. and R. A. Dalrymple, 1982. Numerical modelling of the nearshore region. Research Report # CE-82-24, Ocean Engineering Program, Department of Civil Engineering, University of Delaware.

Kirkgoz, M. S. 1989. An experimental investigation of plunging breaker boundary layers in the transformation zone. Coastal Engineering, 13, pp. 341-356.

Kobayashi, N., G. S. DeSilva and K. D. Watson, 1989. Wave transformation and swash oscillation on gentle and steep slopes. Journal of Geophysical Research, 94, pp. 951-966.

Kraus, N. C. and T. O. Sasaki, 1979. Influence of wave angle and lateral mixing on the longshore current. Marine Science Communications, 5, pp. 91-126.

Larson, M. and N. Kraus, 1991. Numerical model for longshore current for bar and trough beaches. Journal of Waterway, Port, Coastal, and Ocean Engineering, 114, pp. 326-347.

LeMehaute, B., 1962. On non-saturated breakers and wave run-up. Proceedings of the 8th Coastal Engineering Conference, pp. 77-92.

Longuet-Higgins, M. S., 1970. Longshore currents generated by obliquely incident sea waves. Parts 1 and 2. Journal of Geophysical Research, 75, pp. 6778-6789 and pp. 6790-6801.

Longuet-Higgins, M. S., 1972. Recent progress in the study of longshore currents. Waves on Beaches, R. E. Meyer ed., Academic Press, pp. 203-248.

Longuet-Higgins, M. S. and R. W. Stewart, 1960. Changes in the form of short gravity waves on long waves and tidal currents. Journal of Fluid Mechanics, 13, pp. 481-504.

Longuet-Higgins, M. S. and R. W. Stewart, 1962. Radiation stress and mass transport in gravity waves with application to 'surf-beats'. Journal of Fluid Mechanics, 8, pp. 565-583.

Longuet-Higgins, M. S. and R. W. Stewart, 1963, A note on wave set-up. Journal Marine Research, 21, pp. 4-10.

Longuet-Higgins, M. S. and R. W. Stewart, 1964, Radiation stress in water waves, a physical discussion with application. Deep Sea Research, 11, pp. 529-563.

Liu, P. L.-F. and R. A. Dalrymple, 1978. Bottom frictional stresses and longshore currents due to waves with large angles of incidence. Journal of Marine Research, 36, pp. 357-375.

McDougal, W. G. and R. T. Hudspeth, 1983. Wave setup/setdown and longshore current on non-planar beaches. Coastal Engineering, 7, pp. 103-117

Mei, C. C. 1983. The applied dynamics of ocean surface waves. John Wiley and Sons, New York, 740 pp.

Mizuguchi, M. and K. Horikawa, 1978. Experimental study on longshore current velocity distribution. Bulletin of the Faculty of Science and Engineering. Chuo University, 21, pp. 123-150.

Moler, C. B. and G. W. Stewart, 1973. An algorithm for generalized matrix eigenvalue problems. SIAM Journal of Numerical Analysis, 10, No. 2, pp. 241-256.

Munk, W. H., 1949. The solitary wave theory and its application to surf problems. Annals of the New York Academy of Sciences, 51, pp. 376-424.

Nadaoka, K., M. Hino and Y. Koyano, 1989, Structure of the turbulent flow field under breaking waves in the surf zone. Journal of Fluid Mechanics, 204, pp. 359-387

Nadaoka, K., and T. Kondoh, 1982, Laboratory measurements of velocity field structure in the surf zone by LDV. Coastal Engineering in Japan, 25, pp. 125-145

Nairn, R. B., J. A. Roelvink and H. Southgate, 1990. Transition width and its implications for modelling surf-zone hydrodynamics. Proceedings of the 22nd Coastal Engineering Conference, pp. 68-81.

Okayasu, A., 1989. Characteristics of turbulence structure and undertow in the surf-zone. Doctoral dissertation, Department of Civil Engineering, University of Tokyo, 119 pp.

Okayasu, A., T. Shibayama and K. Horikawa, 1988. Vertical variation of undertow in the surf-zone. Proceedings of the 21st Coastal Engineering Conference, pp. 478-491.

Okayasu, A., T. Shibayama and N. Mimura, 1986. Velocity field under plunging waves. Proceedings of the 20th Coastal Engineering Conference, pp. 660-674

Oltman-Shay, J., P. A. Howd and W. A. Berkemeier, 1989. Shear instabilities of the mean longshore current 2: Field observations. Journal of Geophysical Research, 94, pp. 18,031-042.

Orszag, S. A. and M. Israeli, 1974. Numerical simulation of viscous incompressible flows. Annual Review of Fluid Mechanics, 6, pp. 281-318.

Otta, A. K., 1992. Unsteady free surface waves in region of arbitrary shape. Doctoral dissertation, Department of Civil Engineering, University of Delaware. In preparation.

Phillips, O. M., 1977. The dynamics of the upper ocean. Cambridge University Press, 336 pp.

Putnam, J. A., W. H. Munk and M. A. Traylor, 1949. The prediction of longshore currents. Transactions of the American Geophysical Union, 30, pp. 337-345.

Roelvink, J. A. and M. J. F. Stive, 1988. Bar generating cross-shore flow mechanisms on a beach. Journal of Geophysical Research, 94, pp. 4785-4800.

Sallenger, A. H. and P. A. Howd, 1989. Nearshore bars and break-point hypothesis. Coastal Engineering, 12, pp. 301-313.

Schaffer, H. A., 1990. Infragravity water waves induced by short-wave groups. Series paper # 50, Institute of Hydrodynamics and Hydraulic Engineering, Technical University of Denmark, 168 pp.

Shemer, L., N. Dodd and E. B. Thornton, 1991. Slow-time modulation of finite depth nonlinear water waves: Relation to longshore current oscillations. Journal of Geophysical Research, 96, pp. 7105-7113.

Stive, M. J. F., 1984. Energy dissipation in waves breaking on gentle slopes. Coastal Engineering, 8, pp. 99-127.

Stive, M. J. F. and J. A. Battjes, 1984. A model for offshore sediment transport. Proceedings of the 20th Coastal Engineering Conference, pp. 1420-1436.

Stive, M. J. F. and H. J. deVriend, 1987. Quasi-3D nearshore current modelling: Wave induced secondary currents. Proceedings of a special conference on coastal hydrodynamics, ASCE, Newark, pp. 356-370.

Stive, M. J. F. and H. G. Wind, 1982. A study of radiation stress and set-up in the nearshore region. Coastal Engineering, 6, pp. 1-26.

Stive, M. J. F. and H. G. Wind, 1986. Cross-shore mean flow in the surf-zone. Coastal Engineering, 10, pp. 325-340.

Svendsen, I. A., 1984a. Wave heights and set-up in a surf-zone. Coastal Engineering, 8, pp. 303-329.

Svendsen, I. A., 1984b. Mass flux and undertow in a surf-zone. Coastal Engineering, 8, pp. 347-365.

Svendsen, I. A. 1987. Analysis of surf zone turbulence. Journal of Geophysical Research, 92, pp. 5115-24.

Svendsen, I. A. and J. B. Hansen, 1976. Deformation up to breaking of periodic waves on a beach. Proceedings of the 15th Coastal Engineering Conference, pp. 477-496.

Svendsen, I. A. and J. B. Hansen, 1986. Interaction of waves and currents over a longshore bar. Proc. 20th Coastal Engineering Conference, pp. 1580-1594.

Svendsen, I. A. and J. B. Hansen, 1988. Cross-shore currents in surf-zone modelling. Coastal Engineering, 12, pp. 23-42.

Svendsen, I. A. and R. S. Lorenz, 1989. Velocities in combined undertow and longshore currents. Coastal Engineering, 13, pp. 55-79.

Svendsen, I. A. and P. A. Madsen, 1981. Energy dissipation in hydraulic jumps and breaking waves. Progress report # 55, Institute of Hydrodynamics and Hydraulic Engineering, Technical University of Denmark, pp. 39-47.

Svendsen, I. A., P. A. Madsen and J. B. Hansen, 1978. Wave characteristics in the surf-zone. Proceedings of the 16th Coastal Engineering Conference, pp. 520-539.

Svendsen, I. A. and Putrevu, U. 1990. Nearshore circulation with 3-D profiles. Proceedings of the 22nd Coastal Engineering Conference. pp. 241-254.

Svendsen, I. A., H. A. Schaffer and J. B. Hansen, 1987. The interaction between the undertow and boundary layer flow on a beach. Journal of Geophysical Research 92, pp. 11,845-856.

Symmonds, G., D. A. Huntley and A. J. Bowen, 1982. Two dimensional surf-beat: Long wave generation by a time-varying break point. Journal of Geophysical Research, 87, pp. 492-498.

Tang, E. and R. A. Dalrymple, 1988. Rip currents and wave groups. Nearshore Sediment Transport, R. J. Seymour, ed., Plenum Publishing Corporation, pp. 205-230.

Thornton, E. B., 1970. Variation of longshore current across the surf zone. Proceedings of the 12th Coastal Engineering Conference, pp. 291-308.

Thornton, E. B. and R. T. Guza, 1986. Surf-zone longshore currents and random waves: Field data and models. Journal of Physical Oceanography, 16, pp. 1165-1178.

Townsend, A. A., 1976. The structure of turbulent shear flow. Cambridge University Press, Cambridge, 429 pp.

Vemulakonda, S. R., 1984. Erosion control of scour during construction; Report 7, CURRENT – A wave induced current model. Technical Report # HL-80-3, Department of the Army, Waterways Experiment Station, Corps of Engineers, Vicksburg, Mississippi, 101 pp.

Visser, P. J. 1982. The proper longshore current in a wave basin. Report no. 82-1, Communications on Hydraulics, Department of Civil Engineering, Delft University of Technology, 86 pp.

Visser, P. J., 1984. A mathematical model of uniform longshore currents and comparison with laboratory data. Communications on Hydraulics. Report 84-2, Department of Civil Engineering, Delft University of Technology, 151 pp.

White, F. M., 1986. Fluid mechanics (second ed.). McGraw-Hill Book Company, New York, 732 pp.

Whitford, D. J., 1988. Wind and wave forcing of longshore currents across a barred beach. Doctoral dissertation. Naval Postgraduate School. 205 pp.

Wind, H. G. and C. B. Vreugdenhil, 1986. Rip current generation near structures. Journal of Fluid Mechanics, 171, pp. 459-476.

Wright, L. D., R. T. Guza and A. D. Short, 1982. Dynamics of a high energy dissipative surf-zone. Marine Geology, 45, pp. 41-62.

Wu, C.-S., E. B. Thornton and R. T. Guza, 1985. Waves and longshore currents: Comparison of a numerical model with field data. Journal of Geophysical Research, 90, pp. 4951-4958.

Wu, N. T., 1987. Numerical simulation of wave induced turbulent boundary layers. Master's thesis, Department of Civil Engineering, University of Delaware, 114 pp.